Regulation and Function of the Extracellular Matrix in *Candida* species biofilms

By

Eddie Gonzalez Dominguez Jr.

A dissertation submitted in partial fulfilment of

the requirements for the degree of

Doctor of Philosophy

(Cellular and Molecular Pathology)

At the

UNIVERSITY OF WISCONSIN-MADISON

2018

Date of final oral examination: 07/20/2018

The dissertation is approved by the following members of the Final Oral Committee:

David Andes, Professor, Medicine

Nancy Keller, Professor, Medical Microbiology and Immunology

Bruce Klein, Professor, Pediatrics

Christina Hull, Professor, Biomolecular Chemistry

Regulation and Function of the Extracellular Matrix in *Candida* species biofilms

Eddie G. Dominguez

Under the supervision of Professor David R. Andes

University of Wisconsin-Madison

Believed to be the predominant microbial growth form found in nature, biofilms are an organized community of microorganisms residing on a surface embedded in extracellular matrix (ECM). In pathogens the ECM acts as a protective barrier against the host innate immune response and enhances drug resistance.

Candida infections have the highest mortality rates of all nosocomial infections due to their ability to form difficult to treat biofilms on indwelling medical devices. Prior studies of the *C. albicans* matrix implicated the polysaccharides α-mannan and β-glucan, which forms a mannan-glucan complex (MGCx), as having a role in the high levels of drug resistance associated with biofilms. However, mechanisms of resistance involving the ECM of *Candida tropicalis, Candida parapsilosis,* and *Candida glabrata* bifoilms still remain unclear.

This work utilized biochemical, pharmacological, and genetic approaches to identify mechanisms of resistance in these non-*albicans Candida* (NAC) species with respect to the ECM. Enzymatic inhibition or hydrolyzation of either of these polysaccharides resulted in increased susceptibility to antifungal drug treatments. These results suggested a conserved matrix structure and function among these *Candida* species.

Genes known to regulate production and modification of the polysaccharide component of the ECM, in *C. albicans,* were knocked out in each of the NAC species. Biochemical analysis of wild-type NAC species matrices revealed the presence of the previously identified MGCx

featuring a structurally conserved polysaccharide backbone of α-1,6-mannan and β-1,6-glucan. These results argue for a conserved functionality of the ECM among the species.

Components of the ECM are theorized to be produced within the cell, packaged into extracellular vesicles (EVs), exported from within the cell, and constructed extracellularly through a number of proteins and enzymes. Here we use mutants defective in the endosomal sorting complexes required for transport (ESCRT) pathway to measure ECM carbohydrate content and function. A subset of defective mutants showed decreased levels of mannan/glucan, decreased quantity of EVs and enhanced susceptibility to antifungal drug treatments. These results argued that in *C. albicans* biofilms EVs are not only capable of cell-cell communication, as commonly seen in many organisms, but are also responsible for matrix production and biofilm drug resistance.

Table of Contents

ACKNOWLEDGEMENTS

First and foremost, I want to extend my sincerest thanks to my thesis advisor, Dr. David Andes. Words cannot express how thankful I am that he took me on as a student and provided me with a healthy research environment which allowed me to grow not only as a person, but as a scientist as well. I would not have the level of skills, both professionally and individually, if it wasn't for his guidance. I am grateful to have been part of such a wonderful research group during my time at UW-Madison.

I also would like to extend my thanks to the members of my thesis committee: Dr. Bruce Klein, Dr. Christina Hull, Dr. Kurt Reed, and Dr. Nancy Keller. Each year I looked forward to our annual meetings and the level of feedback each member provided at these times. The levels of expertise that each member brought from their respective areas of pathogenic fungi, allowed for discussions to emerge that stimulated growth of my own project in ways I never would of thought on my own. I would like to especially thank Dr. Christina Hull for the extra guidance and opportunities she provided me when she extended a position to me as an MBTG trainee.

I would like to thank the members of the Andes and Nett lab for all of the support, mentorship, and camaraderie throughout my dissertation. Working so closely with another lab who focused on the host side of *Candida* infections allowed for the inspiration of ideas and experiments which I never would have considered without their valuable input. I especially want to extend my thanks to long time lab members Hiram Sanchez and Dr. Robert Zarnowski. Hiram taught me numerous skills that were invaluable throughout my tenure in the lab and his general upbeat attitude gave the lab such a warm friendly atmosphere. My sincerest thanks go out to Robert and his family. Not only did he teach me the majority of the skills I needed to be successful in my projects, he was always kind, patient, and willing to take the time out of his own work schedule to brainstorm and provide his expertise towards my projects. Additionally, being so far

from home, he and his family welcomed me with open arms providing a level of support much needed. I will be forever thankful for what he and his family have done for me.

I would also like to thank the current and past graduate and undergraduates in the Andes lab: Dr. Kaitlin Mitchell, Dr, Nate Feirer, Dr. Miao Zhao, Antonio Covelli, Dr. Chad Johnson, John Kernien, and Riley Jones. I especially want to thank two of the undergraduates I mentored, Keeley Choy and Caitlin Baltus, for all of their assistance and general enthusiasm for being in the lab.

Thank you to the Cellular and Molecular Pathology Graduate Program for providing me the opportunity to train and become a scientist in one of the best research Universities in the country. A special thanks to Joanne Thornton for all of her help and tireless efforts in coordinating events and ensuring that things move along smoothly for us students within the program. I would also like to thank the Science and Medicine Graduate Research Scholars (SciMed GRS) program for financial support and the Molecular Biosciences Training Grant (MBTG) for financial support and additional training and mentorship.

Lastly, I would like to extend a special thank you to my family and a few special friends, whose support these past 5 years has been invaluable and I can never thank you enough: Gloria, Sarah, Amanda, and Sharon.

Chapter 1: Literature Review

Candida Biofilm Tolerance: Comparison of Planktonic and Biofilm Resistance Mechanisms

The contents of this section were published as a book chapter:

Eddie G. Dominguez and David R. Andes. "*Candida* Biofilm tolerance: Comparison of Planktonic and Biofilm Resistance Mechanisms". *Candida albicans*: Cellular and Molecular Biology. Springer International Publishing Switzerland 2017.

ABSTRACT:

Candida species are opportunistic fungal pathogens residing as commensal organisms in approximately 70% of the human population. During times of decreased immune function, *Candida spp.* are able to transition from harmless members of the human microbiota into pathogens capable of causing life threatening infections boasting mortality rates as high as 50%. Commonly adhering to implanted medical devices, *Candida spp* grow as highly structured biofilms with inherent resistance to antifungal drug therapies and the host immune system. A multitude of investigations have found this resistance to be multifactorial involving mechanisms associated with planktonic antifungal resistance (efflux pump activity) along with biofilm-specific mechanisms. One biofilm-specific mechanism involves the complex extracellular matrix. Components of the matrix, specifically β-glucan, mannan, and extracellular DNA, have been found to promote resistance against multiple antifungal drug classes. Here we will review molecular mechanisms contributing to *Candida* biofilm drug resistance.

Introduction:

Candida species is an opportunistic fungal pathogen which exists as a commensal organism in the alimentary, gastrointestinal, and genitourinary tract of approximately 70% of the human population [1-6]. In a healthy human, the fungus typically exists in harmony with the normal microbiotic flora of the host. However, in an immunocompromised or immunologically weak host, such as patients receiving chemotherapy, transplant recipients, and patients in the intensive care unit, *Candida* is among the most common pathogens and there is risk for spread beyond the mucosa which is associated with mortality in up to half of patients [7-9]. These lethal cases of candidiasis are often a result of biofilm formation, often on implanted medical devices. In fact, some case series suggest that up to 70% of *Candida* bloodstream infection is linked to biofilm infection of vascular catheters. Considered to be the predominant microbial growth form found in nature, biofilms are an organized community of microbial cells adhered to a surface and

enveloped in an extracellular matrix (ECM) with properties that are distinct from their planktonic counterparts [10, 11]. Microbial biofilms exist within environments that are both biotic (aquatic, plant tissues, or mammalian tissues) and abiotic (indwelling medical devices). Microbial species that form biofilms on solid surfaces, such as *Candida* sp., *Staphylococcus* sp., *Streptococcus* sp., and *Escherichia coli,* each form a biofilm with structure, development, and unique properties that are distinct [10]. Whilst each of these organisms have the capability to form a biofilm on its own, it is becoming clear they often occur in multispecies biofilms due to different species of bacteria and bacterial and fungi that thrive as a result of shared virulence attributes [12].

Antimicrobial tolerance is an obstacle to the treatment of numerous biofilm infections [13, 14]. *Candida* biofilms display innate resistance to all available drug classes and withstand antifungal concentrations up to 1000-fold higher than those which are effective towards non-biofilm planktonic cells [15-18]. Due to this inherent increased resistance to anti-fungal drugs, the recommended course of treatment for individuals afflicted with a *Candida* biofilm infection is extirpation of the afflicted device. *Candida* biofilm infections that are not successfully treated have a poor prognosis for the afflicted individual with an associated mortality rate as high as 50% [8, 9, 19-21].

Antifungal resistance is an intrinsic biofilm characteristic and one of the many phenotypic changes that occurs upon transition to this mode of growth [22, 23]. During the later phases of development the resistant phenotype is most pronounced, however drug resistance is able to be detected within minutes to hours of adhesion to a surface [22]. Genetic mutations do not account for this observed resistance since biofilm cells re-cultured in planktonic conditions revert back to a susceptibility phenotype to antifungals. Furthermore, it is clear that multiple mechanisms contribute throughout the various stages of biofilm growth to the drug resistance phenotype [24-26].

Overview of Antifungal Drug Classes and Planktonic *Candida* Resistance Mechanisms

Triazoles- The triazoles represent the most commonly used of all antifungal classes. Azole antifungal drugs inhibit *Candida* growth by targeting the enzyme lanosterol 14 α-demethylase (encoded by *ERG11*) which is necessary to convert lanosterol to ergosterol. This depletion of ergosterol in the fungal membrane causes the accumulation of toxic sterol intermediates which then lead to growth arrest [27-30]. As with almost all types of antimicrobials, prolonged use has been linked to drug resistance, however acquired *Candida* drug resistance is relatively uncommon [24, 31, 32]. Long-term treatment of oral or esophageal candidiasis as reported in HIV/AIDS, especially in the pre-HAART era [24, 33] was associated with high rates of resistance. The reported mechanisms of *C. albicans* azole resistance have included *ERG11* point mutations (S405F, Y132H, R467K, and G464S), gene amplifications, and mitotic recombination events within *ERG11* or the drug efflux pumps (*Cdr1p, Cdr2p, and Mdr1p)* which result in their increased expression [34-42]. Acquired resistance in *C. glabrata* is even more common. Conversely, resistance in *C. parapsilosis* and *C. tropicalis* is uncommon [41, 43-46]. However, intrinsic resistance during biofilm growth is universal among all *Candida* species. Cells within a biofilm environment tolerate 1,000-fold higher azole concentrations than their planktonic counterparts, acquiring resistance as early as 4-6 hours after initial adherence to a surface, resulting in ineffective triazole treatment [26, 47, 48].

Polyenes – The polyene antifungals were the first available for systemic therapy. These polyenes are amphiphilic molecules allowing for binding with sterols, primarily ergosterol, in the fungal cell membrane. This binding alters the transition temperature of the cell membrane, decreasing membrane fluidity and permeability. Release of monovalent ions (K^+, Na^+, H^+, and Cl^-) and small organic molecules ultimately leads to death of cell [49, 50]. Amphotericin B is a potent antifungal but is reserved for patients with severe systemic fungal infections due to the severe and potentially lethal side effects, the most important of which is renal toxicity. Resistance to amphotericin B is rare but has been described in case reports from cancer patients undergoing

chemotherapy and individuals undergoing prolonged prophylactic therapy [24]. The specific mechanisms of acquired polyene resistance are mechanistically poorly defined, but thought to involve alterations to cell membrane composition. Resistance has been linked to sterol changes in *C. glabrata* [51] as well as in genetically altered strains that are defective in sterol C5,6 – desaturase which produce little ergosterol [29, 52]. As with the triazoles, biofilms exhibit resistance to amphotericin B as well, but only 10-100 times as much as their planktonic counterparts in comparison to the 1,000 fold greater resistance associated with triazoles [53]. Unfortunately, the concentrations needed for effective therapy are not achievable during systemic administration.

Echinocandins – The echinocandins represent the most recently available antifungal drug class. They act via inhibition of β-1,3 glucan synthase, which is a key component of *Candida* cell walls [54-56]. Inhibition of this enzyme at the cell wall results in osmotic instability within the cell ultimately leading to lysis of the cell [57]. Clinical trial results suggest superiority over other antifungals for invasive candidiasis, likely due to its cidal activity and relative safety of this drug class. While, resistance remains relatively uncommon among all *Candida* species, treatment failures among *C. glabrata* have been emerging more rapidly. Point mutations along “hot spot” regions of the Fks1 subunits, located specifically among the range of amino acids from Phe641 – Pro649 and Arg1361, are the most commonly seen mechanisms of acquired resistance among this class of drugs and have been observed in *C. albicans* and homologous regions in *C. glabrata FKS2* gene [55, 56, 58-67]. As with the other antifungal drug classes, biofilms are intrinsically more resistant to echinocandins than their planktonic counterparts by approximately 2-20 fold [53, 68].

5-FC/Flucytosine – Flucytosine is a pyrimidine analogue that is metabolized in the pyrimidine salvage pathway by a cytosine deaminase into a toxic version of UTP. Upon incorporation, RNA synthesis is halted [69, 70]. Flucytosine also decreases the availability of nucleotides for DNA synthesis via conversion into a metabolite that inhibits thymidylate

synthetase [70]. Emergence of resistance with flucytosine monotherapy is relatively rapid. This resistance is due to mutations in the cytosine permease gene *FCY2,* which is responsible for escorting flucytosine into the cell, or in the cytosine deaminase gene *FCY1* [69]. Due to this rapid rate of acquired resistance, flucytosine is almost generally administered to patients in conjunction with amphotericin B and/or azole antifungals [71].

***Candida* Biofilm Resistance Mechanisms:**

Candida biofilms have been the subject of numerous investigations. Initial studies into the mechanisms of drug resistance primarily explored mechanisms previously linked to drug tolerance in planktonic cells. Mutations in genes that encode drug target enzymes, such as *ERG11* and *FKS1*and alterations in the composition of the plasma membrane have all been linked to planktonic cell resistance but have not been demonstrated to contribute to biofilm resistance [60, 72-74].

Role of efflux pumps

As described above, the over expression of efflux pumps, coupled with the reduction of antifungal accumulation within the cell, is a key mechanism of resistance for planktonic *Candida*. [72]. Ramage et al. examined if upregulation of efflux pumps may also contribute drug tolerance during biofilm growth. They found increased transcription of both *MDR1* and *CDR1* in 24 hr *C. albicans* biofilms when compared to their planktonic counterparts of the same growth stage [75]. Genetic manipulation, via deletion, of *MDR1, CDR1,* and/or *CDR2* was conducted in order to investigate the role of efflux pumps on triazole resistance during biofilm growth. Hypersensitivity to fluconazole was displayed by these mutants during both planktonic and biofilm growth, but not in biofilms grown for 24 – 48 hrs of the same mutant strain. This suggested that during the mature biofilm stage efflux pumps do not significantly contribute to drug resistance [75].

Mukherjee et al. explored the impact of efflux pumps at three phases of biofilm development including early (0 – 11 hr), intermediate (12 – 30 hr), and mature (31 – 72 hr) time points in comparison to their planktonic counterparts [76]. Single, double, and triple mutants of these three main efflux pump genes showed no increase in susceptibility to fluconazole during the mature biofilm growth phase; however, in the early phase (6 hr) the double and triple efflux pump mutants displayed a modest increase in azole susceptibility as compared to the parent strains [76]. Loss of a single efflux pump had little to no effect in regards to biofilm resistance, even at the earliest time points as seen in the double and triple mutants. This suggested that not only do efflux pumps function in a cooperative manner, but that they also contribute to resistance during the early biofilm developmental stages opposed to the later mature stages. To further investigate this observation, transcriptional analysis of efflux pump genes were conducted on 12 and 48 hr biofilms which found with elevated expression levels of said genes during the earlier less mature phase in comparison to the older mature phase [76]. Additional studies directed at *C. glabrata* and *C. tropicalis* also suggested efflux pumps more than likely contribute to biofilm drug resistance during the early phases of growth [26, 46].

Influence of sterol synthesis

Mukherjee et al. explored the role of plasma membrane changes during biofilm formation, as changes in sterol synthesis have been linked to amphotericin B and ergosterol resistance during planktonic growth, as described above [76-78]. Initial studies examined the levels of sterols during different stages of biofilm development and found that early phase biofilms contained relatively similar levels of ergosterol as that of time matched planktonic cells. However, as biofilm development continued, the ergosterol levels reduced to 50% of the levels measured for planktonic conditions [76]. Furthermore, the sterol profile of intermediate and mature biofilms was different than planktonic cultures of the same age. Specifically, concentrations of ergosterol decreased as the biofilms aged and were replaced by intermediate sterols such as zymosterol,

4,14-dimethylzymosterol, and obtusifoliol [76]. This finding suggested that during the early stages of biofilm development ergosterol is an effective target for drug therapy, but as biofilms continue to grow and mature their dependency upon ergosterol decreases, potentially limiting the efficacy azole and polyene antifungals which target ergosterol.

Global transcriptional analysis also showed increased levels of *ERG11* transcription during the early phase growth stage of *C. albicans* biofilms in comparison to planktonic cells of the same age [22, 79]. A second gene that plays a role in ergosterol biosynthesis, *ERG25,* was found to be upregulated in intermediate and mature biofilms when compared to planktonic cultures of the same age [79]. *ERG25* encodes a putative C-4 sterol methyl oxidase which is believed to play a role in the biosynthesis of ergosterol intermediates via C4-demethylation [79]. The conversion of lanosterol to nonergosterol intermediates, such as eburicol and 14-methyl fecosterol, is a role that this enzyme is theorized to perform in biofilms. Additional studies directly testing the role of membrane changes in the biofilm drug-resistant phenotype have not been reported.

Impact of cell density and quorum sensing

Another trait contributing to the enhanced drug resistance observed during biofilm growth is the relatively large fungal burden [80, 81]. This relationship has also been described for planktonic cells, with higher inoculums producing higher MICs [82, 83]. Based upon these studies, Perumal et al. examined the role of high cell density on antifungal resistance by comparing the susceptibility levels of planktonic yeast cultures with those of intact and disrupted biofilms [80]. Similar to findings in planktonic cells, high cell density cultures displayed higher levels of resistance to azoles when compared to cultures of lower density in the biofilm state.

Quorum sensing is the signaling process linked to control of cell density in the biofilm state. Two key quorum sensing molecules, tyrosol and farnesol, have opposing roles during biofilm development. Tyrosol promotes the hyphal state of biofilms whereas farnesol promotes

the yeast state [84-87]. In addition to the roles of fungal morphogenesis and fungal development, quorum sensing molecules have also been implicated as having potential antifungal activity. Studies in which biofilm cells are co-treated with antifungal drugs (azoles and polyenes) and quorum sensing molecules have demonstrated a synergistic effect [84, 88]. Sharma et al. found that farnesol is able to reduce drug extrusion, of azoles, through the ABC transporters CaCdr1p and CaCdr2p, which may in part explain the synergistic effect observed with a triazole [88].

Contribution of biofilm extracellular matrix

The production of extracellular matrix is a distinctive feature of biofilms [89, 90]. This matrix encompasses the cells within the biofilm and promotes cohesion among the cells within as well as adhesion to surfaces [91, 92]. Furthermore, the matrices of most microbes have been found capable of absorption numerous environmental components. For example, the surrounding matrix has been shown to retain water and nutrients [91]. However, the most studied aspect of the extracellular matrix is its ability to create a protective physical barrier between biofilm cells and its surrounding environment. This proves to be vital to the organism's survival when growing on the surface of an indwelling device by providing protection from pharmacological agents and the hosts innate immune system [93, 94].

The Douglas group performed the first studies on fungal biofilms using *C. albicans* to investigate the potential role of the extracellular matrix on drug resistance and the importance of environmental conditions on overall matrix production [16]. Since this initial study a number of labs have investigated the matrix composition and role in drug resistance in fungal biofilms. A recent detailed analysis of the *C. albicans* matrix identified each of the four macromolecules classes. Relative composition of the matrix based upon dry weight included 55% protein, 25% carbohydrate, 15% lipid, and 5% nucleic acid [90]. Proteomic analysis revealed 458 distinct entries which included protein classes involved in carbohydrate and amino acid metabolism [95-97]. Analysis of the carbohydrate fraction revealed the presence of three polysaccharides, β-1,3

glucan, β-1,6 glucan, and α-1,6 mannan with α-1,2 linked branches. Identified lipids included neutral and polar glycerolipids in addition to a small portion of sphingolipids [90]. The nucleic acids found consisted mainly of non-coding sequences of DNA [90].

Nett et al. examined the relationship between biofilm resistance and matrix by taking purified matrix material from biofilms and adding it to planktonic cells prior to antifungal susceptibility testing [98]. The addition of matrix rendered the planktonic cells resistant to antifungal drug to a degree that was similar to that seen in mature biofilms. This suggested that matrix material is interacting or sequestering antifungals preventing them from reaching their intended targets. Using radiolabeled fluconazole, they found that cultures containing matrix were able to sequester the azole drug from their intended targets, consistent with this theory. Genetic studies seeking the component responsible for this process implicated the carbohydrate β-1,3 glucan [98, 99]. This drug sequestration phenomenon has been found to relatively non-specific with regard to the antifungal drug as resistance linked to matrix protection has been shown important for triazoles, polyenes, flucytosine, and echinocandins [68, 100]. Studies conducted on biofilms formed by other *Candida* spp., namely *C. glabrata, C. parapsilosis,* and *C. tropicalis* also displayed this matrix antifungal mechanism as well as affinity towards β-1,3 glucans role in biofilm resistance [68, 101-104].

The first investigation into the genetic control of production of matrix β-1,3 glucan have shown that the β-1,3 glucan synthase Fks1p is required for production of this polysaccharide [68]. Subsequent delivery to the matrix has been found to be regulated in a complementary fashion by three glucan modifier proteins Bgl2p, Phr1p, and Xog1p [68, 99, 105]. Additionally, Nobile et al. identified a transcription factor, Zap1p, that is critical for control of matrix production [106]. Zap1p was found to negatively regulate production of β-1,3 glucan by hydrolysis of matrix carbohydrates through the control of two glucoamylases *GCA1* and *GCA2*. It is also speculated to influence matrix production through quorum sensing pathways based upon its control over alcohol dehydrogenases ADH5, CSH1, and LFD6 enzymes [106].

Recent work has also shown that the drug resistance phenotype is not solely due to β-1,3 glucan. In fact, each of the three polysaccharides identified in the carbohydrate fraction of the extracellular matrix were found to cooperate as a mannan-glucan complex to facilitate drug resistance in *C. albicans* biofilm. Mitchell et al. further investigated the genetic implications of the loss of genes which regulate production and modification of mannan and glucan within the extracellular matrix. They found that a subset of mutants had reduced levels of all three polysaccharides, lower levels of total matrix, and increased susceptibility towards antifungals. The β-1,3 glucan synthase gene (*FKS1),* two genes regulating matrix β-1,6 glucan (*BIG1* and *KRE5*), and seven genes regulating matrix mannan (*ALG11, MNN4-4, MNN9, PMR1, VAN1,* and *VRG4*) all prominently displayed the aforementioned phenotype. Surprisingly though when biofilms containing mutants from the various pathways were mixed and grown with one another, matrix structure and functionality was restored [89]. This observation in addition to studies pharmacologically manipulating the matrix components demonstrated that the matrix constituents were assembled after export from the cell.

Extracellular DNA (eDNA) has also been found to impact the drug resistance phenotype seen in biofilms. This finding is based upon investigations that showing an increase in susceptibility of *C. albicans* biofilms to two classes of antifungals (echinocandins and polyenes) when co-treated with DNase [107, 108]. It is still unclear how the eDNA is mechanistically contributing to drug resistance [90].

Presence of persister cells

Persister cells are a subpopulation of dormant cells found within biofilms which exhibit a higher tolerance to multiple drug classes [109, 110]. They are defined as the population of microbes remaining after antimicrobial exposure and were first described for amphotericin B. The cells are capable of reconstituting new biofilms containing the same percentage of resistant persister cells (0.01 – 0.02 %). These characteristics suggest they serve as the primary

component of recurring fungal infections [111]. Although the underlying mechanism for the production of persister cells is still unclear, Sun et al. showed they rapidly emerged upon surface adhesion, reaching a state of saturation 1by 2 hours [111]. The genetic basis underlying the persister cell lifestyle remains unclear.

Conclusion

The ability of *Candida* spp. to transition into a biofilm lifestyle allows this organism to thrive in even the healthy human host. This survival is attributed to the intrinsically high levels tolerance of conventional antifungal therapies and the host's innate immune response. The process appears multifactorial with resistance mechanisms varying by the phase of biofilm development.

Efflux pumps play an important role during the early phase of development. This mechanism of resistance is most prevalent during the stage at which the planktonic cells begin to adhere to a surface and transition into a biofilm state. As the biofilm matures the role played by these efflux pumps diminishes and instead biofilm-specific mechanisms are predominant. The earliest biofilm specific mechanism is the production of persister cells, which are phenotypic variants of the parent cells that are resistant to antifungals and provide a mechanism for regrowth of the organism after high levels of drug exposure. As biofilms continue to mature an extracellular matrix is produced which contains a multitude of components that work together to provide multi-layers of protection to the cells which now reside within this material. Carbohydrates of the matrix, specifically β-1,3 glucan, β-1,6 glucan, and α-1,6 mannan with α-1,2 linked branches, sequester a variety of antifungals providing drug resistance to mature biofilms. A secondary component, extracellular DNA, also promotes drug resistance to popular antifungals further contributing to this phenotype.

Biofilms contain many overlapping and redundant mechanisms which allow them to survive in hostile environments and evade drug treatments resulting in poor prognosis for patients. Compositional, structural, and biochemical analysis of biofilms and their components have

allowed us to better understand this complex organism and potentially develop innovative therapies to better combat infections. However, there are still many unknowns, such as the role of host factors and their interaction with matrix components during infection or do the components of duel-species biofilms interact with one another to further enhance drug resistance? Additional investigations addressing questions such as these are still necessary in order to fully comprehend the nature and full potential of fungal biofilms.

References

1. Ruhnke, M. and G. Maschmeyer, *Management of mycoses in patients with hematologic disease and cancer -- review of the literature.* Eur J Med Res, 2002. **7**(5): p. 227-35.
2. Meiller, T.F., et al., *A novel immune evasion strategy of candida albicans: proteolytic cleavage of a salivary antimicrobial peptide.* PLoS One, 2009. **4**(4): p. e5039.
3. Schulze, J. and U. Sonnenborn, *Yeasts in the gut: from commensals to infectious agents.* Dtsch Arztebl Int, 2009. **106**(51-52): p. 837-42.
4. Sobel, J.D., *Vaginitis.* N Engl J Med, 1997. **337**(26): p. 1896-903.
5. Kabir, M.A., M.A. Hussain, and Z. Ahmad, *Candida albicans: A Model Organism for Studying Fungal Pathogens.* ISRN Microbiol, 2012. **2012**: p. 538694.
6. Rosenbach, A., et al., *Adaptations of Candida albicans for growth in the mammalian intestinal tract.* Eukaryot Cell, 2010. **9**(7): p. 1075-86.
7. Pfaller, M.A., et al., *Variation in Candida spp. distribution and antifungal resistance rates among bloodstream infection isolates by patient age: report from the SENTRY Antimicrobial Surveillance Program (2008-2009).* Diagn Microbiol Infect Dis, 2010. **68**(3): p. 278-83.
8. Pfaller, M.A. and D.J. Diekema, *Epidemiology of invasive candidiasis: a persistent public health problem.* Clin Microbiol Rev, 2007. **20**(1): p. 133-63.
9. Pfaller, M.A., et al., *Results from the ARTEMIS DISK Global Antifungal Surveillance Study: a 6.5-year analysis of susceptibilities of Candida and other yeast species to fluconazole and voriconazole by standardized disk diffusion testing.* J Clin Microbiol, 2005. **43**(12): p. 5848-59.
10. Nobile, C.J. and A.D. Johnson, *Candida albicans Biofilms and Human Disease.* Annu Rev Microbiol, 2015. **69**: p. 71-92.
11. Kolter, R. and E.P. Greenberg, *Microbial sciences: the superficial life of microbes.* Nature, 2006. **441**(7091): p. 300-2.
12. Roder, H.L., S.J. Sorensen, and M. Burmolle, *Studying Bacterial Multispecies Biofilms: Where to Start?* Trends Microbiol, 2016.
13. Mah, T.F., *Biofilm-specific antibiotic resistance.* Future Microbiol, 2012. **7**(9): p. 1061-72.
14. Romling, U. and C. Balsalobre, *Biofilm infections, their resilience to therapy and innovative treatment strategies.* J Intern Med, 2012. **272**(6): p. 541-61.
15. Chandra, J., et al., *Biofilm formation by the fungal pathogen Candida albicans: development, architecture, and drug resistance.* J Bacteriol, 2001. **183**(18): p. 5385-94.
16. Douglas, L.J., *Candida biofilms and their role in infection.* Trends in Microbiology, 2003. **11**(1): p. 30-36.
17. Donlan, R.M. and J.W. Costerton, *Biofilms: survival mechanisms of clinically relevant microorganisms.* Clin Microbiol Rev, 2002. **15**(2): p. 167-93.
18. Ramage, G., et al., *Candida biofilms: an update.* Eukaryot Cell, 2005. **4**(4): p. 633-8.
19. Kojic, E.M. and R.O. Darouiche, *Candida Infections of Medical Devices.* Clinical Microbiology Reviews, 2004. **17**(2): p. 255-267.

20. Mayer, F.L., D. Wilson, and B. Hube, *Candida albicans pathogenicity mechanisms.* Virulence, 2013. **4**(2): p. 119-28.
21. Al-Fattani, M.A. and L.J. Douglas, *Penetration of Candida biofilms by antifungal agents.* Antimicrob Agents Chemother, 2004. **48**(9): p. 3291-7.
22. Finkel, J.S. and A.P. Mitchell, *Genetic control of Candida albicans biofilm development.* Nat Rev Microbiol, 2011. **9**(2): p. 109-18.
23. Tobudic, S., et al., *Antifungal susceptibility of Candida albicans in biofilms.* Mycoses, 2012. **55**(3): p. 199-204.
24. White, T.C., K.A. Marr, and R.A. Bowden, *Clinical, cellular, and molecular factors that contribute to antifungal drug resistance.* Clin Microbiol Rev, 1998. **11**(2): p. 382-402.
25. Marie, C. and T.C. White, *Genetic Basis of Antifungal Drug Resistance.* Curr Fungal Infect Rep, 2009. **3**(3): p. 163-169.
26. Ramage, G., et al., *Fungal biofilm resistance.* Int J Microbiol, 2012. **2012**: p. 528521.
27. Kelly, S.L., et al., *Mode of action and resistance to azole antifungals associated with the formation of 14 alpha-methylergosta-8,24(28)-dien-3 beta,6 alpha-diol.* Biochem Biophys Res Commun, 1995. **207**(3): p. 910-5.
28. Lupetti, A., et al., *Molecular basis of resistance to azole antifungals.* Trends Mol Med, 2002. **8**(2): p. 76-81.
29. Kelly, S.L., et al., *Resistance to fluconazole and cross-resistance to amphotericin B in Candida albicans from AIDS patients caused by defective sterol delta5,6-desaturation.* FEBS Lett, 1997. **400**(1): p. 80-2.
30. Shimokawa, O. and H. Nakayama, *Increased sensitivity of Candida albicans cells accumulating 14 alpha-methylated sterols to active oxygen: possible relevance to in vivo efficacies of azole antifungal agents.* Antimicrob Agents Chemother, 1992. **36**(8): p. 1626-9.
31. Ostrosky-Zeichner, L., et al., *An insight into the antifungal pipeline: selected new molecules and beyond.* Nat Rev Drug Discov, 2010. **9**(9): p. 719-27.
32. Cleveland, A.A., et al., *Changes in incidence and antifungal drug resistance in candidemia: results from population-based laboratory surveillance in Atlanta and Baltimore, 2008-2011.* Clin Infect Dis, 2012. **55**(10): p. 1352-61.
33. Law, D., et al., *High prevalence of antifungal resistance in Candida spp. from patients with AIDS.* J Antimicrob Chemother, 1994. **34**(5): p. 659-68.
34. White, T.C., *The presence of an R467K amino acid substitution and loss of allelic variation correlate with an azole-resistant lanosterol 14alpha demethylase in Candida albicans.* Antimicrob Agents Chemother, 1997. **41**(7): p. 1488-94.
35. Lamb, D.C., et al., *The mutation T315A in Candida albicans sterol 14alpha-demethylase causes reduced enzyme activity and fluconazole resistance through reduced affinity.* J Biol Chem, 1997. **272**(9): p. 5682-8.
36. Sanglard, D., et al., *Amino acid substitutions in the cytochrome P-450 lanosterol 14alpha-demethylase (CYP51A1) from azole-resistant Candida albicans clinical isolates contribute to resistance to azole antifungal agents.* Antimicrob Agents Chemother, 1998. **42**(2): p. 241-53.

37. Sanglard, D., et al., *Mechanisms of resistance to azole antifungal agents in Candida albicans isolates from AIDS patients involve specific multidrug transporters.* Antimicrob Agents Chemother, 1995. **39**(11): p. 2378-86.
38. Marichal, P., et al., *Contribution of mutations in the cytochrome P450 14alpha-demethylase (Erg11p, Cyp51p) to azole resistance in Candida albicans.* Microbiology, 1999. **145 (Pt 10)**: p. 2701-13.
39. Albertson, G.D., et al., *Multiple efflux mechanisms are involved in Candida albicans fluconazole resistance.* Antimicrob Agents Chemother, 1996. **40**(12): p. 2835-41.
40. White, T.C., *Increased mRNA levels of ERG16, CDR, and MDR1 correlate with increases in azole resistance in Candida albicans isolates from a patient infected with human immunodeficiency virus.* Antimicrob Agents Chemother, 1997. **41**(7): p. 1482-7.
41. vanden Bossche, H., et al., *Characterization of an azole-resistant Candida glabrata isolate.* Antimicrob Agents Chemother, 1992. **36**(12): p. 2602-10.
42. Coste, A., et al., *Genotypic evolution of azole resistance mechanisms in sequential Candida albicans isolates.* Eukaryot Cell, 2007. **6**(10): p. 1889-904.
43. Silva, A.P., et al., *Transcriptional profiling of azole-resistant Candida parapsilosis strains.* Antimicrob Agents Chemother, 2011. **55**(7): p. 3546-56.
44. Vandeputte, P., et al., *Mechanisms of azole resistance in a clinical isolate of Candida tropicalis.* Antimicrob Agents Chemother, 2005. **49**(11): p. 4608-15.
45. Cannon, R.D., et al., *Efflux-mediated antifungal drug resistance.* Clin Microbiol Rev, 2009. **22**(2): p. 291-321, Table of Contents.
46. Bizerra, F.C., et al., *Characteristics of biofilm formation by Candida tropicalis and antifungal resistance.* FEMS Yeast Res, 2008. **8**(3): p. 442-50.
47. Ramage, G., et al., *Standardized method for in vitro antifungal susceptibility testing of Candida albicans biofilms.* Antimicrob Agents Chemother, 2001. **45**(9): p. 2475-9.
48. Lamfon, H., et al., *Susceptibility of Candida albicans biofilms grown in a constant depth film fermentor to chlorhexidine, fluconazole and miconazole: a longitudinal study.* J Antimicrob Chemother, 2004. **53**(2): p. 383-5.
49. Baginski, M. and J. Czub, *Amphotericin B and its new derivatives - mode of action.* Curr Drug Metab, 2009. **10**(5): p. 459-69.
50. Gray, K.C., et al., *Amphotericin primarily kills yeast by simply binding ergosterol.* Proc Natl Acad Sci U S A, 2012. **109**(7): p. 2234-9.
51. Vandeputte, P., et al., *Reduced susceptibility to polyenes associated with a missense mutation in the ERG6 gene in a clinical isolate of Candida glabrata with pseudohyphal growth.* Antimicrob Agents Chemother, 2007. **51**(3): p. 982-90.
52. Kelly, S.L., et al., *Resistance to fluconazole and amphotericin in Candida albicans from AIDS patients.* Lancet, 1996. **348**(9040): p. 1523-4.
53. Tobudic, S., et al., *In vitro activity of antifungal combinations against Candida albicans biofilms.* J Antimicrob Chemother, 2010. **65**(2): p. 271-4.
54. Denning, D.W., *Echinocandin antifungal drugs.* Lancet, 2003. **362**(9390): p. 1142-51.
55. Perlin, D.S., *Mechanisms of echinocandin antifungal drug resistance.* Ann N Y Acad Sci, 2015. **1354**: p. 1-11.

56. Shapiro, R.S., N. Robbins, and L.E. Cowen, *Regulatory circuitry governing fungal development, drug resistance, and disease.* Microbiol Mol Biol Rev, 2011. **75**(2): p. 213-67.
57. Chaffin, W.L., et al., *Cell wall and secreted proteins of Candida albicans: identification, function, and expression.* Microbiol Mol Biol Rev, 1998. **62**(1): p. 130-80.
58. Perlin, D.S., *Resistance to echinocandin-class antifungal drugs.* Drug Resist Updat, 2007. **10**(3): p. 121-30.
59. Hernandez, S., Lopez-Ribot, J. L., Najvar, L. K., McCarthy, D. I., Bocanegra, R., and J. R. Graybill, *Caspofungin resistance in Candida albicans: correlating clinical outcome with laboratory susceptibility testing of three isogenic isolates serially obtained from a patient with progressive Candida esophagitis.* Antimicrobial agents and chemotherapy, 2004. **48**(4): p. 1382 - 1383.
60. Balashov, S.V., S. Park, and D.S. Perlin, *Assessing resistance to the echinocandin antifungal drug caspofungin in Candida albicans by profiling mutations in FKS1.* Antimicrob Agents Chemother, 2006. **50**(6): p. 2058-63.
61. Desnos-Ollivier, M., et al., *Mutations in the fks1 gene in Candida albicans, C-tropicalis, and C-krusei correlate with elevated caspofungin MICs uncovered in AM3 medium using the method of the European Committee on Antibiotic Susceptibility Testing.* Antimicrobial Agents and Chemotherapy, 2008. **52**(9): p. 3092-3098.
62. Laverdiere, M., et al., *Progressive loss of echinocandin activity following prolonged use for treatment of Candida albicans oesophagitis.* Journal of Antimicrobial Chemotherapy, 2006. **57**(4): p. 705-708.
63. Park, S., et al., *Specific substitutions in the echinocandin target Fks1p account for reduced susceptibility of rare laboratory and clinical Candida sp. isolates.* Antimicrob Agents Chemother, 2005. **49**(8): p. 3264-73.
64. Perlin, D.S., *Echinocandin Resistance in Candida.* Clin Infect Dis, 2015. **61 Suppl 6**: p. S612-7.
65. Garcia-Effron, G., S. Park, and D.S. Perlin, *Correlating echinocandin MIC and kinetic inhibition of fks1 mutant glucan synthases for Candida albicans: implications for interpretive breakpoints.* Antimicrob Agents Chemother, 2009. **53**(1): p. 112-22.
66. Johnson, M.E., S.K. Katiyar, and T.D. Edlind, *New Fks hot spot for acquired echinocandin resistance in Saccharomyces cerevisiae and its contribution to intrinsic resistance of Scedosporium species.* Antimicrob Agents Chemother, 2011. **55**(8): p. 3774-81.
67. Katiyar, S.K. and T.D. Edlind, *Role for Fks1 in the intrinsic echinocandin resistance of Fusarium solani as evidenced by hybrid expression in Saccharomyces cerevisiae.* Antimicrob Agents Chemother, 2009. **53**(5): p. 1772-8.
68. Nett, J.E., et al., *Role of Fks1p and matrix glucan in Candida albicans biofilm resistance to an echinocandin, pyrimidine, and polyene.* Antimicrob Agents Chemother, 2010. **54**(8): p. 3505-8.

69. White, T.C., K.A. Marr, and R.A. Bowden, *Clinical, cellular, and molecular factors that contribute to antifungal drug resistance.* Clinical Microbiology Reviews, 1998. **11**(2): p. 382-+.
70. Hope, W., Tabernero, L, Denning, DW, and MJ Anderson, *Molecular Mechanisms of Primary Resistance to Flucytosice in Candida albicans.* Antimicrobial agents and chemotherapy, 2004. **48**(11): p. 4377 - 4386.
71. Pappas, P.G., et al., *Clinical practice guidelines for the management of candidiasis: 2009 update by the Infectious Diseases Society of America.* Clin Infect Dis, 2009. **48**(5): p. 503-35.
72. Morschhauser, J., *The genetic basis of fluconazole resistance development in Candida albicans.* Biochim Biophys Acta, 2002. **1587**(2-3): p. 240-8.
73. Stevens, D.A., et al., *Escape of Candida from caspofungin inhibition at concentrations above the MIC (Paradoxical effect) accomplished by increased cell wall chitin; Evidence for beta-1,6-glucan synthesis inhibition by caspofungin.* Antimicrobial Agents and Chemotherapy, 2006. **50**(9): p. 3160-3161.
74. Bizerra, F.C., et al., *Changes in cell wall synthesis and ultrastructure during paradoxical growth effect of caspofungin on four different Candida species.* Antimicrob Agents Chemother, 2011. **55**(1): p. 302-10.
75. Ramage, G., et al., *Investigation of multidrug efflux pumps in relation to fluconazole resistance in Candida albicans biofilms.* J Antimicrob Chemother, 2002. **49**(6): p. 973-80.
76. Mukherjee, P.K., et al., *Mechanism of fluconazole resistance in Candida albicans biofilms: phase-specific role of efflux pumps and membrane sterols.* Infect Immun, 2003. **71**(8): p. 4333-40.
77. Ghannoum, M.A. and L.B. Rice, *Antifungal agents: mode of action, mechanisms of resistance, and correlation of these mechanisms with bacterial resistance.* Clin Microbiol Rev, 1999. **12**(4): p. 501-17.
78. Kontoyiannis, D.P., *Efflux-mediated resistance to fluconazole could be modulated by sterol homeostasis in Saccharomyces cerevisiae.* J Antimicrob Chemother, 2000. **46**(2): p. 199-203.
79. Nett, J.E., et al., *Time course global gene expression analysis of an in vivo Candida biofilm.* J Infect Dis, 2009. **200**(2): p. 307-13.
80. Perumal, P., S. Mekala, and W.L. Chaffin, *Role for cell density in antifungal drug resistance in Candida albicans biofilms.* Antimicrob Agents Chemother, 2007. **51**(7): p. 2454-63.
81. Seneviratne, C.J., et al., *Cell density and cell aging as factors modulating antifungal resistance of Candida albicans biofilms.* Antimicrobial Agents and Chemotherapy, 2008. **52**(9): p. 3259-3266.
82. Nguyen, M.H. and C.Y. Yu, *Influence of incubation time, inoculum size, and glucose concentrations on spectrophotometric endpoint determinations for amphotericin B, fluconazole, and itraconazole.* J Clin Microbiol, 1999. **37**(1): p. 141-5.
83. Riesselman, M.H., K.C. Hazen, and J.E. Cutler, *Determination of antifungal MICs by a rapid susceptibility assay.* J Clin Microbiol, 2000. **38**(1): p. 333-40.

84. Wongsuk, T., P. Pumeesat, and N. Luplertlop, *Fungal quorum sensing molecules: Role in fungal morphogenesis and pathogenicity.* J Basic Microbiol, 2016. **56**(5): p. 440-7.
85. - Hornby J. M., J.E.C., Lisec A. D., Tasto J. J., Jahnke B., Shoemaker R., Dussault P., and K. W. Nickerson, *Quorum sensing in the dimorphic fungus Candida albicans is mediated by farnesol.* Applied and Environmental Microbiology, 2001. **67**: p. 2982 - 2992.
86. Ramage, G., et al., *Inhibition of Candida albicans biofilm formation by farnesol, a quorum-sensing molecule.* Appl Environ Microbiol, 2002. **68**(11): p. 5459-63.
87. Lindsay, A.K., et al., *Farnesol and cyclic AMP signaling effects on the hypha-to-yeast transition in Candida albicans.* Eukaryot Cell, 2012. **11**(10): p. 1219-25.
88. Sharma, M. and R. Prasad, *The quorum-sensing molecule farnesol is a modulator of drug efflux mediated by ABC multidrug transporters and synergizes with drugs in Candida albicans.* Antimicrob Agents Chemother, 2011. **55**(10): p. 4834-43.
89. Mitchell, K.F., et al., *Community participation in biofilm matrix assembly and function.* Proc Natl Acad Sci U S A, 2015. **112**(13): p. 4092-7.
90. Zarnowski, R., et al., *Novel entries in a fungal biofilm matrix encyclopedia.* MBio, 2014. **5**(4): p. e01333-14.
91. Flemming, H.C. and J. Wingender, *The biofilm matrix.* Nat Rev Microbiol, 2010. **8**(9): p. 623-33.
92. O'Toole, G.A., *To build a biofilm.* J Bacteriol, 2003. **185**(9): p. 2687-9.
93. Costerton, J.W., P.S. Stewart, and E.P. Greenberg, *Bacterial biofilms: a common cause of persistent infections.* Science, 1999. **284**(5418): p. 1318-22.
94. Donlan, R.M., *Biofilm formation: a clinically relevant microbiological process.* Clin Infect Dis, 2001. **33**(8): p. 1387-92.
95. Al-Fattani, M.A. and L.J. Douglas, *Biofilm matrix of Candida albicans and Candida tropicalis: chemical composition and role in drug resistance.* J Med Microbiol, 2006. **55**(Pt 8): p. 999-1008.
96. Faria-Oliveira, F., et al., *Methodologies to generate, extract, purify and fractionate yeast ECM for analytical use in proteomics and glycomics.* BMC Microbiol, 2014. **14**: p. 244.
97. Thomas, D.P., S.P. Bachmann, and J.L. Lopez-Ribot, *Proteomics for the analysis of the Candida albicans biofilm lifestyle.* Proteomics, 2006. **6**(21): p. 5795-804.
98. Nett, J., et al., *Putative role of beta-1,3 glucans in Candida albicans biofilm resistance.* Antimicrob Agents Chemother, 2007. **51**(2): p. 510-20.
99. Nett, J.E., et al., *Genetic basis of Candida biofilm resistance due to drug-sequestering matrix glucan.* J Infect Dis, 2010. **202**(1): p. 171-5.
100. Vediyappan, G., T. Rossignol, and C. d'Enfert, *Interaction of Candida albicans biofilms with antifungals: transcriptional response and binding of antifungals to beta-glucans.* Antimicrob Agents Chemother, 2010. **54**(5): p. 2096-111.
101. Kuhn, D.M., et al., *Antifungal susceptibility of Candida biofilms: unique efficacy of amphotericin B lipid formulations and echinocandins.* Antimicrob Agents Chemother, 2002. **46**(6): p. 1773-80.

102. Mitchell, K.F., et al., *Role of matrix beta-1,3 glucan in antifungal resistance of non-albicans Candida biofilms.* Antimicrob Agents Chemother, 2013. **57**(4): p. 1918-20.
103. Yi, S., et al., *Alternative mating type configurations (a/alpha versus a/a or alpha/alpha) of Candida albicans result in alternative biofilms regulated by different pathways.* PLoS Biol, 2011. **9**(8): p. e1001117.
104. Fernandes, T., S. Silva, and M. Henriques, *Candida tropicalis biofilm's matrix--involvement on its resistance to amphotericin B.* Diagn Microbiol Infect Dis, 2015. **83**(2): p. 165-9.
105. Taff, H.T., et al., *A Candida biofilm-induced pathway for matrix glucan delivery: implications for drug resistance.* PLoS Pathog, 2012. **8**(8): p. e1002848.
106. Nobile, C.J., et al., *Biofilm matrix regulation by Candida albicans Zap1.* PLoS Biol, 2009. **7**(6): p. e1000133.
107. Martins, M., et al., *Presence of extracellular DNA in the Candida albicans biofilm matrix and its contribution to biofilms.* Mycopathologia, 2010. **169**(5): p. 323-31.
108. Martins, M., et al., *Addition of DNase improves the in vitro activity of antifungal drugs against Candida albicans biofilms.* Mycoses, 2012. **55**(1): p. 80-5.
109. LaFleur, M.D., C.A. Kumamoto, and K. Lewis, *Candida albicans biofilms produce antifungal-tolerant persister cells.* Antimicrob Agents Chemother, 2006. **50**(11): p. 3839-46.
110. Lewis, K., *Multidrug tolerance of biofilms and persister cells.* Curr Top Microbiol Immunol, 2008. **322**: p. 107-31.
111. Sun, J., et al., *Candida albicans Amphotericin B-Tolerant Persister Formation is Closely Related to Surface Adhesion.* Mycopathologia, 2016. **181**(1-2): p. 41-9.
112. Taff, H.T., et al., *Mechanisms of Candida biofilm drug resistance.* Future Microbiol, 2013. **8**(10): p. 1325-37.

Figure 1 *Candida* biofilm resistance mechanisms. **a** Resistance mechanisms at the biofilm community level. **b** Resistance mechanisms at the cellular level [112]

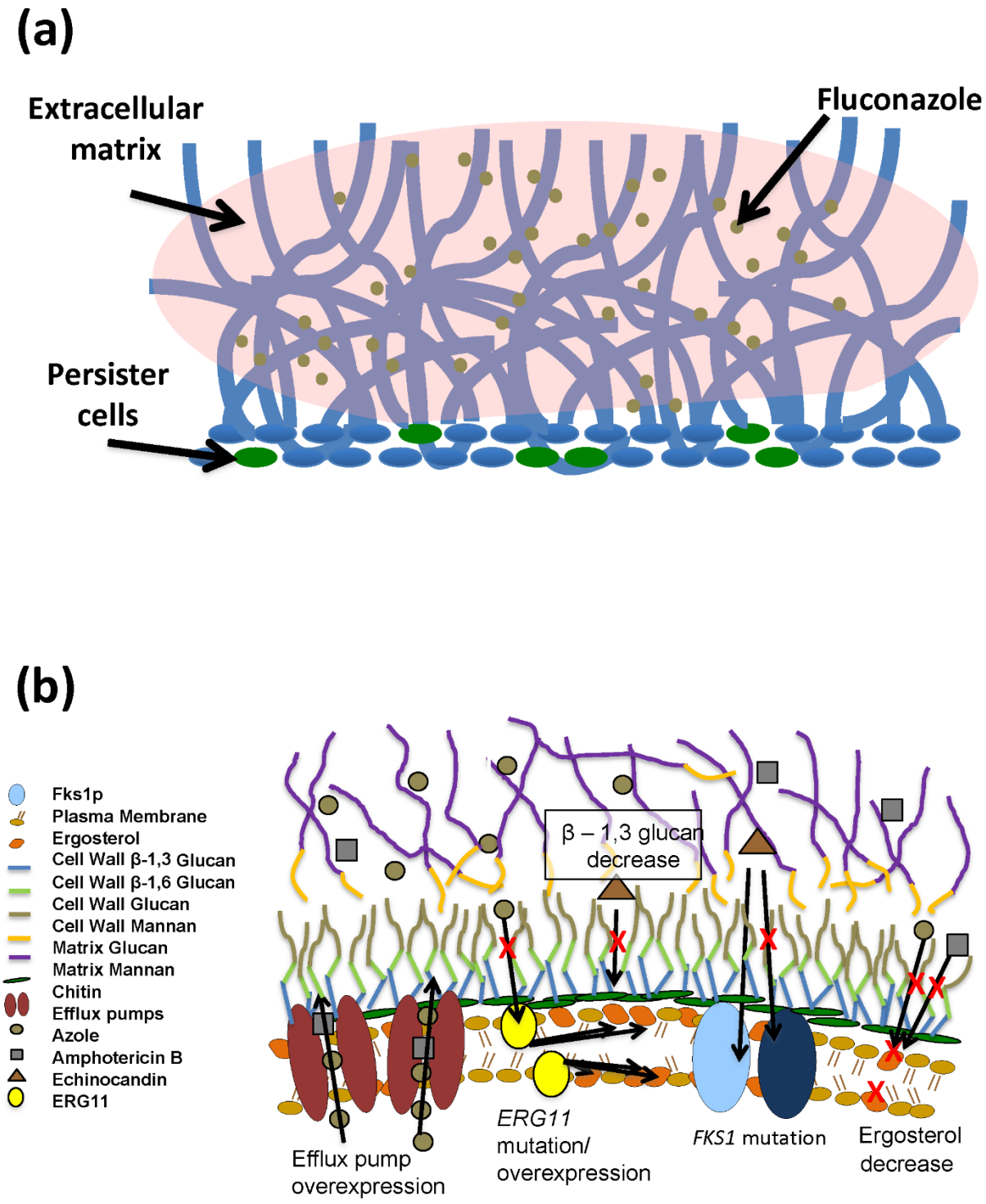

Chapter 2

Conservation and Divergence in the *Candida* species Biofilm Matrix Mannan-Glucan Complex Structure, Function, and Genetic Control

The contents of this section were published:

Eddie Dominguez, Robert Zarnowski, Hiram Sanchez, Antonio S. Covell[a], William M. Westler, Parastoo Azadi, Jeniel Nett, Aaron P. Mitchell, and David R. Andes. Conservation and Divergence in the *Candida* species Biofilm Matrix Mannan-Glucan Complex Structure, Function, and Genetic Control. MBio. 2018 Apr 3; 9(2):00451-18. PMCID: PMC5885036.

E. Dominguez performed and analyzed susceptibility testing, biofilm growth assays, and created new mutant strains. R. Zarnowski performed gas chromatography analyses, matrix co-purification, and created new mutant strains. H. Sanchez performed fluconazole sequestration assays and SEM. A. Covelli grew biofilms in roller bottles. W. Westler and P. Azadi are collaborators from the University of Georgia, Athens, and conducted and analyzed NMR data. J. Nett edited the manuscript. A. Mitchell is a collaborator from Carnegie Mellon University, Pittsburgh, interpreted data and wrote the manuscript. D. Andes supervised the study, interpreted data, and wrote the manuscript.

ABSTRACT

Candida biofilms resist the effects of available antifungal therapies. Prior studies with *Candida albicans* biofilms show that an extracellular matrix mannan-glucan complex (MGCx) contributes to antifungal sequestration, leading to drug resistance. Here we implement biochemical, pharmacologic, and genetic approaches to explore a similar mechanism of resistance for the three most common clinically encountered non-*albicans Candida* species (NAC). Our findings reveal that each *Candida* spp. biofilm synthesizes a mannan-glucan complex, and that the antifungal-protective function of this complex is conserved. Structural similarities extended primarily to the polysaccharide backbone (α1,6-mannan and β1,6 glucan). Surprisingly, biochemical analysis uncovered stark differences in the branching side chains of the MGCx among the species. Consistent with the structural analysis, similarities in the genetic control of MGCx production for each *Candida* spp. also appeared limited to the synthesis of the polysaccharide backbone. Each species appear to employ a unique subset of modification enzymes for MGCx synthesis, likely accounting for the observed side chain diversity. Our results argue for the conservation of matrix function among *Candida* spp. While biogenesis is preserved at the level of the mannan-glucan complex backbone, divergence emerges for construction of branching side chains. Thus, the MGCx backbone represents an ideal drug target for effective pan-*Candida* species biofilm therapy.

Importance

Candida species, the most common fungal pathogens, frequently grow as a biofilm. These adherent communities tolerate extremely high concentrations of antifungals, due in large part, to a protective extracellular matrix. The present studies define the structural, functional, and genetic similarities and differences in the biofilm matrix from the four most common *Candida* species. Each species synthesizes an extracellular mannan-glucan complex (MGCx) which contributes to sequestration of antifungal drug, shielding the fungus from this external assault. Synthesis of a

common polysaccharide backbone appears conserved. However, subtle structural differences in the branching side chains likely rely upon unique modification enzymes, which are species-specific. Our findings identify MGCx backbone synthesis as a potential pan-*Candida* biofilm therapeutic target.

INTRODUCTION

Candida species are among the most common causes of fungal infection worldwide (1). More than a hundred *Candida* species have been identified, but fewer than two dozen have been implicated in human disease. *Candida albicans* is the predominant clinical species, however, other *Candida* species are increasingly encountered (1-5). Four species, *C. albicans, C. tropicalis, C. parapsilosis,* and *C. glabrata,* account for nearly 95% of all infections. While the epidemiology of infection varies among these species, their disease manifestations are similar. Likewise, their general virulence attributes appear mostly conserved (6-17). Among these factors, the ability to live in the biofilm state is arguably responsible for a majority of invasive infections (18-24).

In a biofilm, microbes are protected from antimicrobials by an organism-produced extracellular matrix (25-30). Hence, biofilm-related infections are challenging to cure (18, 31-33). The structure, function, and genetic control of this process was recently defined for *C. albicans (34-41).* Biochemical investigation identified a unique mannan-glucan complex composed of three polysaccharide building blocks, α 1,6 mannan, β1,6 and β1,3 glucans(40). These polysaccharides assemble extracellularly to form a complex capable of impeding antifungal delivery through drug sequestration (39, 42). While recent studies have shed light on this process in *C. albicans* biofilms, only few studies have begun to explore matrix production and function of other *Candida* spp, and there is a paucity of detailed structure-function knowledge for these emerging pathogens (27, 40, 43-47). Furthermore, the genetic pathways linked to matrix production or function in non-albicans *Candida* species remains unexplored. Elucidation of matrix biogenesis mechanisms in these emergent species thus addresses an intriguing biological question as well as a critical medical need.

Here, we present evidence of a conserved matrix mannan and glucan complex backbone (MGCx) which contributes to profound drug resistance exhibited by the four most prevalent *Candida* species. We show that select matrix synthesis *C. albicans* orthologs play a similar role

across *Candida* species to synthesize a common polysaccharide backbone. However, structural and molecular divergence in matrix assembly is suggested by subtle differences in matrix branching and absence of the involvement of matrix modification enzyme orthologs. Our findings argue that broad-spectrum *Candida* biofilm drug discovery should target the level of MGCx backbone synthesis as opposed to side chain synthesis.

RESULTS

Comparison of *Candida* spp. biofilm growth and architecture.

We determined basic parameters of biofilm development for three non-albicans *Candida* species: *C. parapsilosis, C. tropicalis,* and the more distantly related *C. glabrata*. We also included wild type *C. albicans* as a standard for comparison. Biofilm formation begins with adherence of cells to the substrate, and we found marked differences among the species in this property (Fig 1A). Despite a similar inoculum, the yield of adherent cells was ~5-fold lower for *C. parapsilosis* and *C. glabrata* than that measured for either *C. albicans* or *C. tropicalis*. Biofilm maturation over the next 24 hours erased these differences in cell number estimates (Fig 1B), thus indicating that all four species reach a similar sessile equilibrium under in vitro growth conditions. Scanning electron microscopy of mature biofilms revealed that each of the species, with the exception of *C. glabrata,* demonstrated a preponderance of filamentous or elongated cell growth (Fig 1C). In addition, abundant extracellular matrix material encased the cells within each biofilm (marked by white arrows). We extended our comparison to examine in vivo biofilm formed in the lumen of a rat vascular catheter. Basic architecture in this model recapitulated the biofilm characteristics observed in vitro: filamentous cells were present in *C. albicans*, *C. parapsilosis* and *C. tropicalis* biofilms, and extracellular matrix material was abundant. In fact, extracellular matrix appeared more pronounced in vivo than in vitro, likely due to the contribution of host components (48). These results indicate that mature biofilms of the three non-albicans *Candida* species resemble those of *C. albicans* in terms of cellular content, matrix accumulation, and, for *C. parapsilosis* and *C. tropicalis*, presence of filamentous cells.

To determine the chemical nature of biofilm extracellular matrix material from each species, we used a large-scale, roller bottle apparatus for biofilm production and matrix isolation as described previously (49). Under these conditions, net biofilm biomass was comparable among the species (**Fig 2A**), as it was in the small-scale experiments described above. The amount of biofilm matrix dry mass in relation to the total biomass was relatively similar across species **(Fig 2B)**, but the relative abundance of each macromolecular matrix component varied among the species **(Fig 2C–2G)**. Specifically, the protein component was greatest for *C. albicans,* while carbohydrate component was greatest for *C. parapsilosis* and *C. glabrata*. The extracellular DNA (eDNA) component was comparable among the species (**Fig 2F**). These results are consistent with a prior investigation (47), and indicate that macromolecular components vary slightly in their relative contributions to overall matrix composition.

Detection of matrix MGCx in non-*albicans* species.

The mannan-glucan complex (MGCx) is a signature feature of the *C. albicans* biofilm (40). The MGCx is comprised of an α-1,6 mannan backbone and β 1,6 glucan (40). Based on our previous report, the MGCx constitute approximately 20% of the total carbohydrate pool in the *C. albicans* matrix. The MGCx isolated from the NAC biofilm matrices constituted 13.5%, 34.8%, and 17.0%, in *C. tropicalis, C, parapsilosis,* and *C. glabrata,* respectively **(Table 2)**. Further gas chromatography revealed presence of both mannan and glucan in the matrix of each non-*albicans Candida* biofilm **(Fig 3A)**. The *C. albicans* MGCx has a mannan:glucan ratio of 89:11 (40). We found a mannan:glucan ratios of 64:25 for *C. tropicalis,* 83:12 for *C. parapsilosis,* and 93:7 for *C. glabrata* **(Fig 3A and Table 2)**. These findings are consistent with the production of an MGCx by each non-*albicans* species, though each species' MGCx may have distinct structural features.

NMR analyses performed on total purified NAC MGCx revealed compelling structural similarities as well as striking differences among the species' neutral matrix polysaccharides **(Fig. 3B-C, Table 1, and Supplemental Table S1)**. Control analysis of *C. albicans* samples revealed several α- and β-Man spin systems that resembled the high- and low- molecular weight F2 and F17 glucomannans (HMW and LMW GMs, respectively) we reported previously(40). Of particular relevance, we found multiple signals specific for α-1→2-Manα-1→2 residues enclosed within branched regions, such as those found in the MGCx side chains. Several of these spin systems **(Fig. 3A and 3B, peaks B, D, H, I, K, and L)** were common to *C. albicans*, *C. parapsilosis*, and *C. tropicalis*. Fewer spin systems were common to *C. albicans* and *C. glabrata* **(Fig. 3B, peaks C, I, K, and L)**, as may be expected from their greater phylogenetic distance. We also found peaks characteristic of □1,6-glucan in 2D NMR analysis **(Fig. 3B, peaks P and O)**. In addition to differences in presence or absence of specific peaks, differences among the polysaccharide compositions were also evident from the quantitative differences among individual anomeric peaks **(Fig. 3B and Table 1)**.

We used a biochemical approach to test for a physical interaction among the matrix polysaccharide components. Specifically, we assessed the glycosyl composition of matrix polysaccharides following a series of neutral sugar purification and fractionation steps. For each species fraction we identified both mannan and glucan in the high molecular weight (HMW) and low molecular weight (LMW) fractions. Co-migration of both mannan and glucan components strongly suggests the presence of covalent bonds between those two polymers, however their definite nature is not completely understood. This observation is consistent with co-elution of each monosugar as a distinct mannan-glucan complex polysaccharide the NAC biofilm matrix (**Table 2**). However, in keeping with analysis described above, the ratios of mannan and glucan varied somewhat across the species suggesting structural differences in this matrix component among the NAC. In addition, there were several distinct mannan-glucan complexes of varying

size for *C. glabrata*. These co-fractionation results support the model that each non-*albicans* species produces a biofilm matrix MGCx.

We also used pharmacologic and enzymatic approaches to test predictions of the MGCx model. Both polysaccharides are required for MGCx assembly in this model, hence disruption of either mannan or glucan alone would be predicted to decrease matrix accumulation of the other (40). To inhibit matrix mannan production, we utilized tunicamycin, an inhibitor of N-glycosylation, and α-mannosidase, an enzyme which hydrolyses and degrades mannan (39). Either tunicamycin or α-mannosidase treatment of biofilm reduced the matrix mannan content on average by 28% and 25%, respectively **(Fig 3C and 3D)**. Each treatment caused a concomitant decrease in the concentration of glucan that was nearly identical in magnitude (25% and 27%, respectively) **(Fig 3C and 3D).** The finding that matrix glucan accumulation is dependent upon matrix mannan supports the model that polysaccharide interaction leading to an MGCx is conserved across these *Candida* species (39).

Mannan-glucan matrix function in NAC species.

Prior studies have linked a majority of the *C. albicans* biofilm-resistance phenotype to sequestration of antifungal drugs by the extracellular matrix (28, 34, 36, 37, 39, 50-52). The MGCx appears strongly linked to this drug sequestration phenomenon. Therefore, we examined the drug susceptibility of biofilms both in vitro and in vivo using a rat vascular catheter model for each of the *Candida* species (53, 54) **(Fig 4A and 4B)**. For *C. albicans, C. tropicalis, and C. glabrata,* the highest soluble concentration of the antifungal, fluconazole (1000 μg/ml, which is more than 1000 times the planktonic MIC) did not appreciably impact biofilm cell burden in either model, consistent with prior biofilm antifungal testing for these species (55-58). For the strain of *C. parapsilosis* studied, treatment was more effective when compared to the other species.

However, the fluconazole concentration needed for effective treatment remained 100 times greater than that associated with planktonic efficacy. These results confirm that biofilms of these species are dramatically less sensitive to fluconazole than planktonic cells. To evaluate drug sequestration as a mechanism underlying the biofilm-associated drug resistance, we tracked radiolabeled fluconazole within the biofilm of each *Candida* species. Nearly all of the antifungal accumulated in the biofilm matrix for each species **(Fig 4C)**. Interestingly, despite the fact that each species was exposed to a similar concentration of fluconazole, the total sequestered drug concentrations were lower in the NAC biofilms. Because matrix levels are relatively similar among the species **(Fig 2B)**, we speculate that differences in matrix-drug binding affinity among the species account for differences in drug accumulation.

We further explored the capacity of NAC matrices to interact with fluconazole using one-dimensional ^{1}H NMR. In our experiments, interactions of the antifungal drug with the matrix were evident by changes in the intensity of ^{1}H peaks upon increasing concentrations of matrix material. Similarly to our previous report(40), the signals of both aromatic and azole protons decreased as a function of increasing concentation of matrices, suggesting that both the aromatic ring and the heterocyclic triazole rings were involved in interactions with matrix components. Interestingly, each NAC matrix had a distinct drug-binding dynamics profile **(Fig. 4D)**. The degree of interaction in this assay was greatest for *C. albicans,* consistent with differences in matrix affinity among the species.

If the MGCx is responsible for functional drug sequestration, then MGCx disruption should increase biofilm drug susceptibility. We tested this prediction through pharmacological and enzymatic treatments. Mannan accumulation was reduced by either tunicamycin or α-mannosidase treatment, as shown above. In addition, both mannan and β-1,6 glucan accumulation were reduced by brefeldin A treatment (59). These treatments alone did not influence biofilm cell viability. However, each treatment augmented the activity of fluconazole,

resulting in a profound killing of biofilm cells **(Fig 4D)**. These effects were biofilm-specific, as these agents did not enhance the activity of fluconazole against planktonic cells **(Supplemental Fig 1)**. In sum, these results support the hypothesis that MGCx contributes to sequestration of antifungals to promote biofilm resistance across *Candida* species.

Genetic determinants of NAC matrix MGCx structure and function.

In order to identify genetic determinants of matrix production across *Candida* species we used a candidate gene approach. Hypothesizing genetic conservation among species, we identified orthologs of 12 *C. albicans* genes shown to be involved in production or modification of matrix mannan or β-1,6 glucan (**Table 3**) **(34, 39)**. We successfully constructed homozygous deletion mutants for the genes in each species with the exceptions of *ALG11* and *VRG4* in *C. tropicalis, BIG1, KRE5*, and *VRG4* in *C. parapsilosis,* and *KRE5* and *VRG4* in *C. glabrata*. We speculate that these genes may be essential in the respective species. Most of the mutants formed biofilms similar to their reference strains. However, three mutants formed biofilms with reduced cell numbers (**Supplemental Fig 2**), including *C. parapsilosis mnn11Δ/Δ, pmr1Δ/Δ* and *phr1Δ/Δ* and *C. glabrata mnn11Δ* and *big1Δ*.

We examined each of the mutant biofilms by electron microscopy to visualize biofilm architecture and matrix deposition. Biofilm architecture seemed largely unaffected by the mutations, but there was a striking reduction of visible extracellular matrix in seven of the mutant biofilm strains **(Fig 5)**. This suggests that each of these genes is required for biofilm matrix production in the respective NAC species.

We next examined the influence of the genetic disruptions on the biofilm resistance phenotype in vitro (**Fig 5 and Supplemental Fig 3 and 4**). Surprisingly, despite the importance of each of these genes for biofilm resistance in *C. albicans,* only a small subset impacted

susceptibility in the NAC biofilms. Specifically, we found a total of seven of 29 deletion mutants exhibiting enhanced biofilm drug susceptibility (**Fig 6A)**. For *C. tropicalis,* fluconazole susceptible strains included the mannan synthesis mutants *mnn9Δ/Δ* and *van1Δ/Δ*, and the β-1,6 glucan synthesis mutant, *kre5Δ/Δ*. Among the *C. parapsilosis* mutants screened, we identified three mannan synthesis mutants, *mnn9Δ/Δ*, *van1Δ/Δ*, and *pmr1Δ/Δ*. Interestingly, two of the *C. parapsilosis* orthologs were also relevant for *C. tropicalis* (*mnn9Δ/Δ,* and *van1Δ/Δ*). Only a single mutant from *C. glabrata* exhibited a biofilm susceptibility phenotype: a putative enzyme for β-1,6 glucan synthesis (*big1Δ*). The susceptibility to fluconazole appeared specific to the biofilm state, as planktonic MICs for all mutants were unchanged (**Fig 6A**). The biofilm susceptibility phenotype was reversed for all strains in which we reintroduced a wildtype copy of the deleted gene (**Supplemental Fig 5**).

For three *C. parapsilosis* mutants (*mnn9Δ/Δ, pmr1Δ/Δ,* and *van1*Δ/Δ) complementation was not successful; consequently, we examined multiple independent deletion mutant strains to verify the enhanced antifungal susceptibility phenotype (**Supplemental Fig 6**). Antifungal biofilm susceptibility was similarly assessed for two additional drugs, amphotericin B and micafungin (**Supplemental Figure S4**). Enhanced susceptibility was observed for the majority of mutants, consistent with a pan-antifungal mechanism. These results show that inferred defects in mannan or β-1,6 glucan production can cause increased biofilm drug susceptibility in NAC species.

We explored the clinical relevance of these findings using the rat catheter in vivo biofilm model. Enhanced fluconazole efficacy was observed for representative mannan or β-1,6 glucan synthesis mutants from each species (**Fig 6B**). These results support the hypothesis that increased biofilm drug susceptibility that results from impaired mannan or β-1,6 glucan synthesis is relevant in a model infection environment.

To determine directly if matrix mannan and glucan are required for drug sequestration in the NAC biofilm mutants, we carried out ^{3}H-fluconazole binding assays. Compared to the

respective wildtype strain, each of the mannan and glucan mutant strains had decreased matrix sequestration of radiolabeled drug **(Fig 6C)**. These findings strengthen the conclusion from our pharmacological and enzymatic matrix disruption treatments that mannan and glucan contribute to matrix drug sequestration. However, variability in the degree of sequestration relative to the change susceptibility suggests the potential of additional mechanisms as previously described(28).

To identify matrix changes associated with increased biofilm susceptibility, we harvested matrix from biofilms of each mutant and assayed for total carbohydrate and specifically for mannan and glucan **(Fig 6D and 5E).** We found that each of the seven of the mutants had significantly lower levels of the corresponding polysaccharide than the reference strain with remaining amounts less than 50% of wild-type on average (**Fig 6E**). Furthermore, genetic disruption of either a mannan or glucan synthase was associated with a lower content of both mannan and glucan. This observation is consistent with the model that the MGCx accounts for the drug resistant phenotype of the NAC biofilms. Unfortunatley, matrix quantities did not allow for complementary NMR analysis. Because the synthesis pathways for each carbohydrate are distinct, inhibition of one pathway would not be expected to lead to a biochemical reduction in the non-impacted pathway components. Our findings suggest that there is an extracellular physical interaction among the matrix components that is conserved among *Candida* species.

DISCUSSION

We theorized that the MGCx, recently described in *C. albicans,* is conserved and promotes the drug-resistance phenotype across *Candida* species. In order to address this question, in this study, we first utilized large-scale biofilm growth and matrix composition analysis. We find that each of the major matrix polysaccharide constituents is required for assembly and function of matrix across *Candida* species. At the structural level, several complementary assays corroborate the presence of an MGCx in diverse *Candida* species. Specifically, we identified a

α-1,6 mannan backbone with α-1,2 branches and β-1,6 glucan in the matrix. Analysis of the glycosyl composition of matrix following fractionation also revealed co-elution of mannan and glucan components. Additionally, both pharmacologic and genetic studies revealed co-dependence of accumulation of matrix mannan and glucan. Phenotypic studies documented the central role of this polysaccharide complex in matrix sequestration and biofilm-specific drug resistance under both in vitro and in vivo conditions.

However, refined NMR analysis of the complex as well as phenotypic and genotypic assays suggested meaningful differences in the MGCx among the *Candida* species. Specifically, the relative ratios of the mannan and glucan components varied among the four species. Additionally, while NMR analysis revealed similar mannan and glucan backbone features, there were differences in branching patterns and length. The *C. parapsilosis* matrix mostly resembled low-molecular weight glucomannans of *C. albicans*. The abundance of α-1→6-linked Man residues along with a substantially increased content of terminal Manα-1→2 residues indicated the presence of a similar α-1→6-linked Man backbone structure, but with shorter side chains consisting of a blend of α-1→2- and α-1→3-linked Man residues. The lack of β-Man for *C. parapsilosis* matrix was unique, as β-Man was observed for the other species. The matrix of *C. tropicalis* exhibited characteristics similar to *C. albicans* and *C. parapsilosis*. Like the latter, this pool contained amounts of α-1→2-Manα-1→2 and 1→6-linked Man as well as of β-Man residues that were comparable to those measured in *C. albicans*. On the other hand, *C. tropicalis* matrix neutral carbohydrates did not contain any 3-linked Man residues, whereas there was a larger terminal Man α-1→2 residue content along with more 1→6-linked Man. This pattern suggests more branching but relatively shorter side chains. Based on measured distribution of 2,6-Manα-1→6 and α-1→2-Manα-1→2 residues, it appeared that the overall branching pattern is bit less diverse than that observed in *C. albicans* matrix. The analysis of *C. glabrata* matrix neutral carbohydrates revealed the most distinct highly branched structure, which also contained well-defined linear regions without any branching Man residues present. This observation suggested

an uneven and infrequent distribution of side chains in this carbohydrate pool as reflected by the presence of only one type of α-1→2-Manα-1→2 signal, whereas the amount of terminal Manα-1→2 residue indicated a side chain length distribution type resembling the one determined in *C. albicans*. Unlike the latter, *C. glabrata* matrix neutral carbohydrates did not contain 3-linked Man residues, while the content of β-Man was significantly reduced, but still detectable. Overall, the major Man residues were similar amongst all four tested *Candida* species. However, the relative proportion of the residues varied significantly, likely due to differences in the degree of branching, the length of side chains, and the presence of unique residues such as β-Man or 3-linked Man. We speculate these structural differences in the MGCx and potentially other non-carbohydrate constituents determine the unique sequestration properties of the NAC.

Our genetic studies reveal both similarities and differences among the species with regard to the genetic pathways responsible for production of matrix. It was initially surprising that the only orthologous mutants in the NAC that impacted the antifungal resistance phenotype were those linked to component synthesis alone. Conversely, the mutants with putative glucan and mannan modification function based upon the *C. albicans* MGCx structure had no apparent impact on NAC matrix production. A plausible explanation for this observation is divergence in the genetic pathways responsible the differences in the impact of *C. albicans* orthologous mutants in the NAC species. Researchers have often assumed that if a yeast species is related to another yeast species (especially within the same genus), the underlying molecular and cellular mechanisms must also be closely related. However, even within a *Candida* clade, the genetic relatedness between any two NAC species is often larger than the genetic distance between man and reptiles (60). There is ample precedent for genetic re-wiring among the *Candida* species, including for biofilm formation pathways (13, 15, 16, 61-63). While sequence identity is not a great predictor of function, the amino acid similarity across species for these *C. albicans* matrix-resistance genes was only modest.

Another potential explanation for the lack of genetic conservation is distinct differences in MGCx branching structure. We favor this model due to the biochemical differences that support a model of altered matrix branch-chain structure across species. The latter model suggests that enzymes needed for production of the matrix backbone may be useful for pan-*Candida* biofilm development of useful therapies, while targeting modification enzymes would be predicted to be less effective across species. In future work, careful characterization the remaining genetic components of the NAC biofilm synthesis pathway will help to elucidate additional therapeutic targets.

MATERIALS AND METHODS

Ethics Statement. All animal procedures were approved by the Institutional Animal Care and Use Committee at the University of Wisconsin according to the guidelines of the Animal Welfare Act, The Institute of Laboratory Animal Resources Guide for the Care and Use of Laboratory Animals, and Public Health Service Policy. The approved animal protocol number is DA0031.

Media. Strains were stored in 15% (vol/vol) glycerol stock at −80°C and maintained on yeast extract-peptone-dextrose (YPD) agar. Prior to biofilm experiments, all *Candida* strains were grown at 30°C in YPD and biofilms were grown in RPMI 1640 buffered with morpholinepropanesulfonic acid (RPMI-MOPS).

Strains and strain construction. Strains used for this study are listed in **Table 2** and the genotypes of strains constructed in the present studies are shown in **Table S2**. The parent strains CAY3764, CPL2H1, and HTL were used to create homozygous deletion strains using fusion PCR disruption cassettes as previously described for *C. tropicalis, C. parapsilosis*, and *C. glabrata,* respectively (6, 64-66). Correct integration was confirmed by PCR. At least two independent mutants were created for each gene of interest. The primers used for strain construction and confirmation are listed in **Table S3**.

C. tropicalis mutant strain construction was conducted using the background strain of CAY3764 which is auxotrophic for *LEU2* and *HIS1 (66)*. The primers used for strain construction and confirmation are listed in **Table S3**. For *C. parapsilosis* strain construction we used the background strain of CPL2H1 which is auxotrophic for *LEU2 and HIS1*, as described by Holland et al (6). The first allele was deleted by replacing one allele with *HIS1* from *C. dubliniensis*, and the second with *LEU2* from *C. maltosa. C. glabrata* transformations were conducted using auxotrophic HTL (*HIS3, LEU2, TRP1)* background strain (63). Candidate genes were deleted by replacing the allele with the gene conferring resistance to the antibiotic nourseothricin. All mutant strains were confirmed by PCR using primers inside nourseothricin and a primer outside of the integration sites at both the 5′ and 3′ end of the gene.

Complementation of *C. tropicalis* and *C. parapsilosis* mutant strains with a single wild-type gene copy used selection for nourseothricin resistance, whereas complementation of *C. glabrata* mutant strains used selection for hygromycin B resistance. A single copy of the gene was reintroduced to its endogenous location within the genome. Briefly, each ORF (plus 1 kb upstream and downstream) was amplified by PCR, and using the PCR fusion method, a cassette was created with either hygromycin B or nourseothricin at the tail end of the PCR product. This fusion PCR product was then transformed into their respective species using the same method as previously described for mutant construction. Colony PCR was used to verify all genotypes, primers are listed in **Table S3**.

In vitro biofilm models. Biofilms were grown in one of four models: 96-well or 6-well polystyrene plate, polystyrene roller-bottle, or glass coverslip. Ninety six-well flat-bottom polystyrene plates were used to assess biofilm adherence, maturation, and treatment effect as previously described (67, 68). The *Candida* species inocula (10^6 cells/ml) was prepared by growth in YPD with uridine overnight at 30°C, followed by dilution in RPMI-MOPS based on hemocytometer counts. The 6-well plate assay was used to assess matrix composition. For this assay, 1 ml of culture was

inoculated in each well. After a 60 min adherence period at 30°C, the non-adherent inoculum was removed and 1 ml of fresh medium (RPMI-MOPS) was applied to each well. Plates were incubated at 37°C for 48 h on an orbital shaker set at 50 rpm. Media was removed and fresh medium was added midway through the incubation period. The coverslip assay was used for in vitro biofilm imaging. Briefly, in vitro biofilms were grown on sterile coverslips (Thermanox) in sterile 12 well plates that had previously been coated with 10 µl of human NaEDTA plasma each and allowed to dry at 30°C. 40 µl of yeast in RPMI, were counted and diluted as in the biofilm models described above, was added to each coverslip for 60 min at 30°C. The initial inoculum was then removed and the plates incubated in 1 ml RPMI+MOPS+5% NaEDTA human plasma for 20 h at 37°C and 50 rpm on an orbital shaker for an additional 24 h. A rolling bottle system was used to generate matrix for analyses (49). Briefly, aliquots of *C. albicans* grown in RPMI-MOPS were used to inoculate a polystyrene roller. Bottles were placed on a roller apparatus (Wheaton Science Products, Millville, NJ), rolling at the rate of 20 rpm at 37°C. After 24 h, the biofilm culture medium was replaced with fresh media and the bottles were incubated for another 24 h. At least three biological replicates were performed in each assay.

In vitro biofilm and planktonic antifungal susceptibility testing. A tetrazolium salt XTT [2,3-bis-(2-methoxy-4-nitro-5-sulfophenyl)-2H-tetrazolium-5-carboxanilide inner salt] reduction assay was used to measure in vitro biofilm drug susceptibility (69, 70). Biofilms were formed in the wells of 96-well microtiter plates, as described above. After a 6 h biofilm formation period, the biofilms were washed with phosphate-buffered saline (PBS) twice to remove non-adherent cells. Fresh RPMI-MOPS and drug dilutions were added, followed by additional periods of incubation (48 h). The antifungals studies included fluconazole at 4 to 1,000 mg/ml, amphotericin B at 125 to 0.5 µg/mL and micafungiun at 125 to 0.5 µg/mL. For experiments with tunicamycin (1.0 µg/mL) and brefeldin A (0.6 µg/mL) biofilms were treated alone or in combination with fluconazole after an

initial 6hr growth phase. Biofilms treated with α-mannosidase (0.78 U/mL; Jack Bean; Sigma) were grown for 24hrs before a 24-h dose either alone or in combination with fluconazole. Drug treatments were reapplied after 24 h, and plates were incubated for an additional 24 h. Following treatment with 90 µl XTT (0.75 mg/ml) and 10 µl phenazine methosulfate (3.20 mg/ml) for 30 min, absorbance at 492 nm was measured using an automated plate reader. The percent reduction in biofilm growth was calculated using the reduction in absorbance compared to that of controls with no antifungal treatment. Assays were performed in triplicate, and significant differences were measured by analysis of variance (ANOVA) with pairwise comparisons using the Holm-Sidak method. The CLSI M27 A3 broth microdilution susceptibility method was used to examine the activities of fluconazole against planktonic *Candida.* sp (71). Endpoints were assessed after 24 h by visible turbidity in triplicate assays.

Biofilm SEM. In vitro biofilms from sterile coverslips were grown as described above. Following a 24 h incubation period, media was replaced with 1 ml of fixative (4% formaldehyde, 1% glutaraldehyde in PBS) and coverslips were incubated at 4°C for 24 hours. The coverslips were then washed with PBS and treated with 1% osmium tetroxide for 30 min at ambient temperature. After a series of alcohol washes (30 to 100%), final desiccation was performed by critical-point drying. Coverslips were mounted, palladium – gold coated, and imaged in a scanning electron microscope (LEO 1530) at 3 kV. The images were assembled using Adobe Photoshop 7.0.1.

Matrix isolation from roller bottle and 6-well biofilms. A rolling bottle system was used to generate matrix for composition analyses (49). After incubation for 48 h, media was removed and the *Candida* biofilms were dislodged by spatula and gently sonicated to avoid cell wall disruption (sonication with a 6mm microtip at 20 kHz with an amplitude of 30% for 8 min). The aggregate biofilm was then centrifuged to separate fungal cells and matrix. The supernatant-containing matrix was then collected and lyophilized. The sample was re-suspended in water and dialyzed

(molecular weight cutoff of 3.5 kDa) for 5 days and again lyophilized yielding the "crude" biofilm matrix. Overall, a total of 400 bottles of the matrix corresponding to the biofilm area of 59.5m^2 were collected for analysis.

Matrix was similarly collected from 6-well plates, as published previously(34). Following incubation, biofilms were harvested by removing and discarding the medium, washing each well with 1 ml of ddH_2O, and then removal of biofilms using a spatula. Biofilms were collected in 1 ml of ddH_2O per well, and then sonicated for 20 min. The soluble matrix was then separated from the cells by centrifuging the samples at 2,880 x *g* for 20 min at 4^o C.

Biofilm Matrix Analysis. Dry Weight. Following biofilm matrix collection described above, matrix was lyophilized, and weighed to obtain total biomass for each biofilm. Carbohydrate analysis. The carbohydrate concentration of crude matrix was determined colorimetrically (492 nm) using the phenol-sulfuric acid method (72). Structural analysis was performed after a series of purification and fractionation steps, including size exclusion chromatography. Protein analysis. The protein concentration of the crude matrix sample was assessed colorimetrically at 562 nm using the BCA protein assay kit (Pierce Biotechnology, Rockford, IL) (73). Nucleic acid analysis Nucleic acid concentrations were measured spectrophotometrically (260 nm) (74). Monosaccharide Analysis Sugars were detected and quantified by gas liquid chromatography-flame ionization detector (GLC-FID) on a Shimadzu GC-2010 system after conversion to alditol acetate derivatives as previously described (75). A 50% cyanopropylmethyl/50% phenylmethyl polysiloxane column was used (Restek) with the same GLC conditions as previously described (76). Data for each monosaccharide was calculated and presented as a percentage of the total detected sugars. Lipid analysis. Lipids were extracted from the desalted lyophilized matrix powder with a mixture of CHCl3 and MeOH (2:1, by volume) as described elsewhere (77). Methylation of fatty acids was performed using 0.5 ml of 14% BF3 in MeOH, and methyl esters

were recovered with hexane. Fatty acid methyl esters were analyzed by gas chromatography using a Hewlett-Packard 5890 (Hewlett-Packard, Palo Alto, CA). eDNA analysis. Extracellular DNA was isolated from NAC matrices using the MasterPure™ Yeast DNA Purification Kit (Epicentre Biotechnologies, Madison, WI) Nucleic acid concentrations were measured spectrophotometrically with a NanoDrop 1000 spectrophotometer (Thermo Fisher Scientific, San Jose, CA). The average measured ratio of absorbance at 260/280 nm was about ~ 1.8, which indicated pure free-of-contaminants DNA.

Nuclear Magnetic Resonance (NMR) of neutral carbohydrates. Following isolation, matrix samples were resuspended in 1 ml of 20 mM bis-Tris/HCl (pH 6.5) loading buffer and fractionated on a HiPrep™ 26/10 Desalting column prepacked with Sephadex™ G-25 Fine (GE Healthcare Life Sciences, Uppsala, Sweden). Column-dialyzed fractions were then separated on an anion exchanger HiPrep™ 16/10 DEAE FF column (GE Healthcare Life Sciences) equilibrated with 20 mM bis-Tris/HCl (pH 6.5). Elution was carried out in a 20 mM bis-Tris/HCl (pH 6.4)/0.5 M NaCl buffer system at a flow rate of 1 ml/min in a linear gradient of salt from 0 to 100% in 20 column volumes. Neutral free carbohydrates were detected in flow-through fractions, which were then pooled, lyophilized, resuspended in 2 ml of 150 mM NH_4HCO_3, and applied to gel filtration on a Superdex™ 200 10/300 GL column (GE Healthcare Life Sciences). Matrix components were eluted at a flow rate of 0.5 ml/min and 1 ml fractions were collected. All chromatographic separation steps were performed at room temperature on the high-performance liquid chromatography ÄKTA-Purifier 10 system (GE Healthcare Life Sciences). All buffers used were filtered through 0.2 µm nylon membrane filters (Nalgene, Rochester, NY) and degassed prior to use. Isolated polysugar fractions were lyophilized, resuspended in a small volume of water, and incubated at 55°C overnight in order to decompose and remove any remaining ammonium bicarbonate. These steps were repeated until all of the salt was removed and the isolated sugars

appeared as an anamorphous cotton-like material after the final lyophilization. The molecular weight of biofilm matrix neutral carbohydrates was estimated using size exclusion column calibration with a set of Leuconostoc spp. dextran standards, which included 100 kDa, 70 kDa, 40 kDa, 25 kDa, and 6 kDa polymers.

To elucidate the structure of the isolated carbohydrates, we utilized a combination of 1D 1H-NMR and 2D HSQC NMR experiments as well as known chemical shift assignments characteristic of individual mannosyl and glucosyl motifs in mannan and glucan structures based on previously published studies (78-82). All data were collected at 70°C on a Bruker Biospin Avance III 500 MHz NMR spectrometer (Bruker BioSpin GmbH, Rheinstetten, Germany) equipped with a 5 mm triple resonance, cryogenic probe, CPTXI 500 H-C/N-D. One dimensional spectra were collected with 32 acquisitions using a standard one pulse experiment. The spectral width was 10 ppm centered at 4.7 ppm. The relaxation delay time was 2 s with an acquisition time of 3.3 s (32768 data points). Thirty-two acquisitions were collected. Multiplicity edited, phase sensitive, echo-antiecho ^{1}H HSQC spectra were obtained using 4 acquisitions per indirect time point with ^{1}H decoupling during acquisition(83). Matched swept adiabatic ^{13}C inversion pulses were used. The raw data matrix size was 2048 × 128 blocks. Spectra were collected with a relaxation time delay of 2 s and an acquisition time of 0.2 s with sweep widths of 10 ppm (^{1}H) and 65 ppm (^{13}C), respectively. The center of the spectrum was 4.7 ppm (^{1}H) and 82 ppm (^{13}C).

Matrix Carbohydrate Fractionation and Analysis for a MGCx. Additional structural analysis was performed after a series of purification and fractionation steps to further ascertain the presence of a mannan-glucan complex. These steps includes size exclusion chromatography followed by separation on an anion exchanger HiPrep 16/10 DEAE FF column (GE Healthcare Life Sciences). Neutral free carbohydrates were collected in flow through fractions, which were pooled and applied to gel filtration on a HighPrep 16/60 Sephacryl S-300 HR column (GE

Healthcare Life Sciences), yielding 22 individual polysaccharide peaks, F1 to F22. The molecular weight of biofilm matrix neutral carbohydrates was determined using size exclusion column calibration with a set of *Leuconostoc* species dextran standards (polymers with molecular weights [in thousands] of 100, 70, 40, 25, and 6). Both HMW and LMW fractinos were examined by GC for monosugar analysis. Matrix monosugar composition and quantification was performed on alditol acetate derivatives by GLC-FID (Shimadzu GC-2010 system; Shimadzu Co., Kyoto, Japan).

In vivo *Candida* venous catheter biofilm model. A jugular vein rat central venous catheter infection model was used for in vivo biofilm studies (53). *Candida* strains were grown to logarithmic phase in YPD at 30°C. Following a 24 h conditioning period after catheter placement, infection was achieved by intraluminal instillation of 500 ml of *C. albicans* (10^6 cells/ml). After an adherence period of 6 h, the catheter volume was withdrawn and the catheter was flushed with heparinized saline. Following a 24 h incubation period the catheters were removed a prepared for SEM imaging, as described above. The images were assembled using Adobe Photoshop 7.0.1.as described above. For drug treatment experiments, fluconazole (250 µg/ml) was instilled in the catheter after 24 h of biofilm growth. After a 24 h drug treatment period, the post treatment viable burden of *Candida* biofilm on the catheter surface was measured by viable plate counts on Sabouraud's dextrose agar (SDA) following removal of the biofilm by sonication and vortexing. We utilized three replicates for each condition.

Sequestration of ^{3}H fluconazole in biofilms. Radiolabeled fluconazole was used in an assay to assess drug retention in biofilms formed in 6-well plates (84). Biofilms were grown for 48 hrs in 6 well polystyrene plates as described above, washed, and then incubated with 8.48 x 10^5 cpm of ^{3}H fluconazole (Moravek Biochemicals; 50 µM, 0.001 mCi/mL in ethanol) in RPMI-MOPS for 30 min at 37^o C with orbital shaking at 50 rpm. Unlabeled fluconazole (20 µM) in RPMI-MOPS

was added for an additional 15-min incubation period. After washing, biofilms and matrix were collected and isolated as described above. For a subset of biofilm cells, cells were disrupted by bead beating to yield cell wall and intracellular portions. Samples were added to a Tri-Carb 2100TR liquid scintillation analyzer after adding ScintiSafe 30% LSC mixture to each sample fraction. Three technical replicates were averaged, the SEs calculated, with values compared to the reference strain using pairwise comparisons with ANOVA with the Holm-Sidak method.

Fluconazole-matrix interaction determination. Interactions between the biofilm matrix and fluconazole were also probed using one-dimensional ^{1}H-NMR. Data were collected at 37°C on a Bruker Biospin Avance III 600 MHz NMR spectrometer (Bruker BioSpin GmbH) equipped with a 1.7 mm triple resonance, cryogenic probe, CPTXI 500 H-C/N-D. One-dimensional spectra were collected with 512 acquisitions using a one pulse sequence experiment with water suppression and excitation sculpting with gradients (zgesgp). The spectral width was 16 ppm centered at 4.7 ppm. The relaxation delay time was 2 s. The approach was based on monitoring chemical shifts of fluconazole-specific protons in the absence and presence of the biofilm matrix under pH controlled conditions In this study, all tested reactions were prepared in PBS (pH 7.2) and fluconazole was used at a constant concentration of 0.653 mM. In this drug/matrix system, interactions were represented by decreasing in signal intensities of the chemical shift peaks of protons present in fluconazole.

Acknowledgement:

This study made use of the National Magnetic Resonance Facility at Madison, which is supported by NIH grant P41GM103399 (NIGMS), old number: P41RR002301. Equipment was purchased with funds from the University of Wisconsin-Madison, the NIH P41GM103399, S10RR02781,

S10RR08438, S10RR023438, S10RR025062, S10RR029220), the NSF (DMB-8415048, OIA-9977486, BIR-9214394), and the USDA.

References

1. **Pfaller MA, Diekema DJ.** 2007. Epidemiology of invasive candidiasis: a persistent public health problem. Clinical microbiology reviews **20:**133-163.
2. **Pfaller MA, Andes DR, Diekema DJ, Horn DL, Reboli AC, Rotstein C, Franks B, Azie NE.** 2014. Epidemiology and outcomes of invasive candidiasis due to non-albicans species of Candida in 2,496 patients: data from the Prospective Antifungal Therapy (PATH) registry 2004-2008. PloS one **9:**e101510.
3. **Cleveland AA, Farley MM, Harrison LH, Stein B, Hollick R, Lockhart SR, Magill SS, Derado G, Park BJ, Chiller TM.** 2012. Changes in incidence and antifungal drug resistance in candidemia: results from population-based laboratory surveillance in Atlanta and Baltimore, 2008-2011. Clinical infectious diseases : an official publication of the Infectious Diseases Society of America **55:**1352-1361.
4. **Lockhart SR, Iqbal N, Cleveland AA, Farley MM, Harrison LH, Bolden CB, Baughman W, Stein B, Hollick R, Park BJ, Chiller T.** 2012. Species identification and antifungal susceptibility testing of Candida bloodstream isolates from population-based surveillance studies in two U.S. cities from 2008 to 2011. Journal of clinical microbiology **50:**3435-3442.
5. **Andes DR, Safdar N, Baddley JW, Alexander B, Brumble L, Freifeld A, Hadley S, Herwaldt L, Kauffman C, Lyon GM, Morrison V, Patterson T, Perl T, Walker R, Hess T, Chiller T, Pappas PG, Investigators T.** 2016. The epidemiology and outcomes of invasive Candida infections among organ transplant recipients in the United States: results of the Transplant-Associated Infection Surveillance Network (TRANSNET). Transplant infectious disease : an official journal of the Transplantation Society **18:**921-931.
6. **Holland LM, Schroder MS, Turner SA, Taff H, Andes D, Grozer Z, Gacser A, Ames L, Haynes K, Higgins DG, Butler G.** 2014. Comparative phenotypic analysis of the major fungal pathogens Candida parapsilosis and Candida albicans. PLoS pathogens **10:**e1004365.
7. **Porman AM, Alby K, Hirakawa MP, Bennett RJ.** 2011. Discovery of a phenotypic switch regulating sexual mating in the opportunistic fungal pathogen Candida tropicalis. Proceedings of the National Academy of Sciences of the United States of America **108:**21158-21163.
8. **Moran GP, Coleman DC, Sullivan DJ.** 2011. Comparative genomics and the evolution of pathogenicity in human pathogenic fungi. Eukaryotic cell **10:**34-42.
9. **Thompson DS, Carlisle PL, Kadosh D.** 2011. Coevolution of morphology and virulence in Candida species. Eukaryotic cell **10:**1173-1182.
10. **Maestre-Reyna M, Diderrich R, Veelders MS, Eulenburg G, Kalugin V, Bruckner S, Keller P, Rupp S, Mosch HU, Essen LO.** 2012. Structural basis for promiscuity and specificity during Candida glabrata invasion of host epithelia. Proceedings of the National Academy of Sciences of the United States of America **109:**16864-16869.
11. **Trofa D, Gacser A, Nosanchuk JD.** 2008. Candida parapsilosis, an emerging fungal pathogen. Clinical microbiology reviews **21:**606-625.
12. **Lackey E, Vipulanandan G, Childers DS, Kadosh D.** 2013. Comparative evolution of morphological regulatory functions in Candida species. Eukaryotic cell **12:**1356-1368.
13. **Butler G, Rasmussen MD, Lin MF, Santos MA, Sakthikumar S, Munro CA, Rheinbay E, Grabherr M, Forche A, Reedy JL, Agrafioti I, Arnaud MB, Bates S, Brown AJ, Brunke S, Costanzo MC, Fitzpatrick DA, de Groot PW, Harris D, Hoyer LL, Hube B, Klis FM, Kodira C, Lennard N, Logue ME, Martin R, Neiman AM, Nikolaou E, Quail MA, Quinn J, Santos MC, Schmitzberger FF, Sherlock G, Shah P, Silverstein KA, Skrzypek MS, Soll D, Staggs R, Stansfield I, Stumpf MP, Sudbery PE, Srikantha T, Zeng Q, Berman J, Berriman M, Heitman J, Gow NA, Lorenz MC, Birren BW, Kellis**

M, Cuomo CA. 2009. Evolution of pathogenicity and sexual reproduction in eight Candida genomes. Nature **459:**657-662.
14. **Papon N, Courdavault V, Clastre M, Bennett RJ.** 2013. Emerging and emerged pathogenic Candida species: beyond the Candida albicans paradigm. PLoS pathogens **9:**e1003550.
15. **Priest SJ, Lorenz MC.** 2015. Characterization of Virulence-Related Phenotypes in Candida Species of the CUG Clade. Eukaryotic cell **14:**931-940.
16. **Chen YL, Konieczka JH, Springer DJ, Bowen SE, Zhang J, Silao FG, Bungay AA, Bigol UG, Nicolas MG, Abraham SN, Thompson DA, Regev A, Heitman J.** 2012. Convergent Evolution of Calcineurin Pathway Roles in Thermotolerance and Virulence in Candida glabrata. G3 **2:**675-691.
17. **Kaur R, Domergue R, Zupancic ML, Cormack BP.** 2005. A yeast by any other name: Candida glabrata and its interaction with the host. Current opinion in microbiology **8:**378-384.
18. **Chandra J, Kuhn DM, Mukherjee PK, Hoyer LL, McCormick T, Ghannoum MA.** 2001. Biofilm formation by the fungal pathogen Candida albicans: development, architecture, and drug resistance. Journal of bacteriology **183:**5385-5394.
19. **Uppuluri P, Pierce CG, Lopez-Ribot JL.** 2009. Candida albicans biofilm formation and its clinical consequences. Future microbiology **4:**1235-1237.
20. **Ramage G, Saville SP, Thomas DP, Lopez-Ribot JL.** 2005. Candida biofilms: an update. Eukaryotic cell **4:**633-638.
21. **Desai JV, Mitchell AP, Andes DR.** 2014. Fungal biofilms, drug resistance, and recurrent infection. Cold Spring Harbor perspectives in medicine **4**.
22. **Blankenship JR, Mitchell AP.** 2006. How to build a biofilm: a fungal perspective. Current opinion in microbiology **9:**588-594.
23. **Andes DR, Safdar N, Baddley JW, Playford G, Reboli AC, Rex JH, Sobel JD, Pappas PG, Kullberg BJ, Mycoses Study G.** 2012. Impact of treatment strategy on outcomes in patients with candidemia and other forms of invasive candidiasis: a patient-level quantitative review of randomized trials. Clinical infectious diseases : an official publication of the Infectious Diseases Society of America **54:**1110-1122.
24. **Kojic EM, Darouiche RO.** 2004. Candida infections of medical devices. Clinical microbiology reviews **17:**255-267.
25. **Branda SS, Vik S, Friedman L, Kolter R.** 2005. Biofilms: the matrix revisited. Trends in microbiology **13:**20-26.
26. **Flemming HC, Wingender J.** 2010. The biofilm matrix. Nature reviews. Microbiology **8:**623-633.
27. **Baillie GS, Douglas LJ.** 2000. Matrix polymers of *Candida biofilms* and their possible role in biofilm resistance to antifungal agents. The Journal of antimicrobial chemotherapy **46:**397-403.
28. **Taff HT, Mitchell KF, Edward JA, Andes DR.** 2013. Mechanisms of Candida biofilm drug resistance. Future microbiology **8:**1325-1337.
29. **Vediyappan G, Rossignol T, d'Enfert C.** 2010. Interaction of Candida albicans biofilms with antifungals: transcriptional response and binding of antifungals to beta-glucans. Antimicrobial agents and chemotherapy **54:**2096-2111.
30. **Katragkou A, Chatzimoschou A, Simitsopoulou M, Dalakiouridou M, Diza-Mataftsi E, Tsantali C, Roilides E.** 2008. Differential activities of newer antifungal agents against Candida albicans and Candida parapsilosis biofilms. Antimicrobial agents and chemotherapy **52:**357-360.
31. **Costerton JW, Stewart PS, Greenberg EP.** 1999. Bacterial biofilms: a common cause of persistent infections. Science **284:**1318-1322.

32. **Hall-Stoodley L, Stoodley P.** 2009. Evolving concepts in biofilm infections. Cellular microbiology **11:**1034-1043.
33. **Mah TF, O'Toole GA.** 2001. Mechanisms of biofilm resistance to antimicrobial agents. Trends in microbiology **9:**34-39.
34. **Taff HT, Nett JE, Zarnowski R, Ross KM, Sanchez H, Cain MT, Hamaker J, Mitchell AP, Andes DR.** 2012. A Candida biofilm-induced pathway for matrix glucan delivery: implications for drug resistance. PLoS pathogens **8:**e1002848.
35. **Nett JE, Sanchez H, Cain MT, Ross KM, Andes DR.** 2011. Interface of Candida albicans biofilm matrix-associated drug resistance and cell wall integrity regulation. Eukaryotic cell **10:**1660-1669.
36. **Nett JE, Crawford K, Marchillo K, Andes DR.** 2010. Role of Fks1p and matrix glucan in Candida albicans biofilm resistance to an echinocandin, pyrimidine, and polyene. Antimicrobial agents and chemotherapy **54:**3505-3508.
37. **Nett JE, Sanchez H, Cain MT, Andes DR.** 2010. Genetic basis of Candida biofilm resistance due to drug-sequestering matrix glucan. The Journal of infectious diseases **202:**171-175.
38. **Nobile CJ, Nett JE, Hernday AD, Homann OR, Deneault JS, Nantel A, Andes DR, Johnson AD, Mitchell AP.** 2009. Biofilm matrix regulation by Candida albicans Zap1. PLoS biology **7:**e1000133.
39. **Mitchell KF, Zarnowski R, Sanchez H, Edward JA, Reinicke EL, Nett JE, Mitchell AP, Andes DR.** 2015. Community participation in biofilm matrix assembly and function. Proceedings of the National Academy of Sciences of the United States of America **112:**4092-4097.
40. **Zarnowski R, Westler WM, Lacmbouh GA, Marita JM, Bothe JR, Bernhardt J, Lounes-Hadj Sahraoui A, Fontaine J, Sanchez H, Hatfield RD, Ntambi JM, Nett JE, Mitchell AP, Andes DR.** 2014. Novel entries in a fungal biofilm matrix encyclopedia. mBio **5:**e01333-01314.
41. **Lopez-Ribot JL.** 2014. Large-scale biochemical profiling of the Candida albicans biofilm matrix: new compositional, structural, and functional insights. mBio **5:**e01781-01714.
42. **Mitchell KF, Zarnowski R, Andes DR.** 2016. Fungal Super Glue: The Biofilm Matrix and Its Composition, Assembly, and Functions. PLoS pathogens **12:**e1005828.
43. **Rajendran R, Sherry L, Lappin DF, Nile CJ, Smith K, Williams C, Munro CA, Ramage G.** 2014. Extracellular DNA release confers heterogeneity in Candida albicans biofilm formation. BMC microbiology **14:**303.
44. **Martins M, Uppuluri P, Thomas DP, Cleary IA, Henriques M, Lopez-Ribot JL, Oliveira R.** 2010. Presence of extracellular DNA in the Candida albicans biofilm matrix and its contribution to biofilms. Mycopathologia **169:**323-331.
45. **Al-Fattani MA, Douglas LJ.** 2006. Biofilm matrix of Candida albicans and Candida tropicalis: chemical composition and role in drug resistance. Journal of medical microbiology **55:**999-1008.
46. **Fernandes T, Silva S, Henriques M.** 2015. Candida tropicalis biofilm's matrix--involvement on its resistance to amphotericin B. Diagnostic microbiology and infectious disease **83:**165-169.
47. **Silva S, Henriques M, Martins A, Oliveira R, Williams D, Azeredo J.** 2009. Biofilms of non-Candida albicans Candida species: quantification, structure and matrix composition. Medical mycology **47:**681-689.
48. **Nett JE, Zarnowski R, Cabezas-Olcoz J, Brooks EG, Bernhardt J, Marchillo K, Mosher DF, Andes DR.** 2015. Host contributions to construction of three device-associated Candida albicans biofilms. Infection and immunity **83:**4630-4638.
49. **Zarnowski R, Sanchez H, Andes DR.** 2016. Large-scale production and isolation of Candida biofilm extracellular matrix. Nature protocols **11:**2320-2327.

50. **Robbins N, Uppuluri P, Nett J, Rajendran R, Ramage G, Lopez-Ribot JL, Andes D, Cowen LE.** 2011. Hsp90 governs dispersion and drug resistance of fungal biofilms. PLoS pathogens **7:**e1002257.
51. **Mukherjee PK, Chandra J, Kuhn DM, Ghannoum MA.** 2003. Mechanism of fluconazole resistance in Candida albicans biofilms: phase-specific role of efflux pumps and membrane sterols. Infection and immunity **71:**4333-4340.
52. **Ramage G, Bachmann S, Patterson TF, Wickes BL, Lopez-Ribot JL.** 2002. Investigation of multidrug efflux pumps in relation to fluconazole resistance in Candida albicans biofilms. The Journal of antimicrobial chemotherapy **49:**973-980.
53. **Andes D, Nett J, Oschel P, Albrecht R, Marchillo K, Pitula A.** 2004. Development and characterization of an in vivo central venous catheter Candida albicans biofilm model. Infection and immunity **72:**6023-6031.
54. **Pierce CG, Uppuluri P, Tristan AR, Wormley FL, Jr., Mowat E, Ramage G, Lopez-Ribot JL.** 2008. A simple and reproducible 96-well plate-based method for the formation of fungal biofilms and its application to antifungal susceptibility testing. Nature protocols **3:**1494-1500.
55. **Maiolo EM, Oliva A, Furustrand Tafin U, Perrotet N, Borens O, Trampuz A.** 2016. Antifungal activity against planktonic and biofilm Candida albicans in an experimental model of foreign-body infection. The Journal of infection **72:**386-392.
56. **Silva S, Henriques M, Oliveira R, Williams D, Azeredo J.** 2010. In vitro biofilm activity of non-Candida albicans Candida species. Current microbiology **61:**534-540.
57. **Kuhn DM, Chandra J, Mukherjee PK, Ghannoum MA.** 2002. Comparison of biofilms formed by Candida albicans and Candida parapsilosis on bioprosthetic surfaces. Infection and immunity **70:**878-888.
58. **Maiolo EM, Furustrand Tafin U, Borens O, Trampuz A.** 2014. Activities of fluconazole, caspofungin, anidulafungin, and amphotericin B on planktonic and biofilm Candida species determined by microcalorimetry. Antimicrobial agents and chemotherapy **58:**2709-2717.
59. **Nebenfuhr A, Ritzenthaler C, Robinson DG.** 2002. Brefeldin A: deciphering an enigmatic inhibitor of secretion. Plant physiology **130:**1102-1108.
60. **Baldauf SL, Palmer JD.** 1993. Animals and fungi are each other's closest relatives: congruent evidence from multiple proteins. Proceedings of the National Academy of Sciences of the United States of America **90:**11558-11562.
61. **Dalal CK, Zuleta IA, Mitchell KF, Andes DR, El-Samad H, Johnson AD.** 2016. Transcriptional rewiring over evolutionary timescales changes quantitative and qualitative properties of gene expression. eLife **5**.
62. **Ding C, Vidanes GM, Maguire SL, Guida A, Synnott JM, Andes DR, Butler G.** 2011. Conserved and divergent roles of Bcr1 and CFEM proteins in Candida parapsilosis and Candida albicans. PloS one **6:**e28151.
63. **Schwarzmuller T, Ma B, Hiller E, Istel F, Tscherner M, Brunke S, Ames L, Firon A, Green B, Cabral V, Marcet-Houben M, Jacobsen ID, Quintin J, Seider K, Frohner I, Glaser W, Jungwirth H, Bachellier-Bassi S, Chauvel M, Zeidler U, Ferrandon D, Gabaldon T, Hube B, d'Enfert C, Rupp S, Cormack B, Haynes K, Kuchler K.** 2014. Systematic phenotyping of a large-scale Candida glabrata deletion collection reveals novel antifungal tolerance genes. PLoS pathogens **10:**e1004211.
64. **Chang DC, Grant GB, O'Donnell K, Wannemuehler KA, Noble-Wang J, Rao CY, Jacobson LM, Crowell CS, Sneed RS, Lewis FM, Schaffzin JK, Kainer MA, Genese CA, Alfonso EC, Jones DB, Srinivasan A, Fridkin SK, Park BJ, Fusarium Keratitis Investigation T.** 2006. Multistate outbreak of Fusarium keratitis associated with use of a contact lens solution. Jama **296:**953-963.

65. **Istel F, Schwarzmuller T, Tscherner M, Kuchler K.** 2015. Genetic Transformation of Candida glabrata by Electroporation. Bio-protocol **5**.
66. **Mancera E, Porman AM, Cuomo CA, Bennett RJ, Johnson AD.** 2015. Finding a Missing Gene: EFG1 Regulates Morphogenesis in Candida tropicalis. G3 **5:**849-856.
67. **Ramage G, Vande Walle K, Wickes BL, Lopez-Ribot JL.** 2001. Standardized method for in vitro antifungal susceptibility testing of Candida albicans biofilms. Antimicrobial agents and chemotherapy **45:**2475-2479.
68. **Taff HT, Nett JE, Andes DR.** 2012. Comparative analysis of Candida biofilm quantitation assays. Medical mycology **50:**214-218.
69. **Nett JE, Cain MT, Crawford K, Andes DR.** 2011. Optimizing a Candida biofilm microtiter plate model for measurement of antifungal susceptibility by tetrazolium salt assay. Journal of clinical microbiology **49:**1426-1433.
70. **Ramage G, Lopez-Ribot JL.** 2005. Techniques for antifungal susceptibility testing of Candida albicans biofilms. Methods in molecular medicine **118:**71-79.
71. **Institute CLS.** 2007. Reference method for broth microdilution antifungal susceptibility testing of yeasts, 3rd edition. Approved standard M27-A3. , Clinical Laboratory Standards Institute. Clinical Laboratory Standards Institute, Wayne, PA.
72. **Dubois M, Gilles K, Hamilton JK, Rebers PA, Smith F.** 1951. A colorimetric method for the determination of sugars. Nature **168:**167.
73. **Smith PK, Krohn RI, Hermanson GT, Mallia AK, Gartner FH, Provenzano MD, Fujimoto EK, Goeke NM, Olson BJ, Klenk DC.** 1985. Measurement of protein using bicinchoninic acid. Analytical biochemistry **150:**76-85.
74. **Sandhu LC, Warters RL, Dethlefsen LA.** 1985. Fluorescence studies of Hoechst 33342 with supercoiled and relaxed plasmid pBR322 DNA. Cytometry **6:**191-194.
75. **Henry RJ, Blakeney AB, Harris PJ, Stone BA.** 1983. Detection of neutral and aminosugars from glycoproteins and polysaccharides as their alditol acetates. Journal of chromatography **256:**419-427.
76. **Sassaki GL, Gorin PA, Souza LM, Czelusniak PA, Iacomini M.** 2005. Rapid synthesis of partially O-methylated alditol acetate standards for GC-MS: some relative activities of hydroxyl groups of methyl glycopyranosides on Purdie methylation. Carbohydr Res **340:**731-739.
77. **Zarnowski R, Jaromin A, Certik M, Czabany T, Fontaine J, Jakubik T, Iqbal MC, Grandmougin-Ferjani A, Kozubek A, Pietr SJ.** 2004. The oil of Adenanthera pavonina L. seeds and its emulsions. Zeitschrift fur Naturforschung. C, Journal of biosciences **59:**321-326.
78. **Shibata N, Kobayashi H, Okawa Y, Suzuki S.** 2003. Existence of novel beta-1,2 linkage-containing side chain in the mannan of Candida lusitaniae, antigenically related to Candida albicans serotype A. European journal of biochemistry **270:**2565-2575.
79. **Shibata N, Suzuki A, Kobayashi H, Okawa Y.** 2007. Chemical structure of the cell-wall mannan of Candida albicans serotype A and its difference in yeast and hyphal forms. The Biochemical journal **404:**365-372.
80. **Shibata N, Okawa Y.** 2010. Enzymatic synthesis of new oligosaccharides using mannosyltransferases from Candida species and their NMR assignments. Biological & pharmaceutical bulletin **33:**895-899.
81. **Lowman DW, Ensley HE, Greene RR, Knagge KJ, Williams DL, Kruppa MD.** 2011. Mannan structural complexity is decreased when Candida albicans is cultivated in blood or serum at physiological temperature. Carbohydr Res **346:**2752-2759.
82. **Lowman DW, West LJ, Bearden DW, Wempe MF, Power TD, Ensley HE, Haynes K, Williams DL, Kruppa MD.** 2011. New insights into the structure of (1-->3,1-->6)-beta-D-glucan side chains in the Candida glabrata cell wall. PloS one **6:**e27614.

83. **Boyer RD, Johnson R, Krishnamurthy K.** 2003. Compensation of refocusing inefficiency with synchronized inversion sweep (CRISIS) in multiplicity-edited HSQC. J Magn Reson **165:**253-259.
84. **Downs JS, Arslanian S, de Bruin WB, Copeland VC, Doswell W, Herman W, Lain K, Mansfield J, Murray PJ, White N, Charron-Prochownik D.** 2010. Implications of type 2 diabetes on adolescent reproductive health risk: an expert model. Diabetes Educ **36:**911-919.

Figure Legends

Figure 1. NAC form biofilms with variable characteristics. (A) Biofilm adhesion of reference strains for *C. albicans, C. tropicalis, C. parapsilosis,* and *C. glabrata* was assessed using an XTT assay in a 96-well polystyrene plate assay after 1 hour for adherence. * reflects a statistically significant ($p<0.001$) lower concentration for *C. parapsilosis* and *C. glabrata* based upon ANOVA using the Holm-Sikak method for pairwise comparison. (B) Mature biofilm formation for each of the four species was quantified in a 96-well format using an XTT endpoint after 24 hours of incubation. * reflects a statistically significant ($p<0.001$) lower concentration for *C. glabrata* based upon ANOVA using the Holm-Sikak method for pairwise comparison. (C) Mature biofilm architecture of wild-type biofilms from in vitro coverslips and the in vivo rat catheter model was assessed visually using SEM imaging after 24 hours of incubation. The white arrow indicates extracellular matrix material and scale bars represent 20 µm.

Figure 2. NAC form biofilm matrix of variable quantity and quality. (A) Total biofilm mass was assessed by dry weight measurements from in vitro biofilms grown in polystyrene roller bottles (3 replicates of 20 bottles per species). * reflects a statistically significant ($p<0.001$) lower values for *C. tropicalis* and *C. glabrata* based upon ANOVA using the Holm-Sikak method for pairwise comparison. (B) Biofilm matrix biomass was quantified by dry weight following matrix separation from biofilm cells. Biofilms were grown in polystyrene roller bottles (3 replicates of 5 bottles per species). ** reflects a statistically lower values for *C. tropicalis* ($p=0.003$) and *C. glabrata* ($p=0.005$) difference between strains based upon ANOVA using the Holm-Sikak method for pairwise comparison. (C) Biofilm matrix total carbohydrate concentration was assessed using the phenol-sulfuric acid assay. The results were normalized by matrix biomass. * reflects a statistically lower concentrations for *C. parapsilosis* ($p=0.009$) and *C. glabrata* ($p=0.002$) based upon ANOVA using the Holm-Sikak method for pairwise comparison. (D) Relative percent

monosugar composition (Rha= rhamnose, Rib= ribose, Man= mannose, Glu= glucose) in the biofilm matrix of *C. albicans, C. tropicalis, C parapsilosis,* and *C. glabrata.* * reflects a statistically significant ($p<0.001$) difference between strains based upon ANOVA. (E) Biofilm matrix total protein concentration was assessed using the BCA. The results were normalized by matrix biomass. * reflects statistically lower concentrations for *C. tropicalis, C. parapsilosis,* and *C. glabrata* ($p<0.001$) compared to *C. albicans* based upon ANOVA using the Holm-Sikak method for pairwise comparison. (F) Biofilm matrix total eDNA. The results were normalized by matrix biomass. * reflects a statistically lower concentrations for *C. tropicalis, C. parapsilosis,* and *C. glabrata* ($p<0.001$) compared to *C. albicans* based upon ANOVA using the Holm-Sikak method for pairwise comparison. (G) Biofilm matrix total lipid concentration was assessed using gas chromatography. The results were normalized by matrix biomass. * reflects a statistically lower concentrations for *C. tropicalis, C. parapsilosis,* and *C. glabrata* compared to *C. albicans* based upon ANOVA using the Holm-Sikak method for pairwise comparison.

Figure 3. Comparative chromatographic fractionation and NMR analysis of carbohydrates from the *Candida* species biofilm extracellular matrix. (A) Comparison of the 500-MHz ^{1}H NMR spectra of purified neutral matrix polysaccharides from *C. albicans, C. tropicalis, C. parapsilosis,* and *C. glabrata* biofilm matrix. See Table 1. (B) Comparison of *C. albicans* NMR spectra spin systems to each of the NAC species (*C. tropicalis, C. parapsilosis,* and *C. glabrata,* respectively) as reflected by HSQC and NOESY data. (C) Carbohydrates in the matrix of WT biofilms treated with tunicamycin, and (D) α-mannosidase were quantified using gas chromatography. Data are presented as percentages of the reference strain, with mean and SEs shown. All values were significantly lower than the reference according to ANOVA as indicted by the *.

Figure 4. NAC biofilm drug resistance phenotype and mechanism. (A) Biofilm antifungal susceptibility (fluconazole 125 or 1000 µg/ml for 48h) of wild-type *C. albicans, C. tropicalis, C. parapsilosis,* and *C. glabrata* was assessed using an XTT assay in a 96-well polystyrene plate assay. * reflects a statistically significant ($p<0.001$) difference between strains based upon ANOVA using the Holm-Sikak method for pairwise comparison. (B) Biofilm antifungal susceptibility (fluconazole 250 µg/ml after 24h exposure) of wild-type *C. albicans, C. tropicalis, C. parapsilosis,* and *C. glabrata* was assessed using viable counts from the rat vascular catheter biofilm model. (C) Fluconazole sequestration and binding to the *Candida* species biofilm extracellular matrix. Sequestration of ^{3}H-labeled fluconazole was assessed using in vitro intact biofilms as well as the extracellular matrix and intracellular components. (D) Fluconazole binding to the NAC biofilm extracellular matrices. Fluconazole interactions with the tested matrices studied by one-dimensional ^{1}H NMR at 600 MHz were determined as decreasing of the intensity of chemical shift peaks characteristic of protons present either in the heterocyclic azole rings or the aromatic ring of the drug. Spectra were recorded at the constant fluconazole concentration of 0.653 mM and matrix concentrations ranged from 0 up to 8 mg/ml. (E) Biofilms were treated with pharmacological inhibitors of mannan or glucan or a mannan hydrolysis enzyme both with and without 1,000 µg/mL fluconazole for all species except *C. parapsilosis* for which we used 250 µg/mL. Efficacy was assessed in a 96-well plate format for quantification with the XTT assay. * reflects a statistically significant ($p<0.001$) difference between the combination and either treatment alone based upon ANOVA using the Holm-Sidak method for pairwise comparison.

Figure 5. Genetic control of NAC biofilm extracellular matrix production. Mature biofilm architecture from in vitro coverslips was assessed visually using SEM imaging after 24 hours of incubation. The white arrow indicates extracellular matrix material and scale bars represent 20 µm.

Figure 6. Genetic control of NAC biofilm drug resistance and extracellular matrix production. (A) The percent of reduction in biofilm formation following 48-h treatment with fluconazole compared with untreated biofilms, as quantified using the 96-well XTT assay. The null mutant (Δ/Δ) is shown for each gene of interest. The figure represents data from three assay replicates of a representative example of 3 biological replicates. * reflects a statistically significant ($p<0.001$) difference between reference and mutant based upon ANOVA using the Holm-Sidak method for pairwise comparison. The minimum inhibitory concentration (MIC) of fluconazole for planktonic cells of the Δ/Δ strains is shown below. (B) The NAC species reference strains, kre5Δ/Δ, van1Δ/Δ and big1 Δ/Δ mutants were tested in vivo using a rat central venous catheter model, with the effects of fluconazole or saline treatment compared with the reference strains for from *C. tropicalis, C. parapsilosis,* and *C. glabrata,* respectively. Biofilms were quantified using viable cell counts following treatment. The figure represents the mean and standard deviation from three replicates. The * symbol indicates CFUs were significantly different from the reference strain ($p<0.001$) based upon ANOVA using the Holm-Sikak method for pairwise comparison. (C) Intact biofilms grown from the reference and mutant strains were exposed to [^{3}H] fluconazole, washed, and harvested. Scintillation counting was performed in triplicate to determine the fluconazole content in the intact biofilms and the isolated matrix. Standard deviations are shown. (D) Mature in vitro biofilms from the reference strain and null mutants were assayed for matrix carbohydrate concentration using the phenol sulfuric acid method. The data with each mutant is presented as a percentage of quantity from the reference strain. The figure represents data from three biologic and three assay replicates. The * symbol indicates that glucan measurements were significantly different ($p<0.0001$) based upon ANOVA compared to the reference strain. (E) Mature in vitro biofilms from the reference strain and null mutants were assayed for matrix glucan and mannan concentrations by gas chromatography. The data with each mutant is presented as a percentage of quantity from the reference strain. The figure represents data from three biologic

and three assay replicates. The * symbol indicates that glucan measurements were significantly different ($p<0.0001$) based upon ANOVA compared to the reference strain.

Figure 1

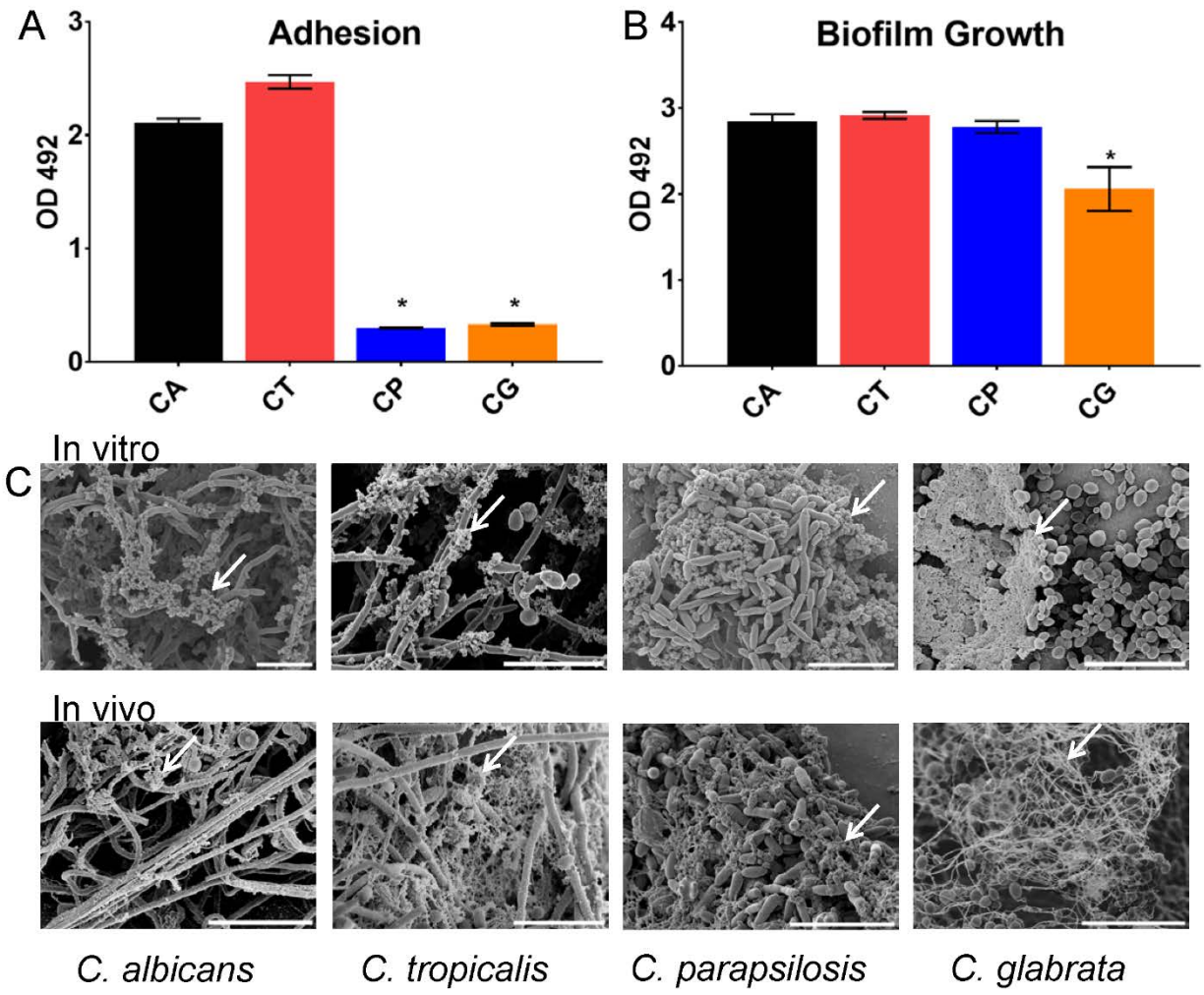
A
Adhesion
OD 492
0
1
2
3
CA
CT
CP
CG
*
*
B
Biofilm Growth
OD 492
0
1
2
3
4
CA
CT
CP
CG
*
C
In vitro
In vivo
C. albicans
C. tropicalis
C. parapsilosis
C. glabrata

Figure 2

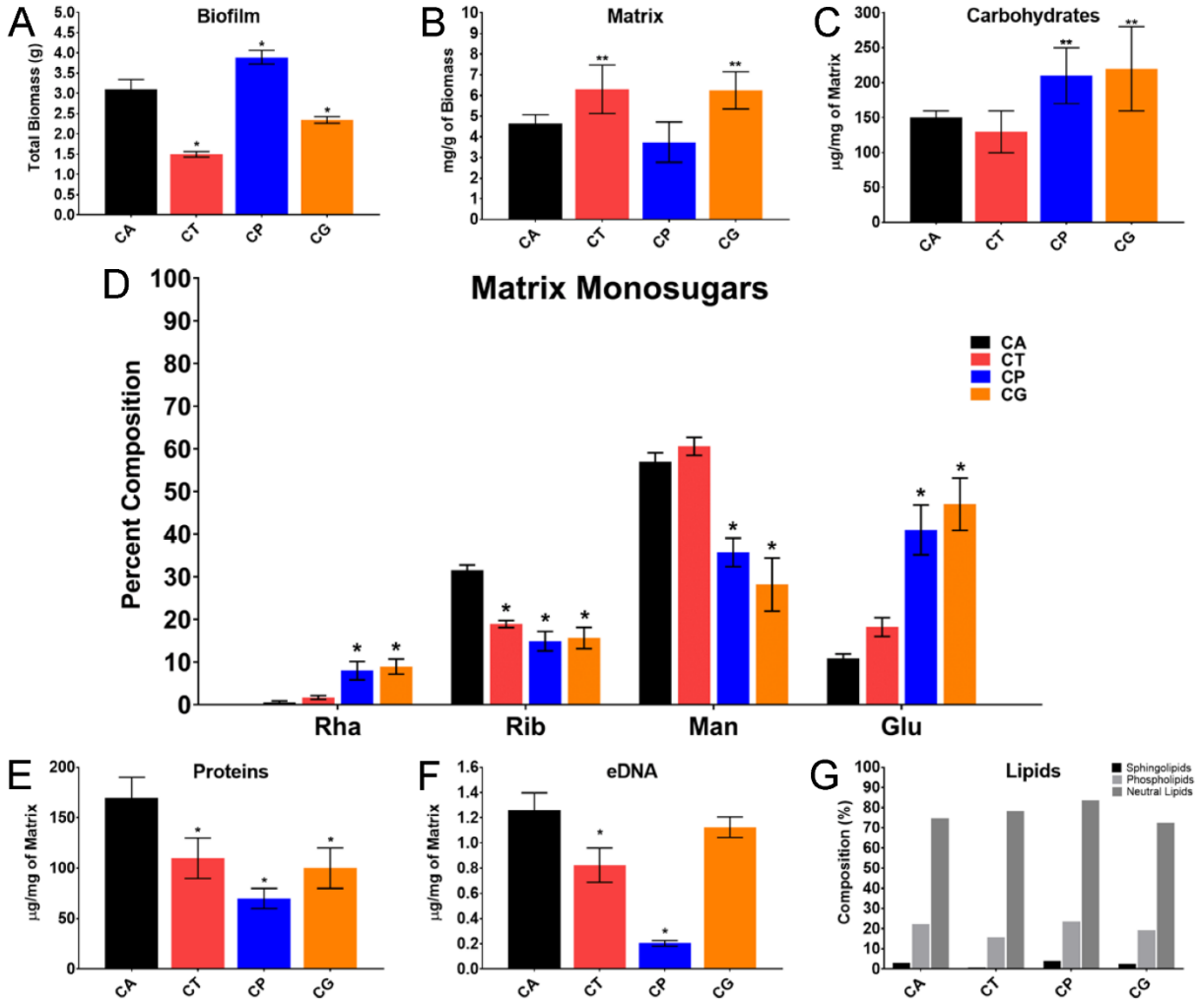
A
Biofilm
Total Biomass (g)
B
Matrix
mg/g of Biomass
C
Carbohydrates
µg/mg of Matrix
D
Matrix Monosugars
Percent Composition
CA
CT
CP
CG
Rha
Rib
Man
Glu
E
Proteins
µg/mg of Matrix
F
eDNA
µg/mg of Matrix
G
Lipids
Composition (%)
Sphingolipids
Phospholipids
Neutral Lipids

Figure 3

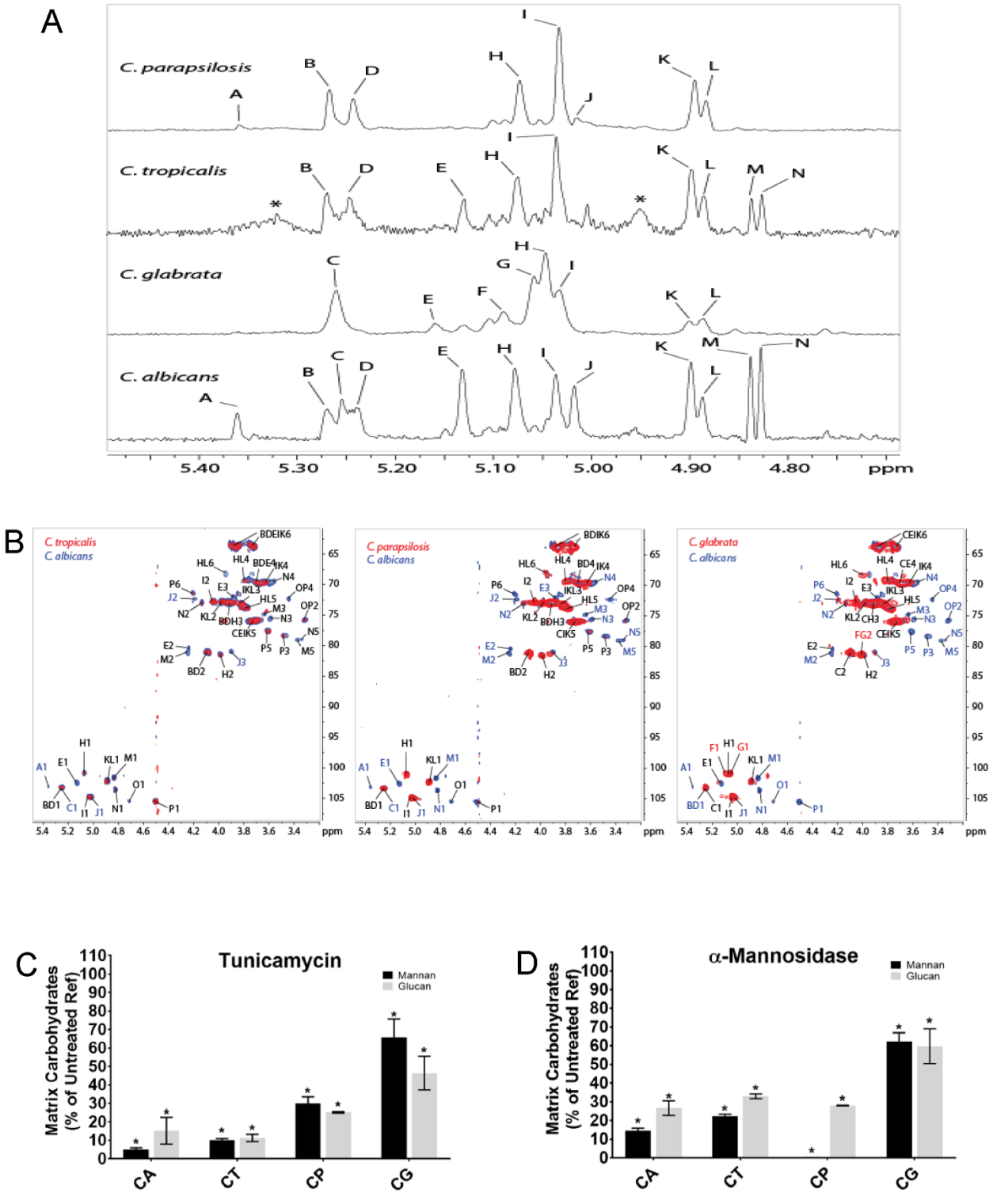
A
C. parapsilosis
C. tropicalis
C. glabrata
C. albicans
5.40
5.30
5.20
5.10
5.00
4.90
4.80
ppm
B
C. tropicalis
C. albicans
C. parapsilosis
C. albicans
C. glabrata
C. albicans
C
Tunicamycin
Mannan
Glucan
Matrix Carbohydrates (% of Untreated Ref)
CA
CT
CP
CG
D
α-Mannosidase
Mannan
Glucan
Matrix Carbohydrates (% of Untreated Ref)
CA
CT
CP
CG

Figure 4

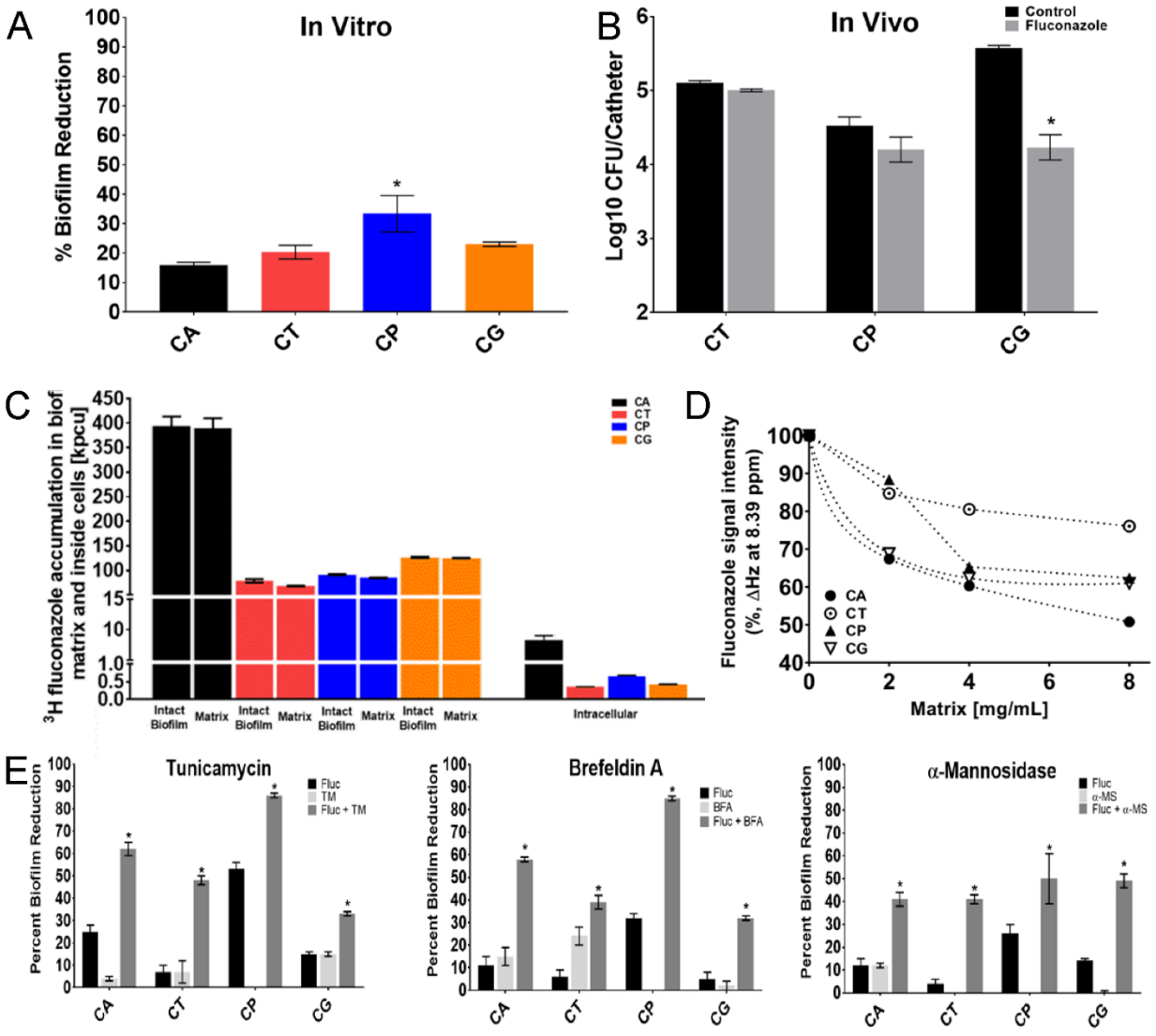
A
In Vitro
% Biofilm Reduction
CA
CT
CP
CG
B
In Vivo
Control
Fluconazole
Log10 CFU/Catheter
CT
CP
CG
C
CA
CT
CP
CG
Intact Biofilm
Matrix
Intracellular
D
Fluconazole signal intensity (%, ΔHz at 8.39 ppm)
Matrix [mg/mL]
E
Tunicamycin
Fluc
TM
Fluc + TM
Brefeldin A
BFA
Fluc + BFA
α-Mannosidase
α-MS
Fluc + α-MS
Percent Biofilm Reduction

Figure 5

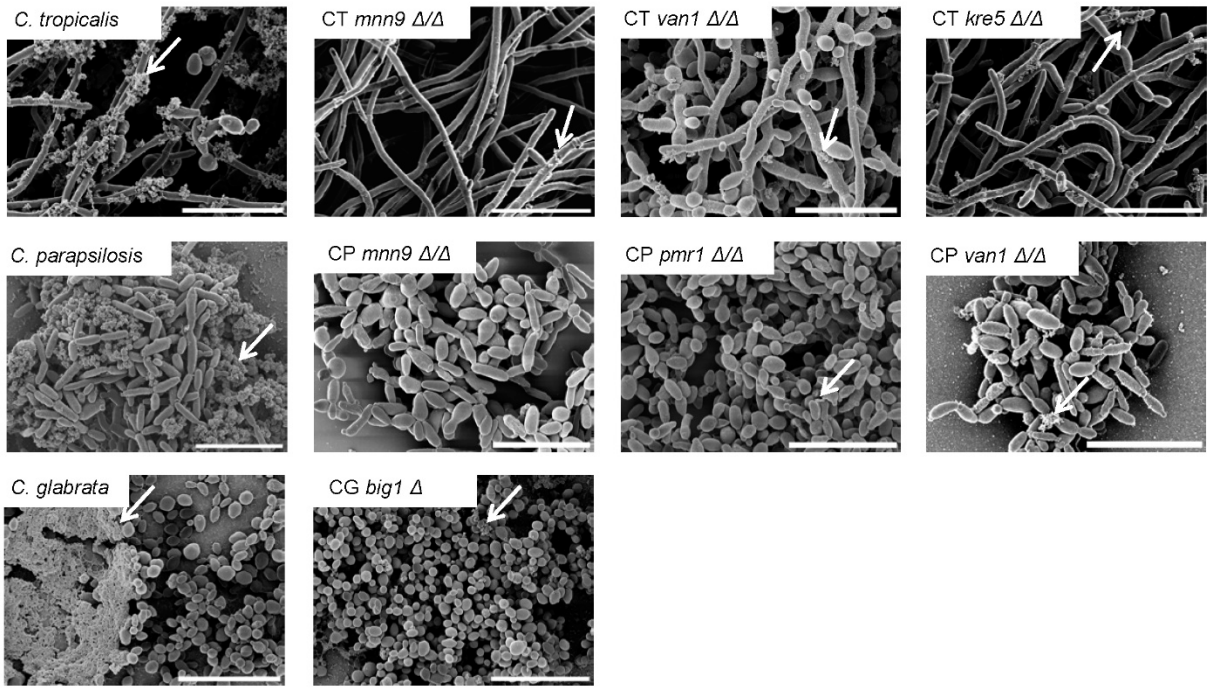
C. tropicalis
CT mnn9 Δ/Δ
CT van1 Δ/Δ
CT kre5 Δ/Δ
C. parapsilosis
CP mnn9 Δ/Δ
CP pmr1 Δ/Δ
CP van1 Δ/Δ
C. glabrata
CG big1 Δ

Figure 6

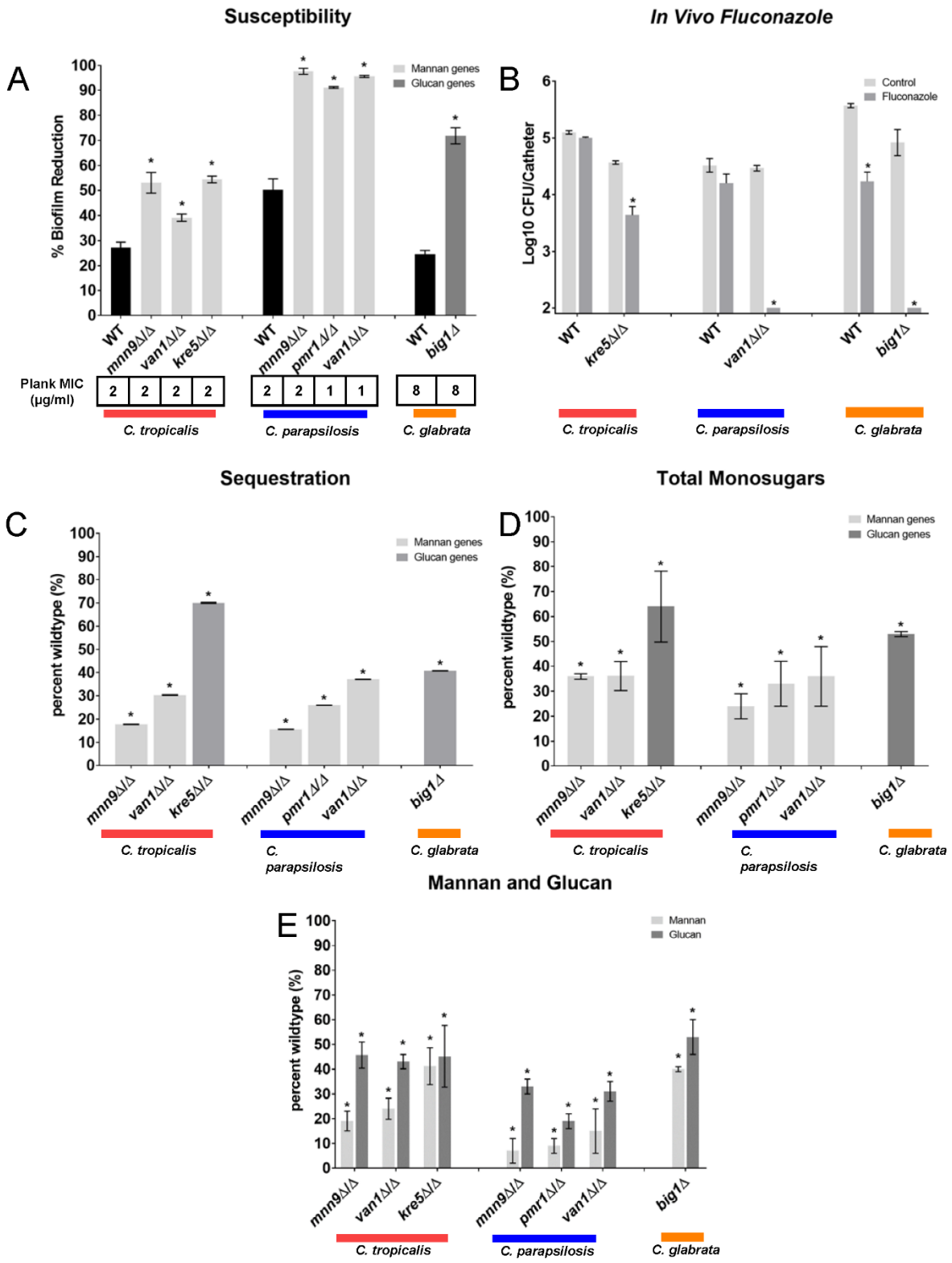
Susceptibility
A
% Biofilm Reduction
Mannan genes
Glucan genes
WT
mnn9Δ/Δ
van1Δ/Δ
kre5Δ/Δ
pmr1Δ/Δ
big1Δ
Plank MIC (μg/ml)
2 2 2 2
2 2 1 1
8 8
C. tropicalis
C. parapsilosis
C. glabrata
In Vivo Fluconazole
B
Log10 CFU/Catheter
Control
Fluconazole
Sequestration
C
percent wildtype (%)
Total Monosugars
D
Mannan and Glucan
E
Mannan
Glucan

Table 1. Percentages of the different residues found in each sample following 1D 1H-NMR. Blank cells indicate that the residue was not found. F 2 and F17 refer to high and low molecular weight MGCx previously reported in the biofilm matrix of *C. albicans* (40).

No.	Residue	CA	CG	CT	CP	F2	F17
i	β-1-2-Manα-1-P					1.8	
ii	α-1-2-Manα-1-P					1.8	0.4
A	α-1-2-Manα-1-3-	3.7			2.1	0.9	1.1
B	α-1-2-Manα-1-2-	4.3		9.5	11.5	5.4	
C	α-1-2-Manα-1-2-	7.2	21.8			7.1	14.1
D	α-1-2-Manα-1-2-	7.4		10.5	12.8	9.3	15.6
E	β-1-2-Manα-1-2-	11.9	5.7	9.1		13	4.1
F	2,6-Manα-1-6-(l)[a]		5.3				
G	2,6-Manα-1-6- (l)		15.1				1.6
H	2,6-Manα-1-6-(b)[b]	15.6	28.2	18.5	18.1	10.8	13.4
I	Manα-1-2-	13.5	14.1	23.7	29.1	10.6	20.9
J	3-Manα-1-2-	7.2			4.4		
K	Manα-1-6-	10.6	6.4	13.5	15.6	16.1	15.8
L	6-Manα-1-6-	6.4	3.5	7.2	6.3	2.4	6.6
M	β-1-2-Manβ-1-2-	5.4		3.7		10.3	3.2
N	Manβ-1-2-	6.7		4.4		10.3	3.2

CA = *C. albicans,* CG = *C. glabrata,* CT = *C.* tropicalis, CP = *C. parapsilosis*

[a] l denotes residues within a linear region, i. e. residues whose neighbors are not branching residues.

[b] b denotes residues within a branched region, i. e. residues whose neighbors are branching residues.

Table 2. Carbohydrate distribution in *Candida* species matrix following neutral sugar purification and fractionation.

Candida species	Carbohydrate type				
	Bound	Neutral			
	[%]	[%]	MWF	Man:Glu ratio	Content [%]
CT	86.5	13.5	HMWF	72:28	2.6
			HMWF	19:81	4.3
			LMWF	73:27	0.9
CP	65.2	34.8	HMWF	13:87	20.9
			LMWF	10:90	13.9
CG	83.0	17.0	HMWF	95:5	0.4
			HMWF	82:18	1.0
			HMWF	61:39	1.6
			HMWF	52:48	3.4
			HMWF	27:73	0.8
			LMWF	80:20	1.1
			LMWF	50:50	1.7

CT= *C. tropicalis,* CP= *C. parapsilosis,* CG= *C. glabrata,* HMWF= high molecular weight fraction, LMWF= low molecular weight fraction* Carbohydrate type indicates whether carbohydrate is either associated with the uncharged neutral fraction or the charged bound fraction (glycoproteins). MWF indicates molecular weight type for each isolated polymer within the neutral carbohydrate pool, whereas HMWF and LMWF indicate high molecular weight fraction and low molecular weight fraction, respectively. Values are percentages of the listed fractions in the total matrix carbohydrate pool.

Table 3. *C. tropicalis, C. parapsilosis,* and *C. glabrata* mutant strains used in this study.

C. tropicalis

Gene name	Systemic name	Genotype	Strain name	Description*	Homology**
MNN9	CTRG_02261	Δ/Δ	URZ565	α-1,6 Mannosyltransferase	85.6
MNN11	CTRG_04663	Δ/Δ	URZ567	α-1,6 Mannosyltransferase	67.9
VAN1	CTRG_05614	Δ/Δ	URZ570	α-1,6 Mannosyltransferase	94.4
MNN4-4	CTRG_05766	Δ/Δ	URZ566	Mannosylphosphate transferase	55.2
PMR1	CTRG_04916	Δ/Δ	URZ569	Ca^{2+}/Mn^{2+} ATPase	88.2
XOG1	CTRG_04334	Δ/Δ	URZ571	β-1,3 Glucanase	75.8
BGL2	CTRG_00169	Δ/Δ	URZ562	β-1,3 Glucosyltransferase	61.5
PHR1	CTRG_03942	Δ/Δ	URZ568	β-1,3 Glucosyltransferase	75.2
BIG1	CTRG_04070	Δ/Δ	URZ563	β-1,6 Glucan Synthesis	70.3
KRE5	CTRG_02572	Δ/Δ	URZ564	β-1,6 Glucan Synthesis	65.7

C. parapsilosis

Gene name	Systemic name	Genotype	Strain name	Description*	Homology**
ALG11	CPAR2_601300	Δ/Δ	EGD136	α-1,2 Mannosyltransferase	58.4
MNN9	CPAR2_806810	Δ/Δ	EGD194	α-1,6 Mannosyltransferase	78.2
MNN11	CPAR2_106380	Δ/Δ	EGD144	α-1,6 Mannosyltransferase	55.9
VAN1	CPAR2_807920	Δ/Δ	EGD184	α-1,6 Mannosyltransferase	73.7
MNN4-4	CPAR2_106570	Δ/Δ	EGD149	Mannosylphosphate transferase	36.0
PMR1	CPAR2_31360	Δ/Δ	EGD141	Ca^{2+}/Mn^{2+} ATPase	82.7
XOG1	CPAR2_106000	Δ/Δ	EGD150	β-1,3 Glucanase	64.2
BGL2	CPAR2_401600	Δ/Δ	EGD147	β-1,3 Glucosyltransferase	72.7
PHR1	CPAR2_302140	Δ/Δ	EGD188	β-1,3 Glucosyltransferase	59.7

C. glabrata

Gene name	Systemic name	Genotype	Strain name	Description*	Homology**
ALG11	CAGL0D01122g	Δ	EGD125	α-1,2 Mannosyltransferase	29.5
MNN9	CAGL0L12804g	Δ	EGD128	α-1,6 Mannosyltransferase	52.4
MNN11	CAGL0G07491g	Δ	EGD124	α-1,6 Mannosyltransferase	25.7

VAN1	CAGL0B02321g	Δ	EGD137	α-1,6 Mannosyltransferase	49.4
MNN4-4	CAGL0H01793g	Δ	EGD121	Mannosylphosphate transferase	26.4
PMR1	CAGL0J01870g	Δ	EGD143	Ca^{2+}/Mn^{2+} ATPase	60.0
XOG1	CAGL0G09515g	Δ	EGD134	β-1,3 Glucanase	52.2
BGL2	CAGL0G00220g	Δ	EGD127	β-1,3 Glucosyltransferase	65.3
PHR1(GAS2)	CAGL0M13849g	Δ	EGD131	β-1,3 Glucosyltransferase	57.1
BIG1	CAGL0L11528g	Δ	EGD129	β-1,6 Glucan Synthesis	23.2

*Based on *Candida* or *Saccharomyces* Genome Database.

**Protein Sequence Alignment to *Candida albicans* (percent)

Supporting Information Legends

Figure S1. Planktonic cell growth following pharmacologic and enzymatic treatments. Planktonic cells were grown in 96-well round bottom plates for 24 h and quantified using XTT. For experiments with TM (at 1.0 μg/ml) and BFA (at 0.6 μg/ml), biofilms or cells were grown for 6 h and then treated for 24 h before quantification. Experiments with α-mannosidase (α-MS; at 0.78 U/ml) used biofilms or cells first grown for 24 h before 24-h treatment. The mean of three technical replicates and SEs are shown.

Figure S2. Biofilm formation capacity for non-albicans *Candida* mutants in the mannan and glucan pathways. Mature biofilm burden for each of the select deletion mutants was quantified in a 96-well format using an XTT endpoint after 24 hours of incubation. * reflects a statistically significant ($p<0.001$) difference between strains based upon ANOVA.

Figure S3. NAC biofilm drug susceptibility in mutants without an enhanced susceptibility phenotype. (A-C) The percent of reduction in biofilm formation following 48-h treatment with fluconazole compared with untreated biofilms, as quantified using the 96-well XTT assay. The null mutant (Δ/Δ) is shown for each gene of interest. The figure represents data from three assay replicates of a representative example of 3 biological replicates. * reflects a statistically significant ($p<0.001$) difference between reference and mutant based upon ANOVA using the Holm-Sikak method for pairwise comparison.

Figure S4. Polyene and echinocandin biofilm activity against fluconazole-susceptible NAC mutants. Following growth for 6 h, biofilms were treated with either 0.5 μg/ml amphotericin B or micafungin for 48 h. Biofilms were quantified using the 96-well XTT assay, and reduction was

determined by comparing treated and untreated biofilms. All mutants were significantly more susceptible to treatment than the referent strain (*P < 0.001, **P < 0.05). The mean of three technical replicates and SEs are shown.

Figure S5. Complemented *C. tropical* and *C. glabrata* glucan and mannan synthesis mutant biofilms are susceptible to fluconazole. Following growth for 6 h, biofilms were treated with 1,000 μg/ml fluconazole for 48 h. Biofilms were quantified using the 96-well XTT assay, and reduction was determined by comparing treated and untreated biofilms. All mutants were significantly more susceptible to treatment than the referent strain (P < 0.001). Each of the complemented strains exhibited resistance similar to the reference strains. The mean of three technical replicates and SEs are shown.

Figure S6. Multiple independent transformants of noncomplemented mutant strains are susceptible to fluconazole. Following growth for 6 h, biofilms were treated with 1,000 μg/ml fluconazole for 48 h. Biofilms were quantified using the 96-well XTT assay, and reduction was determined by comparing treated and untreated biofilms. Two or three independent transformants were tested for each homozygous deletion mutant. All mutants were significantly more susceptible to treatment than the referent strain (P < 0.001). A different biological replicate is presented here than in Figure 5A. The mean of three technical replicates and SEs are shown.

Figure S1

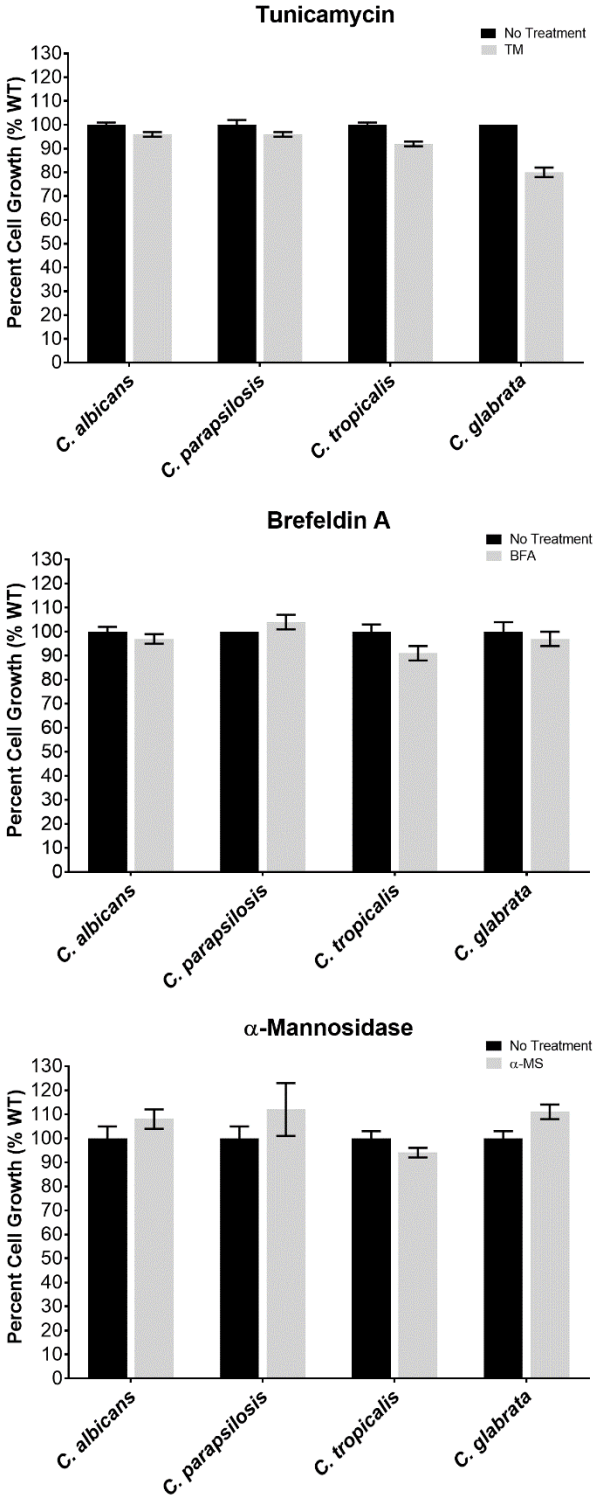
Tunicamycin
No Treatment
TM
Percent Cell Growth (% WT)
C. albicans
C. parapsilosis
C. tropicalis
C. glabrata
Brefeldin A
No Treatment
BFA
Percent Cell Growth (% WT)
C. albicans
C. parapsilosis
C. tropicalis
C. glabrata
α-Mannosidase
No Treatment
α-MS
Percent Cell Growth (% WT)
C. albicans
C. parapsilosis
C. tropicalis
C. glabrata

Figure S2

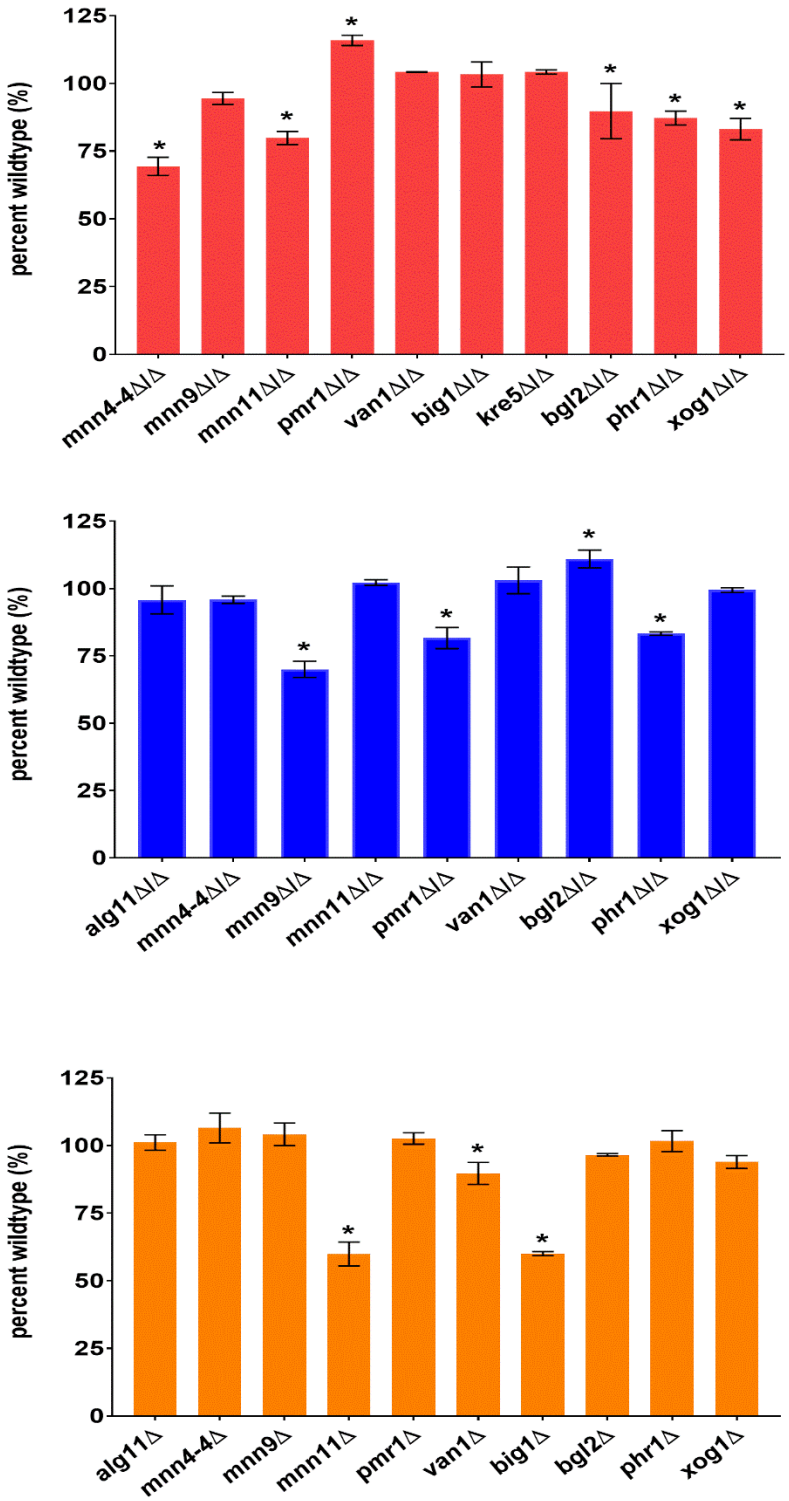
percent wildtype (%)
125
100
75
50
25
0
mnn4-4Δ/Δ
mnn9Δ/Δ
mnn11Δ/Δ
pmr1Δ/Δ
van1Δ/Δ
big1Δ/Δ
kre5Δ/Δ
bgl2Δ/Δ
phr1Δ/Δ
xog1Δ/Δ
percent wildtype (%)
125
100
75
50
25
0
alg11Δ/Δ
mnn4-4Δ/Δ
mnn9Δ/Δ
mnn11Δ/Δ
pmr1Δ/Δ
van1Δ/Δ
bgl2Δ/Δ
phr1Δ/Δ
xog1Δ/Δ
percent wildtype (%)
125
100
75
50
25
0
alg11Δ
mnn4-4Δ
mnn9Δ
mnn11Δ
pmr1Δ
van1Δ
big1Δ
bgl2Δ
phr1Δ
xog1Δ

Figure S3

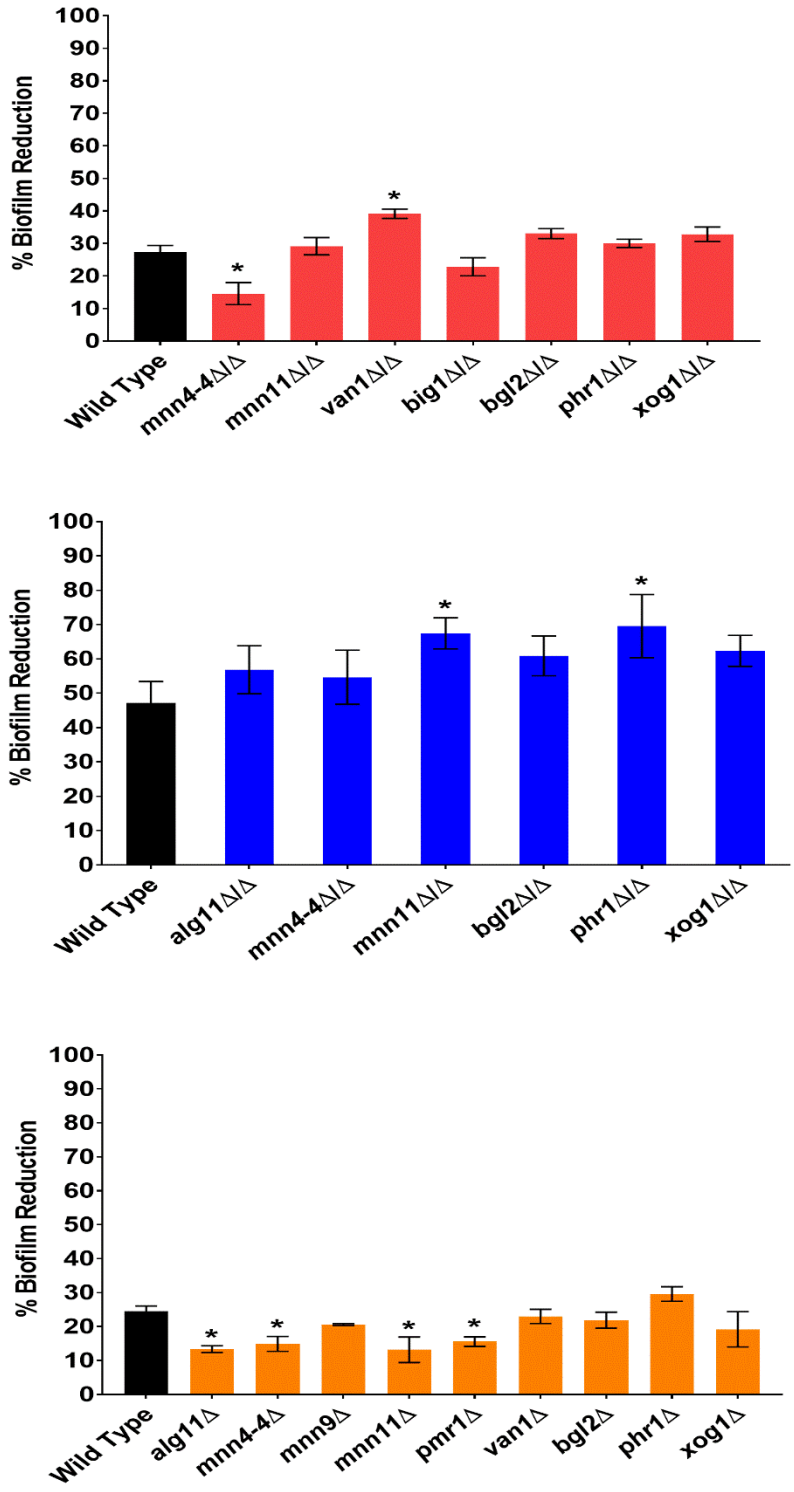
% Biofilm Reduction
100
90
80
70
60
50
40
30
20
10
0
*
*
Wild Type
mnn4-4ΔlΔ
mnn11ΔlΔ
van1ΔlΔ
big1ΔlΔ
bgl2ΔlΔ
phr1ΔlΔ
xog1ΔlΔ
% Biofilm Reduction
100
90
80
70
60
50
40
30
20
10
0
*
*
Wild Type
alg11ΔlΔ
mnn4-4ΔlΔ
mnn11ΔlΔ
bgl2ΔlΔ
phr1ΔlΔ
xog1ΔlΔ
% Biofilm Reduction
100
90
80
70
60
50
40
30
20
10
0
*
*
*
*
Wild Type
alg11Δ
mnn4-4Δ
mnn9Δ
mnn11Δ
pmr1Δ
van1Δ
bgl2Δ
phr1Δ
xog1Δ

Figure S4

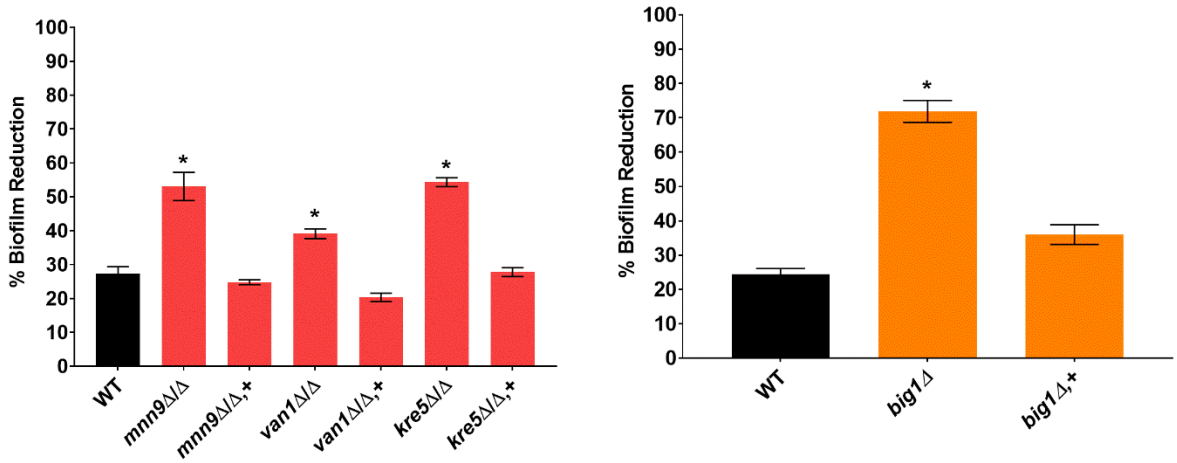
% Biofilm Reduction
100
90
80
70
60
50
40
30
20
10
0
*
*
*
WT
mnn9Δ/Δ
mnn9Δ/Δ,+
van1Δ/Δ
van1Δ/Δ,+
kre5Δ/Δ
kre5Δ/Δ,+
% Biofilm Reduction
100
90
80
70
60
50
40
30
20
10
0
*
WT
big1Δ
big1Δ,+

Figure S5

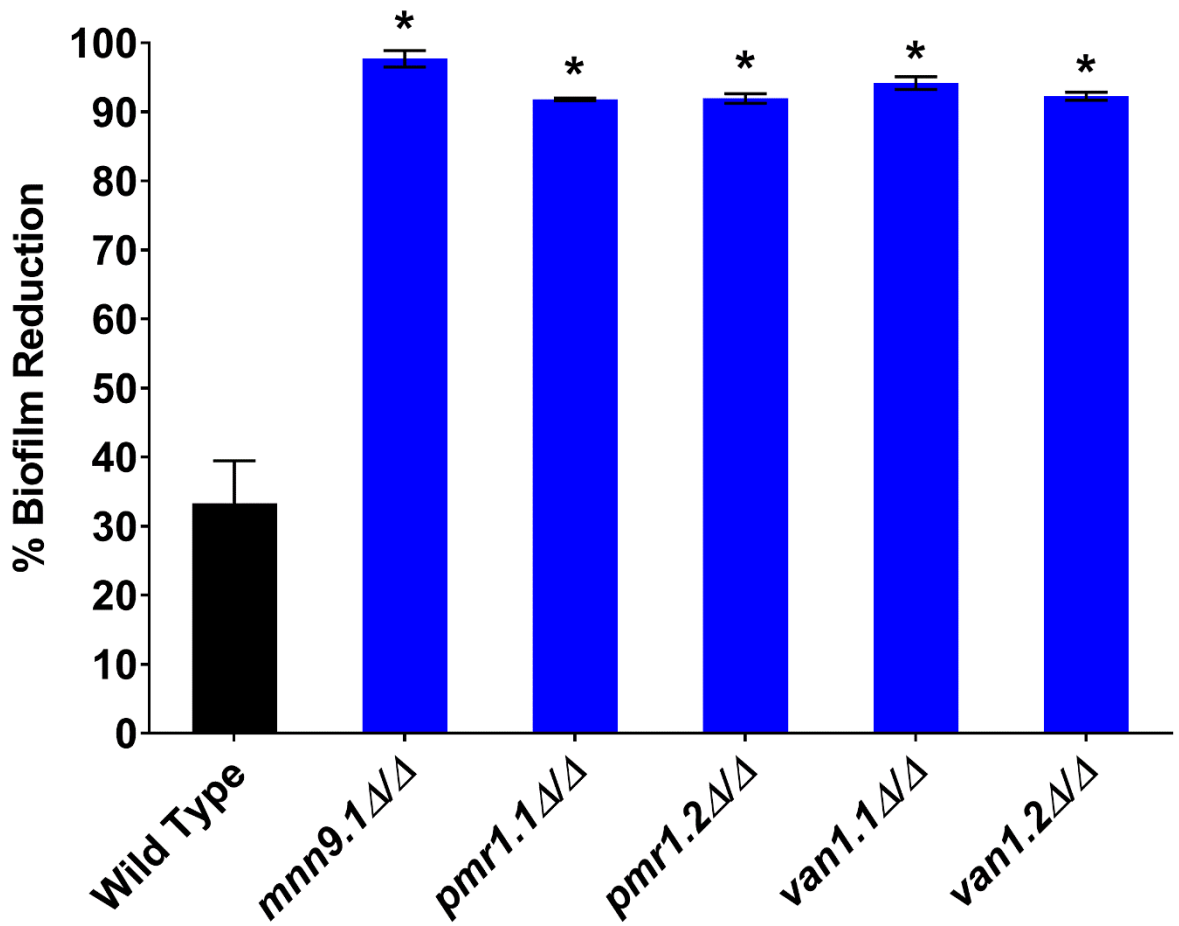
% Biofilm Reduction
100
90
80
70
60
50
40
30
20
10
0
*
*
*
*
*
Wild Type
mnn9.1Δ/Δ
pmr1.1Δ/Δ
pmr1.2Δ/Δ
van1.1Δ/Δ
van1.2Δ/Δ

Figure S6

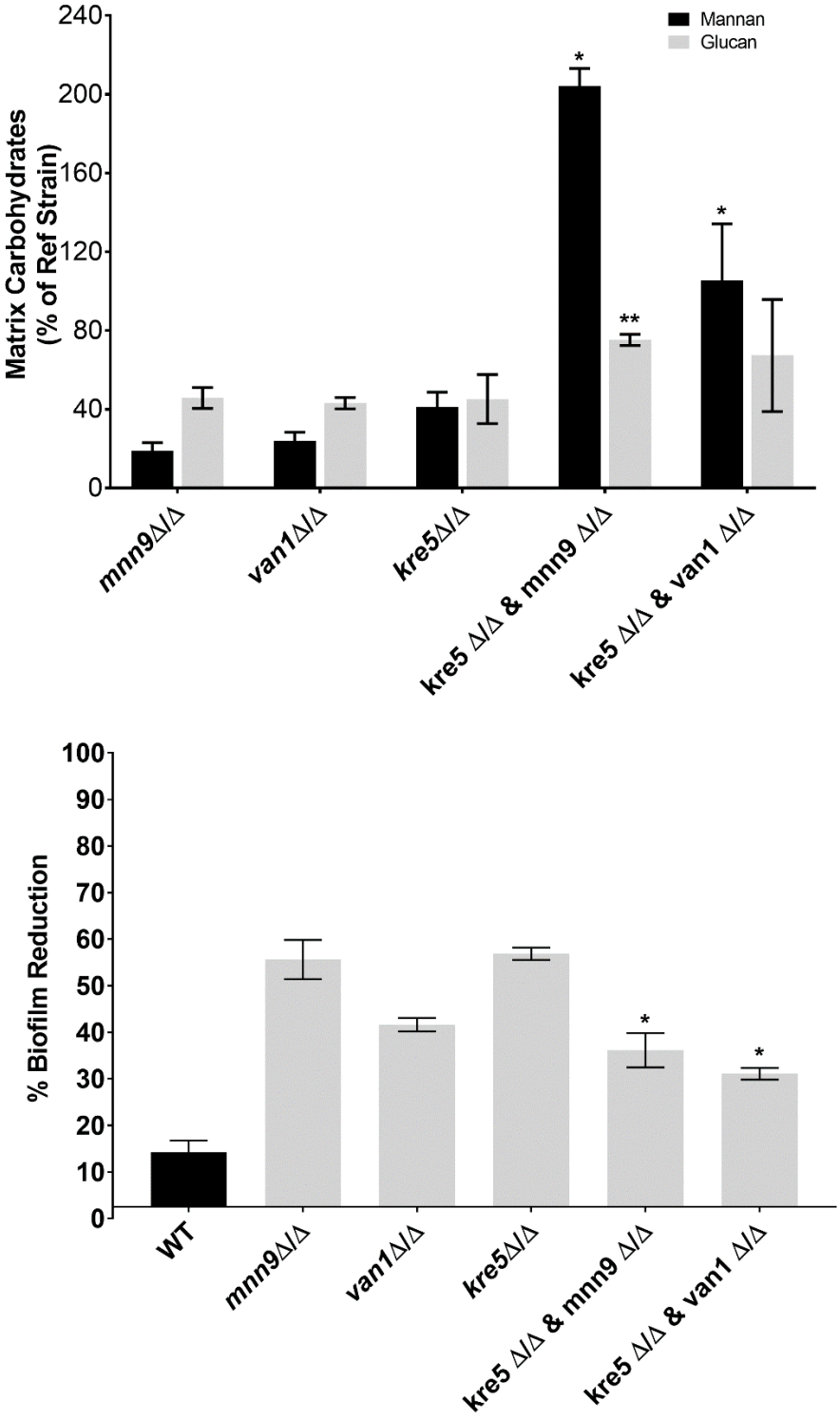
Mannan
Glucan
Matrix Carbohydrates (% of Ref Strain)
240
200
160
120
80
40
0
*
**
*
mnn9Δ/Δ
van1Δ/Δ
kre5Δ/Δ
kre5 Δ/Δ & mnn9 Δ/Δ
kre5 Δ/Δ & van1 Δ/Δ
% Biofilm Reduction
100
90
80
70
60
50
40
30
20
10
0
*
*
WT
mnn9Δ/Δ
van1Δ/Δ
kre5Δ/Δ
kre5 Δ/Δ & mnn9 Δ/Δ
kre5 Δ/Δ & van1 Δ/Δ

Table S1. 2D HSQC NMR **c**hemical shift assignment of the major spin systems found in *C. albicans, C. glabrata, C. tropicalis,* and *C. parapsilosis*

Candida albicans

No.	Residue	Chemical shift (ppm)						
		1	**2**	**3**	**4**	**5**	**6**	**6'**
A	α-1-2-Manα-1-3-	5.36	4.08	3.98	3.76	3.76	3.86	3.73
		103.2	*81.2*	*72.9*	*69.2*	*76.1*	*63.8*	
B	α-1-2-Manα-1-2-	5.26	4.09	3.94	3.74	3.69	3.86	3.73
		103.3	*81.2*	*72.9*	*69.2*	*76.0*	*63.8*	
C	α-1-2-Manα-1-2-	5.25	4.10	3.95	3.73	3.75	3.87	3.74
		103.3	*81.2*	*72.9*	*69.2*	*76.0*	*64.0*	
D	α-1-2-Manα-1-2-	5.24	4.08	3.89	3.70	3.72	3.86	3.73
		103.3	*81.2*	*73.1*	*69.2*	*76.1*	*63.8*	
E	β-1-2-Manα-1-2-	5.13	4.24	3.85	3.61	3.72	3.86	3.73
		102.8	*80.5*	*73.1*	*69.7*	*76.1*	*63.8*	
F	2,6-Manα-1-6- (l)							
G	2,6-Manα-1-6- (l)							
H	2,6-Manα-1-6- (b)	5.07	4.00	3.93	3.78	3.80	3.95	3.74
		101.0	*73.0*	*73.0*	*69.3*	*73.6*	*68.4*	
I	Manα-1-2-	5.03	4.05	3.83	3.64	3.74	3.86	3.73
		104.9	*72.9*	*73.2*	*69.7*	*76.1*	*63.8*	
J	3-Manα-1-2-	5.01	4.21	3.91	3.77	3.77	3.86	3.73
		104.9	*72.4*	*81.0*	*69.1*	*76.0*	*63.8*	
K	Manα-1-6-	4.90	3.98	3.80	3.76	3.67	3.86	3.73
		102.3	*73.0*	*73.4*	*69.4*	*75.7*	*63.8*	
L	6-Manα-1-6-	4.89	3.99	3.83	3.76	3.78	3.95	3.74
		102.3	*73.0*	*73.3*	*69.4*	*73.9*	*68.4*	
M	β-1-2-Manβ-1-2-	4.84	4.25	3.66	3.60	3.39	3.74	
		101.8	*81.3*	*74.9*	*69.6*	*79.1*	*63.8*	
N	Manβ-1-2-	4.83	4.13	3.60	3.58	3.35	3.89	3.74
		103.7	*73.0*	*75.6*	*69.6*	*79.1*	*63.8*	
O	Glcβ-1-6	4.72	3.35	3.50	3.44	3.47	3.84	3.75
		105.6	*76.1*	*78.5*	*72.5*	*78.5*	*63.6*	
P	β-1-6-Glcβ-1-6	4.51	3.32	3.47	3.44	3.60	4.20	3.85
		105.6	*75.8*	*78.5*	*72.4*	*77.6*	*71.4*	

Candida glabrata

No.	Residue	Chemical shift (ppm)						
		1	**2**	**3**	**4**	**5**	**6**	**6'**
A	α-1-2-Manα-1-3-							
B	α-1-2-Manα-1-2-							
C	α-1-2-Manα-1-2-	5.25	4.09	3.89	3.71	3.75	3.87	3.74
		103.2	*81.2*	*73.1*	*69.8*	*76.0*	*64.0*	
D	α-1-2-Manα-1-2-							
E	β-1-2-Manα-1-2-	5.16	4.26	3.85	3.76			
		102.6	*80.6*	*72.2*	*69.4*			
F	2,6-Manα-1-6- (l)	5.10	4.00					
		100.9	*81.4*					
G	2,6-Manα-1-6- (l)	5.06	4.02					
		101.1	*81.4*					
H	2,6-Manα-1-6- (b)	5.05	4.00	3.90		3.76	3.95	3.74
		101.0	*81.4*	*73.2*		*73.9*	*68.3*	
I	Manα-1-2-	5.04	4.05	3.83	3.64	3.74	3.87	3.74
		104.9	*73.0*	*73.2*	*69.7*	*76.0*	*64.0*	
J	3-Manα-1-2-							
K	Manα-1-6-	4.90	3.98	3.82				
		102.3	*72.9*	*73.2*				
L	6-Manα-1-6-	4.88	3.97	3.82			4.00	3.68
		102.2	*72.9*	*73.2*			*68.5*	
M	β-1-2-Manβ-1-2-							
N	Manβ-1-2-							
O	Glcβ-1-6							
P	β-1-6-Glcβ-1-6							

Candida tropicalis

No.	Residue	Chemical shift (ppm)						
		1	**2**	**3**	**4**	**5**	**6**	**6'**
A	α-1-2-Manα-1-3-							
B	α-1-2-Manα-1-2-	5.27	4.09	3.94	3.72	3.72	3.86	3.73
		103.3	*81.2*	*73.0*	*69.2*	*76.1*	*63.8*	
C	α-1-2-Manα-1-2-							
D	α-1-2-Manα-1-2-	5.25	4.08	3.89	3.70	3.72	3.86	3.73
		103.3	*81.2*	*73.1*	*69.2*	*76.1*	*63.8*	
E	β-1-2-Manα-1-2-	5.13	4.24	3.85	3.61	3.72	3.86	3.73
		102.8	*80.5*	*73.1*	*69.7*	*76.1*	*63.8*	
F	2,6-Manα-1-6- (l)							
G	2,6-Manα-1-6- (l)							
H	2,6-Manα-1-6- (b)	5.07	4.00	3.93	3.78	3.80	3.95	3.74
		101.0	*73.0*	*73.0*	*69.3*	*73.6*	*68.4*	
I	Manα-1-2-	5.03	4.05	3.83	3.64	3.74	3.86	3.73
		104.9	*72.9*	*73.2*	*69.7*	*76.1*	*63.8*	
J	3-Manα-1-2-							
K	Manα-1-6-	4.90	3.98	3.80				
		102.3	*73.0*	*73.4*				
L	6-Manα-1-6-	4.89	3.99					
		102.3	*73.0*					
M	β-1-2-Manβ-1-2-	4.83	4.25					
		101.7	*81.2*					
N	Manβ-1-2-	4.82	4.14					
		103.7	*73.1*					
O	Glcβ-1-6	4.72	3.35	3.50	3.44	3.47	3.84	3.75
			76.1	*78.5*	*72.5*	*78.5*	*63.6*	
P	β-1-6-Glcβ-1-6	4.51	3.32	3.48	3.44	3.61	4.21	3.85
		105.6	*76.0*	*78.5*	*72.5*	*77.7*	*71.6*	

Candida parapsilosis

No.	Residue	Chemical shift (ppm)						
		1	**2**	**3**	**4**	**5**	**6**	**6'**
A	α-1-2-Manα-1-3-	5.36	4.08					
		103.3	*81.3*					
B	α-1-2-Manα-1-2-	5.27	4.09	3.92	3.72	3.72	3.86	3.73
		103.4	*81.2*	*73.0*	*69.5*	*76.1*	*63.8*	
C	α-1-2-Manα-1-2-							
D	α-1-2-Manα-1-2-	5.25	4.08	3.89	3.69	3.72	3.86	3.73
		103.4	*81.2*	*72.9*	*69.9*	*76.1*	*63.8*	
E	β-1-2-Manα-1-2-							
F	2,6-Manα-1-6- (l)							
G	2,6-Manα-1-6- (l)							
H	2,6-Manα-1-6- (b)	5.08	3.98	3.92	3.78	3.78	3.95	3.74
		101.1	*81.6*	*73.0*	*69.4*	*73.8*	*68.4*	
I	Manα-1-2-	5.04	4.05	3.83	3.64	3.74	3.86	3.73
		104.9	*72.8*	*73.4*	*69.8*	*76.1*	*63.8*	
J	3-Manα-1-2-	5.02	4.19	3.92	3.78	3.77	3.85	3.74
		104.9	*72.7*	*81.2*	*69.5*	*76.0*	*63.8*	
K	Manα-1-6-	4.90	3.98	3.80	3.67	3.75	3.86	3.73
		102.4	*72.9*	*73.9*	*69.7*	*76.0*	*63.8*	
L	6-Manα-1-6-	4.88	3.97	3.82	3.78	3.78	3.95	3.74
		102.2	*72.9*	*73.6*	*69.4*	*73.8*	*68.4*	
M	β-1-2-Manβ-1-2-							
N	Manβ-1-2-							
O	Glcβ-1-6	4.70	3.35	3.50	3.41	3.47	3.83	3.75
		105.7	*75.9*	*78.5*	*72.4*	*78.5*	*63.4*	
P	β-1-6-Glcβ-1-6	4.50	3.31	3.49	3.41	3.61	4.21	3.85
		105.7	*75.8*	*78.5*	*72.4*	*77.6*	*71.6*	

Table S2. *C. tropicalis, C. parapsilosis,* and *C. glabrata* mutant strains developed in this study. List of genes under study, the strain names, and strain genotypes for strains constructed and utilized in these studies.

C. tropicalis

Gene	Strain	Genotype	Source
Reference	CAY2597	*C. tropicalis* wild type strain	(Ref 5)
Reference	CAY3764	*his1Δ::FRT/his1Δ::FRT, leu2Δ::FRT/leu2Δ::FRT*	(Ref 5)
big1 $^{-/-}$	EGD192	*his1Δ::FRT/his1Δ::FRT, leu2Δ::FRT/leu2Δ::FRT, big1::C.m LEU2/big1::C.d HIS1*	This study
bgl2 $^{-/-}$	EGD151	*his1Δ::FRT/his1Δ::FRT, leu2Δ::FRT/leu2Δ::FRT, bgl2::C.m LEU2/bgl2::C.d HIS1*	This study
bgl2 $^{-/-}$	EGD152	*his1Δ::FRT/his1Δ::FRT, leu2Δ::FRT/leu2Δ::FRT, bgl2::C.m LEU2/bgl2::C.d HIS1*	This study
kre5 $^{-/-}$	EGD186	*his1Δ::FRT/his1Δ::FRT, leu2Δ::FRT/leu2Δ::FRT, kre5::C.m LEU2/kre5::C.d HIS1*	This study
kre5 $^{-/-}$	EGD187	*his1Δ::FRT/his1Δ::FRT, leu2Δ::FRT/leu2Δ::FRT, kre5::C.m LEU2/kre5::C.d HIS1*	This study
kre5 $^{-/-}$,+	URZ492	*his1Δ::FRT/his1Δ::FRT, leu2Δ::FRT/leu2Δ::FRT, kre5::C.m LEU2/kre5::C.d HIS1,C.m leu2::KRE5-NAT1*	This study
mnn4-4 $^{-/-}$	EGD155	*his1Δ::FRT/his1Δ::FRT, leu2Δ::FRT/leu2Δ::FRT, mnn4-4::C.m LEU2/mnn4-4::C.d HIS1*	This study
mnn4-4 $^{-/-}$	EGD157	*his1Δ::FRT/his1Δ::FRT, leu2Δ::FRT/leu2Δ::FRT, mnn4-4::C.m LEU2/mnn4-4::C.d HIS1*	This study
mnn9 $^{-/-}$	EGD179	*his1Δ::FRT/his1Δ::FRT, leu2Δ::FRT/leu2Δ::FRT, mnn9::C.m LEU2/mnn9::C.d HIS1*	This study
mnn9 $^{-/-}$	EGD182	*his1Δ::FRT/his1Δ::FRT, leu2Δ::FRT/leu2Δ::FRT, mnn9::C.m LEU2/mnn9::C.d HIS1*	This study
mnn9 $^{-/-}$,+	URZ494	*his1Δ::FRT/his1Δ::FRT, leu2Δ::FRT/leu2Δ::FRT, mnn9::C.m LEU2/mnn9::C.d HIS1,C.m leu2::MNN9-NAT1*	This study
mnn11 $^{-/-}$	EGD159	*his1Δ::FRT/his1Δ::FRT, leu2Δ::FRT/leu2Δ::FRT, mnn11::C.m LEU2/mnn11::C.d HIS1*	This study
mnn11 $^{-/-}$	EGD160	*his1Δ::FRT/his1Δ::FRT, leu2Δ::FRT/leu2Δ::FRT, mnn11::C.m LEU2/mnn11::C.d HIS1*	This study
phr1 $^{-/-}$	EGD171	*his1Δ::FRT/his1Δ::FRT, leu2Δ::FRT/leu2Δ::FRT, phr1::C.m LEU2/phr1::C.d HIS1*	This study
phr1 $^{-/-}$	EGD173	*his1Δ::FRT/his1Δ::FRT, leu2Δ::FRT/leu2Δ::FRT, phr1::C.m LEU2/phr1::C.d HIS1*	This study
pmr1 $^{-/-}$	EGD163	*his1Δ::FRT/his1Δ::FRT, leu2Δ::FRT/leu2Δ::FRT, pmr1::C.m LEU2/pmr1::C.d HIS1*	This study
pmr1 $^{-/-}$	EGD165	*his1Δ::FRT/his1Δ::FRT, leu2Δ::FRT/leu2Δ::FRT, pmr1::C.m LEU2/pmr1::C.d HIS1*	This study
van1 $^{-/-}$	EGD168	*his1Δ::FRT/his1Δ::FRT, leu2Δ::FRT/leu2Δ::FRT, van1::C.m LEU2/van1::C.d HIS1*	This study
van1 $^{-/-}$	EGD169	*his1Δ::FRT/his1Δ::FRT, leu2Δ::FRT/leu2Δ::FRT, van1::C.m LEU2/van1::C.d HIS1*	This study

van1 $^{-/-}$,+	URZ497	*his1Δ::FRT/his1Δ::FRT, leu2Δ::FRT/leu2Δ::FRT, van1::C.m LEU2/van1::C.d HIS1, C.d his1::VAN1-NAT1*	This study
xog1 $^{-/-}$	EGD176	*his1Δ::FRT/his1Δ::FRT, leu2Δ::FRT/leu2Δ::FRT, xog1::C.m LEU2/xog1::C.d HIS1*	This study
xog1 $^{-/-}$	EGD177	*his1Δ::FRT/his1Δ::FRT, leu2Δ::FRT/leu2Δ::FRT, xog1::C.m LEU2/xog1::C.d HIS1*	This study

C. parapsilosis

Gene	Strain	Genotype	Source
Reference	CLIB214	*C. parapsilosis* wild type strain	
Reference	CPL2H1	*leu2Δ::FRT/leu2Δ::FRT, his1Δ::FRT/his1Δ::FRT*	
alg11 $^{-/-}$	EGD136	*leu2Δ::FRT/leu2Δ::FRT, his1Δ::FRT/his1Δ::FRT, alg11::C.m LEU2/alg11::C.d HIS1*	This study
bgl2 $^{-/-}$	EGD146	*leu2Δ::FRT/leu2Δ::FRT, his1Δ::FRT/his1Δ::FRT, bgl2::C.m LEU2/bgl2::C.d HIS1*	This study
bgl2 $^{-/-}$	EGD147	*leu2Δ::FRT/leu2Δ::FRT, his1Δ::FRT/his1Δ::FRT, bgl2::C.m LEU2/bgl2::C.d HIS1*	This study
mnn4-4 $^{-/-}$	EGD148	*leu2Δ::FRT/leu2Δ::FRT, his1Δ::FRT/his1Δ::FRT, mnn4-4::C.m LEU2/mnn4-4::C.d HIS1*	This study
mnn4-4 $^{-/-}$	EGD149	*leu2Δ::FRT/leu2Δ::FRT, his1Δ::FRT/his1Δ::FRT, mnn4-4::C.m LEU2/mnn4-4::C.d HIS1*	This study
mnn4-4 $^{-/-}$,+	URZ488	*leu2Δ::FRT/leu2Δ::FRT, his1Δ::FRT/his1Δ::FRT, mnn4-4::C.m LEU2/mnn4-4::C.d HIS1, C.m leu2::MNN4-4-NAT1*	This study
mnn9 $^{-/-}$	EGD193	*leu2Δ::FRT/leu2Δ::FRT, his1Δ::FRT/his1Δ::FRT, mnn9::C.m LEU2/mnn9::C.d HIS1*	This study
mnn9 $^{-/-}$	EGD194	*leu2Δ::FRT/leu2Δ::FRT, his1Δ::FRT/his1Δ::FRT, mnn9::C.m LEU2/mnn9::C.d HIS1*	This study
mnn9 $^{-/-}$,+	URZ485	*leu2Δ::FRT/leu2Δ::FRT, his1Δ::FRT/his1Δ::FRT, mnn9::C.m LEU2/mnn9::C.d HIS1, C.d his1::MNN9-NAT1*	This study
mnn11 $^{-/-}$	EGD144	*leu2Δ::FRT/leu2Δ::FRT, his1Δ::FRT/his1Δ::FRT, mnn11::C.m LEU2/mnn11::C.d HIS1*	This study
mnn11 $^{-/-}$	EGD145	*leu2Δ::FRT/leu2Δ::FRT, his1Δ::FRT/his1Δ::FRT, mnn11::C.m LEU2/mnn11::C.d HIS1*	This study
mnn11 $^{-/-}$,+	URZ486	*leu2Δ::FRT/leu2Δ::FRT, his1Δ::FRT/his1Δ::FRT, mnn11::C.m LEU2/mnn11::C.d HIS1, C.m leu2::MNN11-NAT1*	This study
phr1 $^{-/-}$	EGD188	*leu2Δ::FRT/leu2Δ::FRT, his1Δ::FRT/his1Δ::FRT, phr1::C.m LEU2/phr1::C.d HIS1*	This study
phr1 $^{-/-}$	EGD189	*leu2Δ::FRT/leu2Δ::FRT, his1Δ::FRT/his1Δ::FRT, phr1::C.m LEU2/phr1::C.d HIS1*	This study
phr1 $^{-/-}$,+	URZ491	*leu2Δ::FRT/leu2Δ::FRT, his1Δ::FRT/his1Δ::FRT, phr1::C.m LEU2/phr1::C.d HIS1, C.m leu2::PHR1-NAT1*	This study
pmr1.1 $^{-/-}$	EGD141	*leu2Δ::FRT/leu2Δ::FRT, his1Δ::FRT/his1Δ::FRT, pmr1::C.m LEU2/pmr1::C.d HIS1*	This study
pmr1.2 $^{-/-}$	EGD142	*leu2Δ::FRT/leu2Δ::FRT, his1Δ::FRT/his1Δ::FRT, pmr1::C.m LEU2/pmr1::C.d HIS1*	This study
pmr1 $^{-/-}$,+	URZ520	*leu2Δ::FRT/leu2Δ::FRT, his1Δ::FRT/his1Δ::FRT, pmr1::C.m LEU2/pmr1::C.d HIS1, C.m leu2::PMR1-NAT1*	This study

van1 $^{-/-}$	EGD184	*leu2Δ::FRT/leu2Δ::FRT, his1Δ::FRT/his1Δ::FRT, van1::C.m LEU2/van1::C.d HIS1*	This study
van1 $^{-/-}$	EGD185	*leu2Δ::FRT/leu2Δ::FRT, his1Δ::FRT/his1Δ::FRT, van1::C.m LEU2/van1::C.d HIS1*	This study
van1 $^{-/-}$,+	URZ510	*leu2Δ::FRT/leu2Δ::FRT, his1Δ::FRT/his1Δ::FRT, van1::C.m LEU2/van1::C.d HIS1, C.m leu2::VAN1-NAT1*	This study
xog1 $^{-/-}$	EGD150	*leu2Δ::FRT/leu2Δ::FRT, his1Δ::FRT/his1Δ::FRT, xog1::C.m LEU2/xog1::C.d HIS1*	This study
xog1 $^{-/-}$,+	URZ499	*leu2Δ::FRT/leu2Δ::FRT, his1Δ::FRT/his1Δ::FRT, xog1::C.m LEU2/xog1::C.d HIS1, C.m leu2::XOG1-NAT1*	This study

C. glabrata

Gene	Strain	Genotype	Source
Reference	ATCC2001	*C. glabrata* wild type strain	
Reference	HTL	*his3*Δ::FRT, *leu2*Δ::FRT, *trp1*Δ::FRT	
alg11 Δ	EGD125	*his3*Δ::FRT, *leu2*Δ::FRT, *trp1*Δ::FRT, *alg11*Δ::NAT1	This study
alg11 Δ	EGD126	*his3*Δ::FRT, *leu2*Δ::FRT, *trp1*Δ::FRT, *alg11*Δ::NAT1	This study
bgl2 Δ	EGD127	*his3*Δ::FRT, *leu2*Δ::FRT, *trp1*Δ::FRT, *bgl2*Δ::NAT1	This study
big1 Δ	EGD129	*his3*Δ::FRT, *leu2*Δ::FRT, *trp1*Δ::FRT, *big1*Δ::NAT1	This study
big1 Δ	EGD130	*his3*Δ::FRT, *leu2*Δ::FRT, *trp1*Δ::FRT, *big1*Δ::NAT1	This study
big1 Δ,+	URZ508	*his3*Δ::FRT, *leu2*Δ::FRT, *trp1*Δ::FRT, *big1*Δ::NAT1 / NAT1::BIG1-HygB	This study
mnn4-4 Δ	EGD121	*his3*Δ::FRT, *leu2*Δ::FRT, *trp1*Δ::FRT,*mnn4-4*Δ::NAT1	This study
mnn4-4 Δ	EGD122	*his3*Δ::FRT, *leu2*Δ::FRT, *trp1*Δ::FRT,*mnn4-4*Δ::NAT1	This study
mnn9 Δ	EGD128	*his3*Δ::FRT, *leu2*Δ::FRT, *trp1*Δ::FRT, *mnn9*Δ::NAT1	This study
mnn11 Δ	EGD124	*his3*Δ::FRT, *leu2*Δ::FRT, *trp1*Δ::FRT, *mnn11*Δ::NAT1	This study
phr1 Δ	EGD131	*his3*Δ::FRT, *leu2*Δ::FRT, *trp1*Δ::FRT, *phr1*Δ::NAT1	This study
phr1 Δ	EGD132	*his3*Δ::FRT, *leu2*Δ::FRT, *trp1*Δ::FRT, *phr1*Δ::NAT1	This study
pmr1 Δ	EGD143	*his3*Δ::FRT, *leu2*Δ::FRT, *trp1*Δ::FRT, *pmr1*Δ::NAT1	This study
van1 Δ	EGD137	*his3*Δ::FRT, *leu2*Δ::FRT, *trp1*Δ::FRT, *van1*Δ::NAT1	This study
van1 Δ	EGD138	*his3*Δ::FRT, *leu2*Δ::FRT, *trp1*Δ::FRT, *van1*Δ::NAT1	This study
xog1 Δ	EGD134	*his3*Δ::FRT, *leu2*Δ::FRT, *trp1*Δ::FRT, *xog1*Δ::NAT1	This study
xog1 Δ	EGD135	*his3*Δ::FRT, *leu2*Δ::FRT, *trp1*Δ::FRT, *xog1*Δ::NAT1	This study

Table S3. Primers used for Mutant Strain Creation and Confirmation. List of primers used to for genetic modification of strains as well as those used to confirm correct modifications.

C. tropicalis

Gene	Function	Primers
BGL2	Knockout	Upstream F: 5' – GCCTTACGTTTTTGATCTTATT Upstream R: 5' – CACGGCGCGCCTAGCAGCGGGACCAAAAATGATAACGAGAGT Auxotrophic marker F: 5' – CCGCTGCTAGGCGCGCCGTGACCAGTGTGATGGATATCTGC Auxotrophic marker R: 5' – GCAGGGATGCGGCCGCTGACAGCTCGGATCCACTAGTAACG Downstream F: 5' – GTCAGCGGCCGCATCCCTGCTCGTTTTAGAATATCCTATTTGC Downstream R: 5' – GTATTTTCCATGTTGCCATCTA Nested Fusion F: 5' – GTCATGGTGAAGAGAAGTTTTT Nested Fusion R: 5' – TAACTAATCCCTGGTAATTTGG Internal Check F: 5' – GCAATTCAAATACTTAGCAGGT Internal Check R: 5' – TTTCTAGAAGAATCCCAAACAC Upstream Check F: 5' – TAGTATGGCAATGGTGTCAG Downstream Check R: 5' – ATTGAGCCAGTTCAAAATGT His Upstream Check F: 5` – AAAATCAATGGGCATTCTCG His Downstream Check R: 5` – TGGGAAGCAGACATTCAACA Leu Upstream Check F: 5` – GAAGTTGGTGACGCGATTGT Leu Downstream Check F: 5` – TTCCCCTTCAATGTATGCAA
BIG1	Knockout	Upstream F: 5' – CTAGTGTTTGTCGGTGTGTG Upstream R: 5' – CACGGCGCGCCTAGCAGCGGTTTTCTTCCTCGTTTTTCAA Auxotrophic marker F: 5' – CCGCTGCTAGGCGCGCCGTGACCAGTGTGATGGATATCTGC Auxotrophic marker R: 5' – GCAGGGATGCGGCCGCTGACAGCTCGGATCCACTAGTAACG Downstream F: 5' – GTCAGCGGCCGCATCCCTGCTTTATCTTATTTGTCACCACCA Downstream R: 5' – GGTGTTGAATATCAACCAACTT Nested Fusion F: 5' – TTTCTCTTCAACTCCTGTTTCT Nested Fusion R: 5' – GAACAAGTGGTGTTGACAGTT Internal Check F: 5' – TAGTCACTTGTCGAGTTACACC Internal Check R: 5' – AAAGTCTTCAAAAAGGATACGA Upstream Check F: 5' – GGTATCATCACCAGCTTTGT Downstream Check R: 5' – TTCAGAAGAATCAGGGTCTG His Upstream Check F: 5` – AAAATCAATGGGCATTCTCG His Downstream Check R: 5` – TGGGAAGCAGACATTCAACA Leu Upstream Check F: 5` – GAAGTTGGTGACGCGATTGT Leu Downstream Check F: 5` – TTCCCCTTCAATGTATGCAA
KRE5	Knockout	Upstream F: 5' – ATGAAATGTTTCCTAAAAATGC Upstream R: 5' – CACGGCGCGCCTAGCAGCGGATCGTTATATGTTTCGGTTTTC Auxotrophic marker F: 5' – CCGCTGCTAGGCGCGCCGTGACCAGTGTGATGGATATCTGC Auxotrophic marker R: 5' – GCAGGGATGCGGCCGCTGACAGCTCGGATCCACTAGTAACG Downstream F: 5' – GTCAGCGGCCGCATCCCTGCCCTGAATCGGAGTTTTTATTAG Downstream R: 5' – TACGTAATTTTGAACACCAAGA Nested Fusion F: 5' – GAATGAAATTGTGGGTACTTTT Nested Fusion R: 5' – TTTCAATTCATCTGTTTCTTCA Internal Check F: 5' – TACTAATCGTGAGGAGGCTTAT Internal Check R: 5' – AGTTTGTCAAAGTGGTTAGCTT Upstream Check F: 5' – CGACCACATCACAATGATAG Downstream Check R: 5' – TCAGCATCGTAAAACATTTG His Upstream Check F: 5` – AAAATCAATGGGCATTCTCG His Downstream Check R: 5` – TGGGAAGCAGACATTCAACA Leu Upstream Check F: 5` – GAAGTTGGTGACGCGATTGT Leu Downstream Check F: 5` – TTCCCCTTCAATGTATGCAA
KRE5	Compliment	Upstream/ORF F: 5' – ATGCGAAATCATTACTATACGA Upstream/ORF R: 5' – CACGGCGCGCCTAGCAGCGGATTCAGGAATAGCACGTGAA Antibiotic marker F: 5' – CCGCTGCTAGGCGCGCCGTGGATATCAAGCTTGCCTCGTCC

		Antibiotic marker R: 5' – GCAGGGATGCGGCCGCTGACTTACTTTCTGCGCACTTAACTTC Downstream F: 5' – GTCAGCGGCCGCATCCCTGCGCACGTGCACTTGTTAGATA Downstream R: 5' – TTTTACGTAATTTTGAACACCA Nested Fusion F: 5' – ATGAAATGTTTCCTAAAAATGC Nested Fusion R: 5' – TTTCAATTCATCTGTTTCTTCA Internal Check F: 5' – TACTAATCGTGAGGAGGCTTAT Internal Check R: 5' – AGTTTGTCAAAGTGGTTAGCTT Upstream Check F: 5' – GGTGGCACCGATAATACAT Downstream Check R: 5' – ATCGTTATATGTTTCGGTTTTC Nourseothricin Upstream Check F: 5` – TGGTTTCGTTGTTGTTTCTTAT Nourseothricin Downstream Check R: 5` – TTATGAGCTTGATCCAACTTCT
MNN4-4	Knockout	Upstream F: 5' – CACGACCTATTTCCTAATAACA Upstream R: 5' – CACGGCGCGCCTAGCAGCGGATGTGAAATGTGAAATGCTAAA Auxotrophic marker F: 5' – CCGCTGCTAGGCGCGCCGTGACCAGTGTGATGGATATCTGC Auxotrophic marker R: 5' – GCAGGGATGCGGCCGCTGACAGCTCGGATCCACTAGTAACG Downstream F: 5' – GTCAGCGGCCGCATCCCTGCACATAAATCTCTTATTAACAAACAAAC Downstream R: 5' – TGTTAGAAAAGAATTAACAGTTAGTGA Nested Fusion F: 5' – CCATGGTACATAAACAATTGAA Nested Fusion R: 5' – AAAGATCCAGAAAAGAGACAAA Internal Check F: 5' – AAATGGGAAGAATTGTTTAATG Internal Check R: 5' – TCACTTGGATTTTCAACAACTA Upstream Check F: 5' – TTATGAAATTAACACAAACATGG Downstream Check R: 5' – TTCAATGTGAAAGATCAGGA His Upstream Check F: 5` – AAAATCAATGGGCATTCTCG His Downstream Check R: 5` – TGGGAAGCAGACATTCAACA Leu Upstream Check F: 5` – GAAGTTGGTGACGCGATTGT Leu Downstream Check F: 5` – TTCCCCTTCAATGTATGCAA
MNN9	Knockout	Upstream F: 5' – ATGATTATGGATGGAGTTGATT Upstream R: 5' – CACGGCGCGCCTAGCAGCGGATATTCGTTTCCTGTTTTGTTT Auxotrophic marker F: 5' – CCGCTGCTAGGCGCGCCGTGACCAGTGTGATGGATATCTGC Auxotrophic marker R: 5' – GCAGGGATGCGGCCGCTGACAGCTCGGATCCACTAGTAACG Downstream F: 5' – GTCAGCGGCCGCATCCCTGCTCCCATTATACACAGTGAATTT Downstream R: 5' – TCAAAATGACCAACATATAAAGA Nested Fusion F: 5' – CAAATTGTTGCTACAACTAGGA Nested Fusion R: 5' – ATTTGGATAACCACAAATCAAT Internal Check F: 5' – TTCGTGGTTTATCTTTTCTTCT Internal Check R: 5' – CTCTATGAACATCAGCATTGAC Upstream Check F: 5' – TGAAAGTTTGAATGAACAAAAA Downstream Check R: 5' – TTGAACATCAACATCAGCTT His Upstream Check F: 5` – AAAATCAATGGGCATTCTCG His Downstream Check R: 5` – TGGGAAGCAGACATTCAACA Leu Upstream Check F: 5` – GAAGTTGGTGACGCGATTGT Leu Downstream Check F: 5` – TTCCCCTTCAATGTATGCAA
MNN9	Compliment	Upstream/ORF F: 5' – TGATTAAGTTTGATATGATGGAA Upstream/ORF R: 5' – CACGGCGCGCCTAGCAGCGGACCTAATAGTTATAGAACACAACAATG Antibiotic marker F: 5' – CCGCTGCTAGGCGCGCCGTGGATATCAAGCTTGCCTCGTCC Antibiotic marker R: 5' – GCAGGGATGCGGCCGCTGACTTACTTTCTGCGCACTTAACTTC Downstream F: 5' – GTCAGCGGCCGCATCCCTGCAATATACTTCCCATTATACACAGTGA Downstream R: 5' – TATTTATAATCAAAATGACCAACA Nested Fusion F: 5' – AATGATGATTATGGATGGAGTT Nested Fusion R: 5' –TAAGGTTGAACATCAACATCAG Internal Check F: 5' – TTCGTGGTTTATCTTTTCTTCT Internal Check R: 5' – CTCTATGAACATCAGCATTGAC Upstream Check F: 5' – ATTTATGGAAACTCATGGAGAA Downstream Check R: 5' – ATATTCGTTTCCTGTTTTGTTT Nourseothricin Upstream Check F: 5` – TCGTTGTTGTTTCTTATTCTGG Nourseothricin Downstream Check R: 5` – TCAGTAAATCCTTCAGCAGTAA
MNN11	Knockout	Upstream F: 5' – CAGCATCTAGTGAAAATAGCAA Upstream R: 5' – CACGGCGCGCCTAGCAGCGGAGCCAATCTTTGATAAGTTGAT Auxotrophic marker F: 5' – CCGCTGCTAGGCGCGCCGTGACCAGTGTGATGGATATCTGC Auxotrophic marker R: 5' – GCAGGGATGCGGCCGCTGACAGCTCGGATCCACTAGTAACG Downstream F: 5' – GTCAGCGGCCGCATCCCTGCAAAACAAGAACACGAAAATCAT Downstream R: 5' – ACTTTATTGCTGATGGAGAAGT Nested Fusion F: 5' – AATATCGAGGTCATTTCTTTTG Nested Fusion R: 5' – ATTATGAAGTGTTTTCCGAATC Internal Check F: 5' – TAACTTATCCAAAAGGTCATCC Internal Check R: 5' – GTTTTTACCAACATCCTTGAAT Upstream Check F: 5' – AGAGAGGTGGGATTACCCTA Downstream Check R: 5' – GGAACCATTACAAAAACTGC

		His Upstream Check F: 5` – AAAATCAATGGGCATTCTCG His Downstream Check R: 5` – TGGGAAGCAGACATTCAACA Leu Upstream Check F: 5` – GAAGTTGGTGACGCGATTGT Leu Downstream Check F: 5` – TTCCCCTTCAATGTATGCAA
PHR1	Knockout	Upstream F: 5' – TGTAAATAATTGCTGCAAAAAG Upstream R: 5' – CACGGCGCGCCTAGCAGCGGTATGTGGATAAGGATTGTAGCA Auxotrophic marker F: 5' – CCGCTGCTAGGCGCGCCGTGACCAGTGTGATGGATATCTGC Auxotrophic marker R: 5' – GCAGGGATGCGGCCGCTGACAGCTCGGATCCACTAGTAACG Downstream F: 5' – GTCAGCGGCCGCATCCCTGCTTGTCTGTTTTCTAAATTCGTG Downstream R: 5' – AATATCTTTCAAAAATGGGATG Nested Fusion F: 5' – ATTATCCTCATCTACTCGTTGG Nested Fusion R: 5' – AAATTGGAAGAAGATGGTATTG Internal Check F: 5' – TAGAGAAATCCCAGTTGGTTAC Internal Check R: 5' – TGTACCAGAACCAGAACTAACA Upstream Check F: 5' – CCCTGTCTTGTTTTTACGAC Downstream Check R: 5' – AGGATCCGGATTAGGTTTAG His Upstream Check F: 5` – AAAATCAATGGGCATTCTCG His Downstream Check R: 5` – TGGGAAGCAGACATTCAACA Leu Upstream Check F: 5` – GAAGTTGGTGACGCGATTGT Leu Downstream Check F: 5` – TTCCCCTTCAATGTATGCAA
PMR1	Knockout	Upstream F: 5' – AATTGTGGAGATGGTAAAGAAG Upstream R: 5' – CACGGCGCGCCTAGCAGCGGAAGGAGTGTTGTGTGTTGTAAA Auxotrophic marker F: 5' – CCGCTGCTAGGCGCGCCGTGACCAGTGTGATGGATATCTGC Auxotrophic marker R: 5' – GCAGGGATGCGGCCGCTGACAGCTCGGATCCACTAGTAACG Downstream F: 5' – GTCAGCGGCCGCATCCCTGCCCAGAAGTGTGGTATGTGTGTA Downstream R: 5' – ATTTCTAGGTTGTGCTAATGGT Nested Fusion F: 5' – TTAAAGAGTTGGGTAAAAATGG Nested Fusion R: 5' – TTCCTTCTAATAATCCAACACC Internal Check F: 5' – AACTTTGGGTTCTGTTAATGTC Internal Check R: 5' – AATACCAATATCAGCCAATTTC Upstream Check F: 5' – TAATTTTGTTGATGTTGAAGGT Downstream Check R: 5' – GGTGCATGATGATAATTTGTAA His Upstream Check F: 5` – AAAATCAATGGGCATTCTCG His Downstream Check R: 5` – TGGGAAGCAGACATTCAACA Leu Upstream Check F: 5` – GAAGTTGGTGACGCGATTGT Leu Downstream Check F: 5` – TTCCCCTTCAATGTATGCAA
VAN1	Knockout	Upstream F: 5' – CAGAACGCGTAAAATATATGAA Upstream R: 5' – CACGGCGCGCCTAGCAGCGGATCCTTGGTAGTCATTCAAGTC Auxotrophic marker F: 5' – CCGCTGCTAGGCGCGCCGTGACCAGTGTGATGGATATCTGC Auxotrophic marker R: 5' – GCAGGGATGCGGCCGCTGACAGCTCGGATCCACTAGTAACG Downstream F: 5' – GTCAGCGGCCGCATCCCTGCCACCTCCTTGATTATCTTTGAT Downstream R: 5' – AAGTATTTAGTGGCTCATTTGC Nested Fusion F: 5' – GAAACGTGATGAAATAATGAAA Nested Fusion R: 5' – TATTTGCTGGTGTAATGAGTGT Internal Check F: 5' – TCTGACTGTTCTCCAGATGATA Internal Check R: 5' – AAATCATCTTCACTAGGCTCAT Upstream Check F: 5' – ATATAGGAGTCATTTATCAGGTGAA Downstream Check R: 5' – CTATTAGCGCTATCGGTTATTC His Upstream Check F: 5` – AAAATCAATGGGCATTCTCG His Downstream Check R: 5` – TGGGAAGCAGACATTCAACA Leu Upstream Check F: 5` – GAAGTTGGTGACGCGATTGT Leu Downstream Check F: 5` – TTCCCCTTCAATGTATGCAA
VAN1	Compliment	Upstream/ORF F: 5' – TAGGAGTCATTTATCAGGTGAA Upstream/ORF R: 5' – CACGGCGCGCCTAGCAGCGGTAATCAAGGAGGTGCTAACTCT Antibiotic marker F: 5' – CCGCTGCTAGGCGCGCCGTGGATATCAAGCTTGCCTCGTCC Antibiotic marker R: 5' – GCAGGGATGCGGCCGCTGACTTACTTTCTGCGCACTTAACTTC Downstream F: 5' – GTCAGCGGCCGCATCCCTGCTTCTGATTTATTGTTTAGTGCAA Downstream R: 5' – GAAGAAACAGGAATTTCAAGTAA Nested Fusion F: 5' – GCGGGAAAGGAAGACAAAA Nested Fusion R: 5' – GACCACTTATATTCTCCTTGGT Internal Check F: 5' – TCTGACTGTTCTCCAGATGATA Internal Check R: 5' – AAATCATCTTCACTAGGCTCAT Upstream Check F: 5' – GCAGAACGCGTAAAATATATGA Downstream Check R: 5' – ATCCTTGGTAGTCATTCAAGTC Nourseothricin Upstream Check F: 5` – CTTTGGATGGTTCTTTCACTAC Nourseothricin Downstream Check R: 5` – ATTCACATGGATTACAAAACCC
XOG1	Compliment	Upstream F: 5' – CGCACAACAGATTAAATTAGAA Upstream R: 5' – CACGGCGCGCCTAGCAGCGGAAAGCAATAATAAAACGTGGAT Auxotrophic marker F: 5' – CCGCTGCTAGGCGCGCCGTGACCAGTGTGATGGATATCTGC

		Auxotrophic marker R: 5’ – GCAGGGATGCGGCCGCTGACAGCTCGGATCCACTAGTAACG Downstream F: 5’ – GTCAGCGGCCGCATCCCTGCTCGTCGGTTTATAGAGATTTTT Downstream R: 5’ – GTCTGATGTATTTGAACACGAG Nested Fusion F: 5’ – TGTTTGTTTTGTTTTGTGGTAT Nested Fusion R: 5’ – GGTAGTGGAAAATGTTGAAAGT Internal Check F: 5’ – CAGTTAATTAATGCTGTGGCTA Internal Check R: 5’ – GTTGATCAATGTCACGAGATAA Upstream Check F: 5’ – TTTTTCTTCGTCTCCAACAC Downstream Check R: 5’ – CCTAATGTTGTTTCCTTACCTC His Upstream Check F: 5` – AAAATCAATGGGCATTCTCG His Downstream Check R: 5` – TGGGAAGCAGACATTCAACA Leu Upstream Check F: 5` – GAAGTTGGTGACGCGATTGT Leu Downstream Check F: 5` – TTCCCCTTCAATGTATGCAA

C. parapsilosis

Gene	Function	Primers
ALG11	Knockout	Upstream F: 5’ – ATATGCAATGTGCCATTTAG Upstream R: 5’ –CACGGCGCGCCTAGCAGCGGTGGACGAGTGCTCTCTCTTA Auxotrophic marker F: 5’ – CCGCTGCTAGGCGCGCCGTGACCAGTGTGATGGATATCTGC Auxotrophic marker R: 5’ – GCAGGGATGCGGCCGCTGACAGCTCGGATCCACTAGTAACG Downstream F: 5’ – GTCAGCGGCCGCATCCCTGCTTGCAATCGTTTGTCTGTAT Downstream R: 5’ – TGGGTAACTTTTTCACCAGT Nested Fusion F: 5’ – CAAAATGTTGTTGTAAACACG Nested Fusion R: 5’ – ACACGAATTTGGAAATCATC Internal Check F: 5’ – CTAGTCCCCTCACAGAAATG Internal Check R: 5’ – AGTGGAAAGTAGTTGCTCCA Upstream Check F: 5’ – ATTGCGTATCGTGGATATAG Downstream Check R: 5’ – GAAAATTGCAAACGATACAT His Upstream Check F: 5` – AAAATCAATGGGCATTCTCG His Downstream Check R: 5` – TGGGAAGCAGACATTCAACA Leu Upstream Check F: 5` – GAAGTTGGTGACGCGATTGT Leu Downstream Check F: 5` – TTCCCCTTCAATGTATGCAA
BGL2	Knockout	Upstream F: 5’ – AATGATTGTATCGCGAAAGT Upstream R: 5’ –CACGGCGCGCCTAGCAGCGGTTGCAAGATTTTGTTGTTGA Auxotrophic marker F: 5’ – CCGCTGCTAGGCGCGCCGTGACCAGTGTGATGGATATCTGC Auxotrophic marker R: 5’ – GCAGGGATGCGGCCGCTGACAGCTCGGATCCACTAGTAACG Downstream F: 5’ – GTCAGCGGCCGCATCCCTGCACTGGTGAGTTTTCATTCGT Downstream R: 5’ – GATTTCAACCACATCCAAAT Nested Fusion F: 5’ – ATGCTAGGGGAAATTTAAGG Nested Fusion R: 5’ – AACACCACTTTCCGACATAC Internal Check F: 5’ – TATCCAACCAAACAACAACA Internal Check R: 5’ – CAATGCTTTTCAACATCTGA Upstream Check F: 5’ – CCTTCAAGAGCAAATGTATC Downstream Check R: 5’ – CCACAACAGCACTTCTTATT His Upstream Check F: 5` – AAAATCAATGGGCATTCTCG His Downstream Check R: 5` – TGGGAAGCAGACATTCAACA Leu Upstream Check F: 5` – GAAGTTGGTGACGCGATTGT Leu Downstream Check F: 5` – TTCCCCTTCAATGTATGCAA
MNN4-4	Knockout	Upstream F: 5’ – TTTGGTTGTTACTGGAGACC Upstream R: 5’ –CACGGCGCGCCTAGCAGCGGGTGACTTGCTTGTGTCAAAC Auxotrophic marker F: 5’ – CCGCTGCTAGGCGCGCCGTGACCAGTGTGATGGATATCTGC Auxotrophic marker R: 5’ – GCAGGGATGCGGCCGCTGACAGCTCGGATCCACTAGTAACG Downstream F: 5’ – GTCAGCGGCCGCATCCCTGCTAGGGTTGGTTACTCAAGCA Downstream R: 5’ – TGCCACGTTTCAACATAAT Nested Fusion F: 5’ – CATCTATATCCACTCCTCGAA Nested Fusion R: 5’ – ACAACTGATGGGTTTTCAAC Internal Check F: 5’ – GAAAAAGTTTTGTTGGATCG Internal Check R: 5’ – ATCTCAGTTTGCGTTTTCAT Upstream Check F: 5’ – GGGGATCTTCACTAACAAAT Downstream Check R: 5’ – AGGCGGTAGAAATTCAAG His Upstream Check F: 5` – AAAATCAATGGGCATTCTCG His Downstream Check R: 5` – TGGGAAGCAGACATTCAACA Leu Upstream Check F: 5` – GAAGTTGGTGACGCGATTGT Leu Downstream Check F: 5` – TTCCCCTTCAATGTATGCAA
MNN9	Compliment	Upstream F: 5’ – AAGGAAAAGAAGGAGAAAGC Upstream R: 5’ –CACGGCGCGCCTAGCAGCGGGGGATATATCAACGCAATGT

		Auxotrophic marker F: 5' – CCGCTGCTAGGCGCGCCGTGACCAGTGTGATGGATATCTGC Auxotrophic marker R: 5' – GCAGGGATGCGGCCGCTGACAGCTCGGATCCACTAGTAACG Downstream F: 5' – GTCAGCGGCCGCATCCCTGCAACGGTAACACAGGTGTAGG Downstream R: 5' – GCGTCTTTGTTTTCCTTAGT Nested Fusion F: 5' – TTGGATGAGTGGAAGAGAAC Nested Fusion R: 5' – CAGCTTAGAATCGCTTGACT Internal Check F: 5' – CCAAGAAGGAAGAAGTGTTG Internal Check R: 5' – TCAAGTGGTAAAATGGGAAC Upstream Check F: 5' – CTAAAAAGGAAGCTTCTGC Downstream Check R: 5' – TGATTTCCTGATTTGTTGTC His Upstream Check F: 5` – AAAATCAATGGGCATTCTCG His Downstream Check R: 5` – TGGGAAGCAGACATTCAACA Leu Upstream Check F: 5` – GAAGTTGGTGACGCGATTGT Leu Downstream Check F: 5` – TTCCCCTTCAATGTATGCAA
MNN11	Knockout	Upstream F: 5' – GTGATCAAATTCGTCTTGGT Upstream R: 5' –CACGGCGCGCCTAGCAGCGGATTTGGATGATGGTTGATGT Auxotrophic marker F: 5' – CCGCTGCTAGGCGCGCCGTGACCAGTGTGATGGATATCTGC Auxotrophic marker R: 5' – GCAGGGATGCGGCCGCTGACAGCTCGGATCCACTAGTAACG Downstream F: 5' – GTCAGCGGCCGCATCCCTGCTGTATCTAAAGACAAGCTTTGAA Downstream R: 5' – CTACAACTTTCCCAAACAGG Nested Fusion F: 5' – TGCAAAGAATATGAACACTCC Nested Fusion R: 5' – ACACTTGACGGTTCAAGAAG Internal Check F: 5' – AGTTGAACAAGCACCACTTT Internal Check R: 5' – CTTCACAATCGGAAATCAGT Upstream Check F: 5' – TGATTACTGTTTTGGTTGCT Downstream Check R: 5' – ATGTGAGACTGTTGCTCAAT His Upstream Check F: 5` – AAAATCAATGGGCATTCTCG His Downstream Check R: 5` – TGGGAAGCAGACATTCAACA Leu Upstream Check F: 5` – GAAGTTGGTGACGCGATTGT Leu Downstream Check F: 5` – TTCCCCTTCAATGTATGCAA
PHR1	Knockout	Upstream F: 5' – TTTCTCCTAACAAGGTCACG Upstream R: 5' –CACGGCGCGCCTAGCAGCGGTAGTGGTAGTGCGAAGTGTG Auxotrophic marker F: 5' – CCGCTGCTAGGCGCGCCGTGACCAGTGTGATGGATATCTGC Auxotrophic marker R: 5' – GCAGGGATGCGGCCGCTGACAGCTCGGATCCACTAGTAACG Downstream F: 5' – GTCAGCGGCCGCATCCCTGCAAATGAAAGAAAAAGGCTGA Downstream R: 5' – AGACAGACAATGCAGGACTT Nested Fusion F: 5' – ATAGTCGTCTCGCCACTTTA Nested Fusion R: 5' – ACAAGACGTTGGATGAATGT Internal Check F: 5' – TGGACCATGATGAATGTATG Internal Check R: 5' – GATGGGAGCAGAATGAGTAG Upstream Check F: 5' – GTGGTAGACATGAATTGCTC Downstream Check R: 5' – TTGGACACCAGTATTTATCC His Upstream Check F: 5` – AAAATCAATGGGCATTCTCG His Downstream Check R: 5` – TGGGAAGCAGACATTCAACA Leu Upstream Check F: 5` – GAAGTTGGTGACGCGATTGT Leu Downstream Check F: 5` – TTCCCCTTCAATGTATGCAA
PMR1	Knockout	Upstream F: 5' – CCCAATGCAAAGGTTATACT Upstream R: 5' –CACGGCGCGCCTAGCAGCGGTATATCTTTCGGGTGTTTGG Auxotrophic marker F: 5' – CCGCTGCTAGGCGCGCCGTGACCAGTGTGATGGATATCTGC Auxotrophic marker R: 5' – GCAGGGATGCGGCCGCTGACAGCTCGGATCCACTAGTAACG Downstream F: 5' – GTCAGCGGCCGCATCCCTGCATCGAATGCAAACTCTTGTT Downstream R: 5' – TACGAGGAGGAAAACTCAAG Nested Fusion F: 5' – ATGAGGAGGATAAGGTGGAT Nested Fusion R: 5' – TAAGCAATTCCCCATTACAC Internal Check F: 5' – GCAAAGAGAGAGGGTGTATG Internal Check R: 5' – AATCCGAAAAACGTACTCAA Upstream Check F: 5' – ATGTTGAAGGCATTAAAGTG Downstream Check R: 5' – CATTTTAGAAATGCCAAACA His Upstream Check F: 5` – AAAATCAATGGGCATTCTCG His Downstream Check R: 5` – TGGGAAGCAGACATTCAACA Leu Upstream Check F: 5` – GAAGTTGGTGACGCGATTGT Leu Downstream Check F: 5` – TTCCCCTTCAATGTATGCAA
VAN1	Knockout	Upstream F: 5' – GACAAGCTAGAGCAAGGGTA Upstream R: 5' –CACGGCGCGCCTAGCAGCGGAGGTAATGACGTTGACGTTT Auxotrophic marker F: 5' – CCGCTGCTAGGCGCGCCGTGACCAGTGTGATGGATATCTGC Auxotrophic marker R: 5' – GCAGGGATGCGGCCGCTGACAGCTCGGATCCACTAGTAACG Downstream F: 5' – GTCAGCGGCCGCATCCCTGCATCAGTAGGAAGGCAGGATT Downstream R: 5' – TTTGAACCTGCTGTTTTCTT Nested Fusion F: 5' – ACCCCCAAGATATTTAAAGC

		Nested Fusion R: 5’ – GTGTATTTGGGCTATGCAAT Internal Check F: 5’ – ACAACCGAAGATTTGAAAAA Internal Check R: 5’ – CACTTCACGAGGATTACCAT Upstream Check F: 5’ – TGGTTTAAAGACTTGAATGG Downstream Check R: 5’ – GTTTTCTTGGGTGGTTTTAT His Upstream Check F: 5` – AAAATCAATGGGCATTCTCG His Downstream Check R: 5` – TGGGAAGCAGACATTCAACA Leu Upstream Check F: 5` – GAAGTTGGTGACGCGATTGT Leu Downstream Check F: 5` – TTCCCCTTCAATGTATGCAA
XOG1	Knockout	Upstream F: 5’ – TGGCATACAAAAGAGAACAA Upstream R: 5’ –CACGGCGCGCCTAGCAGCGGATGGTTGTTGTAAATGTGACC Auxotrophic marker F: 5’ – CCGCTGCTAGGCGCGCCGTGACCAGTGTGATGGATATCTGC Auxotrophic marker R: 5’ – GCAGGGATGCGGCCGCTGACAGCTCGGATCCACTAGTAACG Downstream F: 5’ – GTCAGCGGCCGCATCCCTGCTTGGTTAATTTTGGTTTGGT Downstream R: 5’ – ACGTGACTGTGATGTTTGAA Nested Fusion F: 5’ – AACTCATGACACATCCACAA Nested Fusion R: 5’ – TCTTGTGCAAACACCGTAT Internal Check F: 5’ – ACAAAGCAATTGGGTAAAGA Internal Check R: 5’ – GAAATAAACCAGCAGCAGTC Upstream Check F: 5’ – TGTGTGTGTGCTAAGCTAAA Downstream Check R: 5’ – TGAATTTCTCGATCTTTTTG His Upstream Check F: 5` – AAAATCAATGGGCATTCTCG His Downstream Check R: 5` – TGGGAAGCAGACATTCAACA Leu Upstream Check F: 5` – GAAGTTGGTGACGCGATTGT Leu Downstream Check F: 5` – TTCCCCTTCAATGTATGCAA

C. glabrata

Gene	Function	Primers
ALG11	Knockout	Upstream F: 5’ – TCTCCTCTTTGGATGGTAGA Upstream R: 5’ – CCGCTGCTAGGCGCGCCGTGTGTTGCTAAACGCTAACTCA Antibiotic marker F: 5’ – CACGGCGCGCCTAGCAGCGGCAGAATACCCTCCTTGACAG Antibiotic marker R: 5’ – GTCAGCGGCCGCATCCCTGCGCGGCGTTAGTATCGAAT Downstream F: 5’ – GCAGGGATGCGGCCGCTGACCATGTGTTGCCATCATCTAC Downstream R: 5’ – GCCTACAGTTAAGGAATCTGG Nested Fusion F: 5’ – ATATCTGTTGGACCCATTGT Nested Fusion R: 5’ – GGTTTTCCTTCTTCTTACCTG Internal Check F: 5’ – GGTGAGAAAGTTCTGTGGAA Internal Check R: 5’ – ATATCTGCCAGAGAGCCATA Upstream Check F: 5’ – AAGGCGACTTTACCAAAC Downstream Check R: 5’ – ATGTACCGAAAGATCAGAC Nourseothricin Upstream Check F: 5` - CAACTGGAACTTCTCTCAAA Nourseothricin Downstream Check R: 5` - CATTTGTGGTTGGAAGTTAC
BGL2	Knockout	Upstream F: 5’ – TCATCACTTCTCACCACAAA Upstream R: 5’ – CCGCTGCTAGGCGCGCCGTGAGAGTACCAAGGTTAGTGTGCT Antibiotic marker F: 5’ – CACGGCGCGCCTAGCAGCGGCAGAATACCCTCCTTGACAG Antibiotic marker R: 5’ – GTCAGCGGCCGCATCCCTGCGCGGCGTTAGTATCGAAT Downstream F: 5’ – GCAGGGATGCGGCCGCTGACTCGAATTCGGTTATGACTTT Downstream R: 5’ – AGACTGATGGAAAAATCCAA Nested Fusion F: 5’ – AGGAGGCACAGAGAAACAC Nested Fusion R: 5’ – TAGTTTTGGAGAAGGGTGAG Internal Check F: 5’ – CTGTTGCAGCTTTAGCATTT Internal Check R: 5’ – CAGTGCTTTTCAACATCAGA Upstream Check F: 5’ – TTCGTCAAGAGACTAGATGG Downstream Check R: 5’ – ACAGGTTGAAAACCATTTTA Nourseothricin Upstream Check F: 5` - CAACTGGAACTTCTCTCAAA Nourseothricin Downstream Check R: 5` - CATTTGTGGTTGGAAGTTAC
BIG1	Knockout	Upstream F: 5’ – ATCTTGCCAGGTCTCAGTAA Upstream R: 5’ – CCGCTGCTAGGCGCGCCGTGTCTTGACTGCCATTAAACAG Antibiotic marker F: 5’ – CACGGCGCGCCTAGCAGCGGCAGAATACCCTCCTTGACAG Antibiotic marker R: 5’ – GTCAGCGGCCGCATCCCTGCGCGGCGTTAGTATCGAAT Downstream F: 5’ – GCAGGGATGCGGCCGCTGACCAGTTGAAGTATGATCTTGCATA Downstream R: 5’ – TCAACTGGATAGAAGGTCGT Nested Fusion F: 5’ – CTGCTTCAAAGAGGCTAGAA Nested Fusion R: 5’ – AGTGATGTTTCAGCTCTGGT Internal Check F: 5’ – GCTCTAGCGAGTAGTCTGGA Internal Check R: 5’ – CGTAGTATTTTTGGCGCTAT Upstream Check F: 5’ – ACCTGCACAGTATTCCATT

		Downstream Check R: 5' – CTGGTGACGTTGTAAGAAAG Nourseothricin Upstream Check F: 5` - CAACTGGAACTTCTCTCAAA Nourseothricin Downstream Check R: 5` - CATTTGTGGTTGGAAGTTAC
BIG1	Compliment	Upstream/ORF F: 5' – TTCATCTATCTTGCCAGGTCTC Upstream/ORF R: 5' – CACGGCGCGCCTAGCAGCGGGAGAGCTAGTTTCCCCTCT Antibiotic marker F: 5' – CCGCTGCTAGGCGCGCCGTGGTATAGTGCTTGCTGTTCGAT Antibiotic marker R: 5' – GCAGGGATGCGGCCGCTGACATTTTATGATGGAATGAATGG Downstream F: 5' – GTCAGCGGCCGCATCCCTGCATTACAGTTGAAGTATGATCTTG Downstream R: 5' – GCTGGCATGATATGGAGATT Nested Fusion F: 5' – TATTCGGTATCTGCTTCAAAGA Nested Fusion R: 5' – GTGGTAAGAGTATTGTAGCTGA Internal Check F: 5' – GCTCTAGCGAGTAGTCTGGA Internal Check R: 5' – CGTAGTATTTTTGGCGCTAT Upstream Check F: 5' – ACCTGCACAGTATTCCATTATA Downstream Check R: 5' – AATAATGCGTGAATTTGTGACT HygB Upstream Check F: 5` - TGGAAATCTGGAAATCTGGTT HygB Downstream Check R: 5` - ATCGGTATCAATGCCTTCTATC
MNN4-4	Knockout	Upstream F: 5' – TCATTATGAACCTGCAGTGA Upstream R: 5' – CCGCTGCTAGGCGCGCCGTGAGCATTCAAATCCCTTCTTA Antibiotic marker F: 5' – CACGGCGCGCCTAGCAGCGGCAGAATACCCTCCTTGACAG Antibiotic marker R: 5' – GTCAGCGGCCGCATCCCTGCGCGGCGTTAGTATCGAAT Downstream F: 5' – GCAGGGATGCGGCCGCTGACTATTTTAAAGGGCATGTTGG Downstream R: 5' – TATGAAACCGATGAACAATG Nested Fusion F: 5' – AGACATTATTTTGGTGTTGC Nested Fusion R: 5' – GTTATCACCCGTTGACATAG Internal Check F: 5' – AATCTCGAGTCAACTGTGCT Internal Check R: 5' – TTTCCTTCCCTAGGATCTTC Upstream Check F: 5' – CTCTACTCAGACACCGAAGA Downstream Check R: 5' – CAGTTCAAGATGAAGTTTCG Nourseothricin Upstream Check F: 5` - CAACTGGAACTTCTCTCAAA Nourseothricin Downstream Check R: 5` - CATTTGTGGTTGGAAGTTAC
MNN9	Knockout	Upstream F: 5' – AAAGAGACGAGGACAAGGTT Upstream R: 5' – CCGCTGCTAGGCGCGCCGTGAAGAGGCTCCTTTCTTGTTT Antibiotic marker F: 5' – CACGGCGCGCCTAGCAGCGGCAGAATACCCTCCTTGACAG Antibiotic marker R: 5' – GTCAGCGGCCGCATCCCTGCGCGGCGTTAGTATCGAAT Downstream F: 5' – GCAGGGATGCGGCCGCTGACATGTGGTTGCCCTAATGTAA Downstream R: 5' – AAGACAACTTTCGGACTTGA Nested Fusion F: 5' – GTATCAGAAGCAGAAGGTGA Nested Fusion R: 5' – AATAACCGCAGCATACTAAA Internal Check F: 5' – CTGATTTTCAGGTCGGATAG Internal Check R: 5' – GAAAGTTGGGAACATAGCAC Upstream Check F: 5' – CAGAAGCAGAAGCAGTAGC Downstream Check R: 5' – CGACTTTTCTCGAGACACTA Nourseothricin Upstream Check F: 5` - CAACTGGAACTTCTCTCAAA Nourseothricin Downstream Check R: 5` - CATTTGTGGTTGGAAGTTAC
MNN11	Knockout	Upstream F: 5' – TGCTCCCTGAACTTTCTAAC Upstream R: 5' – CCGCTGCTAGGCGCGCCGTGTTCCAAACAGGTATCAGAAAA Antibiotic marker F: 5' – CACGGCGCGCCTAGCAGCGGCAGAATACCCTCCTTGACAG Antibiotic marker R: 5' – GTCAGCGGCCGCATCCCTGCGCGGCGTTAGTATCGAAT Downstream F: 5' – GCAGGGATGCGGCCGCTGACTTTGGGATTCATTGAGCTAT Downstream R: 5' – CACTTACATCGCTTGTCTCA Nested Fusion F: 5' – ACAACTGACGTATGGTCATC Nested Fusion R: 5' – CACCACTGTTATAAAGAATCAA Internal Check F: 5' – GGTACGTGTCGAAGAAGAAG Internal Check R: 5' – TTGATGTTCAAGTTTGTTGG Upstream Check F: 5' – GTGTACTTGTCCTGCAACTC Downstream Check R: 5' – ACTTGGAGACCACCAGTAAT Nourseothricin Upstream Check F: 5` - CAACTGGAACTTCTCTCAAA Nourseothricin Downstream Check R: 5` - CATTTGTGGTTGGAAGTTAC
PHR1	Knockout	Upstream F: 5' – TTCCCTTCATTGACTATTGG Upstream R: 5' – CCGCTGCTAGGCGCGCCGTGCTCCAGGAAAGCAAAAGAT Antibiotic marker F: 5' – CACGGCGCGCCTAGCAGCGGCAGAATACCCTCCTTGACAG Antibiotic marker R: 5' – GTCAGCGGCCGCATCCCTGCGCGGCGTTAGTATCGAAT Downstream F: 5' – GCAGGGATGCGGCCGCTGACAATGGGATCTTGATTATCCTT Downstream R: 5' – ACATGGTTCAATATGGAGGA Nested Fusion F: 5' – AAGAAAGCAATCTCGACGTA Nested Fusion R: 5' – ATATGCCCCAACAACATATC Internal Check F: 5' – AGCTTGCCACAAATGTTATT Internal Check R: 5' – CGAAGTTCAGCTTTTCCTTA

		Upstream Check F: 5’ – CTTAATTAGAGGGAGGAGGA Downstream Check R: 5’ – GAATACCTAGTATCGCCAGA Nourseothricin Upstream Check F: 5` - CAACTGGAACTTCTCTCAAA Nourseothricin Downstream Check R: 5` - CATTTGTGGTTGGAAGTTAC
PMR1	Knockout	Upstream F: 5’ – AGTTCGAAGACGCAAAGAA Upstream R: 5’ – CCGCTGCTAGGCGCGCCGTGGTAATAAGCCTTGATTCAGCA Antibiotic marker F: 5’ – CACGGCGCGCCTAGCAGCGGCAGAATACCCTCCTTGACAG Antibiotic marker R: 5’ – GTCAGCGGCCGCATCCCTGCGCGGCGTTAGTATCGAAT Downstream F: 5’ – GCAGGGATGCGGCCGCTGACATTTTGTCGATGAAGCACTC Downstream R: 5’ – AAACCTGTTTGCTGTGGTAG Nested Fusion F: 5’ – GACGACTCGCAGATATGG Nested Fusion R: 5’ – GCATCTGTGGTTGTAAAGGT Internal Check F: 5’ – CGCTTATATGGGTACTCTGG Internal Check R: 5’ – TCCACCTCTATGCAGTTTTT Upstream Check F: 5’ – AGGAGAAGACAGAGGAGAAG Downstream Check R: 5’ – ATTCAGTTGATTTGGTTGAA Nourseothricin Upstream Check F: 5` - CAACTGGAACTTCTCTCAAA Nourseothricin Downstream Check R: 5` - CATTTGTGGTTGGAAGTTAC
VAN1	Knockout	Upstream F: 5’ – CGAGAGCGATAGTGATAAGG Upstream R: 5’ – CCGCTGCTAGGCGCGCCGTGCACAACGTAATCGTGTATGC Antibiotic marker F: 5’ – CACGGCGCGCCTAGCAGCGGCAGAATACCCTCCTTGACAG Antibiotic marker R: 5’ – GTCAGCGGCCGCATCCCTGCGCGGCGTTAGTATCGAAT Downstream F: 5’ – GCAGGGATGCGGCCGCTGACTACCGTTTGAATTCGTTTCT Downstream R: 5’ – GGGTTCGTTTGGTATTTTT Nested Fusion F: 5’ – AACACCAATCCACTGTAAAA Nested Fusion R: 5’ – AGACACTATACCCCGCTCT Internal Check F: 5’ – GCCAAGAAGAAAAACTTCAA Internal Check R: 5’ – CATCCAAGAATTCAGGTCAT Upstream Check F: 5’ – GTAGCAATTTCCATATTTCG Downstream Check R: 5’ – ACATTCCAATTGAATTTAAGAC Nourseothricin Upstream Check F: 5` - CAACTGGAACTTCTCTCAAA Nourseothricin Downstream Check R: 5` - CATTTGTGGTTGGAAGTTAC
XOG1	Knockout	Upstream F: 5’ – CATCTTCGAATCGTTGTTTT Upstream R: 5’ – CCGCTGCTAGGCGCGCCGTGTCTCCTTGGGTTCTTTAATTT Antibiotic marker F: 5’ – CACGGCGCGCCTAGCAGCGGCAGAATACCCTCCTTGACAG Antibiotic marker R: 5’ – GTCAGCGGCCGCATCCCTGCGCGGCGTTAGTATCGAAT Downstream F: 5’ – GCAGGGATGCGGCCGCTGACAAAGCTGGACAACATTGATT Downstream R: 5’ – GTCGTCAAATTGTCATTCG Nested Fusion F: 5’ – CTTCCCTTTCGATATTCCTT Nested Fusion R: 5’ – TTGGTCTATCAATGCTCAAGT Internal Check F: 5’ – GTTCAGAACCAACCCTTACA Internal Check R: 5’ – AGATCCAGCCACCTCTTAAT Upstream Check F: 5’ – CCGCAAGTAGTCATCTATGT Downstream Check R: 5’ – TCTTCAACTTCTGAATCGTC Nourseothricin Upstream Check F: 5` - CAACTGGAACTTCTCTCAAA Nourseothricin Downstream Check R: 5` - CATTTGTGGTTGGAAGTTAC

Chapter 3

Biofilm Formation and Function of the emerging pathogen *Candida auris*

The contents of this section will be submitted for publication:

Eddie G. Dominguez, Robert Zarnowski, Hau L. Choy, Maio Zhao, Hiram Sanchez, and David R. Andes.

E. Dominguez designed experiments, performed susceptibility assays, analyzed data, characterized all isolates, and wrote the manuscript. R. Zarnowski performed matrix analysis and analyzed data. HL. Choy assisted in susceptibility assays and isolate characterization. M. Zhao performed SEM. H. Sanchez conducted sequestration assays on all isolates. DR. Andes supervised the study, analyzed and interpreted data, and wrote the manuscript.

ABSTRACT

Candida auris is an emerging yeast pathogen which is associated with nosocomial infections, invasive infections, and high rates of mortality. The almost simultaneous emergence across four continents with intrinsic resistance to antifungal drugs; raised the status of this uncommon *Candida* species to a global threat of healthcare associated infections. Here we implement biochemical, enzymatic, and pharmacologic approaches to explore biofilm properties and presence/function of an extracellular matrix (ECM) in 10 *C. auris* isolates. Biochemical analysis revealed the presence of the polysaccharides mannan and glucan within the matrices of all 10 isolates. Pharmacologic treatment of *C. auris* biofilms showed increased levels of resistance, however, when combined with an enzymatic treatment of either mannosidase or glucanase increased levels of susceptibility were observed in all 10 isolates. Further biochemical analysis on 3 isolates treated with mannosidase revealed decreased levels of mannan and glucan within the ECM. Our results argue that in *C. auris* biofilms mannan and glucan have a role in the drug resistance phenotype so commonly associated with *Candida* biofilms.

INTRODUCTION

Candida species are part of the normal microbiota of individuals residing primarily in the alimentary canal, tract, and vagina [1-6]. However, in immunocompromised or immunologically weak individuals, this opportunistic pathogen is able to manifest itself clinically with symptoms ranging from non-life threating, such as mucocutaneous overgrowth, all the way to life-threating such as bloodstream infections [7]. Virulence factors such as the organisms morphology, ability to evade host defense, adherence, and ability to form biofilms [8-16], all play a role in the pathogenicity of *Candida* species. However, as is the case with the majority of *Candida* infections, the pathogens ability to survive within a host in the biofilm state has been shown to be responsible for the majority of invasive infections [17-22]. Furthermore, the presence of an extracellular matrix in *Candida* biofilms has been shown to provide protective properties resulting in high levels of resistance to antifungal drug therapy [23-27].

Candida auris is an emerging yeast pathogen first identified from ear drainage discharge of a Japanese patient in 2009 [28]. Since its identification, countries across the globe have reported new case reports with cultures isolated from multiple sites such as blood, urine, respiratory tract, bile fluid, wounds, and central venous catheter tips [9, 29-35]. *C. auris* also has the capability to persist and contaminate environmental surfaces in healthcare facilities which has led to intra-hospital and inter-hospital outbreaks that originate from a single isolate [36-38]. A large portion of clinical isolates have also been shown to be intrinsically resistant to antifungal drug therapy resulting in high rates of mortality (-60%) and limited treatment options for physicians [36-40]. These two factors

have caused this invasive fungal pathogen to rise to the status of a global threat of healthcare-associated infections at an alarming rate.

Recent studies have provided insight into the organisms planktonic lifestyle [8], however, there is still a distinct lack of knowledge in regards to the biofilm lifestyle. To date there have been only a handful of studies which have addressed the pathogens capability to form biofilms and their susceptibility to popular antifungals such as fluconazole, and amphotericin B [8, 14], but very little is still known in regards to whether *C. auris* biofilms produce an extracellular matrix and the role it may have in drug resistance. Here we present evidence that 10 different *C. auris* isolates, obtained from 5 different regions across the globe, are able to form a biofilm and exhibit drug resistant phenotypes as seen in the four most prevalent *Candida* species. We attribute this drug resistance with the presence of an extracellular matrix which contains components that have been previously linked to the drug resistance phenotype [27, 41, 42].

RESULTS

Biofilm growth and architecture.

Early and mature phases of biofilm growth were quantified using in vitro biofilm assays. The early phase of biofilm growth is defined as the point after one hour of growth following seeding onto a 96 well microtiter plate and mature is defined after a 24hr growth period. A similar inoculum of cells was used as a starting point for all strains and based upon the assessment of adherent cells of the early phase biofilm, there was a significant difference between *C. albicans* and all *C. auris* strains tested (**Supplemental Figure 1A**). In fact, the burden of cells was 5-fold less than that of *C. albicans* however, there was

almost no difference in fungal burden when compared to *C. glabrata.* This was also seen in mature biofilms where the dry biofilm masses were upwards to 9 times less abundant than *C. albicans* biofilms **(Supplemental Figure 1B)**. The inability of *C. glabrata* and *C. auris* to filament [8, 14, 43], and the fact that they form biofilms as a monolayer of cells, are more than likely the underlying cause to the significant decrease of cells observed among these species.

Scanning electron microscopy of mature biofilms was used to visually evaluate biofilm architecture in vitro and in vivo via the rat vascular catheter model (**Figure 1**). As expected, none of the clinical isolates showed any signs of filamentation and instead formed biofilms as a monolayer of cells, as seen in *C. glabrata* biofilms. In fact, the ultrastructure between the two species is almost identical except that *C. glabrata* cells appear to be smaller in size than *C. auris.* All strains, except for B11221, were able to form biofilms in vivo. Cell encasing extracellular matrix was apparent and observed in all clinical isolates.

Antifungal susceptibility testing of *C. auris.*

An in vitro biofilm model was used to assess the biofilm associated drug-resistance phenotype for each of the *C. auris* isolates. An antifungal from each of the three main classes (polyene, azole, echinocandin) was used to assess efficacy against mature biofilms. Minimum inhibitory concentration (MIC) values for planktonic cultures were obtained from a previous study conducted by our lab [12], and used as a reference point for mature biofilm studies (**Supplemental Table 1**).

Mature biofilms, as defined previously, were challenged against 1 µg/ml liposomal amphotericin B required concentrations up to 2 times greater than reported MIC values to actively reduce fungal burden (**Supplemental Figure 2A**). Mature biofilms challenged with 1 mg/ml fluconazole, showed resistance levels 4 – 1000x greater than their planktonic counterparts (**Figure 2**). When challenged against 1 µg/ml of micafungin , which has been shown to be one of the most effective treatment options against *C. auris* [44], resistance levels up to 4 times greater than reported MIC values were observed (**Supplemental Figure 2B**).

***C. auris* biofilm matrix functional analysis and composition.**

A large number of studies have linked the biofilm drug resistance phenotype to the ability of the extracellular matrix to sequester antifungal drugs [26, 42, 45-50]. Using an in vitro biofilm assay, which tracks radiolabeled fluconazole within the biofilm matrix, we tested biofilms from each of the *C. auris* isolates and measured the concentration of fluconazole retained within the matrix and inside the cells. The majority of fluconazole was retained within the matrix (52 – 96%) with varying concentrations reaching the basal layer of cells (**Figure 3**). However, upon removal of the matrix using gentle sonication, we saw up to a 5-fold increase in the amount of fluconazole inside the basal layer of cells, suggesting that the *C. auris* extracellular matrix has a similar drug sequestering capability as seen in other *Candida* species. Additionally, the capability of the matrix to sequester anti-fungal drugs varies with each isolate which is consistent as to what has been observed in other *Candida* species [27, 41, 42].

Prior studies of *Candida* matrices have identified components within the extracellular matrix which play a role in the drug resistance phenotype observed in biofilms, specifically the complex carbohydrates mannan and glucan, which form a mannan-glucan complex (MGCx) [26, 27, 41, 42, 45, 51]. Gas chromatography was used to identify the presence of carbohydrates found within the isolated matrices of all 10 strains (**Figure 4**) and resulted in the detection of mannan and glucan. To elucidate whether these two prominent carbohydrates were playing a role in the observed drug resistance phenotype in *C. auris* biofilms, we used pharmacological and enzymatic treatments to test these interactions.

Treatment with α-mannosidase or zymolase alone had no influence on biofilm cell viability, however, when combined with fluconazole we saw a significant increase in biofilm reduction across all 10 isolates (**Figure 5A, 5B**). Interestingly enough this increase in the efficacy of fluconazole against these *C. auris* biofilms was most prevalent when combined with α-mannosidase opposed to zymolase. Biofilms treated with fluconazole and α-mannosidase resulted in biofilm reduction ranging from 60-95% opposed to the 25-70% range observed in fluconazole and zymolase treated biofilms.

To see whether this increase in drug susceptibility was due to disruption of mannan and/or glucan, we choose three isolates which exhibited the greatest resistance, (B11104, B11221, B11801), and measured the levels of mannan and glucan after α-mannosidase treatment using gas chromatography. We saw a significant decrease of mannan and glucan (50-70%) in each of these strains (**Figure 5C**), compared to untreated strains, suggesting that these carbohydrates have a role in the drug resistance phenotype as seen in other *Candida* species.

Discussion

The ability of a *Candida* species to cause invasive infections has been intimately linked to its ability to form biofilms in patients who are immunocompromised or have serious underlying medical conditions. This statement may also hold true for *C. auris* even though evidence of a biofilm within a patient has yet to be found, regardless of the multiple sites from which *C. auris* has been isolated from which are commonly associated with *C. albicans* biofilm infections [52, 53]. Furthermore, studies have shown that *C. auris* shares a multitude of the virulence factors that are associated with *C. albicans*, such as genes and pathways involved in cell wall modeling and nutrient acquisition, tissue invasion, enzyme secretion, multidrug efflux, and iron acquisition [10, 54-56]. These studies, along with the evidence presented in our current study, show that *C. auris* does have the capability to form biofilms, however whether they are able to within a human host has yet to be seen.

The ability to form a biofilm increases drug resistance not only in *Candida,* but in bacterial pathogens as well. This increased resistance is attributed to the presence of an extracellular matrix which works to sequester antifungals and retain them above the basal layer of cells they need to reach. In *Candida* species a MGCx has been identified which works to enhance the drug resistance phenotype associated with *Candida* biofilms. In *C. albicans* the MGCx is comprised of an α-1,6-mannan backbone with α-1,2 branches and β-1,6-glucan with the same complex being recently identified in *Candida parapsilosis, Candida tropicalis,* and *Candida glabrata,* which contain a similar backbone, but with side chains that are unique for each species. These biofilms, when treated with either α-

mannosidase, tunicamycin, or Brefeldin A, caused a structural breakdown to occur of the complex resulting in increased susceptibility when co-treated with fluconazole [27, 42]. Interesting enough, disruption of mannan and/or glucan in the matrices of *C. auris* biofilms resulted in an increase in susceptibility akin to what we have previously reported for other *Candida* species. These results suggest that not only is mannan and glucan important for drug resistance among the most prevalent *Candida* pathogens, but there may also be a level of evolutionary conservation within the biofilm lifestyle of these species. Furthermore, the levels of functionality and interaction observed between mannan and glucan within these species suggest the potential for the presence of a MGCx, however further studies are necessary in order to validate this hypothesis.

In the current study, we evaluated 10 different *C. auris* clinical isolates and characterized their ability to form biofilms, provided insight to their ultrastructure, measured biofilm resistance against the three main classes of antifungals, performed functional analysis of their matrices, and identified components within their matrices which contribute to drug resistance. Among those components we found mannan and glucan, which are part of MGCx present in the most prevalent pathogenic *Candida* species which may allow for the unique opportunity of alternative methods of targeted drug treatments of biofilm infections with increased efficacy of conventional antifungal therapies. This could allow for physicians to treat said infections in a less invasive manner with the potential to increase overall patient prognosis.

Materials and Methods

Ethics Statement. All animal procedures were approved by the Institutional Animal Care and Use Committee at the University of Wisconsin according to the guidelines of the Animal Welfare Act, The Institute of Laboratory Animal Resources Guide for the Care and Use of Laboratory Animals, and Public Health Service Policy. The approved animal protocol number is DA0031.

Strains and Media:

C. auris isolates obtained from the Centers for Disease Control and Prevention (Table S1) were used for this study.

C. auris strains were stored at -80 ^{o}C in 25% (vol/vol) glycerol and sustained on yeast extract-peptone-dextrose (YPD) medium with uridine. Prior to biofilm experiments, all *C. auris* strains were grown at 30°C in YPD and biofilms were grown in RPMI 1640 (RPMI-1640 Medium, HyClone SH30011.04) buffered with 4-Morpholinepropanesulfonic acid (MOPS, Fisher BP308) at a pH of 7.0.

***In vitro/In vivo* Biofilm Cell Imaging:**

In vitro biofilms were grown on sterile coverslips in 12-well polystyrene plates. 10 µL of FCS was placed on the center of each coverslip and dried at 37^{o} C for 1-2 hours. 40 µL of an inoculum of 10^{8} cells/ml in RPMI-MOPS was placed directly onto the dried FCS and incubated at 37^{o} C for 1 hr. After incubation, all media was removed and 1 ml of RPMI-MOPS supplemented with 5% (vol/vol) FCS was added to each well and incubated for 20 Hr at 37^{o} C with orbital shaking at 50 rpm. The next day media was removed and 1 ml of fixative [4% formaldehyde (vol/vol) and 1% glutaraldehyde in PBS] and incubated at 4^{o} C overnight. Coverslips were then washed with PBS and treated with 1% osmium tetroxide, in PBS, for 30 min at room temperature. Samples were then washed with a series of increasing ethanol dilutions [30-100% (vol/vol)], with 10 min incubations for each wash. Samples were dehydrated

using critical point drying, mounted and coated with palladium. Imaging of samples was done on a SEM LEO 1530 and compiled using Adobe Photoshop CC 2015.5.

In vivo biofilms were grown using rodent biofilm models as previously described [57]. After a 48 hr biofilm formation phase, the implanted medical devices were removed and processed for SEM imaging identically as just described for in vitro biofilms.

Biofilm Formation, Matrix isolation, and Analysis:

Biofilms were grown in 6-well polystyrene plates with extracellular matrix collected from mature 48 hr biofilms as previously described [42, 45]. Cell cultures were grown overnight in YPD medium at 30 ^{o}C with orbital shaking at 200 rpm. Cells were then counted, using a hemocytometer, and resuspended in RPMI-MOPS at 10^6 cells/ml. Biofilms were grown in 6-well plates by inoculating 1 ml of this suspension into each well. Cells were then incubated for 1 hr at 37^{o} C with no shaking to allow for adhesion of cells. After this adhesion period biofilms were then grown at 37^{o} C for 48 hrs on an orbital shaker set at 50 rpm. Medium was replaced at the 24 hr point of this incubation period. Biofilms were harvested by removing and discarding the medium, washing each well with 1 ml of ddH_2O, and then removal of biofilms using a spatula. Biofilms were collected in 1 ml of ddH_2O per well, and then sonicated for 20 min. The soluble matrix was then separated from the biomass by centrifuging the samples at 2,880 x *g* for 20 min at 4^{o} C.

To determine the concentration of mannan and glucan within the matrix, sugars were detected and quantified by gas liquid chromatography-flame ionization detector (GLC-FID) on a Shimadzu GC-2010 system after conversion to alditol acetate derivatives as previously described [58]. A 50% cyanopropylmethyl/50% phenylmethyl polysiloxane column was used (Restek) with the same GLC conditions as previously described [41]. Data for these monosugars were calculated and presented as µg of matrix per mg of biofilm biomass.

Biofilms were quantified through dry weight analysis and metabolic activity. For dry weight analysis biofilms grown in 6 well plates were collected as described above. Biofilms were then lyophilized and weighed to obtain total biomass for each biofilm. Metabolic activity was measured using the XTT assay from the non-treated control wells used in the drug susceptibility assays as described above.

In vitro biofilm antifungal susceptibility testing:

Susceptibility assays were conducted on biofilms grown in 96 well polystyrene plates. Using the same starting inocula as described above, plates were inoculated at 100 µL per well and incubated statically for a 24 hr time period at 37^{o} C. Fresh media and dilutions of amphotericin B (0.016-8 µg/ml), fluconazole (125-1000 µg/ml), or micafungin (0.016-8 µg/ml) were then added followed by a 24 hr incubation period. Biofilms treated with α-mannosidase (0.78 U/ml;jack bean; Sigma) or zymolyase (0.63 U/ml; MP Biomedicals) were grown for 24 hr before a 24-hr dose either alone or in combination with fluconazole.

Biofilms were quantified using a tetrazolium salt XTT {2,3-bis-(2-methoxy-4-nitro-5-sulfophenyl)-2H-tetrazolium-5-carboxanilide inner salt} reduction assay [59, 60]. XTT (80 µL; 0.75 mg/ml), phenazine methosulfate (PMS) (10 µL; 320 µg/ml), and 10 µL of 20% glucose were added for 30 -60 min at 37° C, and an automated plate reader was used to measure absorbance at 492nm. Biofilm reduction was calculated by comparing untreated control biofilms with those with treatment. Assays were performed in triplicate and significant differences were measured by analysis of variance (ANOVA) with pairwise comparisons using the Holm-Sidak method.

Sequestration of ^{3}H Fluconazole in Biofilms:

Radiolabeled fluconazole (Moravek Biochemicals; 50 µM, 0.001 mCi/ml in ethanol) was used in an assay to measure drug retention in biofilms [45, 61]. Biofilms were grown for 48 hrs in 6 well polystyrene plates as described above. Media was removed and biofilms were washed with

sterile water and then incubated with 8.48 x 10^5 cpm of ^{3}H fluconazole in RPMI-MOPS for 30 min at 37^o C with orbital shaking at 50 rpm. Unlabeled fluconazole (20 µM) in RPMI-MOPS was added for an additional 15-min incubation period. After a second wash with sterile water, biofilms and matrix were collected and isolated as described above with cells broken open by bead beating to yield cell wall and intracellular portions. An aliquot of each collected intact biofilm was saved for scintillation counting. To determine cpm, samples were added to a Tri-Carb 2100TR liquid scintillation analyzer after adding ScintiSafe 30% LSC mixture to each sample fraction. Three technical replicates were averaged, the SEs calculated, with values compared to the reference strain using pairwise comparisons with ANOVA with the Holm-Sidak method.

References

1. Ruhnke, M. and G. Maschmeyer, *Management of mycoses in patients with hematologic disease and cancer -- review of the literature.* Eur J Med Res, 2002. **7**(5): p. 227-35.
2. Meiller, T.F., et al., *A novel immune evasion strategy of candida albicans: proteolytic cleavage of a salivary antimicrobial peptide.* PLoS One, 2009. **4**(4): p. e5039.
3. Schulze, J. and U. Sonnenborn, *Yeasts in the gut: from commensals to infectious agents.* Dtsch Arztebl Int, 2009. **106**(51-52): p. 837-42.
4. Sobel, J.D., *Vaginitis.* N Engl J Med, 1997. **337**(26): p. 1896-903.
5. Kabir, M.A., M.A. Hussain, and Z. Ahmad, *Candida albicans: A Model Organism for Studying Fungal Pathogens.* ISRN Microbiol, 2012. **2012**: p. 538694.
6. Rosenbach, A., et al., *Adaptations of Candida albicans for growth in the mammalian intestinal tract.* Eukaryot Cell, 2010. **9**(7): p. 1075-86.
7. Eggimann, P., J. Garbino, and D. Pittet, *Epidemiology of Candida species infections in critically ill non-immunosuppressed patients.* Lancet Infect Dis, 2003. **3**(11): p. 685-702.
8. Larkin, E., et al., *The Emerging Pathogen Candida auris: Growth Phenotype, Virulence Factors, Activity of Antifungals, and Effect of SCY-078, a Novel Glucan Synthesis Inhibitor, on Growth Morphology and Biofilm Formation.* Antimicrob Agents Chemother, 2017. **61**(5).
9. Oh, B.J., et al., *Biofilm formation and genotyping of Candida haemulonii, Candida pseudohaemulonii, and a proposed new species (Candida auris) isolates from Korea.* Med Mycol, 2011. **49**(1): p. 98-102.
10. Sharma, C., et al., *Whole genome sequencing of emerging multidrug resistant Candida auris isolates in India demonstrates low genetic variation.* New Microbes New Infect, 2016. **13**: p. 77-82.
11. Borman, A.M., A. Szekely, and E.M. Johnson, *Isolates of the emerging pathogen Candida auris present in the UK have several geographic origins.* Med Mycol, 2017.
12. Lepak, A.J., et al., *Pharmacodynamic Optimization for Treatment of Invasive Candida auris Infection.* Antimicrob Agents Chemother, 2017.
13. Lockhart, S.R., et al., *Simultaneous Emergence of Multidrug-Resistant Candida auris on 3 Continents Confirmed by Whole-Genome Sequencing and Epidemiological Analyses.* Clin Infect Dis, 2017. **64**(2): p. 134-140.
14. Sherry, L., et al., *Biofilm-Forming Capability of Highly Virulent, Multidrug-Resistant Candida auris.* Emerg Infect Dis, 2017. **23**(2): p. 328-331.
15. Borman, A.M., A. Szekely, and E.M. Johnson, *Comparative Pathogenicity of United Kingdom Isolates of the Emerging Pathogen Candida auris and Other Key Pathogenic Candida Species.* mSphere, 2016. **1**(4).
16. Kumar, D., et al., *Itraconazole-resistant Candida auris with phospholipase, proteinase and hemolysin activity from a case of vulvovaginitis.* J Infect Dev Ctries, 2015. **9**(4): p. 435-7.
17. Chandra, J., et al., *Biofilm formation by the fungal pathogen Candida albicans: development, architecture, and drug resistance.* J Bacteriol, 2001. **183**(18): p. 5385-94.
18. Uppuluri, P., C.G. Pierce, and J.L. Lopez-Ribot, *Candida albicans biofilm formation and its clinical consequences.* Future Microbiol, 2009. **4**(10): p. 1235-7.
19. Ramage, G., et al., *Candida biofilms: an update.* Eukaryot Cell, 2005. **4**(4): p. 633-8.
20. Desai, J.V., A.P. Mitchell, and D.R. Andes, *Fungal biofilms, drug resistance, and recurrent infection.* Cold Spring Harb Perspect Med, 2014. **4**(10).
21. Blankenship, J.R. and A.P. Mitchell, *How to build a biofilm: a fungal perspective.* Curr Opin Microbiol, 2006. **9**(6): p. 588-94.

22. Andes, D.R., et al., *Impact of treatment strategy on outcomes in patients with candidemia and other forms of invasive candidiasis: a patient-level quantitative review of randomized trials.* Clin Infect Dis, 2012. **54**(8): p. 1110-22.
23. Branda, S.S., et al., *Biofilms: the matrix revisited.* Trends Microbiol, 2005. **13**(1): p. 20-6.
24. Flemming, H.C. and J. Wingender, *The biofilm matrix.* Nat Rev Microbiol, 2010. **8**(9): p. 623-33.
25. Baillie, G.S. and L.J. Douglas, *Matrix polymers of Candida biofilms and their possible role in biofilm resistance to antifungal agents.* Journal of Antimicrobial Chemotherapy, 2000. **46**(3): p. 397-403.
26. Taff, H.T., et al., *Mechanisms of Candida biofilm drug resistance.* Future Microbiol, 2013. **8**(10): p. 1325-37.
27. Dominguez, E., et al., *Conservation and Divergence in the Candida Species Biofilm Matrix Mannan-Glucan Complex Structure, Function, and Genetic Control.* MBio, 2018. **9**(2).
28. Satoh, K., et al., *Candida auris sp. nov., a novel ascomycetous yeast isolated from the external ear canal of an inpatient in a Japanese hospital.* Microbiol Immunol, 2009. **53**(1): p. 41-4.
29. Rudramurthy, S.M., et al., *Candida auris candidaemia in Indian ICUs: analysis of risk factors.* J Antimicrob Chemother, 2017. **72**(6): p. 1794-1801.
30. Lee, W.G., et al., *First three reported cases of nosocomial fungemia caused by Candida auris.* J Clin Microbiol, 2011. **49**(9): p. 3139-42.
31. Emara, M., et al., *Candida auris candidemia in Kuwait, 2014.* Emerg Infect Dis, 2015. **21**(6): p. 1091-2.
32. Chowdhary, A., et al., *New clonal strain of Candida auris, Delhi, India.* Emerg Infect Dis, 2013. **19**(10): p. 1670-3.
33. Magobo, R.E., et al., *Candida auris-associated candidemia, South Africa.* Emerg Infect Dis, 2014. **20**(7): p. 1250-1.
34. Calvo, B., et al., *First report of Candida auris in America: Clinical and microbiological aspects of 18 episodes of candidemia.* J Infect, 2016. **73**(4): p. 369-74.
35. Tsay, S., et al., *Notes from the Field: Ongoing Transmission of Candida auris in Health Care Facilities - United States, June 2016-May 2017.* MMWR Morb Mortal Wkly Rep, 2017. **66**(19): p. 514-515.
36. Schelenz, S., et al., *First hospital outbreak of the globally emerging Candida auris in a European hospital.* Antimicrob Resist Infect Control, 2016. **5**: p. 35.
37. Vallabhaneni, S., et al., *Investigation of the First Seven Reported Cases of Candida auris, a Globally Emerging Invasive, Multidrug-Resistant Fungus-United States, May 2013-August 2016.* Am J Transplant, 2017. **17**(1): p. 296-299.
38. Chowdhary, A., et al., *Multidrug-resistant endemic clonal strain of Candida auris in India.* Eur J Clin Microbiol Infect Dis, 2014. **33**(6): p. 919-26.
39. Morales-Lopez, S.E., et al., *Invasive Infections with Multidrug-Resistant Yeast Candida auris, Colombia.* Emerg Infect Dis, 2017. **23**(1): p. 162-164.
40. Kim, M.N., et al., *Candida haemulonii and closely related species at 5 university hospitals in Korea: identification, antifungal susceptibility, and clinical features.* Clin Infect Dis, 2009. **48**(6): p. e57-61.
41. Zarnowski, R., et al., *Novel entries in a fungal biofilm matrix encyclopedia.* MBio, 2014. **5**(4): p. e01333-14.
42. Mitchell, K.F., et al., *Community participation in biofilm matrix assembly and function.* Proc Natl Acad Sci U S A, 2015. **112**(13): p. 4092-7.
43. Rodrigues, C.F., S. Silva, and M. Henriques, *Candida glabrata: a review of its features and resistance.* Eur J Clin Microbiol Infect Dis, 2014. **33**(5): p. 673-88.
44. Sarma, S. and S. Upadhyay, *Current perspective on emergence, diagnosis and drug resistance in Candida auris.* Infect Drug Resist, 2017. **10**: p. 155-165.

45. Taff, H.T., et al., *A Candida biofilm-induced pathway for matrix glucan delivery: implications for drug resistance.* PLoS Pathog, 2012. **8**(8): p. e1002848.
46. Nett, J.E., et al., *Role of Fks1p and matrix glucan in Candida albicans biofilm resistance to an echinocandin, pyrimidine, and polyene.* Antimicrob Agents Chemother, 2010. **54**(8): p. 3505-8.
47. Nett, J.E., et al., *Genetic basis of Candida biofilm resistance due to drug-sequestering matrix glucan.* J Infect Dis, 2010. **202**(1): p. 171-5.
48. Robbins, N., et al., *Hsp90 governs dispersion and drug resistance of fungal biofilms.* PLoS Pathog, 2011. **7**(9): p. e1002257.
49. Mukherjee, P.K., et al., *Mechanism of fluconazole resistance in Candida albicans biofilms: phase-specific role of efflux pumps and membrane sterols.* Infect Immun, 2003. **71**(8): p. 4333-40.
50. Ramage, G., et al., *Investigation of multidrug efflux pumps in relation to fluconazole resistance in Candida albicans biofilms.* J Antimicrob Chemother, 2002. **49**(6): p. 973-80.
51. Mitchell, K.F., et al., *Role of matrix beta-1,3 glucan in antifungal resistance of non-albicans Candida biofilms.* Antimicrob Agents Chemother, 2013. **57**(4): p. 1918-20.
52. Kojic, E.M. and R.O. Darouiche, *Candida infections of medical devices.* Clin Microbiol Rev, 2004. **17**(2): p. 255-67.
53. Nobile, C.J. and A.D. Johnson, *Candida albicans Biofilms and Human Disease.* Annu Rev Microbiol, 2015. **69**: p. 71-92.
54. Sharma, C., et al., *Draft Genome Sequence of a Fluconazole-Resistant Candida auris Strain from a Candidemia Patient in India.* Genome Announc, 2015. **3**(4).
55. Chatterjee, S., et al., *Draft genome of a commonly misdiagnosed multidrug resistant pathogen Candida auris.* BMC Genomics, 2015. **16**: p. 686.
56. Chowdhary, A., C. Sharma, and J.F. Meis, *Candida auris: A rapidly emerging cause of hospital-acquired multidrug-resistant fungal infections globally.* PLoS Pathog, 2017. **13**(5): p. e1006290.
57. Andes, D., et al., *Development and characterization of an in vivo central venous catheter Candida albicans biofilm model.* Infect Immun, 2004. **72**(10): p. 6023-31.
58. Henry, R.J., et al., *Detection of neutral and aminosugars from glycoproteins and polysaccharides as their alditol acetates.* J Chromatogr, 1983. **256**(3): p. 419-27.
59. Taff, H.T., J.E. Nett, and D.R. Andes, *Comparative analysis of Candida biofilm quantitation assays.* Med Mycol, 2012. **50**(2): p. 214-8.
60. Ramage, G. and J.L. Lopez-Ribot, *Techniques for antifungal susceptibility testing of Candida albicans biofilms.* Methods Mol Med, 2005. **118**: p. 71-9.
61. Mansfield, B.E., et al., *Azole drugs are imported by facilitated diffusion in Candida albicans and other pathogenic fungi.* PLoS Pathog, 2010. **6**(9): p. e1001126.

Figure Legends

Figure 1. *C. auris* biofilm ultrastructure. (A) Mature biofilm architecture from in vitro coverslips. (B) Mature biofilm architecture from the in vivo rat catheter model. All biofilms were assessed visually using SEM imaging after 24 hours of incubation. The white arrow indicates extracellular matrix material and scale bars represent 10 µm and 500 µm for the in vivo isolate B11211.

Figure 2. *C. auris* biofilm drug resistance phenotype. Biofilm antifungal susceptibility following 24-h treatment with 1000 µg/ml of fluconazole compared with untreated biofilms. Biofilm reduction was assessed using an XTT assay in a 96-well polystyrene plate assay.

Figure 3. Fluconazole sequestration and binding to the extracellular matrix of *C. auris* biofilms. Sequestration of ^{3}H-labeled fluconazole was assessed using *in vitro* intact biofilms and matrix deprived biofilms. Matrix-deprived biofilms demonstrated an increase of accumulated drug intracellularly and in cell walls as compared to intact biofilms containing matrix. The asterisks indicate statistically significant differences ($p < 0.0001$) between matrix-deprived biofilms and intact biofilms containing matrix based upon unpaired two tailed t-test.

Figure 4. Matrix carbohydrates in the extracellular matrix of *C. auris* biofilms. Mature in vitro biofilms were assayed for matrix mannan and glucan concentrations by gas chromatography. The data for each isolate is presented as µg of matrix/mg of biofilm biomass. Data is represented from three biologic and three assay replicates.

Figure 5. *C. auris* biofilm drug resistance mechanism. (A) Mature biofilms were treated with 1,000 μg/ml fluconazole with and without 0.78 U/ml of the mannan hydrolysis enzyme α-mannosidase. (B) Mature biofilms were treated with 1,000 μg/ml fluconazole with and without 0.63 U/ml of the glucan hydrolysis enzyme zymolase. * reflects a statistically significant ($p < 0.0001$), ** ($p = 0.001$), and *** ($p = 0.01$) difference between the combination and either treatment alone based upon ANOVA using the Holm-Sidak method for pairwise comparison. (C) Mature in vitro biofilms for three of the isolates were assayed for matrix and glucan concentrations, after 24-h growth and 24-h treatment with 0.78 U/ml of α-mannosidase, by gas chromatography. The data for each isolate is presented as a percentage of quantity from the untreated isolate. The figure represents data from three biologic and three assay replicates. * reflects a statistically significant ($p = 0.1$), ** ($p = 0.002$), and *** ($p = 0.0001$) difference between treated and untreated biofilms based upon ANOVA using the Holm-Sidak method for pairwise comparison.

Figure 1

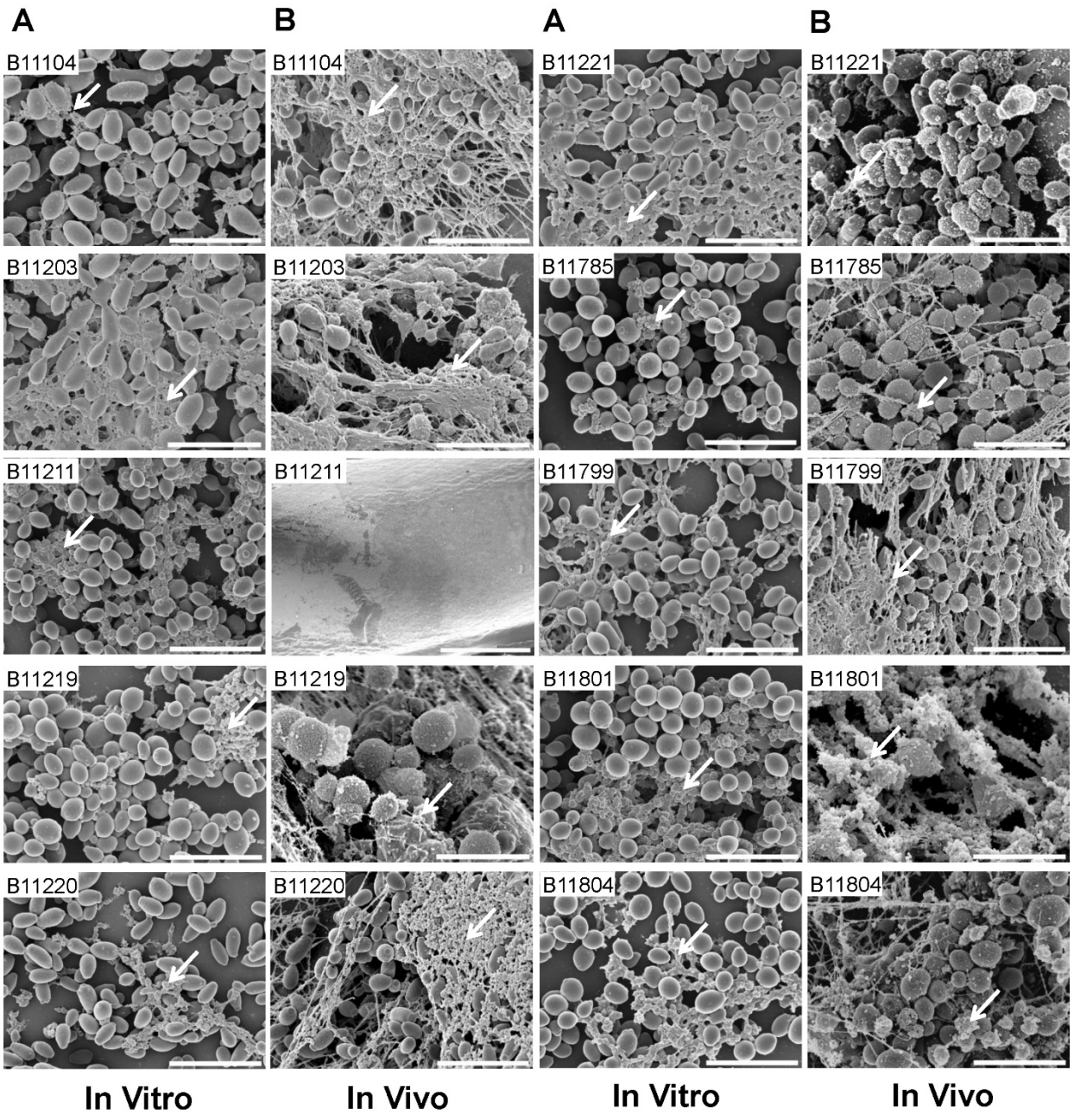
A
B
A
B
B11104
B11104
B11221
B11221
B11203
B11203
B11785
B11785
B11211
B11211
B11799
B11799
B11219
B11219
B11801
B11801
B11220
B11220
B11804
B11804
In Vitro
In Vivo
In Vitro
In Vivo

Figure 2

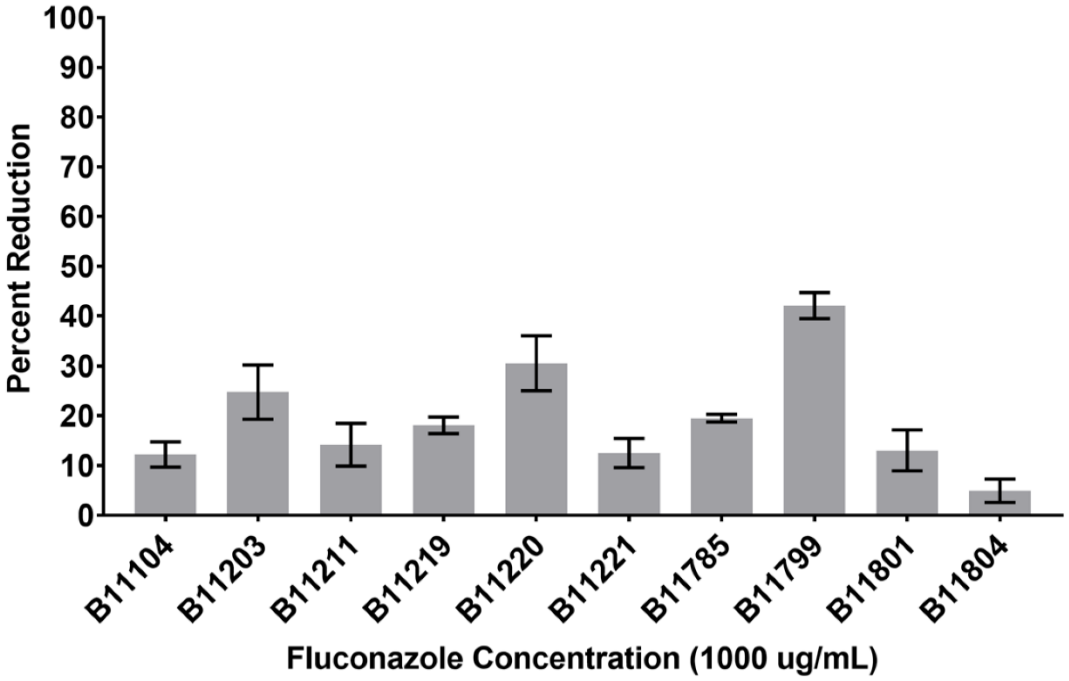
Percent Reduction
100
90
80
70
60
50
40
30
20
10
0
B11104
B11203
B11211
B11219
B11220
B11221
B11785
B11799
B11801
B11804
Fluconazole Concentration (1000 ug/mL)

Figure 3

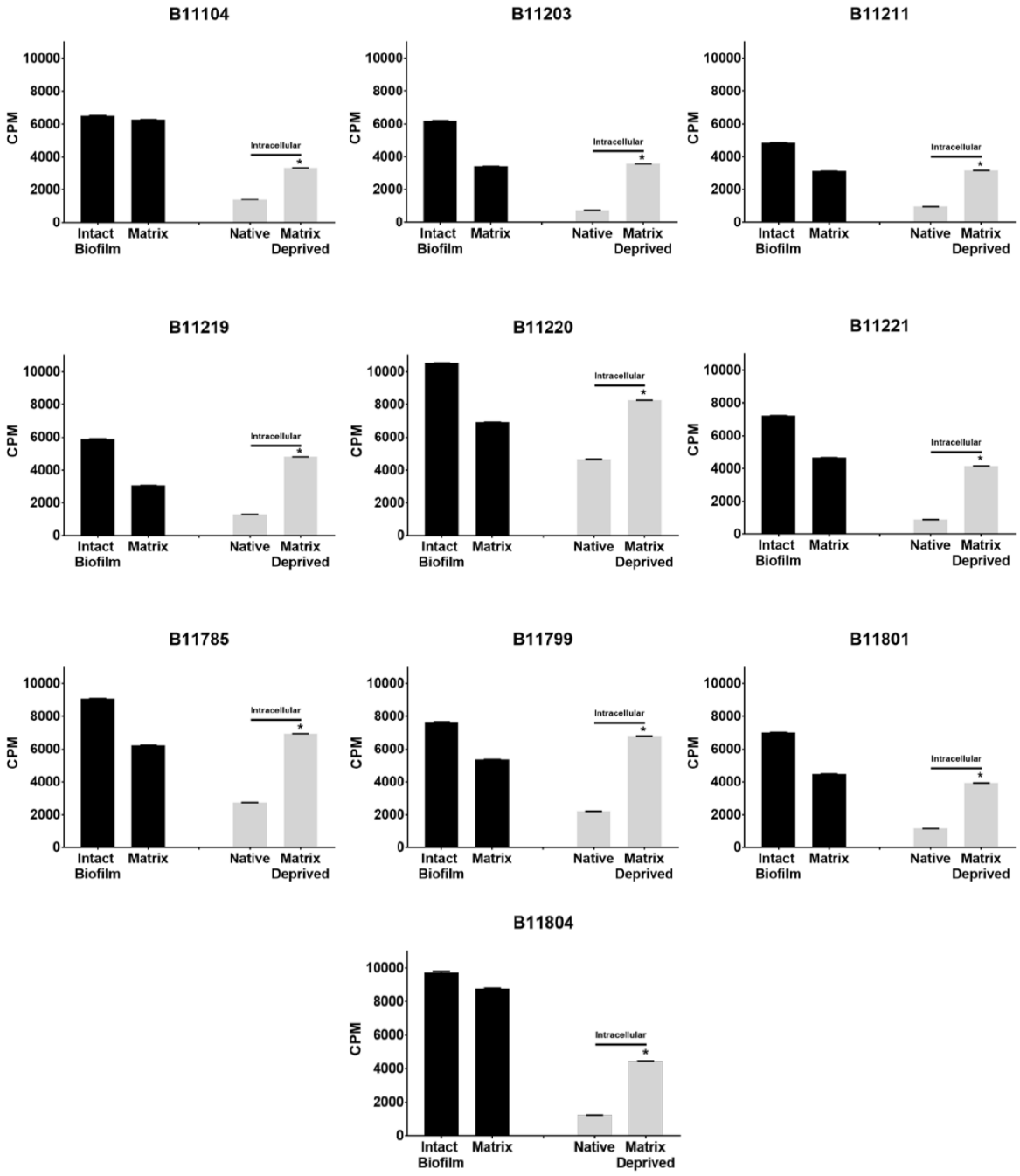
B11104
B11203
B11211
B11219
B11220
B11221
B11785
B11799
B11801
B11804
CPM
10000
8000
6000
4000
2000
0
Intracellular
*
Intact Biofilm
Matrix
Native
Matrix Deprived

Figure 4

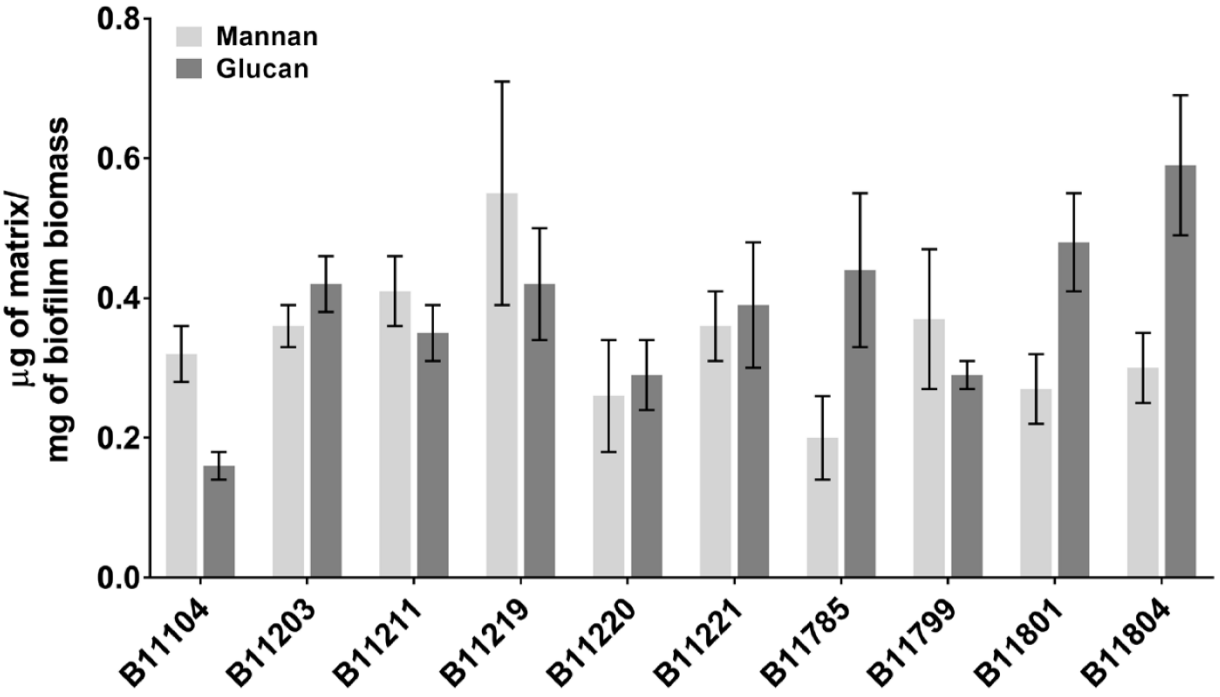
Mannan
Glucan
μg of matrix/
mg of biofilm biomass
0.8
0.6
0.4
0.2
0.0
B11104
B11203
B11211
B11219
B11220
B11221
B11785
B11799
B11801
B11804

Figure 5

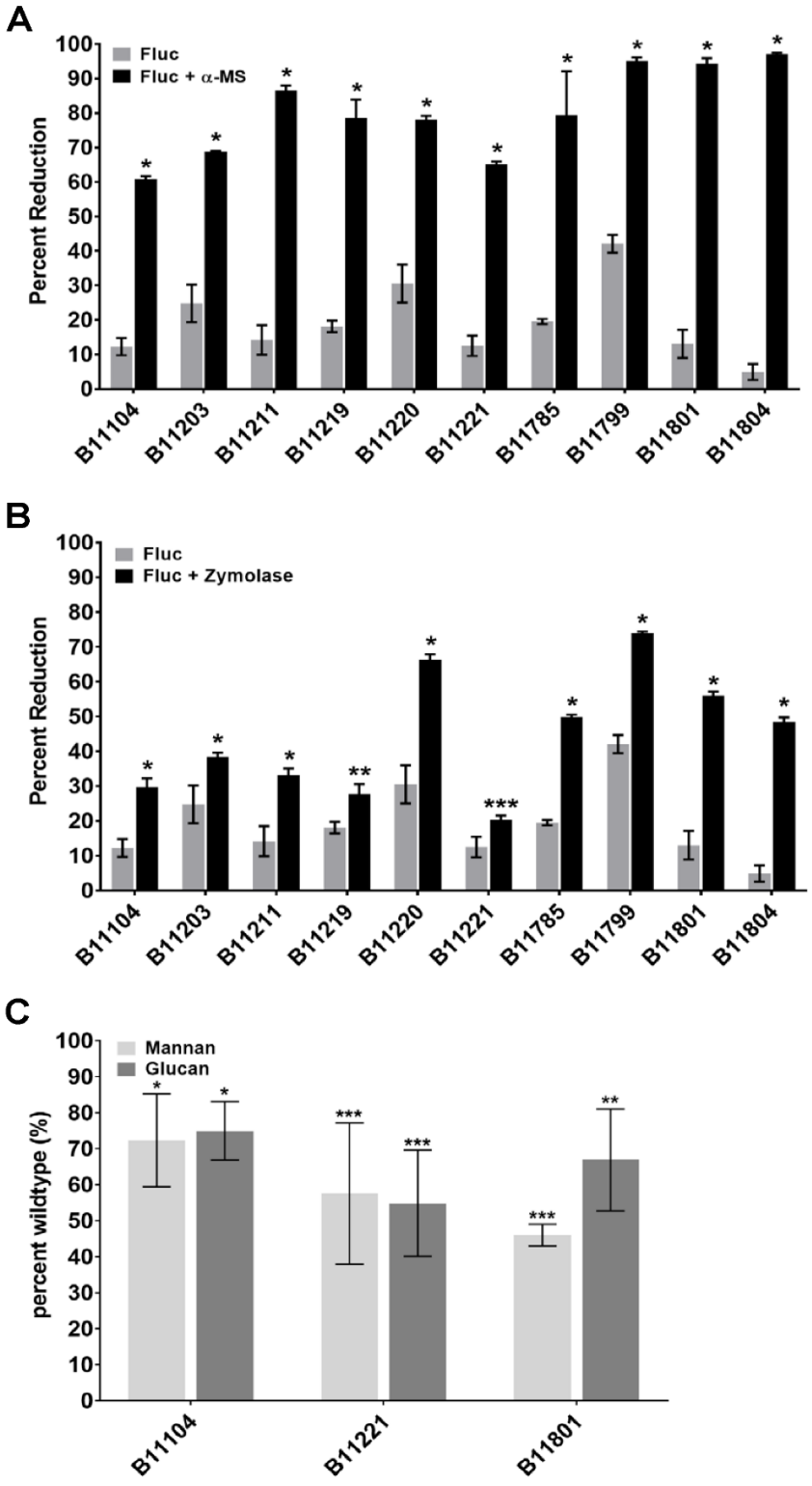
A
Fluc
Fluc + α-MS
Percent Reduction
B11104
B11203
B11211
B11219
B11220
B11221
B11785
B11799
B11801
B11804
B
Fluc
Fluc + Zymolase
Percent Reduction
C
Mannan
Glucan
percent wildtype (%)
B11104
B11221
B11801

Supporting Information Legends

Supplemental Figure S1. *C. auris* forms biofilms. (A) Biofilm adhesion of *C. albicans, C. glabrata,* and *C. auris* isolates was assessed using an XTT assay in a 96-well polystyrene plate assay after 1 hour for adherence. (B) Total biofilm mass was assessed by dry weight measurements from in vitro biofilms grown in 6-well polystyrene plates (3 replicates per strain). * reflects a statistically significant ($p < 0.0001$) difference between *C. glabrata* and *C. auris* as compared to *C. albicans.*

Supplemental Figure S2. Polyene and echinocandin biofilm activity against *C. auris.* Following growth for 24-h, biofilms were treated with either 1 µg/ml amphotericin B or micafungin for 24-h. Biofilms were quantified using the 96-well XTT assay with reduction determined by comparing treated and untreated biofilms. The mean of three technical replicates and SEs are shown.

Table S1. Planktonic Minimum inhibitory Concentration (MIC). The MIC of fluconazole, amphotericin B, and Micafungin for *C. auris* isolates used in this study.

Figure S1

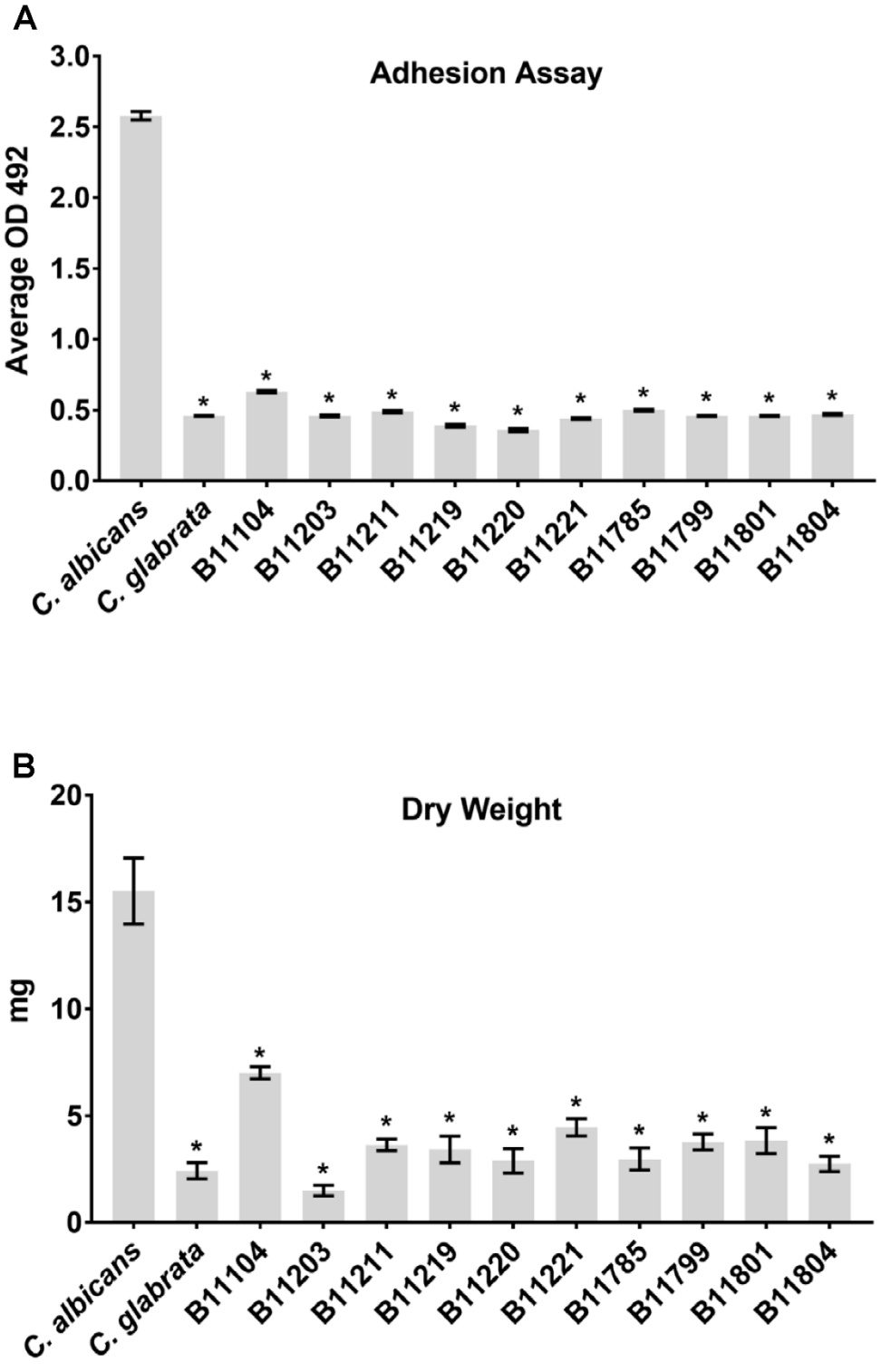
A
Adhesion Assay
Average OD 492
3.0
2.5
2.0
1.5
1.0
0.5
0.0
C. albicans
C. glabrata
B11104
B11203
B11211
B11219
B11220
B11221
B11785
B11799
B11801
B11804
B
Dry Weight
mg
20
15
10
5
0
C. albicans
C. glabrata
B11104
B11203
B11211
B11219
B11220
B11221
B11785
B11799
B11801
B11804

Figure S2

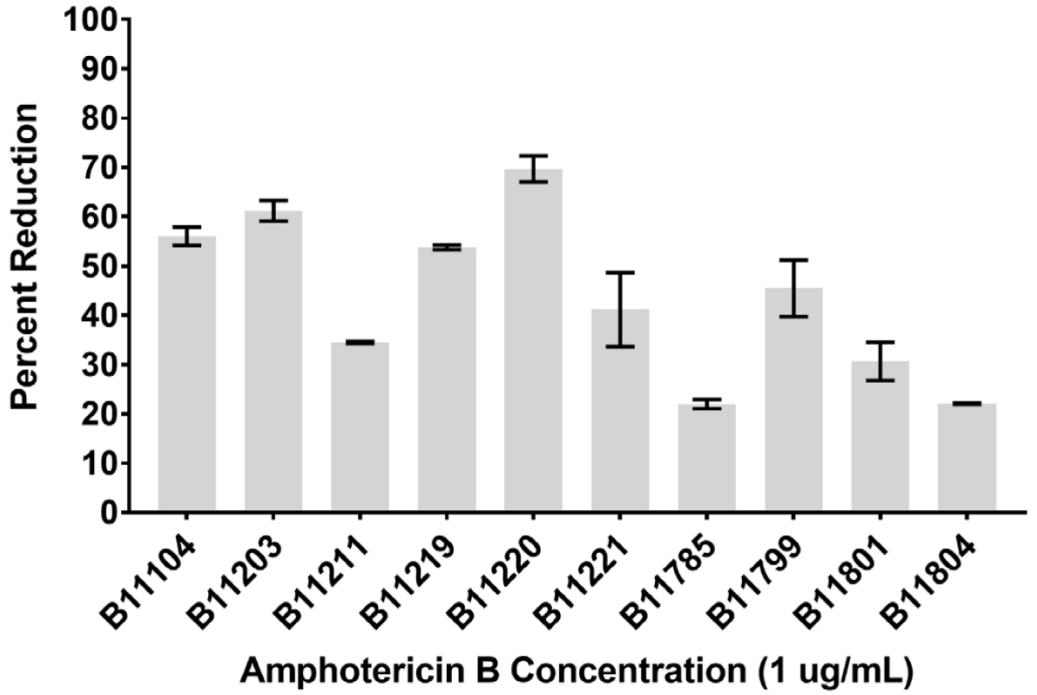
Percent Reduction
100
90
80
70
60
50
40
30
20
10
0
B11104
B11203
B11211
B11219
B11220
B11221
B11785
B11799
B11801
B11804
Amphotericin B Concentration (1 ug/mL)

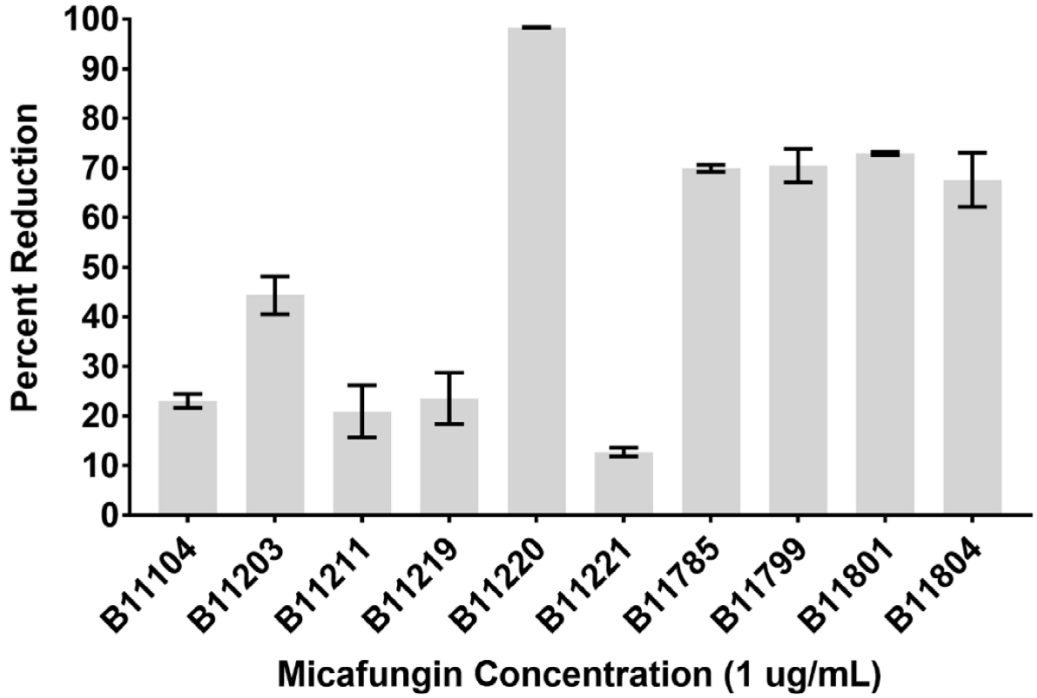
Percent Reduction
100
90
80
70
60
50
40
30
20
10
0
B11104
B11203
B11211
B11219
B11220
B11221
B11785
B11799
B11801
B11804
Micafungin Concentration (1 ug/mL)

Table S1

Table S1. Planktonic MIC (μg/ml)

Strain	Fluconazole	Amphotericin B	Micafungin
B11104	256	1	0.25
B11203	256	4	0.25
B11211	256	0.38	4
B11219	256	3	4
B11220	4	0.38	0.125
B11221	128	0.38	1
B11785	8	1.5	0.5
B11799	16	0.5	2
B11801	16	2	1
B11804	2	0.5	0.5

Chapter 4

Biofilm drug resistance determination by extracellular vesicles

The contents of this section have been submitted for publication and is currently under peer review:

Robert Zarnowski, Hiram Sanchez, Antonio S. Covelli, **Eddie Dominguez**, Anna Jaromin, Jörg Berhardt, Christian Heiss, Parastoo Azadi, Aaron Mitchell, David R. Andes

R. Zarnowski designed, performed experiments, created null mutants, analyzed data, and wrote the manuscript. H. Sanchez performed/analyzed imaging and conducted drug sequestration experiments. AS. Covelli grew biofilms for EV collection and assisted with vesicle experiments. E. Dominguez conducted susceptibility assays, optimized EV add back experiments, and characterized all mutant strains. A. Jaromin is a collaborator from the University of Wroclaw, Poland, and performed TEM and sizing analysis. J. Bernhardt is a collaborator from Ernst-Arndt University, Germany, and assisted with proteomic analysis. C. Heiss and P. Azadi are collaborators from the University of Georgia, Athens, and conducted and analyzed NMR data. A. Mitchell is a collaborator from Carnegie Mellon University, Pittsburgh, and interpreted data and wrote the manuscript. D. Andes supervised the study, interpreted data, and wrote the manuscript.

Abstract

Cells from all kingdoms of life produce extracellular vesicles (EVs). Their cargo is protected from the environment by the surrounding lipid bilayer. EVs from many organisms have been shown to function in cell-cell communication, relaying signals that impact metazoan development, microbial quorum sensing, and pathogenic host-microbe interactions. Here we have investigated the production and functional activities of EVs in a surface-associated microbial community, or biofilm, of the fungal pathogen *Candida albicans*. Crowded communities like biofilms are a context in which EVs are likely to function. Biofilms are noteworthy because they are encased in an extracellular polymeric matrix, and because biofilm cells manifest extreme tolerance to antimicrobial compounds. We found that biofilm EVs are distinct from those produced by free-living planktonic cells, and display strong parallels in composition to biofilm matrix material. The functions of biofilm EVs were defined with a panel of mutants defective in ESCRT subunits orthologs, which are required for normal EV production in diverse eukaryotes. Most ESCRT-defective mutations caused reduced biofilm EV production, reduced matrix polysaccharide levels, and greatly increased sensitivity to the antifungal drug fluconazole. Matrix accumulation and drug hypersensitivity of ESCRT mutants was reversed by addition of wild-type biofilm EVs. Vesicle complementation showed that biofilm EV function derives from specific cargo proteins. Our studies indicate that *C. albicans* biofilm EVs have a pivotal role in matrix production and biofilm drug resistance. Biofilm matrix synthesis is a community enterprise; our prior studies of mixed cell biofilms have demonstrated extracellular complementation. Therefore, EVs function not only in cell-cell communication but also in the sharing of microbial community resources.

Introduction

Vesicles are released externally by cells of bacteria, archaea, and eukaryotes (1-3). These extracellular vesicles (EVs) convey cargo of RNA and protein that is protected by a surrounding lipid bilayer. Classes of EVs have been distinguished based upon their size, cargo, and mechanisms of biogenesis (1-3). Functional analysis has shown that EVs play diverse biological roles in delivery of effectors to target cells. For example, during *Drosophila* wing development, secretion of the morphogenic effector Hedgehog in EVs is required for activation of many of its target genes (4). For many bacterial pathogens, toxin delivery via EVs causes host cell damage or lysis (1). In the case of the eukaryotic protozoan *Trypanosoma brucei*, EVs orchestrate community flight from sources of environmental stress (5). The purpose of EV secretion is thus tailored to each organism's biology and environmental context.

Microorganisms exist predominantly in surface-associated communities called biofilms, which typically have high cell density and include an extracellular polymeric matrix(6). Biofilm cells are notorious for their resistance to antimicrobial treatments (7), a property often determined by multiple mechanisms. Our interest is in the eukaryotic microorganism *Candida albicans*, which poses a severe threat to hospitalized patients with vascular devices due to its capacity for biofilm formation (8, 9). *Candida* proliferates on the surface of these devices as a biofilm (10-12). *Candida* biofilm cells resist available drug therapies (13) and, thus, the only currently effective therapy is removal of medical devices, which is often impossible for critically ill patients (14). One of the central determinants of *C. albicans* biofilm drug resistance is a mannan-glucan complex in the extracellular matrix (15, 16). Our findings reported here show that EVs promote assembly of the mannan-glucan complex and drug resistance. We suggest that drug resistance of other microbial biofilms may also rely upon the efficient sharing of community resources as EV cargo.

Results/Discussion

Production of distinctive biofilm EVs

We have reported that *C. albicans* biofilm extracellular matrix includes a significant phospholipid component (17), a finding that might indicate the presence of EVs in the matrix material. In support of this idea, we observed numerous <100 nm spheres on the surface of biofilm cells (**Fig 1A**) and embedded in the extracellular matrix (**Fig 1B**). EVs, isolated from biofilm(18, 19) and imaged by cryoTEM, were enriched for an exosome population based upon size (20) (**Fig 1C**), though other vesicle types may be included in the preparation. Time course studies revealed that vesicle production peaks at 12-48 h after biofilm initiation (**Fig 1D**); these kinetics parallel the time course of matrix deposition (21). Our results indicate that *C. albicans*, like many other microbes (1), produces biofilm EVs.

EVs are known to be produced by free-living planktonic cells of numerous fungi including *Candida albicans* (1, 22, 23). We assessed the similarity of biofilm and planktonic EVs though comparisons of their sizes and composition. We verified the finding from studies of *Saccharomyces cerevisiae* (24) that two populations of planktonic EVs are produced (**Fig 1E**). There is a 30-200 nm-diameter population that corresponds in size to exosomes, and a larger 200-1000 nm-diameter population that corresponds in size to microvesicles (24). In contrast, biofilm EVs comprise predominantly a 30-200 nm-diameter exosome-sized population (**Fig 1F**). Proteomic analysis revealed that planktonic and biofilm EVs have a considerable proportion of distinct cargo, with 34% of the proteome being unique to the biofilm state (**Fig 2A-C and supplemental Table 1**). In addition, many proteins shared by vesicles from both sources were up to 100-fold more abundant in the biofilm EVs. Our results indicate that EVs produced by biofilms are distinct from those of planktonic cells.

The composition of biofilm EVs pointed toward two prospective roles in biofilm extracellular matrix biogenesis. First, vesicle composition shows a quite high degree of similarity with matrix composition in lipid **(Fig 2G)**, protein **(Fig 2D-F)**, and polysaccharide **(Fig 2H-I)**, thus suggesting that vesicles may be a major source of matrix material. The protein comparison suggests that up to 45% of the proteins in the biofilm matrix may be delivered by vesicles (**Fig 2F**

and Supplemental Table 2). Polysaccharide analysis revealed a predominance of mannan and glucan, two major matrix components, in vesicle cargo (**Fig 2H-I**). The mannan and glucan cargo displayed structural similarity to the biofilm matrix mannan-glucan complex (**Fig 2H-I**), a determinant of biofilm associated drug-resistance (25). Thus, biofilm vesicles may deliver cargo that forms the extracellular matrix. A second possible role is that vesicle cargo have a catalytic function in matrix macromolecule synthesis. Specifically, one of the enriched functional ontology categories for the biofilm EV proteome was polysaccharide modification (**Fig 2A-F)**. These observations suggest that biofilm EVs may deposit cargo that contributes directly to matrix structure, and they may also provide catalytic activities that engage in matrix polysaccharide synthesis.

Role of biofilm EVs in matrix production

We sought to test our hypothesis that biofilm EVs function in matrix biogenesis. The size range of biofilm EVs suggests that they are exosomes (20) and in other eukaryotes exosome production is governed by the endosomal ESCRT pathway (20). In fact, we note that biofilm vesicle cargo includes ESCRT subunits Hse1 and Vps27 (**Supplemental Table 1**). We identified 21 ESCRT subunit homologs in *C. albicans* and created homozygous deletion mutants (**Fig 3A-B**). Strikingly, sixteen of the mutants showed decreased vesicle production (**Fig 3B**). We note that exosome production depends upon only a subset of ESCRT subunits in other eukaryotes(3, 20), in keeping with our observations for *C. albicans*. The ESCRT mutants with reduced EV production enabled us to test whether biofilm vesicles have a role in biofilm matrix biogenesis and function.

We screened the ESCRT vesicle-defective mutants for biofilm matrix-associated phenotypes. All mutants produced a biofilm structure, but a subset had prominent defects in antifungal resistance and matrix production (**Fig 3C-G**). The clinical relevance of these observations was confirmed via demonstration of congruent drug-susceptibility phenotypes in the

rat vascular catheter biofilm model (26) (**Fig 3C**). Our previous studies have shown that biofilm matrix sequesters antifungals to promote drug resistance (15, 16, 27), and we verified that the drug-susceptible ESCRT mutants were also defective in sequestration (**Fig 3E**). We considered two models for the relationship between ESCRT function, biofilm EVs, and matrix biogenesis. One model is that biofilm EVs have a direct role in matrix biogenesis; ESCRT defects cause matrix defects by reducing the levels of vesicles or packaging of functionally relevant cargo. An alternative model is that EVs have no role in matrix biogenesis; ESCRT defects cause matrix defects due to indirect effects. The second model stems from the growing appreciation that ESCRT machinery, with its central role in organelle physiology, has impact on diverse aspects of cell biology(28). We used a "vesicle add-back" protocol to test these models (**Fig 4A**). Specifically, if vesicles have a direct role in matrix biogenesis, then providing wild-type biofilm vesicles to a vesicle-defective ESCRT mutant should restore matrix production and matrix-associated phenotypes. Remarkably, the addition of the wild-type vesicles to drug susceptible ESCRT mutants increased drug resistance dramatically (**Fig 4B**). Furthermore, the addition of wild-type biofilm vesicles restored biofilm matrix architecture and quantities of the key mannan-glucan components (**Fig 4C and D**). These results support the first model: a subset of ESCRT subunits promote matrix biogenesis and function through their role in biofilm EV production.

Biofilm EV function in cargo delivery

Among the proteins in biofilm EVs, several have previously defined roles in biofilm matrix biogenesis and specifically matrix polysaccharide modification (**Supplemental Table 2**) (15, 25). We considered a model in which presence of these proteins as vesicle cargo is central to their functional activity; they are "functional passengers." An alternative model is that they are "coincidental passengers" in vesicles, and that their true function is vesicle-independent. For example, they may function in matrix biogenesis at intracellular sites or after conventional secretion into the extracellular milieu. We deployed our vesicle add-back protocol to test these

models, using mutants in cargo proteins Phr1 and Sun41, which act in the glucan modification pathway (**Fig 4E**). Remarkably, addition of wild-type vesicles to these drug susceptible cargo mutants restored drug resistance. These results favor the functional passenger model - that cargo proteins function to confer biofilm drug resistance as vesicle components, rather than through some vesicle-independent activity.

Our results indicate that biofilm growth of *C. albicans* results in a distinctive EV population and cargo. These findings echo studies of bacterial and eukaryotic cells that show that EV properties reflect environmental and developmental signals (1, 3). Our findings also add a new facet to the understanding of EV function: whereas prior studies have shown a role for EVs in cell-cell signaling, our studies reveal a role for EVs in the sharing of community resources (25), that of biofilm matrix material. Matrix is a pivotal determinant of *C. albicans* biofilm drug resistance, and our results reveal EV-dependence of drug resistance both in vitro and in an animal biofilm infection model. Our findings suggest that EV-based therapeutics (29) may be a useful new platform for anti-biofilm strategies.

Materials and Methods

Fungal strain construction and growth conditions. The parent strain *Candida albicans* SN152 was used to create homozygous deletion strains (**Supplemental Table 6**) using a SOE-PCR-based disruption cassette method employing histidine and lysine auxotrophic markers (30). PCR with primers listed in **Supplemental Table 5** was used to verify genotypes. Complementation of mutant strains with a single gene-of-interest copy used selection for arginine prototrophy. Transformants were selected on minimal medium with the corresponding auxotrophic supplements. Both planktonic and biofilm cultures were grown in RPMI 1640 buffered with 4-morpholinepropanesulfonic acid (MOPS) for all experiments described below(31).

In vitro biofilm models. Biofilms were grown in one of four models: 96-well or 6-well polystyrene plate, polystyrene roller-bottle, or glass coverslip. Ninety six-well flat-bottom polystyrene plates were used to assess biofilm treatment effect as previously described (32, 33). The 6-well plate assay was used to assess matrix composition. The coverslip assay was used for in vitro biofilm SEM imaging. A rolling bottle system was used to generate matrix for analyses (31). At least three biological replicates were performed for each assay.

Matrix isolation from roller bottle and 6-well biofilms. A rolling bottle system was used to generate matrix for composition analyses (31). After incubation for 48 h, media was removed and the *Candida* biofilms were dislodged by spatula and gently sonicated to avoid cell wall disruption (sonication with a 6mm microtip at 20 kHz with an amplitude of 30% for 8 min). The aggregate biofilm was then centrifuged to separate fungal cells and matrix. The supernatant-containing matrix was then collected and lyophilized. Matrix was similarly collected from 6-well plates, as published previously(15).

Large-scale purification of extracellular vesicles. Extracellular vesicles were isolated from both planktonic cultures and large-scale biofilms grown in polystyrene roller bottles(31). The culture media was removed from the bottles, filter-sterilized, and concentrated down to 25 ml using a Vivaflow 200 unit (Sartorius AG, Goettingen, Germany) equipped with a Hydrosart 30 kDa cut-off membrane. The sample was centrifuged at 10,000×*g* for 1 h at 4°C to remove smaller cellular debris. The pellets were discarded, and the resulting supernatant was centrifuged again as described above. The resulting supernatant was then centrifuged at 100,000×*g* for 1.5 h at 4°C. The supernatants were then discarded, and the pellet was then resuspended in PBS (pH 7.2). Next, the sample was subject to size exclusion chromatography on a HighPrep 16/60 Sephacryl™ S-400 HR column (GE Life Sciences) pre-equilibrated with PBS (pH 7.2) containing 0.01% NaN_3. All chromatographic separation steps were performed at room temperature on the

high-performance liquid chromatography ÄKTA-Purifier 10 system (Amersham Biosciences AB, Uppsala, Sweden).

Quantitative vesicle analysis using imaging flow cytometry. Extracellular vesicles were quantified using a combination of imaging flow cytometry, image confirmation, and fluorescence sensitivity in low background samples as previously described (34, 35). Prior to analysis, samples were stained with carboxyfluorescein succinimidyl ester (CSFE) and 1,1'-dioctadecyl-3,3,3',3'-tetramethylindocarbocyanine perchlorate (DiI) at 37^{o}C for 90 min. Excessive dye particles were removed from stained vesicles using illustra microspin G-50 columns (GE Healthcare). All samples were analyzed on the ImageStreamX Mk II flow cytometry system from Amnis Corporation (Seattle, WA, USA) at ×60 magnification with default low flow rate/high sensitivity using the INSPIRE software.

Measurements of extracellular vesicles. The mean particle size of the vesicles dispersions were determined using a Zetasizer Nano-ZS (Malvern Instruments, Malvern, UK). In order to obtain the optimum light scattering intensity, 10 µl of the vesicles suspension was added to 990 µl of PBS. All the measurements were carried out in triplicate at 25°C (36).

Imaging of extracellular vesicles and biofilms. For SEM of biofilms, 40 µl of an inoculum of 10^8 cells/ml in RPMI-MOPS was added to the coverslips and incubated 60 min at 37^{o}C. 1 ml RPMI-MOPS was added to each well and the plates were incubated at 37^{o}C for 20 h1 ml fixative (4% formaldehyde, 1% glutaraldehyde in PBS) was then added to each well prior to incubation at 4°C overnight. Coverslips were then washed with PBS prior to incubation for 30 min in 1% osmium tetroxide. Samples were then serially dehydrated in ethanol (30 to 100%). Critical point drying was used to completely dehydrate the samples prior to palladium-gold coating. Samples were imaged on a SEM LEO 1530, with Adobe Photoshop 7.0.1 used for image compilation (25).

For cryo-TEM, 3 µl of a sample suspensions were pipetted onto a glow-discharged 200 mesh copper grid with a lacey carbon support film (EMS, 1560 Industry Road, Hatfield, PA 19440, USA, #LC200-CU). Before sample application the grid was mounted on a tweezer in the Vitrobot (FEI, 5350 NE Dawson Creek Drive, Hillsboro, OR 97124, USA, model MarkIII). In an automated sequence, excess fluid was blotted off, and the grid was plunge frozen in liquid ethane. Once frozen, the grid was mounted in a precooled cryo transfer sample holder (Gatan,780 Commonwealth Drive, Warrendale, PA 15086, USA, model 626), and inserted into the TEM (Hitachi Ltd., 4026, Kuji-cho, Hitachi-shi, Ibaraki, 319-12, Japan, model HT7700). The samples were observed at 120 kV acceleration voltage and the sample temperature was kept at -170° C.

Gel-free proteome analysis. Enzymatic "in liquid" digestion and mass spectrometric analysis was done at the Mass Spectrometry Facility, Biotechnology Center, University of Wisconsin-Madison. 200 µg of matrix proteins were extracted by precipitation with 15% TCA/60% acetone and then incubated at -20°C for 30 min. The matrix or vesicle preparation was centrifuged at 16,000×*g* for 10 min and the resulting pellets were washed twice with ice-cold acetone followed by an ice-cold MeOH wash. Pelleted proteins were re-solubilized and denatured in 10 µl of 8 M urea in 100 mM NH_4HCO_3 for 10 min, then diluted to 60 µl for tryptic digestion with the following reagents: 3 µl of 25 mM DTT, 4.5 µl of acetonitrile, 36.2 µl of 25 mM NH_4HCO_3, 0.3 µl of 1M Tris-HCl and 6 µl of 100 ng/µl Trypsin Gold solution in 25 mM NH_4HCO_3 (Promega Co., Madison, WI). Digestion was conducted in two stages, first overnight at 37°C, then additional 4 µl of trypsin solution were added and the mixture was incubated at 42°C for additional 2 h. The reaction was terminated by acidification with 2.5% TFA to a final concentration of 0.3%, and then centrifuged at 16,000×*g* for 10 min. Trypsin-generated peptides were analyzed by nanoLC-MS/MS using the Agilent 1100 nanoflow system (Agilent, Palo Alto, CA) connected to a hybrid linear ion trap-orbitrap mass spectrometer (LTQ-Orbitrap, Thermo Fisher Scientific, San Jose, CA) equipped

with a nanoelectrospray ion source. Capillary HPLC was performed using an in-house fabricated column with an integrated electrospray emitter as described elsewhere (37). Sample loading and desalting were achieved using a trapping column in line with the autosampler (Zorbax 300SB-C18, 5 µm, 5 × 0.3 mm, Agilent). The LTQ-Orbitrap was set to acquire MS/MS spectra in a data-dependent mode as follows: MS survey scans from m/z 300 to 2000 were collected in profile mode with a resolving power of 100,000. MS/MS spectra were collected on the 5 most-abundant signals in each survey scan. Dynamic exclusion was employed to increase the dynamic range and maximize peptide identifications. Raw MS/MS data were searched against a concatenated *C. albicans* amino acid sequence database using an in-house MASCOT search engine (38). Identified proteins were further annotated and filtered to 1.5% peptide and 0.1% protein false-discovery-rate with Scaffold Q+ version 3.0 (Proteome Software Inc., Portland, OR) using the protein prophet algorithm (39).

Functional mapping of the extracellular vesicle and matrix proteomes. The *Candida albicans* vesicle and matrix proteomes were analyzed using the Kyoto Encyclopedia of Genes and Genomes (KEGG) (40, 41). Each protein predicted from the *C. albicans* genome assigned a KEGG Ontology ID (KOID) was obtained, and the specific pathway and superpathway membership information retained. This was then correlated with the experimental proteome data, and the number of proteins expressed within a given pathway was then determined. Tabulated proteins were presented as a percentage out of the total number of proteins predicted to belong to a given pathway from the *C. albicans* genome, as determined by KEGG. The visualization of relative quantities of biofilm proteins was also done using KEGG protein functional categorization. On the basis of this hierarchical classification scheme Voronoi treemaps were constructed (42). This approach divides screen space according hierarchy levels where main functional categories determine screen sections on the first level, subsidiary categories on the second level and so forth. The polygonic cells of the deepest level represented functionally classified proteins and

were colored according to relative abundance of each protein that was determined based on total counts of corresponding trypsin-digested peptides.

Isolation and analysis of extracellular vesicle and matrix lipids. Lipids were extracted from the desalted lyophilized extracellular vesicle or matrix powder with a mixture of $CHCl_3$/MeOH (2:1, by vol.) containing 0.1 g/l BHT. The sample was vortexed, incubated in the darkness for 2 h at room temperature and then centrifuged. The separated layer of organic solvents was removed and the pellet was washed with 2 ml of $CHCl_3$/MeOH (2:1, by vol.) and centrifuged. The collected lipid extracts were combined and dried under a stream of nitrogen. After drying, the sample was reconstituted in 0.5 ml of $CHCl_3$/MeOH (2:1, by vol.) and subjected to TLC separation on 20 cm × 20 cm silica gel Si60 plates. Neutral lipids were separated in hexane/ethyl ether/AcOH (90:20:1, by vol.), which yielded triacylglycerols, sterol esters, free fatty acids, and a pool of immobile phospholipids. The latter group was scrapped off the plate, extracted from the silica gel and subjected to another TLC separation in $CHCl_3$/MeOH/AcOH/H_2O (50:37.5:3.5:2, by vol.). This step yielded four classes of glycerolipids (phosphatidylcholine, phosphatidylethanolamine, phosphatidylserine, and phosphatidylinositol) and one class of sphingolipids (sphingomyelins). Lipids were visualized under UV light after spraying plates evenly with a 0.2% solution of fluorescein in EtOH. All isolated lipid classes were scraped off their silica gel plates and re-extracted with $CHCl_3$/MeOH (4:1, by vol.) containing 0.1g/l BHT. Samples were vortexed, incubated overnight at room temperature and then centrifuged in order to remove silica gel particles. 100 μl of 0.05 mg/ml pentadecanoic acid was added to each sample and the organic solvents were evaporated under nitrogen. Next, isolated lipids were subjected to methylation in the presence of 0.5 ml of 14% BF_3 in MeOH. Vials containing the processed lipids were boiled. After cooling, the samples were mixed with 1 ml hexane and 0.5 ml H_2O, vortexed and centrifuged. The top hexane layer containing methyl ester derivatives were transferred to a new clean glass

tube, dried under nitrogen, resuspended in 100 μl hexane and transferred to GC vials. Fatty acid methyl esters were identified by gas chromatography using a Hewlett-Packard 5890 equipped with a capillary column coated with DB-225 (30-m length, 0.25 mm, internal diameter, 0.25 μm; Agilent Technologies, Inc., Wilmington, DE). Peaks were identified by a comparison of retention times with a set of authentic fatty acid standards provided by Supelco. The abundance of fatty acids was calculated from the relative peak areas (17).

Isolation and purification of vesicle and matrix carbohydrates. Delipidated vesicle and matrix pellets containing carbohydrates and proteins were washed twice with acetone, dried under a stream of nitrogen and reconstituted in 3 ml of 20 mM bis-Tris/HCl (pH 6.5) loading buffer. Aliquots were chromatographically desalted on a HiPrep™ 26/10 Desalting column (GE Healthcare Life Sciences, Uppsala, Sweden) and then separated on an anion exchanger HiPrep™ 16/10 DEAE FF column (GE Healthcare Life Sciences) equilibrated with 20 mM bis-Tris/HCl (pH 6.5). Carbohydrate positive flow-through fractions were pooled together, lyophilized, resuspended in 15% acetonitrile in 150 mM ammonium bicarbonate, and applied to gel filtration on a HighPrep 16/60 Sephacryl™ S-300 HR column (GE Healthcare). All chromatographic separation steps were performed at room temperature on the high-performance liquid chromatography ÄKTA-Purifier 10 system (GE Healthcare Life Sciences).

Monosugar composition analysis. Sugars were converted to alditol acetate derivatives according to the procedure described previously (43). Monosugar alditol derivatives were identified and quantified by GLC-FID on a Shimadzu GC-2010 system (Shimadzu Co., Kyoto, Japan) using a (50% cyanopropylphenyl) methylpolysiloxane column (#007-225; 30 m × 0.25 mm with 0.25 μm film thickness,) (Quadrex Co., Woodbridge, CT).

NMR spectroscopy. The samples were dissolved in 100 µl water and precipitated by addition of 900 µl EtOH. After centrifugation, the precipitate was dried, dissolved in D_2O (99.9% D, Sigma-Aldrich), and lyophilized. The sample was then dissolved in 280 µl D_2O (99.96% D, Cambridge Isotope Laboratories) containing 0.5 µl acetone and placed into a 5-mm NMR tube with magnetic susceptibility plugs, matched to D_2O (Shigemi). NMR experiments were recorded at 65 °C on an Agilent Inova-600 spectrometer, equipped with a 5-mm cryoprobe. The 1-D proton experiment was acquired in 8 transients with water presaturation. The 2-D COSY experiment was collected with gradient enhancement in 400 increments of 8 transients each. The 2-D TOCSY and NOESY experiments were acquired with water presaturation in 128 increments of 16 transients each. Spinlock time in TOCSY was 80 ms, and mixing time in NOESY was 200 ms. The gradient-enhanced ^{1}H-^{13}C HSQC experiment with adiabatic 180° carbon pulses and multiplicity editing was acquired in 128 increments of 64 transients each and with a spectral width of 18091 Hz in the carbon dimension. The gradient-enhanced ^{1}H-^{13}C HMBC experiment with adiabatic 180° carbon pulses was acquired in 128 increments of 128 transients each and with a spectral width of 18091 Hz in the carbon dimension. Chemical shifts were measured relative to DSS at 0 ppm in both proton and carbon scales by setting the chemical shift of internal acetone to 2.218 ppm (proton) and 33.0 ppm (carbon). Chemical shifts assignments reported in **Supplemental Tables 3 and 4** were performed based on literature values reported elsewhere (44).

***In vitro* biofilm antifungal susceptibility assay.** A tetrazolium salt XTT [2,3-bis-(2-methoxy-4-nitro-5-sulfophenyl)-2H-tetrazolium-5-carboxanilide inner salt] reduction assay was used to measure in vitro biofilm drug susceptibility (15). The antifungal studied included fluconazole at 1,000 µg/ml. The percent reduction in biofilm growth was calculated using the reduction in absorbance compared to that of controls with no antifungal treatment. Assays were performed in triplicate, and significant differences were measured by one-way analysis of variance (ANOVA) with the post-hoc Bonferroni and Holm methods (45).

In vivo *Candida* venous catheter biofilm model. A jugular vein rat central venous catheter infection model was used for in vivo biofilm studies (26). Following a 24 h incubation period the catheters were removed for quantitative plate count of viable *C. albicans.* For drug treatment experiments, fluconazole (250 µg/ml) was instilled in the catheter after 24 h of biofilm growth. After a 24 h drug treatment period, the post treatment viable burden of *Candida* biofilm on the catheter surface was measured by viable plate counts. We utilized three replicates for each condition.

Ethics Statement. All animal procedures were approved by the Institutional Animal Care and Use Committee at the University of Wisconsin according to the guidelines of the Animal Welfare Act, The Institute of Laboratory Animal Resources Guide for the Care and Use of Laboratory Animals, and Public Health Service Policy. The approved animal protocol number is DA0031.

Sequestration of ^{3}H fluconazole in biofilms. Radiolabeled fluconazole was used in an assay to assess drug retention in biofilms formed in 6-well plates (46). Biofilms were grown for 48 hrs in 6 well polystyrene plates as described above, washed, and then incubated with 8.48 x 10^5 cpm of ^{3}H fluconazole (Moravek Biochemicals; 50 µM, 0.001 mCi/mL in ethanol) in RPMI-MOPS for 30 min at 37^{o} C with orbital shaking at 50 rpm. Unlabeled fluconazole (20 µM) in RPMI-MOPS was added for an additional 15-min incubation period. After washing, biofilms and matrix were collected and isolated as described above. Samples were added to a Tri-Carb 2100TR liquid scintillation analyzer after adding ScintiSafe 30% LSC mixture to each sample fraction. Three biologic and technical replicates were averaged, the SEs calculated, with values compared to the reference strain using pairwise comparisons with ANOVA with the Holm-Sidak method.

EV addback assay. Biofilms were formed in the wells of 96-well microtiter plates, as described above. After a 5 h biofilm formation period, the biofilms were washed with phosphate-buffered saline (PBS) twice and purified EVs at concentrations of 21804±1711 EVs/ml were added. For treatment studies, after an additional hour if incubation, biofilm cultures were amended with fluconazole (1,000 µg/ml) followed by the drug treatment protocol described above. For biofilm matrix studies, the samples were incubated for an additional 24 hours prior to either SEM imaging or matrix isolation for quantitative carbohydrate analysis.

Author contributions: RZ designed, performed experiments, analyzed data, and wrote the manuscript. HS performed and analyzed imaging, animal, and drug sequestration experiments, ASC performed vesicle experiments, ED performed and analyzed biofilm susceptibility and EV add back experiments, AJ performed and analyzed EV sizing experiments, JB analyzed lipidomic and proteomic data, CH and PA analyzed NMR data, APM interpreted data and wrote the manuscript, DRA supervised the study, designed and interpreted data, and wrote the manuscript.

References

1. Brown L, Wolf JM, Prados-Rosales R, Casadevall A. Through the wall: extracellular vesicles in Gram-positive bacteria, mycobacteria and fungi. Nat Rev Microbiol. 2015;13(10):620-30.
2. Choi DH, Kwon YM, Chiura HX, Yang EC, Bae SS, Kang SG, et al. Extracellular Vesicles of the Hyperthermophilic Archaeon "Thermococcus onnurineus" NA1T. Appl Environ Microbiol. 2015;81(14):4591-9.
3. Juan T, Furthauer M. Biogenesis and function of ESCRT-dependent extracellular vesicles. Semin Cell Dev Biol. 2018;74:66-77.
4. Matusek T, Wendler F, Poles S, Pizette S, D'Angelo G, Furthauer M, et al. The ESCRT machinery regulates the secretion and long-range activity of Hedgehog. Nature. 2014;516(7529):99-103.
5. Eliaz D, Kannan S, Shaked H, Arvatz G, Tkacz ID, Binder L, et al. Exosome secretion affects social motility in Trypanosoma brucei. PLoS Pathog. 2017;13(3):e1006245.
6. Hall-Stoodley L, Costerton JW, Stoodley P. Bacterial biofilms: from the natural environment to infectious diseases. Nat Rev Microbiol. 2004;2(2):95-108.
7. Koo H, Allan RN, Howlin RP, Stoodley P, Hall-Stoodley L. Targeting microbial biofilms: current and prospective therapeutic strategies. Nat Rev Microbiol. 2017;15(12):740-55.
8. Pfaller MA, Diekema DJ. Epidemiology of invasive candidiasis: a persistent public health problem. Clinical microbiology reviews. 2007;20(1):133-63.
9. Cleveland AA, Farley MM, Harrison LH, Stein B, Hollick R, Lockhart SR, et al. Changes in Incidence and Antifungal Drug Resistance in Candidemia: Results From Population-Based Laboratory Surveillance in Atlanta and Baltimore, 2008-2011. Clinical infectious diseases : an official publication of the Infectious Diseases Society of America. 2012.
10. O'Toole GA. To build a biofilm. Journal of bacteriology. 2003;185(9):2687-9.
11. Donlan RM, Costerton JW. Biofilms: survival mechanisms of clinically relevant microorganisms. Clinical microbiology reviews. 2002;15(2):167-93.
12. Kojic EM, Darouiche RO. *Candida* infections of medical devices. Clinical microbiology reviews. 2004;17(2):255-67.
13. Mukherjee PK, Zhou G, Munyon R, Ghannoum MA. Candida biofilm: a well-designed protected environment. Med Mycol. 2005;43(3):191-208.
14. Pappas PG, Kauffman CA, Andes D, Benjamin DK, Jr., Calandra TF, Edwards JE, Jr., et al. Clinical practice guidelines for the management of candidiasis: 2009 update by the Infectious Diseases Society of America. Clinical infectious diseases : an official publication of the Infectious Diseases Society of America. 2009;48(5):503-35.
15. Taff HT, Nett JE, Zarnowski R, Ross KM, Sanchez H, Cain MT, et al. A Candida biofilm-induced pathway for matrix glucan delivery: implications for drug resistance. PLoS Pathog. 2012;8(8):e1002848.
16. Nett JE, Sanchez H, Cain MT, Andes DR. Genetic basis of Candida biofilm resistance due to drug-sequestering matrix glucan. The Journal of infectious diseases. 2010;202(1):171-5.
17. Zarnowski R, Westler WM, Lacmbouh GA, Marita JM, Bothe JR, Bernhardt J, et al. Novel entries in a fungal biofilm matrix encyclopedia. MBio. 2014;5(4):e01333-14.
18. Lotvall J, Hill AF, Hochberg F, Buzas EI, Di Vizio D, Gardiner C, et al. Minimal experimental requirements for definition of extracellular vesicles and their functions: a position statement from the International Society for Extracellular Vesicles. Journal of extracellular vesicles. 2014;3:26913.
19. Zaborowski MP, Balaj L, Breakefield XO, Lai CP. Extracellular Vesicles: Composition, Biological Relevance, and Methods of Study. Bioscience. 2015;65(8):783-97.
20. Abels ER, Breakefield XO. Introduction to Extracellular Vesicles: Biogenesis, RNA Cargo Selection, Content, Release, and Uptake. Cell Mol Neurobiol. 2016;36(3):301-12.

21. Mitchell KF, Zarnowski R, Andes DR. Fungal Super Glue: The Biofilm Matrix and Its Composition, Assembly, and Functions. PLoS Pathog. 2016;12(9):e1005828.
22. Vargas G, Rocha JD, Oliveira DL, Albuquerque PC, Frases S, Santos SS, et al. Compositional and immunobiological analyses of extracellular vesicles released by Candida albicans. Cellular microbiology. 2015;17(3):389-407.
23. Matos Baltazar L, Nakayasu ES, Sobreira TJ, Choi H, Casadevall A, Nimrichter L, et al. Antibody Binding Alters the Characteristics and Contents of Extracellular Vesicles Released by Histoplasma capsulatum. mSphere. 2016;1(2).
24. Oliveira DL, Nakayasu ES, Joffe LS, Guimaraes AJ, Sobreira TJ, Nosanchuk JD, et al. Characterization of yeast extracellular vesicles: evidence for the participation of different pathways of cellular traffic in vesicle biogenesis. PloS one. 2010;5(6):e11113.
25. Mitchell KF, Zarnowski R, Sanchez H, Edward JA, Reinicke EL, Nett JE, et al. Community participation in biofilm matrix assembly and function. Proc Natl Acad Sci U S A. 2015;112(13):4092-7.
26. Andes D, Nett J, Oschel P, Albrecht R, Marchillo K, Pitula A. Development and characterization of an in vivo central venous catheter Candida albicans biofilm model. Infection and immunity. 2004;72(10):6023-31.
27. Nett JE, Sanchez H, Cain MT, Ross KM, Andes DR. Interface of Candida albicans biofilm matrix-associated drug resistance and cell wall integrity regulation. Eukaryotic cell. 2011;10(12):1660-9.
28. Lefebvre C, Legouis R, Culetto E. ESCRT and autophagies: Endosomal functions and beyond. Seminars in cell & developmental biology. 2017.
29. Meldolesi J. Exosomes and Ectosomes in Intercellular Communication. Curr Biol. 2018;28(8):R435-R44.
30. Noble SM, Johnson AD. Strains and strategies for large-scale gene deletion studies of the diploid human fungal pathogen Candida albicans. Eukaryot Cell. 2005;4(2):298-309.
31. Zarnowski R, Sanchez H, Andes DR. Large-scale production and isolation of Candida biofilm extracellular matrix. Nature protocols. 2016;11(12):2320-7.
32. Ramage G, Vande Walle K, Wickes BL, Lopez-Ribot JL. Standardized method for in vitro antifungal susceptibility testing of Candida albicans biofilms. Antimicrobial agents and chemotherapy. 2001;45(9):2475-9.
33. Taff HT, Nett JE, Andes DR. Comparative analysis of Candida biofilm quantitation assays. Medical mycology. 2012;50(2):214-8.
34. Headland SE, Jones HR, D'Sa AS, Perretti M, Norling LV. Cutting-edge analysis of extracellular microparticles using ImageStream(X) imaging flow cytometry. Sci Rep. 2014;4:5237.
35. Lannigan J, Erdbruegger U. Imaging flow cytometry for the characterization of extracellular vesicles. Methods. 2017;112:55-67.
36. Jaromin A, Kozubek A, Suchoszek-Lukaniuk K, Malicka-Blaszkiewicz M, Peczynska-Czoch W, Kaczmarek L. Liposomal formulation of DIMIQ, potential antitumor indolo[2,3-b]quinoline agent and its cytotoxicity on hepatoma Morris 5123 cells. Drug Deliv. 2008;15(1):49-56.
37. Martin SE, Shabanowitz J, Hunt DF, Marto JA. Subfemtomole MS and MS/MS peptide sequence analysis using nano-HPLC micro-ESI fourier transform ion cyclotron resonance mass spectrometry. Anal Chem. 2000;72(18):4266-74.
38. Perkins DN, Pappin DJ, Creasy DM, Cottrell JS. Probability-based protein identification by searching sequence databases using mass spectrometry data. Electrophoresis. 1999;20(18):3551-67.
39. Keller A, Purvine S, Nesvizhskii AI, Stolyar S, Goodlett DR, Kolker E. Experimental protein mixture for validating tandem mass spectral analysis. OMICS. 2002;6(2):207-12.
40. Kanehisa M, Goto S. KEGG: kyoto encyclopedia of genes and genomes. Nucleic Acids Res. 2000;28(1):27-30.

41. Kanehisa M, Sato Y, Kawashima M, Furumichi M, Tanabe M. KEGG as a reference resource for gene and protein annotation. Nucleic Acids Res. 2016;44(D1):D457-62.
42. Bernhardt J, Funke S, Hecker M, Siebourg J, editors. Visualizing gene expression data via Voronoi treemaps. Sixth International Symposium on Voronoi diagrams; 2009 23-26 June 2009; Piscataway, NJ: IEEE.
43. Henry RJ, Blakeney AB, Harris PJ, Stone BA. Detection of neutral and aminosugars from glycoproteins and polysaccharides as their alditol acetates. J Chromatogr. 1983;256(3):419-27.
44. Shibata N, Suzuki A, Kobayashi H, Okawa Y. Chemical structure of the cell-wall mannan of Candida albicans serotype A and its difference in yeast and hyphal forms. Biochem J. 2007;404(3):365-72.
45. Aickin M, Gensler H. Adjusting for multiple testing when reporting research results: the Bonferroni vs Holm methods. Am J Public Health. 1996;86(5):726-8.
46. Downs JS, Arslanian S, de Bruin WB, Copeland VC, Doswell W, Herman W, et al. Implications of type 2 diabetes on adolescent reproductive health risk: an expert model. Diabetes Educ. 2010;36(6):911-9.

Figure Legends

Figure 1. *C. albicans* biofilms secrete unique extracellular vesicles. **(A)** A scanning electron micrograph (SEM) of extracellular vesicle-like structures on the surface of *C. albicans* growing in a biofilm. Scale bar indicates 0.6 μm. **(B)** A SEM of extracellular vesicle-like structures within deposits of the extracellular matrix in biofilms. Scale bar indicates 0.5 μm. **(C)** A cryo-TEM of *Candida* biofilm-derived extracellular vesicles are surrounded by a 7-nm-thick lipid bilayer. Scale bar indicates 100 nm. **(D)** Quantitative analysis of extracellular vesicles in *C. albicans* biofilms measured at various culture growth time points. The measurements were done in triplicate using an imaging flow cytometry system and data presented as particles per ml. **(E)** Size distribution of *C. albicans* planktonic extracellular vesicles evaluated by dynamic light scattering. **(F)** Size distribution of *C. albicans* biofilm extracellular vesicles evaluated by dynamic light scattering.

Figure 2. Unique *C. albicans* biofilm extracellular vesicle protein, lipid, and carbohydrate cargo delivers biofilm extracellular matrix components. Biofilm EVs proteomes are shown in orange vs. planktonic EVs shown in blue **(A, B, C)**, whereas extracellular matrix (ECM) is shown in green **(D, E, F)**. Smallest regions **(A, B, D, E)** represent identified proteins and are arranged inside higher level regions according their KEGG functional category and pathway assignment by using a Voronoi treemap layout. **(A, B)** log2 biofilm EVs/planktonic EVs ratios of proteins relative abundances were mapped to a color ramp starting with orange (more protein in biofilm EVs) passing grey (similar protein proportions in biofilm EVs as well as planktonic EVs) reaching blue (more protein in planktonic cells). **(C)** The number of exclusive (blue and orange) and common (white) biofilm EVs and planktonic EVs proteins are illustrated by using a Venn Diagram. **(D, E, F)** Accordingly the proteome comparisons of biofilm EVs (orange) and extracellular matrix (green) are shown. **(G)** Lipidomics profiles in biofilm extracellular vesicles and the extracellular matrix. The treemaps reflect relative amounts of individual lipid species present in extracellular vesicles

(EVs) or extracellular matrix (ECM). The coloration of individual clusters based on their classification showing phospholipids in orange, neutral lipids in red, and sphingolipids in blue. Quantitative differences of biofilm EVs lipids and extracellular matrix lipids are given by using z-scores. Blue illustrates lipids with higher concentrations in biofilm EVs, whereas orange reflect lipids more abundant in extracellular matrix (ECM). **(H)** Comparison of the ^{1}H NMR spectra of purified biofilm EV carbohydrate (top) and extracellular matrix neutral carbohydrates (bottom). The labels refer to chemical shifts listed in **Supplemental Table 3**. **(I)** Overlaid 2D ^{1}H-^{13}C-HSQC NMR spectra of the *C. albicans* extracellular matrix carbohydrate (blue trace) and the biofilm extracellular vesicle (red trace). The labels refer to chemical shifts listed in **Supplemental Table 4**.

Figure 3. ESCRT driven biofilm extracellular vesicles are responsible for drug-resistance due to delivery of macromolecules to the *C. albicans* extracellular matrix. (A) A diagram of the ESCRT machinery involved in sorting cargo via extracellular vesicles. **(B)** Quantitative analysis of biofilm extracellular vesicles in the *C. albicans* wild-type strain and the ESCRT null mutants assessed by the imaging flow cytometry system. The experiment and assays were done in triplicate and data presented as particles per ml. Bars indicate standard deviation of the median. **(C)** The percent of reduction in biofilm formation following 48-h treatment with fluconazole (1 mg/ml) compared with untreated biofilms, as quantified using the 96-well XTT assay. The null deletions and corresponding complemented strains are shown for mutants with fluconazole susceptibility phenotype. The experiments and assays were performed in triplicate. Asterisks indicate values significantly different from the reference strain based on one-way ANOVA with the post-hoc Tukey HSD test. Bars indicate standard deviation of the median. **(D)** Quantification of *in vivo* biofilms using a rat central venous catheter model. Individual fluconazole-susceptible ESCRT null mutants were treated either with fluconazole 250 µg/ml or 0.9M NaCl followed by the CFU

analysis. Three animal and culture replicates per condition. **(E)** Sequestration of ^{3}H-labelled fluconazole by intact biofilms grown from the reference and ESCRT mutant strains. Biofilms were exposed to the radiolabeled drug, washed, and harvested. Scintillation counting was performed in triplicate to determine the fluconazole content in the intact biofilms and the isolated matrix. **(F)** The percent reduction of mannan and glucan concentration in biofilm matrices of fluconazole-susceptible ESCRT null mutants measured by gas chromatography. Three biological and assay replicates per data point. **(G)** Impact of ESCRT null mutants on biofilm architecture and extracellular matrix based upon SEM imaging of mature (24h) *in vitro* biofilms.

Figure 4. Exogenous delivery of wild-type vesicles restores the biofilm drug-resistant phenotype and matrix composition. (A) A diagram depicting the addition of purified wild-type extracellular vesicles from *C. albicans* biofilm cultures to mutant biofilms. **(B)** Effect of exogenous wild-type biofilm extracellular vesicles on biofilm fluconazole susceptibility for select ESCRT null mutants as measured by the 96-well XTT assay. Biofilm cultures of fluconazole sensitive mutant strains amended with wild-type extracellular vesicles (21804±1711 EVs/ml) regain their ability to grow in the presence of fluconazole. Each 541 experiment and assay was performed in triplicate. **(C)** Exogenous wild-type extracellular vesicles rescue matrix production in ESCRT mutant biofilms. The fluconazole susceptible biofilm of HSE1 null mutant does not produce extracellular matrix (upper SEM). The addition of exogenous vesicles restores the mutant's ability to produce the extracellular matrix (lower SEM). Scale bars indicate 11 μm. **(D)** Exogenous extracellular vesicle restore mannan and glucan concentrations in the biofilm matrix of HSE1 null mutant as measured by gas chromatography. Each experiment and assay was performed in triplicate. **(E)** Effect of exogenous biofilm extracellular vesicles on drug susceptibility of select *C. albicans* matrix glucan-modification null mutants as measured by the 96-well XTT assay. The vesicle cargo mutants (PHR1, SUN41) regain their ability to grow in the presence of fluconazole after the

addition of exogenous wild-type extracellular vesicles. Each experiment and assay was performed in triplicate.

Figure 1

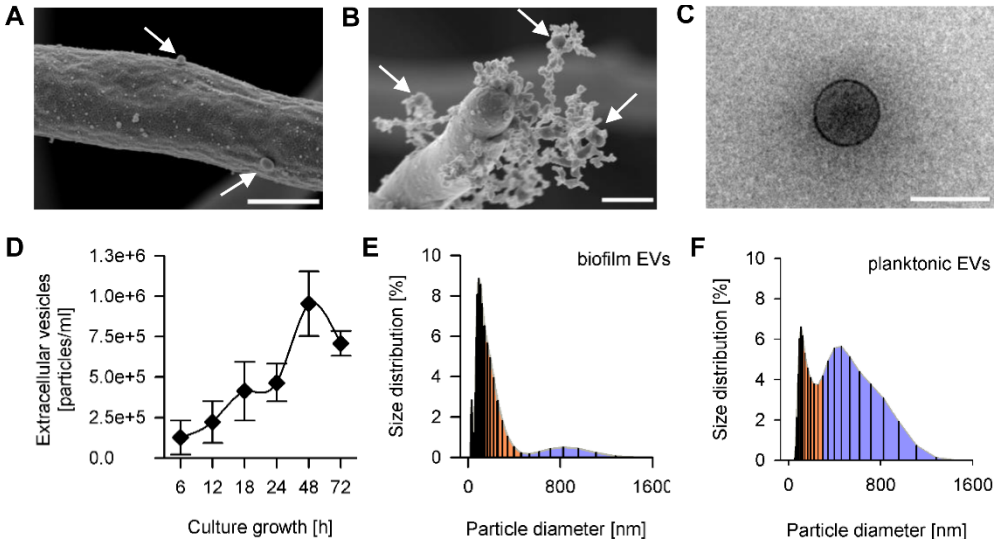
A
B
C
D
E
F
Extracellular vesicles [particles/ml]
1.3e+6
1.0e+6
7.5e+5
5.0e+5
2.5e+5
0.0
6 12 18 24 48 72
Culture growth [h]
Size distribution [%]
biofilm EVs
0 800 1600
Particle diameter [nm]
planktonic EVs
0 800 1600
Particle diameter [nm]

Figure 2

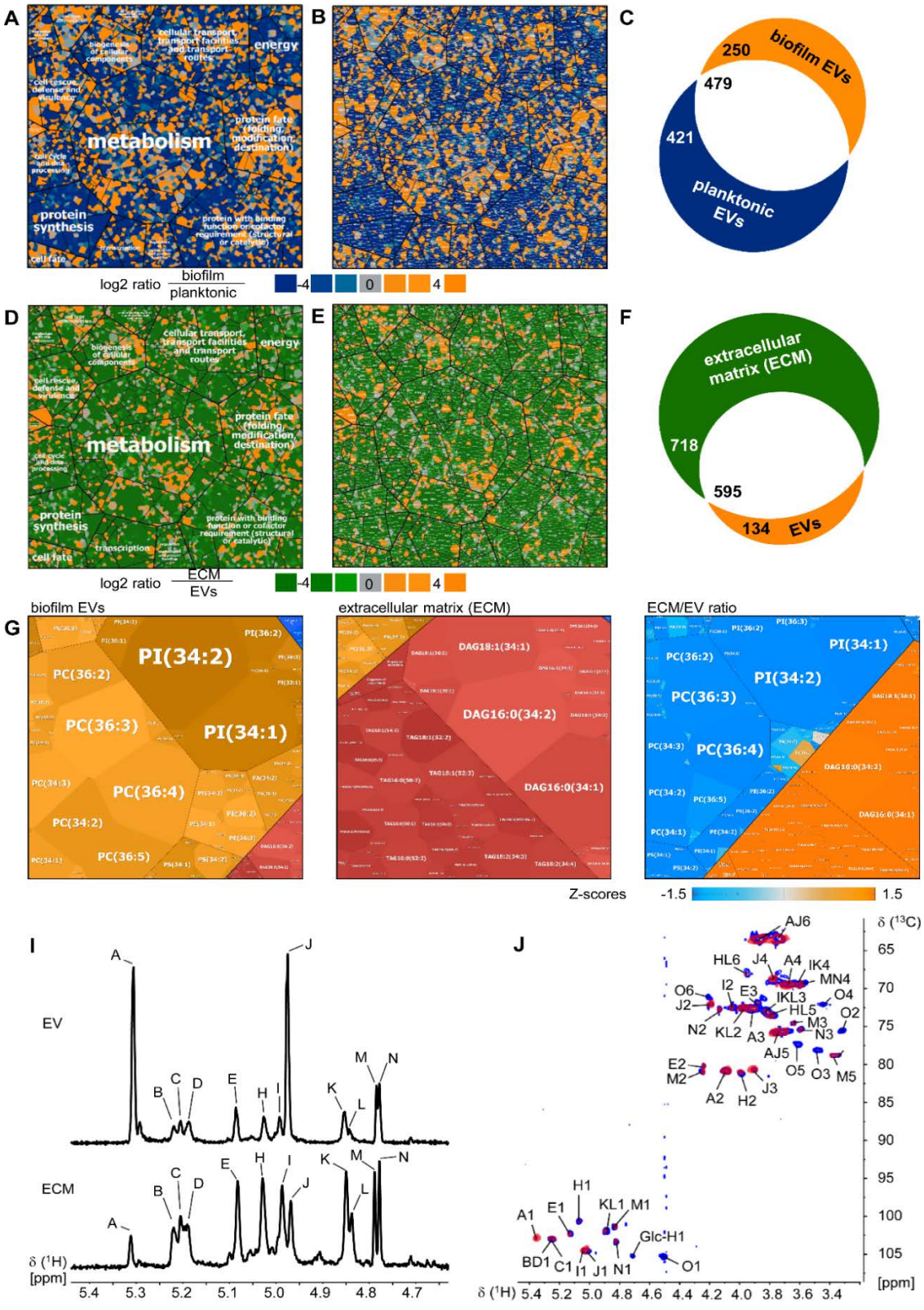
A
B
C
energy
metabolism
protein synthesis
protein fate (folding, modification, destination)
cellular transport, transport facilities and transport routes
biogenesis of cellular components
cell rescue, defense and virulence
cell cycle and DNA processing
protein with binding function or cofactor requirement (structural or catalytic)
cell fate
transcription
log2 ratio biofilm / planktonic
-4 0 4
250
479
421
biofilm EVs
planktonic EVs
D
E
F
extracellular matrix (ECM)
718
595
134
EVs
log2 ratio ECM / EVs
G
biofilm EVs
extracellular matrix (ECM)
ECM/EV ratio
PI(34:2)
PC(36:2)
PC(36:3)
PI(34:1)
PC(36:4)
PC(34:2)
PC(36:5)
DAG18:1(34:1)
DAG16:0(34:2)
DAG16:0(34:1)
PI(34:3)
PC(34:3)
PC(34:1)
Z-scores
-1.5
1.5
I
EV
ECM
A B C D E H I J K L M N
δ (1H) [ppm]
5.4 5.3 5.2 5.1 5.0 4.9 4.8 4.7
J
δ (13C)
AJ6 HL6 J4 A4 IK4 MN4 O6 I2 E3 IKL3 O4 J2 HL5 O2 N2 KL2 A3 M3 N3 AJ5 O5 O3 M5 E2 M2 A2 H2 J3
H1 A1 E1 KL1 M1 Glc-H1 BD1 C1 I1 J1 N1 O1
65 70 75 80 85 90 95 100 105
δ (1H) 5.4 5.2 5.0 4.8 4.6 4.4 4.2 4.0 3.8 3.6 3.4
[ppm]

Figure 3

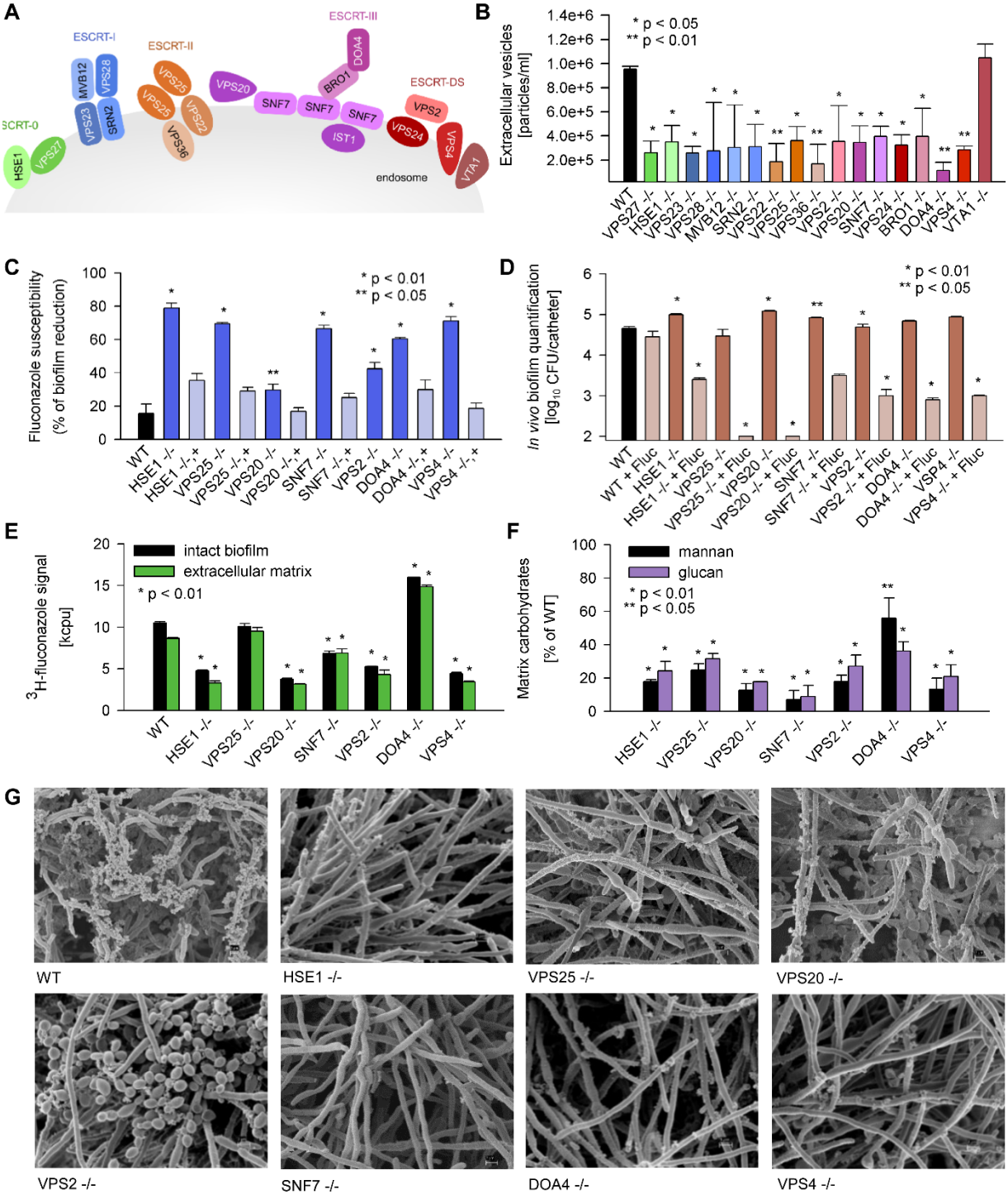
A
ESCRT-0
ESCRT-I
ESCRT-II
ESCRT-III
ESCRT-DS
HSE1
VPS27
VPS23
MVB12
VPS28
SRN2
VPS25
VPS22
VPS36
VPS20
SNF7
BRO1
DOA4
IST1
VPS2
VPS24
VPS4
VTA1
endosome
B
Extracellular vesicles [particles/ml]
* p < 0.05
** p < 0.01
C
Fluconazole susceptibility (% of biofilm reduction)
* p < 0.01
** p < 0.05
D
In vivo biofilm quantification [log10 CFU/catheter]
* p < 0.01
** p < 0.05
E
3H-fluconazole signal [kcpu]
intact biofilm
extracellular matrix
* p < 0.01
F
Matrix carbohydrates [% of WT]
mannan
glucan
* p < 0.01
** p < 0.05
G
WT
HSE1 -/-
VPS25 -/-
VPS20 -/-
VPS2 -/-
SNF7 -/-
DOA4 -/-
VPS4 -/-

Figure 4

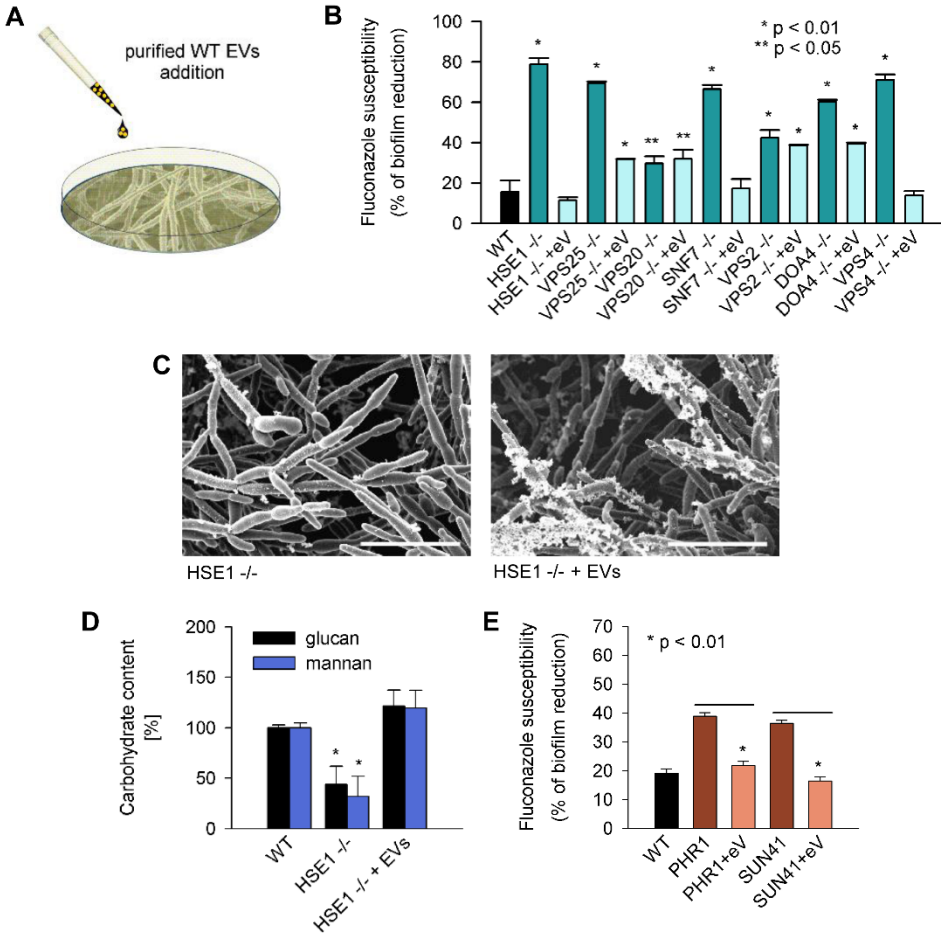
A
purified WT EVs addition
B
Fluconazole susceptibility (% of biofilm reduction)
* p < 0.01
** p < 0.05
WT
HSE1 -/-
HSE1 -/- +eV
VPS25 -/-
VPS25 -/- +eV
VPS20 -/-
VPS20 -/- +eV
SNF7 -/-
SNF7 -/- +eV
VPS2 -/-
VPS2 -/- +eV
DOA4 -/-
DOA4 -/- +eV
VPS4 -/-
VPS4 -/- +eV
C
HSE1 -/-
HSE1 -/- + EVs
D
Carbohydrate content [%]
glucan
mannan
WT
HSE1 -/-
HSE1 -/- + EVs
E
Fluconazole susceptibility (% of biofilm reduction)
* p < 0.01
WT
PHR1
PHR1+eV
SUN41
SUN41+eV

Supplemental Table 1. Biofilm EV compared to Planktonic EV Proteomics Profiles (Only top hits shown)						
Protein Characteristics				**Quantitative Value (Normalized Total Spectra)[1]**		**Biofilm/Planktonic Ratio**
Protein Name	**Gene Name**	**ORF Number**	**UniProt ID**	**Biofilm EVs**	**Planktonic EVs**	
Candidapepsin-6	SAP6	CaO19.12988	Q5AC08	164.74	0.00	biofilm unique
Cell surface Cu-only superoxide dismutase 5	SOD5	CaO19.2060	Q5AD07	52.36	0.00	biofilm unique
Candidapepsin-4	SAP4	CaO19.13139	Q5A8N2	34.28	0.00	biofilm unique
Uncharacterized protein		CAALFM_C602100WA	A0A1D8PPT3	27.96	0.00	biofilm unique
Lipase 4	LIP4	CaO19.2133	Q9P8W1	26.53	0.00	biofilm unique
Rax2p	RAX2	CAALFM_C112510WA	A0A1D8PFE5	22.03	0.00	biofilm unique
Uncharacterized protein		CAALFM_C209800CA	Q59YF6	18.96	0.00	biofilm unique
Profilin	PFY1	CAALFM_C108030WA	Q5A786	17.01	0.00	biofilm unique
Glucan 1,3-beta-glucosidase 2	EXG2	CaO19.10469	Q5AIA1	16.26	0.00	biofilm unique
Uncharacterized protein		CAALFM_CR06030CA	A0A1D8PT50	16.21	0.00	biofilm unique
Predicted GPI-anchored protein 17	PGA17	CaO19.8512	Q5AHA4	16.18	0.00	biofilm unique
Surface antigen protein 2	CSA2	CaO19.10629	Q5A0X8	15.69	0.00	biofilm unique
Uncharacterized protein		CAALFM_C210150WA	A0A1D8PIN7	15.37	0.00	biofilm unique
Kexin	KEX2	CAALFM_C108990CA	A0A1D8PEG3	13.87	0.00	biofilm unique
Ferroxidase	FET34	CAALFM_C600440CA	A0A1D8PPC9	12.48	0.00	biofilm unique
Beta-mannosyltransferase 6	BMT6	CaO19.13045	Q5ABU8	12.23	0.00	biofilm unique
Pbr1p	PBR1	CAALFM_C106370CA	Q5AAN7	10.35	0.00	biofilm unique
Glucose-6-phosphate 1-dehydrogenase	ZWF1	CAALFM_C108980CA	A0A1D8PEG2	9.70	0.00	biofilm unique
Mannan endo-1,6-alpha-mannosidase	DCW1	CaO19.1989	Q5AD78	9.66	0.00	biofilm unique
Rdi1p	RDI1	CAALFM_C305000WA	Q5AND4	9.30	0.00	biofilm unique
Putative NADPH-dependent methylglyoxal reductase	GRP2	CaO19.11785	P83775	9.29	0.00	biofilm unique
Glucose-6-phosphate 1-epimerase		CAALFM_C501230CA	Q5A1Q0	9.26	0.00	biofilm unique
Uncharacterized protein		CAALFM_CR09240CA	A0A1D8PTY0	9.25	0.00	biofilm unique
17-beta-hydroxysteroid dehydrogenase-like protein		CAALFM_C114060WA	A0A1D8PFV8	8.75	0.00	biofilm unique
Induced during hyphae development protein 1	IHD1	CaO19.13183	Q5A8I8	7.72	0.00	biofilm unique
Lysophospholipase	PLB5	CAALFM_C108230CA	A0A1D8PEB1	6.83	0.00	biofilm unique
Fet31p	FET31	CAALFM_C600480CA	A0A1D8PPE2	6.29	0.00	biofilm unique
Uncharacterized protein		CAALFM_C104010CA	A0A1D8PD74	5.97	0.00	biofilm unique
Bleomycin hydrolase	LAP3	CAALFM_CR04480CA	Q5A6L5	5.79	0.00	biofilm unique

[1]Parameters used: minimum 95% peptide threshold, minimum 95% protein threshold and minimum of 2 peptides

Supplemental Table 2. Biofilm EV Compared to Biofilm Matrix Proteomic Profiles (Only top hits shown)						
Protein Characteristics				**Quantitative Value (Normalized Total Spectra)[1]**		
Protein Name	**Gene Name**	**ORF Number**	**UniProt ID**	**Biofilm EVs**	**Extracellular matrix**	**Biofilm/Planktonic Ratio**
Beta-hexosaminidase	HEX1	CAALFM_C503610WA	A0A1D8PNR7	50.95	0.00	EV unique
Gca2p	GCA2	CAALFM_C110550CA	A0A1D8PEW1	49.09	0.00	EV unique
Putative glucan endo-1\3-beta-D-glucosidase	SCW11	CAALFM_C504110WA	A0A1D8PNW1	35.85	0.00	EV unique
Uncharacterized protein		CAALFM_C209800CA	Q59YF6	18.96	0.00	EV unique
Predicted GPI-anchored protein 45	PGA45	CAALFM_C105960WA	Q5AA33	17.04	0.00	EV unique
Predicted GPI-anchored protein 17	PGA17	CAALFM_C203350WA	A0A1D8PGU3	16.18	0.00	EV unique
Uncharacterized protein		CAALFM_C210150WA	A0A1D8PIN7	15.37	0.00	EV unique
Glycolipid 2-alpha-mannosyltransferase 2	MNT2	CAALFM_C301830CA	P46592	13.49	0.00	EV unique
Beta-mannosyltransferase 6	BMT6	CAALFM_C603160CA	A0A1D8PQ28	12.23	0.00	EV unique
Alpha-1,2-mannosyltransferase	MNN24	CAALFM_C201300CA	Q5AD72	11.50	0.00	EV unique
Repressed by EFG1 protein 1	RBE1	CAALFM_C114120CA	Q59ZX3	9.25	0.00	EV unique
Alpha-1,2-mannosyltransferase	MNN26	CAALFM_C703600WA	Q59R28	9.16	0.00	EV unique
Uncharacterized protein		CAALFM_CR07460CA	A0A1D8PTI1	7.65	0.00	EV unique
Chitinase 1	CHT1	CAALFM_CR00180CA	Q5AAH2	7.17	0.00	EV unique
ADP-ribosylation factor	ARF1	CAALFM_CR08700CA	P22274	7.04	0.00	EV unique
Candidapepsin-2	SAP2	CAALFM_CR07800WA	P0DJ06	5.94	0.00	EV unique
Glucan 1,4-alpha-glucosidase	SGA1	CAALFM_C301320CA	Q5AJ73	5.69	0.00	EV unique
Candidapepsin-8	SAP8	CAALFM_C302510CA	Q5AEM6	5.48	0.00	EV unique
Candidapepsin-10	SAP10	CAALFM_C404470WA	Q5A651	4.93	0.00	EV unique
Phosphatidylglycerol/phosphatidylinositol transfer protein (PG/PI-TP)	NPC2	CAALFM_CR01280CA	Q5A8A2	4.17	0.00	EV unique
Beta-mannosyltransferase 1	BMT1	CAALFM_C307180CA	Q5ADQ9	4.01	0.00	EV unique
Emp46p	EMP46	CAALFM_C105960WA	A0A1D8PTF1	3.79	0.00	EV unique
Mid1p	MID1	CAALFM_C503990WA	A0A1D8PNU4	3.47	0.00	EV unique
Axl2p	AXL2	CAALFM_C404170CA	A0A1D8PM01	3.26	0.00	EV unique
Uncharacterized protein		CAALFM_C403480CA	A0A1D8PLU2	2.99	0.00	EV unique
Acid phosphatase	PHO113	CAALFM_CR02180WA	Q59UY6	2.94	0.00	EV unique
Secreted protein	PRY1	CAALFM_C107580CA	Q59PV6	2.82	0.00	EV unique

[1]Parameters used: minimum 95% peptide threshold, minimum 95% protein threshold and minimum of 2 peptides

Supplemental Table 3. 1D ^{1}H NMR chemical shift assignment of the major spin systems found in *C. albicans* extracellular matrix and extracellular vesicles.

Determination of percentages of the different mannose residues found in *C. albicans* biofilm extracellular vesicles and extracellular matix.			
No.	**Residue type**	**Matrix**	**Vesicles**
A	α-1-2-Manα-1-3-	3.7	25.8
B	α-1-2-Manα-1-2-	4.3	4.0
C	α-1-2-Manα-1-2-	7.2	3.2
D	α-1-2-Manα-1-2-	7.4	6.7
E	β-1-2-Manα-1-2-	11.9	6.5
H	2,6-Manα-1-6- (b)	15.6	6.7
I	Manα-1-2-	13.5	5.1
J	3-Manα-1-2-	7.2	23.8
K	Manα-1-6-	10.6	5.8
L	6-Manα-1-6-	6.4	2.1
M	β-1-2-Manβ-1-2-	5.4	3.7
N	Manβ-1-2-	6.7	6.6

Supplemental Table 4. Chemical shift assignment of the major spin systems found in *C. albicans* extracellular vesicles.

Chemical shift assignments of the major spin systems found in *C. albicans* biofilm extracellular vesicles (carbon chemical shifts in italics).								
No.	**Residue type**	**Chemical shift (ppm)**						
		1	**2**	**3**	**4**	**5**	**6**	**6'**
A	α-1-2-Manα-1-3-	5.37	4.10	3.99	3.70	3.77	3.90	3.77
		103.4	*81.4*	*73.1*	*70.1*	*76.2*	*64.1*	
B	α-1-2-Manα-1-2-	5.28	4.11	3.95	3.69	3.78	3.88	3.76
		103.4	*81.4*	*73.1*	*70.2*	*76.2*	*63.9*	
C	α-1-2-Manα-1-2-	5.27	4.12	3.95	3.73	3.78	3.88	3.76
		103.3	*81.2*	*72.9*	*69.2*	*76.2*	*63.9*	
D	α-1-2-Manα-1-2-	5.25	4.11	3.91	3.72	3.78	3.88	3.76
		103.4	*81.4*	*73.1*	*70.2*	*76.2*	*63.9*	
E	β-1-2-Manα-1-2-	5.15	4.26	3.90	3.73	3.78	3.88	3.76
		102.8	*81.2*	*73.1*	*70.2*	*76.2*	*63.9*	
H	2,6-Manα-1-6-(l)	5.09	4.01	3.95	3.73	3.81	3.97	3.73
		101.0	*81.5*	*73.2*	*70.2*	*73.9*	*68.7*	
I	Manα-1-2-	5.05	4.07	3.84	3.67	3.76	3.88	3.76
		104.9	*73.2*	*73.5*	*69.9*	*76.2*	*63.9*	
J	3-Manα-1-2-	5.04	4.21	3.93	3.78	3.76	3.86	3.77
		104.8	*72.6*	*81.2*	*69.2*	*76.3*	*64.1*	
K	Manα-1-6-	4.92	4.01	3.82	3.67	3.81	3.88	3.73
		102.4	*73.1*	*73.9*	*69.7*	*75.8*	*63.9*	
L	6-Manα-1-6-	4.91	4.01	3.82	3.73	3.81	3.97	3.74
		102.4	*73.1*	*73.9*	*69.2*	*75.8*	*68.3*	

M	β-1-2-Manβ-1-2-	4.85	4.26	3.66	3.61	3.40	3.92	3.78
		101.8	*81.0*	*75.2*	*70.0*	*79.2*	*64.3*	
N	Manβ-1-2-	4.84	4.16	3.62	3.60	3.36	3.92	3.75
		103.8	*73.3*	*75.9*	*70.0*	*79.2*	*64.3*	
O	β-1-6-Glcβ-1-6	4.52	3.34	3.49	3.45	3.63	4.22	3.86
		105.7	*76.0*	*78.7*	*72.5*	*77.7*	*71.6*	

Supplemental Table 5. Primer Sequences for Strain Construction

Target Gene Primer Name	Function[1]	Primer Sequence
BRO1 F1	K/O	TTCTTTGGTTTTCTTTCTGAAT
BRO1 F3	K/O	gtcagcggccgcatccctgcACTCTTTTCGGTCATTATCTTG
BRO1 R1	K/O	cacggcgcgcctagcagcggAGGATGTAAGGATAAGTTGGTG
BRO1 R3	K/O	TGAATTTACAGGCGTATATGTG
BRO1 nF	K/O	TTGTCGTTATTGGATTTATTGA
BRO1 nR	K/O	TTTTCCTCCTGCTATAATGTTT
BRO1 intF	K/O	AATGGTTTGATTCATTTTCTTC
BRO1 intR	K/O	TTCAGGTAATGTCACCAAGTTA
BRO1 K/O Check U	K/O	TCCTTTTCATGATCATTGTT
BRO1 K/O Check D	K/O	CCTCCTTATAAACACGTGAA
BRO1 Compl F	Compl	ccgctgctaggcgcgccgtgTTGTCGTTATTGGATTTATTGA
BRO1 Compl R	Compl	gcagggatgcggccgctgacAAAAAGAATTCAAAACATTGCT
BRO1 Compl nF	Compl	GTCATTCAAGCAATTAATGAAA
BRO1 Compl nR	Compl	ACTAAAACCCCAACAAATCAC
BRO1 Compl Check D F	Compl	TACAATTTTGCCACAACTCTAC
BRO1 Compl Check D R	Compl	TTCAGTCAGTTTATTGACAACG
BRO1 Compl Check U F	Compl	ttttgattttgaagctagtgtg
BRO1 Compl Check U R	Compl	GAAAACAATTTTGGTGAGAAAT
DOA4 F1	K/O	TGTTTTTGTTTTTGAGTGTAGC
DOA4 F3	K/O	gtcagcggccgcatccctgcTCGACTTTATCGTCATGATTTA
DOA4 R1	K/O	cacggcgcgcctagcagcggAGTTGGTGGTAATTTAGTTTGG
DOA4 R3	K/O	TAGTCACACCAAAGAAGAAACA
DOA4 nF	K/O	TTTTCAAATTGATATGGATACG
DOA4 nR	K/O	TTAGCACATTCGTGAAGAAAC
DOA4 intF	K/O	GTATCATTGTCGGAAGAAGAAT
DOA4 intR	K/O	CCAAAAGAAAATTCAAAAACTC
DOA4 K/O Check U	K/O	AAGTGATTTTCGTTATCGGTAT
DOA4 K/O Check D	K/O	CATTACTTGCTTCAATGTGG
DOA4 Compl F	Compl	ccgctgctaggcgcgccgtgGCTGCAAAGTTTTCAAATTGAT
DOA4 Compl R	Compl	gcagggatgcggccgctgacATTACTTGCTTCAATGTGGGAA
DOA4 Compl nF	Compl	AGCAATTAATGAAAGAGTTGACT
DOA4 Compl nR	Compl	gtttaaacTCGAAAACGATGTT
DOA4 Compl Check D F	Compl	TTGAACCATACTAAATCGGAG
DOA4 Compl Check D R	Compl	ACCACCACGACCACTAAAAC
DOA4 Compl Check U F	Compl	gaaagaagagatgctattggtg
DOA4 Compl Check U R	Compl	GTTATGTTTTCGTGACACTTCT
HSE1 F1	K/O	CACCTAAGATCCTTTGTTTGTT
HSE1 F3	K/O	gtcagcggccgcatccctgcTCTTCAGTTTCTTTTCTCAAGC
HSE1 R1	K/O	cacggcgcgcctagcagcggGAGGAGGCAAAGTAGTTGTATT
HSE1 R3	K/O	CAATTTATGAACATGAACAAGC
HSE1 Nf	K/O	AACTGAGTTCACTTCAACAACA
HSE1 Nr	K/O	CAATTTATGAACATGAACAAGC
HSE1 intF	K/O	AGAGAGCTTTGAAATTGTCATT
HSE1 intR	K/O	GTGGGTACTGGTTAAAAGTTGT
HSE1 K/O Check U	K/O	TTCCATCTTTGTTGCTATTC
HSE1 K/O Check D	K/O	CTGTTAAAGCTGAAAATCCA
HSE1 Compl F	Compl	ccgctgctaggcgcgccgtgCACCTAAGATCCTTTGTTTGTT
HSE1 Compl R	Compl	gcagggatgcggccgctgacATTGTTGATCCTTCTAAATTGG
HSE1 Compl nF	Compl	GTCATTCAAGCAATTAATGAAA
HSE1 Compl nR	Compl	ACTAAAACCCCAACAAATCAC
HSE1 Compl Check U F	Compl	AGAAGATAAGGCAGACCAAATA
HSE1 Compl Check U R	Compl	TATGCAGGATTTTGATAGTCTG
HSE1 Compl Check U1 R	Compl	AACGTTACACAACCATTGACTA
HSE1 Compl Check D F	Compl	TATAATAGAGCTGCACCTGGAC
HSE1 Compl Check D R	Compl	TGAGGATGAAGAGTTTTTCTCT
MVB12 F1	K/O	ATTCAACAGATCCAGGAAGATA
MVB12 F3	K/O	gtcagcggccgcatccctgcAAACTATTGGTGTTCATCTTCC
MVB12 R1	K/O	cacggcgcgcctagcagcggGATTGAAAAGATTTCGCATATT
MVB12 R3	K/O	AATTCTTTCTTTAAGCCATTTTT

MVB12 nF	K/O	GACATTCATCAACATCAAAAGA
MVB12 nR	K/O	TGGAAATAATCATTACATCGTG
MVB12 intF	K/O	CTCTATATTCTAGCGGATCCAA
MVB12 intR	K/O	TTAATTTCGTTGTCCCAAATA
MVB12 K/O Check U	K/O	ACAATAAAGTATGCAGAATAACAG
MVB12 K/O Check D	K/O	CAAAAGGTTCAGTTTTATAACCA
MVB12 Compl F	Compl	ccgctgctaggcgcgccgtgAAGAAGAAGAAGAAGAAGGAGG
MVB12 Compl R	Compl	gcagggatgcggccgctgacGAAGATTCAGGAATAGTAGTTAAAG
MVB12 Compl nF	Compl	AGCAATTAATGAAAGAGTTGACT
MVB12 Compl nR	Compl	gtttaaacTCGAAAACGATGTT
MVB12 Compl Check D F	Compl	TTGTCAGGTGTTTTGATAATGT
MVB12 Compl Check D R	Compl	CTAAAACCCCAACAAATCACAC
MVB12 Compl Check U F	Compl	atagaaagataccctgtattcca
MVB12 Compl Check U R	Compl	TTTTGCTCTTCCCCTCCTTTT
SNF7 F1	K/O	ACCAGAAAATCTACCATACGAC
SNF7 F3	K/O	gtcagcggccgcatccctgcATTCTTTTTGTTGTTGTTGTTG
SNF7 R1	K/O	cacggcgcgcctagcagcggAAAAAGAAAAGAACCTGGTGTT
SNF7 R3	K/O	TCAGTAGCGTTGACTAACTTTG
SNF7 intF	K/O	GATTTACCAAAGAAGGCAATAG
SNF7 intR	K/O	AATGCTTCTTCATCTTCATCTT
SNF7 nF	K/O	GGAAGAACAACAATATGGAAAT
SNF7 nR	K/O	GTATCGATTTGTGATGTAGCTG
SNF7 K/O Check U	K/O	TTATCATTACCTTCGCAAAC
SNF7 K/O Check D	K/O	TGGTTAATCGACATTAAAGG
SNF7 Compl F	Compl	ccgctgctaggcgcgccgtgCAAGGTGAACAAATACAAAGAA
SNF7 Compl R	Compl	gcagggatgcggccgctgacCAACAACAACAACAAAAAGAA
SNF7 Compl nF	Compl	GAAGTCGACTATGTCATTCAAG
SNF7 Compl nR	Compl	ACCACTAAAACCCCAACAAAT
SNF7 Compl Check UF	Compl	CCATAAAATATTCGGTTTGATT
SNF7 Compl Check U R	Compl	TAATAAAATGCTTTACCGGAAT
SNF7 Compl Check D R	Compl	AAAAATATCCCCACATGTTTAC
SNF7 Compl Check D F	Compl	ATGAATTTGTTGATGAAGATGA
SRN2 F1	K/O	ATTTGGCTTTGTATGGTTAGAC
SRN2 F3	K/O	gtcagcggccgcatccctgcAACGTTCAGGAACTTTTCTCTA
SRN2 R1	K/O	cacggcgcgcctagcagcggTTTTCCTCCCTTATCTTGTTTA
SRN2 R3	K/O	GTCGAATGAACTAACGTTGTAA
SRN2 nF	K/O	AAAGTGTGACTGGTTTGATGTA
SRN2 nR	K/O	ATTGAATACTTTCGAGAGATGG
SRN2 intF	K/O	ATACACCTTGACCAAACTTCTC
SRN2 intR	K/O	TCGATGTAATTTCTCCTTTCTT
SRN2 K/O Check U	K/O	ATGGGTTCATGTACTTGATGAT
SRN2 K/O Check D	K/O	ATGATGAAACTAGTCGAATGAAC
SRN2 Compl F	Compl	ccgctgctaggcgcgccgtgGAGATGTTGTAGTTAATAGAGTCT
SRN2 Compl R	Compl	gcagggatgcggccgctgacAACTAGTCGAATGAACTAACGT
SRN2 Compl nF	Compl	AGCAATTAATGAAAGAGTTGACT
SRN2 Compl nR	Compl	gtttaaacTCGAAAACGATGTT
SRN2 Compl Check U F	Compl	gtattccattgtatcgcctttg
SRN2 Compl Check U R	Compl	TGATCTATAATTTCCAGCTGCT
SRN2 Compl Check D F	Compl	TTGGTGTAGTAGATTGTAGGTG
SRN2 Compl Check D R	Compl	CTAAAACCCCAACAAATCACAC
SRN2 Compl Check D2 F	Compl	GAACAGTTGAGGATGAAGTTTT
SRN2 Compl Check D2 R	Compl	AAGCAACCTTTATTGAGTGAAG
SRN2 Compl Check D3 F	Compl	TAACTCCCTTCTCGGTTTTATT
SRN2 Compl Check D3 R	Compl	ATATACGAGAGCCAAGTCAATC
VPS2 F1	K/O	ATGGAATTTCAATTGTCCTAAA
VPS2 F3	K/O	gtcagcggccgcatccctgcCTATAATTTGTTCAGCAGCTTG
VPS2 R1	K/O	cacggcgcgcctagcagcggATTTACCTTTGAGCTTTTGTTG
VPS2 R3	K/O	TTGCAAATAAACCTCTATCACA
VPS2 nF	K/O	TTCATTCGTAAGAAATTGACAC
VPS2 nR	K/O	ATGACAAATTGCAACAAAATTA
VPS2 intF	K/O	TGGTAAGAAGTTAACACCACAA
VPS2 intR	K/O	AACTATCTAATCGCGCTTGTAA

VPS2 K/O Check U	K/O	AACCTTCACAAACTAAAATTGAA
VPS2 K/O Check D	K/O	CGATTTTGACCTCAAATCATA
VPS2 Compl F	Compl	ccgctgctaggcgcgccgtgTCGACATCTCTCAGTAAATCATAT
VPS2 Compl R	Compl	gcagggatgcggccgctgacTAGAGTTACAATTGAGCTCCAC
VPS2 Compl nF	Compl	AGCAATTAATGAAAGAGTTGACT
VPS2 Compl nR	Compl	gtttaaacTCGAAAACGATGTT
VPS2 Compl Check D F	Compl	GAAGTGACAGTGATACAACATG
VPS2 Compl Check D R	Compl	CAGTAGTGAGGATGAAGAGTTT
VPS2 Compl Check U F	Compl	atttctttcaccaatcaactcg
VPS2 Compl Check U R	Compl	CCTAATACTCTAGTGGCATCTC
VPS20 F1	K/O	GGCTATTTCTAACACAAAAACC
VPS20 F3	K/O	gtcagcggccgcatccctgcTTGCATAGTTTCTAGTTCAACG
VPS20 R1	K/O	cacggcgcgcctagcagcggACAGTTCCTGATAACTCGTAGG
VPS20 R3	K/O	AAGCGTTTTGGTGTAAATAAAT
VPS20 nF	K/O	TTTCCGATACCCTTAATAAAAA
VPS20 nR	K/O	AGCTGTGATATTGTTTGGAGTT
VPS20 intF	K/O	TAAAATAACTGCACAAGACAGG
VPS20 intR	K/O	TGTTCTTCGATTTCATTACTTG
VPS20 K/O Check U	K/O	TTAATTTTTACGGTTGCTTTTT
VPS20 K/O Check D	K/O	TATGTGAAAAACTTGGTTGAAA
VPS20 Compl F	Compl	ccgctgctaggcgcgccgtg GATAATTCATGAAGGTTTATCGATG
VPS20 Compl R	Compl	gcagggatgcggccgctgac GCCTTCCTGATTTTGCAAGA
VPS20 Compl nF	Compl	AGCAATTAATGAAAGAGTTGACT
VPS20 Compl nR	Compl	gtttaaacTCGAAAACGATGTT
VPS20 Compl Check D F	Compl	ATAATGAGATGCAAGTCGAAAA
VPS20 Compl Check D R	Compl	CTAAAACCCCAACAAATCACAC
VPS20 Compl Check U F	Compl	taccctgtattccattgtatcg
VPS20 Compl Check U R	Compl	ATCCAGCCTCTTAGTAATCAAG
VPS22 F1	K/O	AACTTGAGTCAGAGGAATTGAA
VPS22 F3	K/O	gtcagcggccgcatccctgcTTTTTCCATCCATCTTAGATTC
VPS22 R1	K/O	cacggcgcgcctagcagcggTAATCAAAATCAGAAAGGAAGG
VPS22 R3	K/O	GTGGAAGAACTGATAAAGGTGT
VPS22 Nf	K/O	ATCTTAAATTAACTGCTGAACG
VPS22 Nr	K/O	TTAAATGCAAATTTACCAAGTG
VPS22 intF	K/O	TCACTCAAATTGTTCAACTGAT
VPS22 intR	K/O	GACAGTTTTACATCGCACTTTA
VPS22 K/O Check U	K/O	TCACTGGTAAAAGGAGTTAAATG
VPS22 K/O Check D	K/O	AAGTCAAATTAATCAAAGAACCA
VPS22 Compl F	Compl	ccgctgctaggcgcgccgtgGCCATCATTGTAACAAAACCAA
VPS22 Compl R	Compl	gcagggatgcggccgctgacTGAAATTTTCTCGATGTGGAAG
VPS22 Compl nF	Compl	AGCAATTAATGAAAGAGTTGACT
VPS22 Compl nR	Compl	gtttaaacTCGAAAACGATGTT
VPS22 Compl Check U F	Compl	aagataccctgtattccattgt
VPS22 Compl Check U R	Compl	TCACTCATTTATGGTTGTCAAC
VPS22 Compl Check D F	Compl	TCACAATCATACAACACCAATG
VPS22 Compl Check D R	Compl	CAATACCAGCGCTATAACATTG
VPS22 Compl Check D2 F	Compl	GTAGTAGTGGTTGGATCTTGAT
VPS22 Compl Check D2 R	Compl	AAATCATATACGAGAGCCAAGT
VPS22 Compl Check D3 F	Compl	CTTCCATAATTTGCAGCATTTG
VPS22 Compl Check D3 R	Compl	TGAAGAGCCAAATCATATACGA
VPS23 F1	K/O	AGGTTTAATGCTTTTTGGAATA
VPS23 F3	K/O	gtcagcggccgcatccctgcTTATTAATAGGAAGGGGCTGTA
VPS23 R1	K/O	cacggcgcgcctagcagcggTTTTTAGTTATGTGGGTGTTTG
VPS23 R3	K/O	CCAGAATCAACAGTTTACATCA
VPS23 nF	K/O	TCCTTAACAGAACCCATAATTC
VPS23 nR	K/O	CATAGCTAGTGAAAAACGTCAA
VPS23 intF	K/O	CATGTTCAGTTTGGTAGAATTG
VPS23 intR	K/O	TATTAATTTCGGCACTAACCTT
VPS23 K/O Check U	K/O	TCGAACAATAAACACAACAA
VPS23 K/O Check D	K/O	CAAAATATTACCCCTCCAAT
VPS23 Compl F	Compl	ccgctgctaggcgcgccgtgATTTCGAACAATAAACACAACA
VPS23 Compl R	Compl	gcagggatgcggccgctgacCATAGCTAGTGAAAAACGTCAA

VPS23 Compl nF	Compl	GTCATTCAAGCAATTAATGAAA
VPS23 Compl nR	Compl	AAACGATGTTTGCACCAC
VPS23 Compl Check U F	Compl	CCATAAAATATTCGGTTTGATT
VPS23 Compl Check D R	Compl	CAATAGATTAGGCTCTCCTGAC
VPS23 Compl Check D F	Compl	CTACTTCAAACAGACCTGTCCT
VPS23 Compl Check U R	Compl	TTTTTGATGTGTCTTTTGATGT
VPS24 F1	K/O	CAACAATGTCGTCATAACTAGG
VPS24 F3	K/O	gtcagcggccgcatccctgcAAATATAGAGAAATGCCCAAAA
VPS24 R1	K/O	cacggcgcgcctagcagcggGGTTTATTTCTTGTTCAATGGT
VPS24 R3	K/O	ATTTGGTTCTCTTATCCCCTAT
VPS24 nF	K/O	ATACGAATACCTTGTTGTTGCT
VPS24 nR	K/O	TCAATTTCATTCTTCTTTCTTTC
VPS24 intF	K/O	CAAAGAACAGGTATGTGAAAAA
VPS24 intR	K/O	ATTTCATCTAATGCCAATTCA
VPS24 K/O Check U	K/O	AGTCAAGATTTGATTCTCCTTG
VPS24 K/O Check D	K/O	GAATCTGGATTTGGTTCTCTT
VPS24 Compl F	Compl	ccgctgctaggcgcgccgtgAGGGACAATATAATAGAACTGGT
VPS24 Compl R	Compl	gcagggatgcggccgctgacTCATTATTGTCATAACCATTGG
VPS24 Compl nF	Compl	AGCAATTAATGAAAGAGTTGACT
VPS24 Compl nR	Compl	gtttaaacTCGAAAACGATGTT
VPS24 Compl Check U F	Compl	taccctgtattccattgtatcg
VPS24 Compl Check U R	Compl	AAGAGAAAACTTGCAAATCGAT
VPS24 Compl Check U2 F	Compl	gaaagaagagatgctattggtg
VPS24 Compl Check U2 R	Compl	GTGGAAAAGATGAAAAGACGAT
VPS24 Compl Check U3 F	Compl	gtgaatgtgttagaaaagctga
VPS24 Compl Check U3 R	Compl	GCAATAAATCACTGGTCATACA
VPS24 Compl Check D F	Compl	GAAACTTCATGGGCAATTGAA
VPS24 Compl Check D R	Compl	CAATACCAGCGCTATAACATTG
VPS25 F1	K/O	AGTTTGGATGAATAGAAAGCAT
VPS25 F3	K/O	gtcagcggccgcatccctgcTTGATGTTTACGCTAGTCAAAG
VPS25 R1	K/O	cacggcgcgcctagcagcggCAGCAAGAGAAATGAGATTACA
VPS25 R3	K/O	TTTTCAATAACATGCGAATAGA
VPS25 nF	K/O	AAGGAATGGAAGTATCAATTTT
VPS25 nR	K/O	AGGGTCAATTTTGATTGAAGTA
VPS25 intF	K/O	TACTCATTTCCACCATTTTACA
VPS25 intR	K/O	TCGTTATTCTCGTCTATCAACA
VPS25 K/O Check U	K/O	GAATCAAGAGATAAGAGGAGTCA
VPS25 K/O Check D	K/O	AACGTTCATAATTACCCAAATC
VPS25 Compl F	Compl	ccgctgctaggcgcgccgtgAATGTGAAATTAGGGTGAGAAT
VPS25 Compl R	Compl	gcagggatgcggccgctgacCTTGCTAATAGAGAGATGGAGG
VPS25 Compl nF	Compl	AGCAATTAATGAAAGAGTTGACT
VPS25 Compl nR	Compl	gtttaaacTCGAAAACGATGTT
VPS25 Compl Check U F	Compl	taccctgtattccattgtatcg
VPS25 Compl Check U R	Compl	AGTGAAAGTGGAACCTCTAATT
VPS25 Compl Check D F	Compl	AGCCAACACATATATAGAGCAA
VPS25 Compl Check D R	Compl	CTAAAACCCCAACAAATCACAC
VPS27 F1	K/O	GTTATTGCGCTAAGTTCTTCTT
VPS27 F3	K/O	gtcagcggccgcatccctgcTTTGCTTATCTAGAAATATTTAGCC
VPS27 R1	K/O	cacggcgcgcctagcagcggATTTGAATTTGGAGGTTTGATA
VPS27 R3	K/O	TCAGAATGTGATTTTTAATGGA
VPS27 nF	K/O	TGTCAATGTCTGGATGAGTATC
VPS27 nR	K/O	GGTTTTAGTGTTTGGTGAGATT
VPS27 intF	K/O	ATCACAAGATTTATCACAAGCA
VPS27 intR	K/O	GGAGGATAATGAGGTAATGAAA
VPS27 K/O Check U	K/O	GGCACTCAAACTCTCAAGTA
VPS27 K/O Check D	K/O	AATGAATCTTCATCATTTGG
VPS27 Compl F	Compl	ccgctgctaggcgcgccgtgGGTTGGTTGGTAAGGATATTAG
VPS27 Compl R	Compl	gcagggatgcggccgctgacTATAAACCACGACAAACCTACA
VPS27 Compl nF	Compl	CAAGCAATTAATGAAAGAGTTG
VPS27 Compl nR	Compl	ACTAAAACCCCAACAAATCAC
VPS27 Compl Check D F	Compl	TTCGGTTTGATTAGGTTATTTT
VPS27 Compl Check U R	Compl	TAATGATCTCATGGCAATTTTA

VPS27 Compl Check U R	Compl	ATCGTCTGGAGATTAAGAAGAA
VPS27 Compl Check D F	Compl	TCAGAGTAGCACATAATCGAAC
VPS28 F1	K/O	GAATTTGGGAAAGAATTCAATA
VPS28 F3	K/O	gtcagcggccgcatccctgcTCTGTTTCTTGCTTATACGATG
VPS28 R1	K/O	cacggcgcgcctagcagcggTTTATTGTTCGATTTTACGATG
VPS28 R3	K/O	ATCTTCACATTCCTTTCAACTC
VPS28 nF	K/O	AAACTAATAGACCGTTTTCGAC
VPS28 nR	K/O	ACTTGCTCCGATTAAACTAGAA
VPS28 intF	K/O	AACCAAGAAGTTACCAAATCAC
VPS28 intR	K/O	ATCAGCTTCCTCTTGTGTAAGT
VPS28 K/O Check U	K/O	CAACCTCAAAGTATCTGGAAAT
VPS28 K/O Check D	K/O	TGTCTTTACAAAAACTCACTGC
VPS28 Compl F	Compl	ccgctgctaggcgcgccgtgAGACGATATTGTTTAAACTAGCA
VPS28 Compl R	Compl	gcagggatgcggccgctgacGTTCTCTCTTTCTTTCTTGGTG
VPS28 Compl nF	Compl	AGCAATTAATGAAAGAGTTGACT
VPS28 Compl nR	Compl	gtttaaacTCGAAAACGATGTT
VPS28 Compl Check U F	Compl	gattttgaagctagtgtggaaa
VPS28 Compl Check U R	Compl	GTAACTTCTTGGTTGTAAACGT
VPS28 Compl Check D F	Compl	TCAAACCCTGACTCAACAAG
VPS28 Compl Check D R	Compl	CTAAAACCCCAACAAATCACAC
VPS36 F1	K/O	TTTTGAATGCACTAAGTAATCG
VPS36 F3	K/O	gtcagcggccgcatccctgcTATGCTTATGTTGTCTTTTTGC
VPS36 R1	K/O	cacggcgcgcctagcagcggTTTGCTTCTTGTCTCTCTTTTT
VPS36 R3	K/O	ATGAATACTATTGTTCCCCTTG
VPS36 nF	K/O	AGTCGGTCGAGTATATCTCTTG
VPS36 nR	K/O	AGTGGTGTTGATCATGATACTG
VPS36 intF	K/O	TGATATCAAATGGCAAATTCTA
VPS36 intR	K/O	TGTTTATCGTATTCATTCCTCA
VPS36 K/O Check U	K/O	ATAACAACATCTTTCCGTGAAT
VPS36 K/O Check D	K/O	ATGATGATGATTGTCACTTTTG
VPS36 Compl F	Compl	ccgctgctaggcgcgccgtgATTGAAATGATTATAAGCGGGT
VPS36 Compl R	Compl	gcagggatgcggccgctgacTTGCATTGGGTTTTCTATATGT
VPS36 Compl nF	Compl	AGCAATTAATGAAAGAGTTGACT
VPS36 Compl nR	Compl	gtttaaacTCGAAAACGATGTT
VPS36 Compl Check U F	Compl	taccctgtattccattgtatcg
VPS36 Compl Check U R	Compl	TTTTGCTTCTTGTCTCTCTTTT
VPS36 Compl Check D F	Compl	CCTGATTATAGTTTCTTTGGTGC
VPS36 Compl Check D R	Compl	CCACTAAAACCCCAACAAATC
VPS36 Compl Check D2 F	Compl	ATTGGAAAAGTGTGTTGAAGAG
VPS36 Compl Check D2 R	Compl	AAATCATATACGAGAGCCAAGT
VPS36 Compl Check D3 F	Compl	TTGATTAAGGAACAACAGGAGA
VPS36 Compl Check D3 R	Compl	TCGGAAATGACAAATGAATTCA
VPS4 F1	K/O	TCAAATCTCAACGCAAGTATAG
VPS4 F3	K/O	gtcagcggccgcatccctgcACAATTGAAACAAACCATTGTA
VPS4 R1	K/O	cacggcgcgcctagcagcggAAAAATTTCCTCCATATTGTTG
VPS4 R3	K/O	CACGATAATAAACCCTGAAACT
VPS4 nF	K/O	ATTATTTTAACCGCATTTCATC
VPS4 nR	K/O	GACTGAAGAACTGGATAGTGGT
VPS4 intF	K/O	ATGATAATGATGATGCTGACAC
VPS4 intR	K/O	TTCATTAACTGTTGGTCGATTA
VPS4 K/O Check U	K/O	AGTTGCTGGTTCAATTTATG
VPS4 K/O Check D	K/O	AAAAGATCAGTGAATCACCA
VPS4 Compl F	Compl	ccgctgctaggcgcgccgtgTTCTTGGAGAGAGAGAAACATT
VPS4 Compl R	Compl	gcagggatgcggccgctgacAAAGGGTGAAAGACAAAGTA
VPS4 Compl nF	Compl	GAAGTCGACTATGTCATTCAAG
VPS4 Compl nR	Compl	ACTAAAACCCCAACAAATCAC
VPS4 Compl Check U F	Compl	CCATAAAATATTCGGTTTGATT
VPS4 Compl Check U R	Compl	GTCGATCCATTTACAGAACTTT
VPS4 Compl Check D F	Compl	TATAGGCTTCTTCATACCGAGT
VPS4 Compl Check D R	Compl	GGAAAGAAAAATTAACACCTTG
SUN41 F1	K/O	AAGATAGCATTCAACATGACAA
SUN41 R1	K/O	cacggcgcgcctagcagcggAAAGGAACGACTAAAAGAAACA

SUN41 F3	K/O	gtcagcggccgcatccctgcACAAGATACCCCTTTTTCTCTT
SUN41 R3	K/O	TCATTGTCACAACCATTATCTC
SUN41 nF	K/O	ATATCAATTTTTATTGGGCAAC
SUN41 nR	K/O	TATTATTTACTGCTGCATTTGG
SUN41 intF	K/O	TCCTATCACTACTGTCAGTCCA
SUN41 intR	K/O	CAAGTAAGCAATACCATTAGCA
SUN41 K/O Check U	K/O	ACTACCAAGCAAAACATCTACC
SUN41 K/O Check D	K/O	CCTTAGCACTACTAAAGCTGGT
SUN41 Compl F	Compl	ccgctgctaggcgcgccgtgAGATAGCATTCAACATGACAAA
SUN41 Compl R	Compl	gcagggatgcggccgctgacCGTCATTGTCACAACCATTATC
SUN41 Compl nF	Compl	TCAAGCAATTAATGAAAGAGTTG
SUN41 Compl nR	Compl	ggggatcgtttaaacTCG
SUN41 Compl Check U F	Compl	gtattccattgtatcgcctttg
SUN41 Compl Check U R	Compl	GAAAGAATTCCTGCATGTAACT
SUN41 Compl Check D F	Compl	GGCACATCAAATTCGATATCAT
SUN41 Compl Check D R	Compl	TATAACATTGACGAGCAGTAGT

1 K/O – knockout; Compl - complement

Supplemental Table 6. Strain Genotypes			
Gene	**Strain**	**Genotype**	**Ref**
Reference	SN152	*URA3 IRO1 arg4 his1 leu2* *ura3::λimm434 iro1:: λimm434 arg4 his1 leu2*	[1]
bro1 -/-	URZ370	*URA3 IRO1 arg4 his1 leu2 bro1::C.d HIS1* *ura3::λimm434 iro1:: λimm434 arg4 his1 leu2 bro1::C.m LEU2*	This study
bro1 -/-, +	URZ430	*URA3 IRO1 arg4 his1 leu2::BRO1::Nou^R bro1::C.d HIS1* *ura3::λimm434 iro1:: λimm434 arg4 his1 leu2 bro1::C.m LEU2*	This study
doa4 -/-	URZ468	*URA3 IRO1 arg4 his1 leu2 doa4::C.d HIS1* *ura3::λimm434 iro1:: λimm434 arg4 his1 leu2 doa4::C.m LEU2*	This study
doa4 -/-, +	URZ531	*URA3 IRO1 arg4 his1 leu2::DOA4::Nou^R doa4::C.d HIS1* *ura3::λimm434 iro1:: λimm434 arg4 his1 leu2 doa4::C.m LEU2*	This study
hse1 -/-	URZ358	*URA3 IRO1 arg4 his1 leu2 hse1::C.d HIS1* *ura3::λimm434 iro1:: λimm434 arg4 his1 leu2 hse1::C.m LEU2*	This study
hse1 -/-, +	URZ403	*URA3 IRO1 arg4 his1 leu2::HSE1::Nou^R hse1::C.d HIS1* *ura3::λimm434 iro1:: λimm434 arg4 his1 leu2 hse1::C.m LEU2*	This study
mvb12 -/-	URZ477	*URA3 IRO1 arg4 his1 leu2 mvb12::C.d HIS1* *ura3::λimm434 iro1:: λimm434 arg4 his1 leu2 mvb12::C.m LEU2*	This study

vps2 -/-	URZ453	*URA3 IRO1 arg4 his1 leu2 vps2::C.d HIS1* *ura3::λimm434 iro1:: λimm434 arg4 his1 leu2 vps2::C.m LEU2*	This study
vps4 -/-	URZ368	*URA3 IRO1 arg4 his1 leu2 vps4::C.d HIS1* *ura3::λimm434 iro1:: λimm434 arg4 his1 leu2 vps4::C.m LEU2*	This study
vps4 -/-, +	URZ400	*URA3 IRO1 arg4 his1 leu2::VPS4::Nou^R vps4::C.d HIS1* *ura3::λimm434 iro1:: λimm434 arg4 his1 leu2 vps4::C.m LEU2*	This study
vps20 -/-	URZ458	*URA3 IRO1 arg4 his1 leu2 vps20::C.d HIS1* *ura3::λimm434 iro1:: λimm434 arg4 his1 leu2 vps20::C.m LEU2*	This study
vps20 -/-, +	URZ537	*URA3 IRO1 arg4 his1 leu2::VPS20::Nou^R vps20::C.d HIS1* *ura3::λimm434 iro1:: λimm434 arg4 his1 leu2 vps20::C.m LEU2*	This study
vps22 -/-, +	URZ501	*URA3 IRO1 arg4 his1 leu2 vps22::C.d HIS1* *ura3::λimm434 iro1:: λimm434 arg4 his1 leu2 vps22::C.m LEU2*	This study
vps23 -/-	URZ364	*URA3 IRO1 arg4 his1 leu2 vps23::C.d HIS1* *ura3::λimm434 iro1:: λimm434 arg4 his1 leu2 vps23::C.m LEU2*	This study
vps23 -/-, +	URZ418	*URA3 IRO1 arg4 his1 leu2::VPS23::Nou^R vps23::C.d HIS1* *ura3::λimm434 iro1:: λimm434 arg4 his1 leu2 vps23::C.m LEU2*	This study
vps24 -/-	URZ470	*URA3 IRO1 arg4 his1 leu2 vps24::C.d HIS1* *ura3::λimm434 iro1:: λimm434 arg4 his1 leu2 vps24::C.m LEU2*	This study

vps25 -/-	URZ503	*URA3 IRO1 arg4 his1 leu2 vps25::C.d HIS1* *ura3::λimm434 iro1:: λimm434 arg4 his1 leu2 vps25::C.m LEU2*	This study
vps25 -/-, +	URZ534	*URA3 IRO1 arg4 his1 leu2::VPS25::Nou^R vps25::C.d HIS1* *ura3::λimm434 iro1:: λimm434 arg4 his1 leu2 vps25::C.m LEU2*	This study
vps27 -/-	URZ362	*URA3 IRO1 arg4 his1 leu2 vps27::C.d HIS1* *ura3::λimm434 iro1:: λimm434 arg4 his1 leu2 vps27::C.m LEU2*	This study
vps27 -/-, +	URZ398	*URA3 IRO1 arg4 his1 leu2::VPS27::Nou^R vps27::C.d HIS1* *ura3::λimm434 iro1:: λimm434 arg4 his1 leu2 vps27::C.m LEU2*	This study
vps28 -/-	URZ461	*URA3 IRO1 arg4 his1 leu2 vps28::C.d HIS1* *ura3::λimm434 iro1:: λimm434 arg4 his1 leu2 vps28::C.m LEU2*	This study
Vps36 -/-	URZ465	*URA3 IRO1 arg4 his1 leu2 vps36::C.d HIS1* *ura3::λimm434 iro1:: λimm434 arg4 his1 leu2 vps36::C.m LEU2*	This study
Vps36 -/-, +	URZ398	*URA3 IRO1 arg4 his1 leu2::VPS36::Nou^R vps36:C.d HIS1* *ura3::λimm434 iro1:: λimm434 arg4 his1 leu2 vps36::C.m LEU2*	This study
snf7 -/-	URZ362	*URA3 IRO1 arg4 his1 leu2 snf7::C.d HIS1* *ura3::λimm434 iro1:: λimm434 arg4 his1 leu2 snf7::C.m LEU2*	This study
snf7 -/-, +	URZ403	*URA3 IRO1 arg4 his1 leu2::SNF7::Nou^R snf7::C.d HIS1* *ura3::λimm434 iro1:: λimm434 arg4 his1 leu2 snf7::C.m LEU2*	This study

srn2 -/-	URZ482	*URA3 IRO1 arg4 his1 leu2 srn2::C.d HIS1* *ura3::λimm434 iro1:: λimm434 arg4 his1 leu2 srn2::C.m LEU2*	This study
vta1 -/-	URZ524	*URA3 IRO1 arg4 his1 leu2 vta1::C.d HIS1* *ura3::λimm434 iro1:: λimm434 arg4 his1 leu2 vta1::C.m LEU2*	This study
sun41 -/-	URZ376	*URA3 IRO1 arg4 his1 leu2 sun41::C.d HIS1* *ura3::λimm434 iro1:: λimm434 arg4 his1 leu2 sun41::C.m LEU2*	This study
sun41 -/-, +	URZ562	*URA3 IRO1 arg4 his1 leu2::SUN41::Nou^R sun41::C.d HIS1* *ura3::λimm434 iro1:: λimm434 arg4 his1 leu2 sun41::C.m LEU2*	This study
phr1 -/-	KMR101	*URA3 IRO1 arg4 his1 leu2 phr1::C.d HIS1* *ura3::λimm434 iro1:: λimm434 arg4 his1 leu2 phr1::C.m LEU2*	[2]
mnn9 -/-	KMR392	*URA3 IRO1 arg4 his1 leu2 mnn9::C.d HIS1* *ura3::λimm434 iro1:: λimm434 arg4 his1 leu2 mnn9::C.m LEU2*	[3]

1 Noble, S. M. & Johnson, A. D. Strains and strategies for large-scale gene deletion studies of the diploid human fungal pathogen Candida albicans. *Eukaryot Cell* **4**, 298-309, doi:10.1128/EC.4.2.298-309.2005 (2005).

2 Mitchell, K. F. *et al.* Community participation in biofilm matrix assembly and function. *Proc Natl Acad Sci U S A* **112**, 4092-4097, doi:10.1073/pnas.1421437112 (2015).

3 Taff, H. T. *et al.* A Candida biofilm-induced pathway for matrix glucan delivery: implications for drug resistance. *PLoS Pathog* **8**, e1002848, doi:10.1371/journal.ppat.1002848 (2012).

Chapter 5

Conclusions and Future Directions

Extracellular Matrix production and function in NAC species

Previous studies from the Andes lab [1-4] have implicated the ECM exopolysaccharides, mannan and glucan, as having a key role in the drug resistance phenotype commonly associated with *C. albicans* biofilms. Further investigation resulted in the identification of seven mannan matrix-governing genes (*ALG11, MNN9, MNN11, VAN1, MNN4-4, PMR1,* and *VRG4)* and five glucan matrix-governing genes (*BGL2, BIG1, KRE5, PHR1,* and *XOG1).* Genetic disruption of any of these genes resulted in decreased levels of mannan/glucan and increased levels of susceptibility.

With many studies showing that genes retain functionality among species [5-10], we set about creating deletion mutants of these 12 genes in *C. tropicalis, C. parapsilosis,* and *C. glabrata.* Biofilms for each mutant was assayed for composition, function, and structure. Using a combination of enzymatic and pharmacologic methods, production of mannan/glucan was inhibited in NAC species, resulting in decreased levels of matrix and increased susceptibility. These results suggested a conserved role for functionality of ECM mannan and glucan among *Candia* species. The work described here (Chapter 2) identified that *Candida* species synthesize a mannan-glucan complex with a conserved backbone and anti-fungal properties but differences in the side chains produced by each species.

Genetic regulation of mannan and glucan in NAC species

Mutants in all three NAC species in which the deleted gene regulated a post-translational modification (*ALG11, MNN11, MNN4-4, BGL2, PHR1,* and *XOG1)* resulted in no detectable changes in biofilm formation or susceptibility to anti-fungal drug therapy. Surprisingly, the only genes that retained conserved regulatory function across the species were those with roles in the synthesis of mannan/glucan (*MNN9, PMR1, VAN1, BIG1,* and *KRE5).* Even then, this level of

conservation was not only species dependent but also related to how closely related each species was positioned phylogenetically relative to *C. albicans. C. tropicalis* and *C. parapsilosis* are closely related to *C. albicans* and shared two mannan synthesis genes, that once removed, exhibited increased levels of susceptibility (*MNN9* and *VAN1)*. It is still possible that these two species may also share a conserved glucan synthesis gene in *KRE5*; however, we were unable to explore this possibility due to the inability to delete that particular gene from *C. parapsilosis. C. glabrata* contained only one orthologous gene which was the glucan synthase gene *KRE5.* This may be due to how distantly related *C. glabrata* is in comparison to *C. albicans* phylogenetically.

To investigate the finding that only genes involved in synthesis of mannan/glucan appeared to have an impact on ECM function in NAC biofilms, we used a roller bottle system to produce large quantities of biofilm from which we isolated matrices from NAC species. Matrix was purified and outsourced to collaborators who specialize in NMR for structure analyses. NMR analysis revealed a conserved polysaccharide backbone consisting of α-1,6-mannan and β-1,6-glucan with differences in the branching side chains for each species. Given that this backbone formed a MGCx in *C. albicans,* we used a series of purification and fractionation steps to verify the presence of a MGCx in NAC species. Using size exclusion chromatography followed by separation on an anion exchanger, fractions that yielded a polysaccharide peak were then separated by high and low-molecular weight and analyzed for monosugar content using gas chromatography. These experiments verified the presence of the MGCx in both fractions for all NAC species.

These results open the possibility for development of a pan-C*andida* biofilm drug therapy, which targets this conserved MGCx backbone. Biofilms are notoriously difficult to treat and often require removal of infected devices in addition to a spectrum of anti-fungal drug treatments, depending on the type of infection. The identification of a common target across these four species, could allow for increased efficacy during treatment of a biofilm infection in addition to

improved patient prognosis. Furthermore, this work showed that even though these four species exhibit varying phenotypes with regard to biofilm formation and morphology, the function of the ECM is conserved.

NAC species: Future Directions

In spite of the data presented here, there are still unanswered questions. First, which genes regulate the production and modification of side chains present on the MGCx in NAC species? As in *C. albicans,* if these genes are identified and deleted from the genome, would they result in increased susceptibility due to loss of ECM structural integrity? Unfortunately, the answers to these questions would require extensive genetic manipulation of these NAC species genomes. In *C. albicans* there are over 50 genes responsible for regulation of mannan production/post-translational modification and 11 genes for glucan. Advancements in genome editing does make this work feasible in a reasonable amount of time; however, determination of which genes regulate production/modification of side chains will require extensive resources because of the sheer volume of matrix required and the amount of NMR necessary to answer these questions.

Another interesting avenue to explore would be the protein portion of the ECM. In all four species, proteins make up the vast majority of the ECM. Proteomic analysis of *Candida* species matrices revealed approximately 1,017 proteins in *C. albicans,* 433 in *C. tropicalis,* 508 in *C. parapsilosis,* and 205 in *C. glabrata.* All four species shared 162 proteins with 430, 1, 7, and 0 being unique to *C. albicans, C. tropicalis, C. parapsilosis,* and *C. glabrata* respectively (unpublished data). That *C. albicans* has at least double to triple the numbers of proteins relative to the NAC species is attributed to it being a commensal pathogen. Investigation into the shared

and unique proteins of each species could allow for a better understanding of the roles these proteins play in their respective species.

Candida auris

The work in Chapter 3 describes the characterization of biofilms and the ECM of the emerging pathogen *Candida auris.* It was found that each of the isolates tested had the capability to form a biofilm and produced an ECM with functionality seen in other *Candida* species. Mannan and glucan were found in the ECM, and through enzymatic and pharmacologic testing, were determined to play likely roles in drug resistance much like in other *Candida* species. Considering the inherent resistance to anti-fungals this pathogen already possesses at a planktonic level, identifying potential biofilm drug targets is a major aadvance in treating these infections.

Candida auris: Future Directions

While informative, the work done on *C. auris* still leaves much to be done. The identification of mannan/glucan within the ECM of this species begs the question of whether the MGCx is present in this species as well. Verification of this complex would argue that in the ECM of *Candida* biofilms, a functionally conserved complex is produced that serves as a “protector” to the basal layer of cells. Determination of the structure of the ECM would also be informative as would the genes that governing ECM formation. As more studies are conducted on this species, the tools necessary to answer these questions will be developed and offer opportunities for further experiments on the ECM.

Extracellular Matrix assembly in *C. albicans* through Extracellular Vesicles

The work in Chapter 4 describes the delivery of components of the ECM via extracellular vesicles (EVs) and the role they play in ECM assembly and drug resistance. Using a panel of ESCRT-defective mutants, biofilms were assayed for matrix structure, composition, function, and number of EVs. Of the 21 mutants tested, 16 showed decreased levels of vesicle production, and a subset of 7 showed increased levels of susceptibility.

NMR analysis of the contents of EVs showed strikingly similar spectra to those seen in the ECM of *C. albicans.* These similarities suggested that components of the ECM were being produced within the cell and packaged into EVs. EVs were then leaving the cell through exocytosis and releasing their contents outside of the cell, allowing for construction of the ECM. To validate this claim, wild-type (WT) EVs were added to mutants that exhibited increased levels of susceptibility, decreased levels of mannan/glucan, and decreased levels of EVs, and the mutants were then challenged with fluconazole. The addition of exogenous WT EVs restored ECM functionality, EV levels, and matrix architecture back to what is seen in WT. These results indicate that components of the ECM are packaged intracellularly and assembled extracellularly via proteins and enzymes.

Extracellular Vesicles: Future Directions

The next pressing question for this project is what genes govern the packaging of the polysaccharide components in EVs. We know that components of the ECM are packaged into EVs within the cell and constructed extracellularly; however, how and what determines what goes into each EV is not known. Identification of these factors would allow for a better understanding of the complicated process of ECM production. Mutants are currently being constructed for genes with a proposed function related to mannan/glucan assembly or packaging in an effort to answer this question. Potential protein candidates are also being identified through proteomics by

comparing biofilm and planktonic EVs and looking for proteins that are upregulated in or unique to biofilm EVs.

The work presented here has expanded our knowledge of ECM functionality across *Candida* species. The identification of a conserved MGCx has important clinical implications in that this may allow for drug therapies that are effective against the four most prevalent *Candida* pathogens encountered by physicians. Lastly, the identification of EVs as the primary packing and delivery mechanism of ECM, shows a new function for EVs in the sharing of community resources outside of the established cell-cell signaling and environmental/developmental signals for which EVs are already known. It is my hope that these findings expand and lead to new avenues of research to further increase therapeutic options for management of biofilm infections.

References

1. Nett, J., et al., *Putative role of beta-1,3 glucans in Candida albicans biofilm resistance.* Antimicrob Agents Chemother, 2007. **51**(2): p. 510-20.
2. Nett, J.E., et al., *Role of Fks1p and matrix glucan in Candida albicans biofilm resistance to an echinocandin, pyrimidine, and polyene.* Antimicrob Agents Chemother, 2010. **54**(8): p. 3505-8.
3. Mitchell, K.F., et al., *Role of matrix beta-1,3 glucan in antifungal resistance of non-albicans Candida biofilms.* Antimicrob Agents Chemother, 2013. **57**(4): p. 1918-20.
4. Mitchell, K.F., et al., *Community participation in biofilm matrix assembly and function.* Proc Natl Acad Sci U S A, 2015. **112**(13): p. 4092-7.
5. Silva, S., et al., *Candida glabrata, Candida parapsilosis and Candida tropicalis: biology, epidemiology, pathogenicity and antifungal resistance.* FEMS Microbiol Rev, 2012. **36**(2): p. 288-305.
6. Holland, L.M., et al., *Comparative phenotypic analysis of the major fungal pathogens Candida parapsilosis and Candida albicans.* PLoS Pathog, 2014. **10**(9): p. e1004365.
7. Mancera, E., et al., *Finding a Missing Gene: EFG1 Regulates Morphogenesis in Candida tropicalis.* G3 (Bethesda), 2015. **5**(5): p. 849-56.
8. Priest, S.J. and M.C. Lorenz, *Characterization of Virulence-Related Phenotypes in Candida Species of the CUG Clade.* Eukaryot Cell, 2015. **14**(9): p. 931-40.
9. Rodrigues, C.F., S. Silva, and M. Henriques, *Candida glabrata: a review of its features and resistance.* Eur J Clin Microbiol Infect Dis, 2014. **33**(5): p. 673-88.

10. Roetzer, A., T. Gabaldon, and C. Schuller, *From Saccharomyces cerevisiae to Candida glabratain a few easy steps: important adaptations for an opportunistic pathogen.* FEMS Microbiol Lett, 2011. **314**(1): p. 1-9.

Appendix A: Proteomic data for non-*albicans* matrices

Figure 1: Venn Diagram of unique and shared proteins found in the extracellular matrix of *C. albicans, C. tropicalis, C. parapsilosis,* and *C. glabrata*

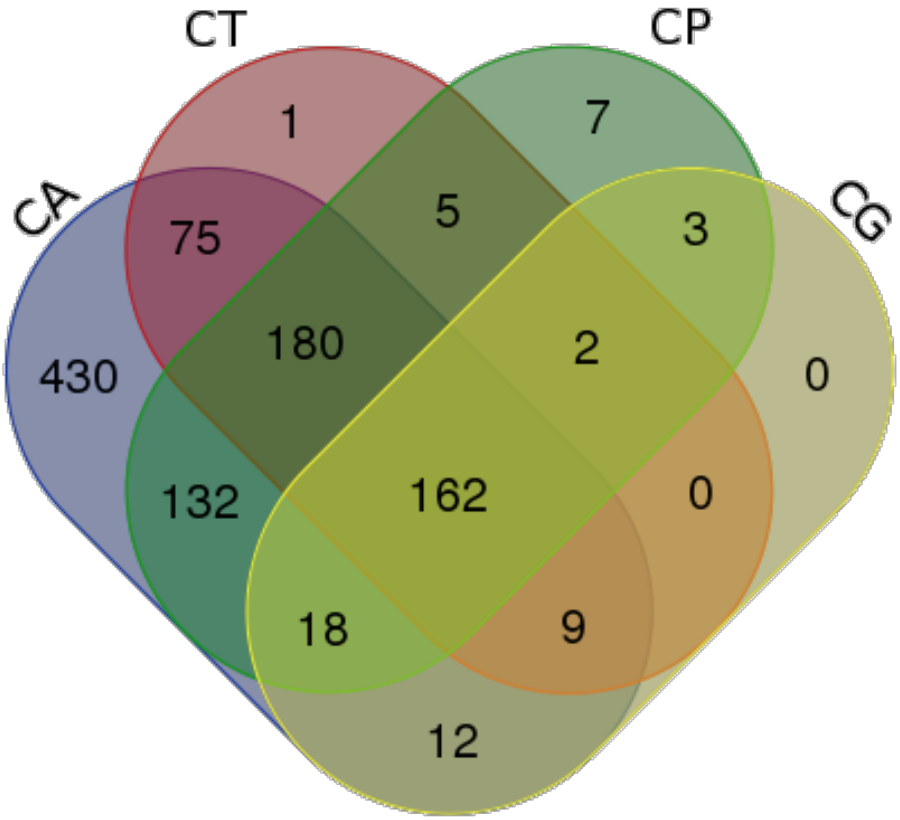

Figure 2: Kegg map of proteins found in the extracellular matrix of *C. albicans, C. tropicalis, C. parapsilosis,* and *C. glabrata* and their respective processes

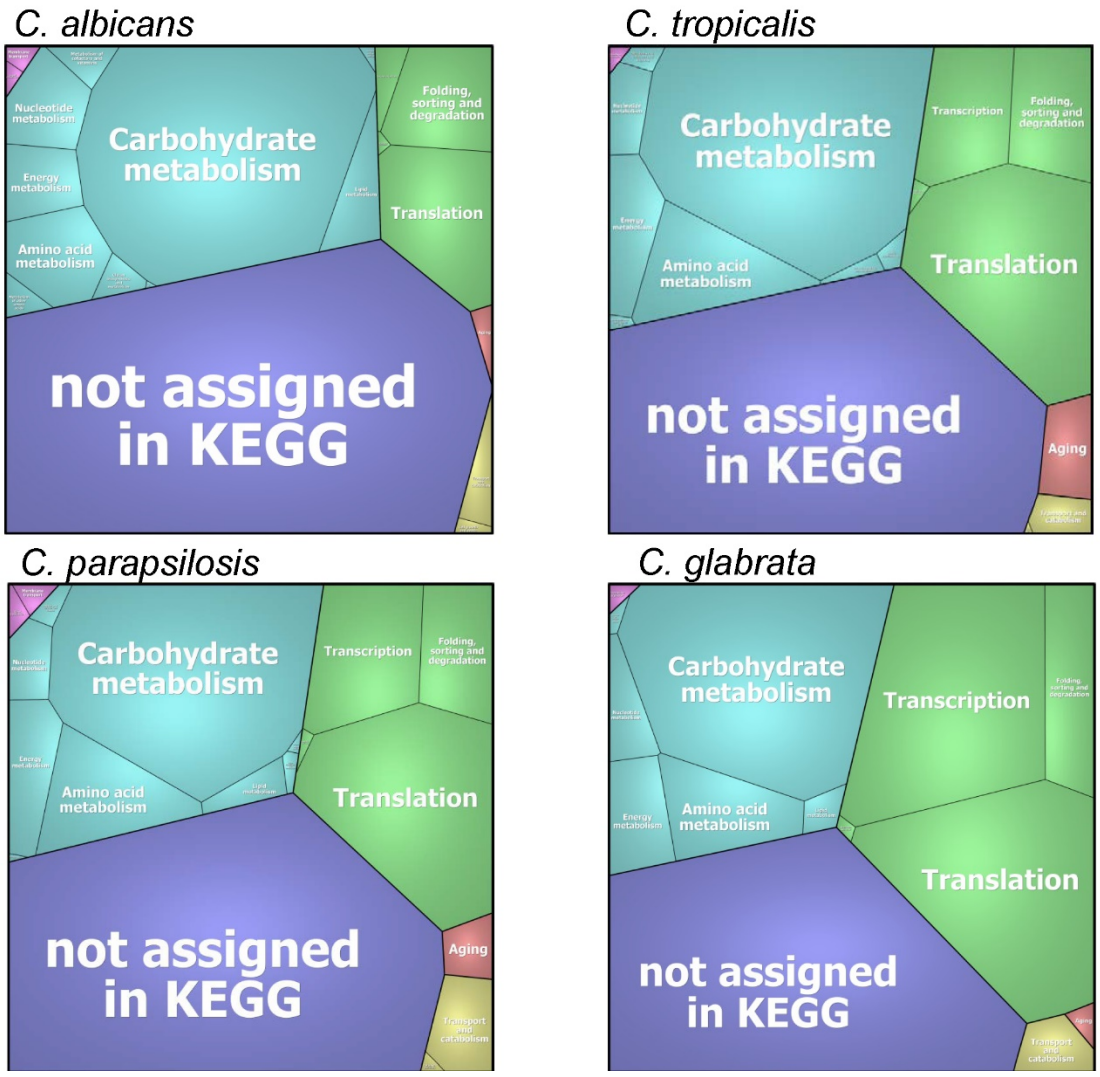

Figure 3: Kegg map of proteins found in the extracellular matrix of *C. albicans, C. tropicalis, C. parapsilosis,* and *C. glabrata* and their relative expression levels

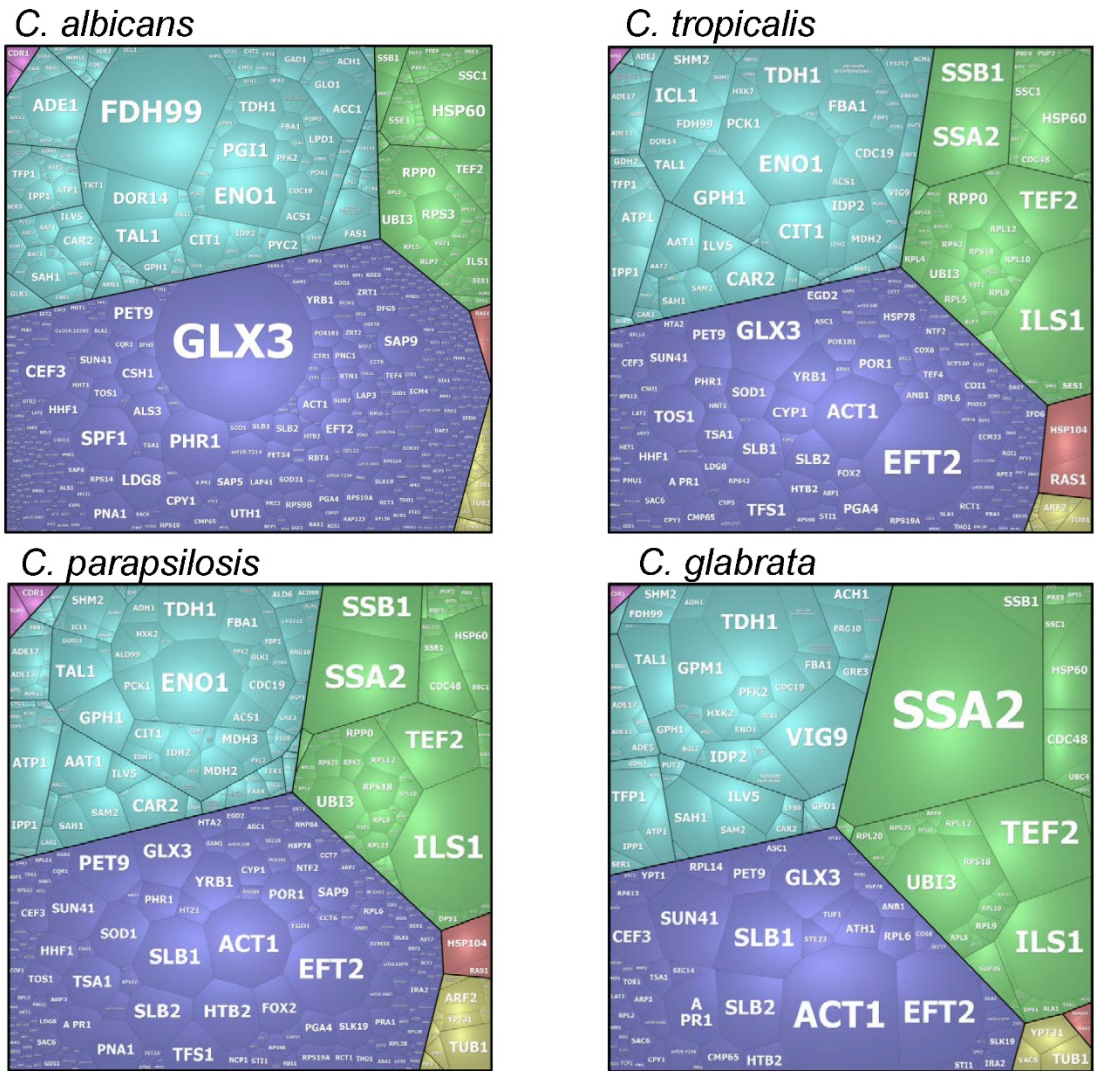

Table 1: Shared Proteins in *C. albicans, C. glabrata, C. parapsilosis, C. tropicalis* extracellular matrix			
Protein Characteristics			
Protein Name	**Gene Name**	**ORF Number**	**Gene Ontology**
Saccharopepsin	APR1	CaO19.1891	fungal-type vacuole [GO:0000324]; aspartic-type endopeptidase activity [GO:0004190]; endopeptidase activity [GO:0004175]
Acetyl-CoA hydrolase (EC 3.1.2.1) (Acetyl-CoA deacylase) (Acetyl-CoA acylase)	ACH1	CaO19.10681	cytoplasm [GO:0005737]; acetyl-CoA hydrolase activity [GO:0003986]; acetyl-CoA metabolic process [GO:0006084]
Acetyl-coenzyme A synthetase (EC 6.2.1.1)	ACS1	CaO19.1743	acetate-CoA ligase activity [GO:0003987]; AMP binding [GO:0016208]; ATP binding [GO:0005524]; acetyl-CoA biosynthetic process from acetate [GO:0019427]
Adenylosuccinate synthetase (AMPSase) (AdSS) (EC 6.3.4.4) (IMP--aspartate ligase)	ADE12	CaO19.4827	cytoplasm [GO:0005737]; adenylosuccinate synthase activity [GO:0004019]; GTP binding [GO:0005525]; magnesium ion binding [GO:0000287]; 'de novo' AMP biosynthetic process [GO:0044208]
Adenylosuccinate lyase (ASL) (EC 4.3.2.2) (Adenylosuccinase)	ADE13	CaO19.3870	N6-(1,2-dicarboxyethyl)AMP AMP-lyase (fumarate-forming) activity [GO:0004018]; 'de novo' AMP biosynthetic process [GO:0044208]; 'de novo' IMP biosynthetic process [GO:0006189]
Bifunctional purine biosynthesis protein ADE17 (Uncharacterized protein)	ADE17	CaO19.492	IMP cyclohydrolase activity [GO:0003937]; phosphoribosylaminoimidazolecarboxamide formyltransferase activity [GO:0004643]; purine nucleotide biosynthetic process [GO:0006164]
Alcohol dehydrogenase I	ADH1	CaO19.3997	oxidoreductase activity [GO:0016491]; zinc ion binding [GO:0008270]
Uncharacterized protein	ALD5	CaO19.5806	oxidoreductase activity, acting on the aldehyde or oxo group of donors, NAD or NADP as acceptor [GO:0016620]
Eukaryotic translation initiation factor 5A (eIF-5A) (eIF-4D)	ANB1	CaO19.10930	cytoplasm [GO:0005737]; ribosome binding [GO:0043022]; translation elongation factor activity [GO:0003746]; positive regulation of translational elongation [GO:0045901]; positive regulation of translational termination [GO:0045905]; translational frameshifting [GO:0006452]
Aminopeptidase 2 (EC 3.4.11.-)	APE2	CaO19.12664	cell wall [GO:0005618]; extracellular region [GO:0005576]; aminopeptidase activity [GO:0004177]; metallopeptidase activity [GO:0008237]; zinc ion binding [GO:0008270]
Uncharacterized protein	ARP3	CaO19.2289	actin cortical patch [GO:0030479]; hyphal tip [GO:0001411]; cellular response to drug [GO:0035690]
Part of 40S ribosomal subunit, putative	ASC1	CaO19.6906	cytosolic small ribosomal subunit [GO:0022627]; GDP-dissociation inhibitor activity [GO:0005092]; ribosome binding [GO:0043022]; signal transducer activity [GO:0004871]; cell adhesion [GO:0007155]; cellular protein localization [GO:0034613]; cellular response to neutral pH [GO:0036244]; cellular response to starvation [GO:0009267]; conjugation with cellular fusion [GO:0000747]; filamentous growth [GO:0030447]; filamentous growth of a population of unicellular organisms in response to biotic stimulus [GO:0036180]; filamentous growth of a population of unicellular organisms in response to neutral pH [GO:0036178]; filamentous growth of a population of unicellular organisms in response to starvation [GO:0036170]; G-protein coupled receptor signaling pathway [GO:0007186]; glucose mediated signaling pathway [GO:0010255]; intracellular signal transduction [GO:0035556]; invasive growth in response to glucose limitation [GO:0001403]; negative regulation of translation

			[GO:0017148]; pathogenesis [GO:0009405]; positive regulation of conjugation with cellular fusion [GO:0031139]; positive regulation of protein autophosphorylation [GO:0031954]; regulation of eIF2 alpha phosphorylation by amino acid starvation [GO:0060733]; regulation of fungal-type cell wall biogenesis [GO:0032995]
Cell wall acid trehalase ATC1 (EC 3.2.1.28) (Alpha,alpha-trehalase) (Alpha,alpha-trehalose glucohydrolase)	ATH1	CaO19.13595	cell wall [GO:0005618]; extracellular region [GO:0005576]; alpha,alpha-trehalase activity [GO:0004555]; carbohydrate binding [GO:0030246]; hydrolase activity [GO:0016787]; carbohydrate metabolic process [GO:0005975]; pathogenesis [GO:0009405]
ATP synthase subunit alpha	ATP1	CaO19.6854	proton-transporting ATP synthase complex, catalytic core F(1) [GO:0045261]; ATP binding [GO:0005524]; proton-transporting ATP synthase activity, rotational mechanism [GO:0046933]; ATP synthesis coupled proton transport [GO:0015986]
ATP synthase subunit beta (EC 3.6.3.14)	ATP2	CaO19.13098	proton-transporting ATP synthase complex, catalytic core F(1) [GO:0045261]; ATP binding [GO:0005524]; proton-transporting ATP synthase activity, rotational mechanism [GO:0046933]; ATP synthesis coupled proton transport [GO:0015986]
Glucan 1,3-beta-glucosidase BGL2 (EC 3.2.1.58) (Exo-1,3-beta-glucanase)	BGL2	CaO19.12034	cell surface [GO:0009986]; cytoplasm [GO:0005737]; extracellular region [GO:0005576]; fungal-type cell wall [GO:0009277]; yeast-form cell wall [GO:0030445]; 1,3-beta-glucanosyltransferase activity [GO:0042124]; glucan exo-1,3-beta-glucosidase activity [GO:0004338]; glucanosyltransferase activity [GO:0042123]; adhesion of symbiont to host [GO:0044406]; carbohydrate metabolic process [GO:0005975]; fungal-type cell wall organization [GO:0031505]; growth of symbiont in host [GO:0044117]; pathogenesis [GO:0009405]; single-species biofilm formation in or on host organism [GO:0044407]; single-species biofilm formation on inanimate substrate [GO:0044011]
Protein BMH2	BMH1	CaO19.3014	cell surface [GO:0009986]; plasma membrane [GO:0005886]; yeast-form cell wall [GO:0030445]; cellular response to heat [GO:0034605]; cellular response to neutral pH [GO:0036244]; chlamydospore formation [GO:0001410]; filamentous growth [GO:0030447]; filamentous growth of a population of unicellular organisms [GO:0044182]; filamentous growth of a population of unicellular organisms in response to biotic stimulus [GO:0036180]; filamentous growth of a population of unicellular organisms in response to heat [GO:0036168]; filamentous growth of a population of unicellular organisms in response to neutral pH [GO:0036178]; pathogenesis [GO:0009405]; positive regulation of filamentous growth of a population of unicellular organisms in response to biotic stimulus [GO:1900445]; positive regulation of filamentous growth of a population of unicellular organisms in response to neutral pH [GO:1900442]; regulation of carbohydrate metabolic process [GO:0006109]
Uncharacterized protein	CAR2	CaO19.13086	cytoplasm [GO:0005737]; identical protein binding [GO:0042802]; ornithine-oxo-acid transaminase activity [GO:0004587]; pyridoxal phosphate binding [GO:0030170]; arginine catabolic process to glutamate [GO:0019544]; arginine catabolic process to proline via ornithine [GO:0010121]

Nucleoside diphosphate kinase (EC 2.7.4.6)	CDC19	CaO19.11059	cell surface [GO:0009986]; cytoplasm [GO:0005737]; hyphal cell wall [GO:0030446]; plasma membrane [GO:0005886]; yeast-form cell wall [GO:0030445]; ATP binding [GO:0005524]; kinase activity [GO:0016301]; magnesium ion binding [GO:0000287]; potassium ion binding [GO:0030955]; pyruvate kinase activity [GO:0004743]; cellular response to starvation [GO:0009267]; filamentous growth [GO:0030447]; filamentous growth of a population of unicellular organisms in response to biotic stimulus [GO:0036180]; filamentous growth of a population of unicellular organisms in response to starvation [GO:0036170]; glycolytic process [GO:0006096]; induction by symbiont of host defense response [GO:0044416]
Cell division control protein 48 (Uncharacterized protein)	CDC48	CaO19.2340	cell surface [GO:0009986]; plasma membrane [GO:0005886]; ATP binding [GO:0005524]; hydrolase activity [GO:0016787]
Suppressor of toxicity of sporidesmin	CDR1	CaO19.6000	integral component of membrane [GO:0016021]; plasma membrane [GO:0005886]; ATP binding [GO:0005524]; xenobiotic-transporting ATPase activity [GO:0008559]; cellular response to drug [GO:0035690]; drug export [GO:0046618]; response to antibiotic [GO:0046677]; response to cycloheximide [GO:0046898]
Elongation factor 3 (EF-3)	CEF3	CaO19.11629	cytoplasm [GO:0005737]; ATP binding [GO:0005524]; ATPase activity [GO:0016887]; translation elongation factor activity [GO:0003746]
Citrate synthase	CIT1	CaO19.4393	citrate (Si)-synthase activity [GO:0004108]; citrate metabolic process [GO:0006101]; tricarboxylic acid cycle [GO:0006099]
Likely calmodulin	CMD1	CaO19.11891	calcium ion binding [GO:0005509]
Cell surface mannoprotein MP65 (EC 3.2.1.-) (Mannoprotein of 65 kDa) (Soluble cell wall protein 10)	CMP65	CaO19.1779	cell surface [GO:0009986]; extracellular region [GO:0005576]; fungal-type cell wall [GO:0009277]; hyphal cell wall [GO:0030446]; yeast-form cell wall [GO:0030445]; hydrolase activity, hydrolyzing O-glycosyl compounds [GO:0004553]; carbohydrate metabolic process [GO:0005975]; cell adhesion [GO:0007155]; cell adhesion involved in single-species biofilm formation [GO:0043709]; cell wall organization [GO:0071555]; cell-substrate adhesion [GO:0031589]; cellular response to glucose starvation [GO:0042149]; cellular response to neutral pH [GO:0036244]; filamentous growth [GO:0030447]; filamentous growth of a population of unicellular organisms in response to neutral pH [GO:0036178]; filamentous growth of a population of unicellular organisms in response to starvation [GO:0036170]; induction by symbiont of host defense response [GO:0044416]; pathogenesis [GO:0009405]
Secreted protein (Uncharacterized protein)	COI1	CaO19.12529	cell surface [GO:0009986]; extracellular region [GO:0005576]
Carboxypeptidase (EC 3.4.16.-)	CPY1	CaO19.1339	vacuole [GO:0005773]; serine-type carboxypeptidase activity [GO:0004185]
6-phosphogluconate dehydrogenase, decarboxylating (EC 1.1.1.44)	DOR14	CaO19.12491	phosphogluconate dehydrogenase (decarboxylating) activity [GO:0004616]; D-gluconate metabolic process [GO:0019521]; pentose-phosphate shunt [GO:0006098]
Aspartyl-tRNA synthetase, cytoplasmic, putative (EC 6.1.1.12)	DPS1-1	CaO19.2407	cytoplasm [GO:0005737]; aspartate-tRNA ligase activity [GO:0004815]; ATP binding [GO:0005524]; nucleic acid binding [GO:0003676]; aspartyl-tRNA aminoacylation [GO:0006422]
Elongation factor 2, putative	EFT2	CaO19.5788	cell surface [GO:0009986]; cytoplasm [GO:0005737]; membrane [GO:0016020]; plasma membrane [GO:0005886]; yeast-form cell wall [GO:0030445]; drug

			binding [GO:0008144]; GTP binding [GO:0005525]; GTPase activity [GO:0003924]; translation elongation factor activity [GO:0003746]; cellular response to drug [GO:0035690]
Enolase (1), putative (EC 4.2.1.11)	ENO1	CaO19.395	biofilm matrix [GO:0097311]; cell surface [GO:0009986]; cytosol [GO:0005829]; extracellular region [GO:0005576]; fungal-type cell wall [GO:0009277]; hyphal cell wall [GO:0030446]; intracellular [GO:0005622]; membrane [GO:0016020]; nucleus [GO:0005634]; phosphopyruvate hydratase complex [GO:0000015]; plasma membrane [GO:0005886]; yeast-form cell wall [GO:0030445]; high molecular weight kininogen binding [GO:0030985]; magnesium ion binding [GO:0000287]; phosphopyruvate hydratase activity [GO:0004634]; entry into host [GO:0044409]; filamentous growth [GO:0030447]; filamentous growth of a population of unicellular organisms in response to biotic stimulus [GO:0036180]; gluconeogenesis [GO:0006094]; glycolytic process [GO:0006096]; induction by symbiont of host defense response [GO:0044416]
Acetyl-CoA acetyltransferase IB (Uncharacterized protein)	ERG10	CaO19.1591	cytoplasm [GO:0005737]; acetyl-CoA C-acetyltransferase activity [GO:0003985]; ergosterol biosynthetic process [GO:0006696]
Likely long chain fatty acid-CoA synthetase Faa4p (Long-chain acyl-CoA synthetase)	FAA4	CaO19.7592	catalytic activity [GO:0003824]; metabolic process [GO:0008152]
Fatty acid synthase subunit alpha (EC 2.3.1.86) [Includes: Acyl carrier	FAS2	CaO19.5949	holo-[acyl-carrier-protein] synthase activity [GO:0008897]; magnesium ion binding [GO:0000287]; fatty acid biosynthetic process [GO:0006633]
Fructose-bisphosphate aldolase	FBA1	CaO19.4618	cell surface [GO:0009986]; cytoplasm [GO:0005737]; fungal-type cell wall [GO:0009277]; hyphal cell wall [GO:0030446]; plasma membrane [GO:0005886]; fructose-bisphosphate aldolase activity [GO:0004332]; zinc ion binding [GO:0008270]; glycolytic process [GO:0006096]; induction by symbiont of host defense response [GO:0044416]; interaction with host [GO:0051701]
Formate dehydrogenase 2 (Potential NAD-formate dehydrogenase)	FDH99	CaO19.638	biofilm matrix [GO:0097311]; cytoplasm [GO:0005737]; formate dehydrogenase (NAD+) activity [GO:0008863]; NAD binding [GO:0051287]; oxidoreductase activity, acting on the CH-OH group of donors, NAD or NADP as acceptor [GO:0016616]; formate catabolic process [GO:0042183]; glycine catabolic process [GO:0006546]
Uncharacterized protein	FRS1	CaO19.10105	cytoplasm [GO:0005737]; ATP binding [GO:0005524]; magnesium ion binding [GO:0000287]; phenylalanine-tRNA ligase activity [GO:0004826]; RNA binding [GO:0003723]; phenylalanyl-tRNA aminoacylation [GO:0006432]
Fumarate hydratase, mitochondrial, putative (EC 4.2.1.2)	FUM11	CaO19.543	tricarboxylic acid cycle enzyme complex [GO:0045239]; fumarate hydratase activity [GO:0004333]; fumarate metabolic process [GO:0006106]; tricarboxylic acid cycle [GO:0006099]
Eukaryotic translation initiation factor 2 subunit gamma (Likely translation initiation factor eIF2 gamma subunit)	GCD11	CaO19.11699	GTP binding [GO:0005525]; GTPase activity [GO:0003924]; translation initiation factor activity [GO:0003743]
NAD-specific glutamate dehydrogenase	GDH2	CaO19.2192	glutamate dehydrogenase (NAD+) activity [GO:0004352]; cellular amino acid metabolic process [GO:0006520]; glutamate catabolic process to 2-oxoglutarate [GO:0019551]
Glyoxalase 3 (EC 4.2.1.130) (Glutathione-independent glyoxalase)	GLX3	CaO19.251	glyoxalase III activity [GO:0019172]; methylglyoxal catabolic process to D-lactate via S-lactoyl-glutathione [GO:0019243]

Alpha-1,4 glucan phosphorylase (EC 2.4.1.1)	GPH1	CaO19.7021	cell surface [GO:0009986]; cytoplasm [GO:0005737]; hyphal cell wall [GO:0030446]; glycogen phosphorylase activity [GO:0008184]; pyridoxal phosphate binding [GO:0030170]; glycogen catabolic process [GO:0005980]
Phosphoglycerate mutase 1	GPM1	CaO19.903	biofilm matrix [GO:0097311]; cell surface [GO:0009986]; cytoplasm [GO:0005737]; fungal-type cell wall [GO:0009277]; hyphal cell wall [GO:0030446]; phosphoglycerate mutase activity [GO:0004619]; glycolytic process [GO:0006096]; interaction with host [GO:0051701]
NAD(P)H-dependent D-xylose reductase I,II	GRE3	CaO19.4317	oxidoreductase activity [GO:0016491]
Glycyl-tRNA synthetase 1	GRS1	CaO19.437	cytoplasm [GO:0005737]; ATP binding [GO:0005524]; glycine-tRNA ligase activity [GO:0004820]; glycyl-tRNA aminoacylation [GO:0006426]
GTP-binding nuclear protein, Ran family member, putative	GSP1	CaO19.12948	nucleus [GO:0005634]; GTP binding [GO:0005525]; GTPase activity [GO:0003924]; chromosome organization [GO:0051276]; intracellular protein transport [GO:0006886]; nucleocytoplasmic transport [GO:0006913]; small GTPase mediated signal transduction [GO:0007264]
Glycogen [starch] synthase, putative (EC 2.4.1.11)	GSY1	CaO19.3278	glycogen (starch) synthase activity [GO:0004373]; glycogen biosynthetic process [GO:0005978]
GMP synthase	GUA1	CaO19.4813	cytoplasm [GO:0005737]; ATP binding [GO:0005524]; GMP synthase (glutamine-hydrolyzing) activity [GO:0003922]; pyrophosphatase activity [GO:0016462]; glutamine metabolic process [GO:0006541]; GMP biosynthetic process [GO:0006177]; GMP metabolic process [GO:0046037]
Glutamyl-tRNA synthetase	GUS1	CaO19.7057	cytosol [GO:0005829]; methionyl glutamyl tRNA synthetase complex [GO:0017102]; mitochondrion [GO:0005739]; nucleus [GO:0005634]; ATP binding [GO:0005524]; glutamate-tRNA ligase activity [GO:0004818]; glutamyl-tRNA aminoacylation [GO:0006424]
Histone H4	HHF1	CaO19.1059	nucleosome [GO:0000786]; nucleus [GO:0005634]; DNA binding [GO:0003677]; DNA-templated transcription, initiation [GO:0006352]; nucleosome assembly [GO:0006334]
Uncharacterized protein	HSP104	CaO19.13747	cell surface [GO:0009986]; ATP binding [GO:0005524]; ATPase activity, coupled [GO:0042623]; cellular heat acclimation [GO:0070370]; cellular response to heat [GO:0034605]; chaperone mediated protein folding requiring cofactor [GO:0051085]; pathogenesis [GO:0009405]; protein metabolic process [GO:0019538]; single-species biofilm formation on inanimate substrate [GO:0044011]
Heat shock protein 60, mitochondrial (60 kDa chaperonin) (Protein Cpn60)	HSP60	CaO19.717	mitochondrion [GO:0005739]; ATP binding [GO:0005524]; cellular response to heat [GO:0034605]; protein refolding [GO:0042026]
Heat shock protein SSA1	HSP70	CaO19.12447	biofilm matrix [GO:0097311]; cell surface [GO:0009986]; cytosol [GO:0005829]; fungal-type cell wall [GO:0009277]; hyphal cell wall [GO:0030446]; plasma membrane [GO:0005886]; yeast-form cell wall [GO:0030445]; ATP binding [GO:0005524]; peptide binding [GO:0042277]; cellular response to heat [GO:0034605]; entry into host cell [GO:0030260]; induction by symbiont of host defense response [GO:0044416]; interaction with host [GO:0051701]; response to toxic substance [GO:0009636]

Heat shock protein 78, mitochondrial, putative	HSP78	CaO19.8501	mitochondrial matrix [GO:0005759]; ATP binding [GO:0005524]
ATP-dependent molecular chaperone HSP82	HSP90	CaO19.6515	cell surface [GO:0009986]; cytoplasm [GO:0005737]; fungal-type cell wall [GO:0009277]; hyphal cell wall [GO:0030446]; membrane [GO:0016020]; plasma membrane [GO:0005886]; ATP binding [GO:0005524]; ATPase activity, coupled [GO:0042623]; cellular response to drug [GO:0035690]; cellular response to heat [GO:0034605]; filamentous growth [GO:0030447]; filamentous growth of a population of unicellular organisms [GO:0044182]; intracellular steroid hormone receptor signaling pathway [GO:0030518]; negative regulation of filamentous growth of a population of unicellular organisms [GO:1900429]; pathogenesis [GO:0009405]; protein folding [GO:0006457]; regulation of apoptotic process [GO:0042981]
Histone H2A	HTA2	CaO19.1051	nuclear chromatin [GO:0000790]; nucleosome [GO:0000786]; DNA binding [GO:0003677]; chromatin silencing [GO:0006342]; DNA repair [GO:0006281]
Histone H2B	HTB2	CaO19.1052	nucleosome [GO:0000786]; nucleus [GO:0005634]; DNA binding [GO:0003677]
Hexokinase (EC 2.7.1.1)	HXK2	CaO19.542	cytoplasm [GO:0005737]; ATP binding [GO:0005524]; glucose binding [GO:0005536]; hexokinase activity [GO:0004396]; cellular glucose homeostasis [GO:0001678]; glycolytic process [GO:0006096]; hexose metabolic process [GO:0019318]
Isocitrate dehydrogenase [NAD] subunit, mitochondrial (EC 1.1.1.41)	IDH1	CaO19.4826	magnesium ion binding [GO:0000287]; NAD binding [GO:0051287]; oxidoreductase activity, acting on the CH-OH group of donors, NAD or NADP as acceptor [GO:0016616]
Isocitrate dehydrogenase [NADP] (EC 1.1.1.42)	IDP1	CaO19.5211	isocitrate dehydrogenase (NADP+) activity [GO:0004450]; magnesium ion binding [GO:0000287]; NAD binding [GO:0051287]; isocitrate metabolic process [GO:0006102]; tricarboxylic acid cycle [GO:0006099]
Isocitrate dehydrogenase [NADP] (EC 1.1.1.42)	IDP2	CaO19.3733	isocitrate dehydrogenase (NADP+) activity [GO:0004450]; magnesium ion binding [GO:0000287]; NAD binding [GO:0051287]; isocitrate metabolic process [GO:0006102]; tricarboxylic acid cycle [GO:0006099]
Isoleucine-tRNA ligase (Probable Isoleucyl-tRNA synthetase)	ILS1	CaO19.2138	cytoplasm [GO:0005737]; aminoacyl-tRNA editing activity [GO:0002161]; ATP binding [GO:0005524]; isoleucine-tRNA ligase activity [GO:0004822]; tRNA binding [GO:0000049]; isoleucyl-tRNA aminoacylation [GO:0006428]
Ketol-acid reductoisomerase, mitochondrial (EC 1.1.1.86) (Acetohydroxy-acid reductoisomerase) (Alpha-keto-beta-hydroxylacyl reductoisomerase)	ILV5	CaO19.7733	mitochondrion [GO:0005739]; isomerase activity [GO:0016853]; ketol-acid reductoisomerase activity [GO:0004455]; metal ion binding [GO:0046872]; isoleucine biosynthetic process [GO:0009097]; valine biosynthetic process [GO:0009099]
Inorganic pyrophosphatase	IPP1	CaO19.3590	biofilm matrix [GO:0097311]; cytoplasm [GO:0005737]; hyphal cell wall [GO:0030446]; inorganic diphosphatase activity [GO:0004427]; magnesium ion binding [GO:0000287]; phosphate-containing compound metabolic process [GO:0006796]
Putative uncharacterized protein	IRA2	CaO19.5219	regulation of GTPase activity [GO:0043087]; signal transduction [GO:0007165]
Importin subunit beta-1 (Uncharacterized protein)	KAP95	CaO19.11165	cytoplasm [GO:0005737]; nuclear membrane [GO:0031965]; nuclear periphery [GO:0034399]; nuclear localization sequence binding [GO:0008139]; protein transporter activity [GO:0008565]; NLS-bearing protein import into nucleus [GO:0006607]; protein import into nucleus, docking [GO:0000059]; protein import

			into nucleus, translocation [GO:0000060]; ribosomal protein import into nucleus [GO:0006610]
Uncharacterized protein	KAR2	CaO19.9564	cell surface [GO:0009986]; extracellular region [GO:0005576]; intracellular [GO:0005622]; ATP binding [GO:0005524]; protein folding [GO:0006457]; SRP-dependent cotranslational protein targeting to membrane, translocation [GO:0006616]
Uncharacterized protein	KGD2	CaO19.6126	oxoglutarate dehydrogenase complex [GO:0045252]; dihydrolipoyllysine-residue succinyltransferase activity [GO:0004149]; tricarboxylic acid cycle [GO:0006099]
Uncharacterized protein	LEU42	CaO19.1375	2-isopropylmalate synthase activity [GO:0003852]; leucine biosynthetic process [GO:0009098]
Homoisocitrate dehydrogenase, mitochondrial	LYS12	CaO19.2525	homoisocitrate dehydrogenase activity [GO:0047046]; magnesium ion binding [GO:0000287]; NAD binding [GO:0051287]; lysine biosynthetic process [GO:0009085]
Saccharopine dehydrogenase [NADP+, L-glutamate-forming], putative (EC 1.5.1.10)	LYS9	CaO19.7448	cytoplasm [GO:0005737]; saccharopine dehydrogenase (NADP+, L-glutamate-forming) activity [GO:0004755]; lysine biosynthetic process via aminoadipic acid [GO:0019878]
Malate dehydrogenase (EC 1.1.1.37)	MDH1	CaO19.12072	biofilm matrix [GO:0097311]; L-malate dehydrogenase activity [GO:0030060]; carbohydrate metabolic process [GO:0005975]; malate metabolic process [GO:0006108]; tricarboxylic acid cycle [GO:0006099]
5-methyltetrahydropteroyltriglutamate-homocysteine methyltransferase	MET6	CaO19.2551	biofilm matrix [GO:0097311]; cell surface [GO:0009986]; fungal-type cell wall [GO:0009277]; hyphal cell wall [GO:0030446]; 5-methyltetrahydropteroyltriglutamate-homocysteine S-methyltransferase activity [GO:0003871]; zinc ion binding [GO:0008270]; cellular response to heat [GO:0034605]; induction by symbiont of host defense response [GO:0044416]; methionine biosynthetic process [GO:0009086]; methionine metabolic process [GO:0006555]
Obg-like ATPase 1	OLA1	CaO19.754	cytoplasm [GO:0005737]; ATP binding [GO:0005524]; ATPase activity [GO:0016887]; GTP binding [GO:0005525]; ribosomal large subunit binding [GO:0043023]; ribosome binding [GO:0043022]
Uncharacterized protein	orf19.11466	CaO19.11466	
Uncharacterized protein	orf19.12079	CaO19.12079	hydrolase activity [GO:0016787]
Glucose-6-phosphate 1-epimerase (Uncharacterized protein)	orf19.1946	CaO19.1946	biofilm matrix [GO:0097311]; carbohydrate binding [GO:0030246]; isomerase activity [GO:0016853]; carbohydrate metabolic process [GO:0005975]
Uncharacterized protein	orf19.338	CaO19.338	mannosyl-oligosaccharide glucosidase activity [GO:0004573]; oligosaccharide metabolic process [GO:0009311]
Uncharacterized protein	orf19.4246	CaO19.4246	mitochondrion [GO:0005739]; glycerophospholipid biosynthetic process [GO:0046474]
Proline-tRNA ligase (Uncharacterized protein)	orf19.6701	CaO19.13993	cytoplasm [GO:0005737]; aminoacyl-tRNA editing activity [GO:0002161]; ATP binding [GO:0005524]; proline-tRNA ligase activity [GO:0004827]; prolyl-tRNA aminoacylation [GO:0006433]
Phosphoenolpyruvate carboxykinase [ATP] (Uncharacterized protein)	PCK1	CaO19.7514	cytosol [GO:0005829]; ATP binding [GO:0005524]; phosphoenolpyruvate carboxykinase (ATP) activity [GO:0004612]; gluconeogenesis [GO:0006094]
Pyruvate decarboxylase (EC 4.1.1.1)	PDC11	CaO19.10395	biofilm matrix [GO:0097311]; cell surface [GO:0009986]; cytoplasm [GO:0005737]; hyphal cell wall [GO:0030446]; plasma membrane [GO:0005886];

			yeast-form cell wall [GO:0030445]; magnesium ion binding [GO:0000287]; pyruvate decarboxylase activity [GO:0004737]; thiamine pyrophosphate binding [GO:0030976]
ADP,ATP carrier protein (Potential mitochondrial inner membrane ATP/ADP translocator)	PET9	CaO19.8545	integral component of membrane [GO:0016021]; membrane [GO:0016020]; mitochondrial inner membrane [GO:0005743]; plasma membrane [GO:0005886]; transporter activity [GO:0005215]; transmembrane transport [GO:0055085]
ATP-dependent 6-phosphofructokinase (ATP-PFK) (Phosphofructokinase) (EC 2.7.1.11) (Phosphohexokinase)	PFK2	CaO19.13893	6-phosphofructokinase complex [GO:0005945]; 6-phosphofructokinase activity [GO:0003872]; ATP binding [GO:0005524]; metal ion binding [GO:0046872]; fructose 6-phosphate metabolic process [GO:0006002]; glycolytic process [GO:0006096]
Phosphoglycerate kinase (EC 2.7.2.3)	PGK1	CaO19.11135	biofilm matrix [GO:0097311]; cell surface [GO:0009986]; cytoplasm [GO:0005737]; external side of plasma membrane [GO:0009897]; fungal-type cell wall [GO:0009277]; hyphal cell wall [GO:0030446]; plasma membrane [GO:0005886]; yeast-form cell wall [GO:0030445]; ATP binding [GO:0005524]; phosphoglycerate kinase activity [GO:0004618]; cell wall organization [GO:0071555]; glycolytic process [GO:0006096]; induction by symbiont of host defense response [GO:0044416]; interaction with host [GO:0051701]
pH-responsive protein 1 (pH-regulated protein 1)	PHR1	CaO19.11310	anchored component of membrane [GO:0031225]; plasma membrane [GO:0005886]; carbohydrate metabolic process [GO:0005975]
Plasma membrane ATPase (EC 3.6.3.6)	PMA1	CaO19.5383	integral component of plasma membrane [GO:0005887]; intracellular membrane-bounded organelle [GO:0043231]; ATP binding [GO:0005524]; hydrogen-exporting ATPase activity, phosphorylative mechanism [GO:0008553]; metal ion binding [GO:0046872]; ATP biosynthetic process [GO:0006754]; hydrogen ion transmembrane transport [GO:1902600]; regulation of intracellular pH [GO:0051453]
Outer mitochondrial membrane protein porin, putative	POR1	CaO19.1042	membrane [GO:0016020]; mitochondrial outer membrane [GO:0005741]; plasma membrane [GO:0005886]; pore complex [GO:0046930]; porin activity [GO:0015288]; voltage-gated anion channel activity [GO:0008308]
Serine/threonine-protein phosphatase (EC 3.1.3.16)	PPH1	CaO19.1683	phosphoprotein phosphatase activity [GO:0004721]
Proteasome component [alpha type 1], putative (EC 3.4.25.1)	PRE5	CaO19.7178	nucleus [GO:0005634]; proteasome core complex [GO:0005839]; proteasome core complex, alpha-subunit complex [GO:0019773]; proteasome storage granule [GO:0034515]; threonine-type endopeptidase activity [GO:0004298]; proteasomal ubiquitin-independent protein catabolic process [GO:0010499]; proteasome-mediated ubiquitin-dependent protein catabolic process [GO:0043161]
Proteasome subunit, putative (EC 3.4.25.1)	PUP2	CaO19.709	nucleus [GO:0005634]; proteasome core complex [GO:0005839]; proteasome core complex, alpha-subunit complex [GO:0019773]; threonine-type endopeptidase activity [GO:0004298]; proteasome-mediated ubiquitin-dependent protein catabolic process [GO:0043161]
Uncharacterized protein	PUT2	CaO19.11457	1-pyrroline-5-carboxylate dehydrogenase activity [GO:0003842]; oxidoreductase activity, acting on the aldehyde or oxo group of donors, NAD or NADP as acceptor [GO:0016620]; glutamate biosynthetic process [GO:0006537]; proline biosynthetic process [GO:0006561]

Ras-like protein 1 (Ras homolog type B)	RAS1	CaO19.1760	intracellular [GO:0005622]; plasma membrane [GO:0005886]; GTP binding [GO:0005525]; small GTPase mediated signal transduction [GO:0007264]
Uncharacterized protein	RCT1	CaO19.7350	outer membrane [GO:0019867]; ribosome [GO:0005840]
Protein rho3, putative	RHO3	CaO19.11018	intracellular [GO:0005622]; membrane [GO:0016020]; GTP binding [GO:0005525]; small GTPase mediated signal transduction [GO:0007264]
Cytochrome b-c1 complex subunit Rieske, mitochondrial (EC 1.10.2.2)	RIP1	CaO19.5893	mitochondrial inner membrane [GO:0005743]; respiratory chain [GO:0070469]; 2 iron, 2 sulfur cluster binding [GO:0051537]; metal ion binding [GO:0046872]; ubiquinol-cytochrome-c reductase activity [GO:0008121]
60S ribosomal protein L10, putative	RPL10	CaO19.10452	cell surface [GO:0009986]; ribosome [GO:0005840]; structural constituent of ribosome [GO:0003735]; translation [GO:0006412]
Ribosomal protein	RPL10A	CaO19.3465	large ribosomal subunit [GO:0015934]; RNA binding [GO:0003723]; structural constituent of ribosome [GO:0003735]; translation [GO:0006412]
Ribosomal protein of the large subunit, putative	RPL12	CaO19.1635	ribosome [GO:0005840]; structural constituent of ribosome [GO:0003735]; translation [GO:0006412]
Ribosomal protein L15	RPL15	CaO19.493	ribosome [GO:0005840]; structural constituent of ribosome [GO:0003735]; translation [GO:0006412]
40S ribosomal protein (S18), putative	RPL18	CaO19.7018	ribosome [GO:0005840]; RNA binding [GO:0003723]; structural constituent of ribosome [GO:0003735]; translation [GO:0006412]
Ribosomal protein, large subunit, putative	RPL23	CaO19.10998	ribosome [GO:0005840]; structural constituent of ribosome [GO:0003735]; translation [GO:0006412]
Ribosomal protein, large subunit, putative	RPL24	CaO19.11269	ribosome [GO:0005840]
60S ribosomal protein L4 subunit, putative	RPL4	CaO19.7217	cell surface [GO:0009986]; membrane [GO:0016020]; ribosome [GO:0005840]; structural constituent of ribosome [GO:0003735]; translation [GO:0006412]
60S ribosomal protein L5 (Likely cytosolic ribosomal protein L5)	RPL5	CaO19.13894	ribosome [GO:0005840]; 5S rRNA binding [GO:0008097]; structural constituent of ribosome [GO:0003735]; translation [GO:0006412]
Likely cytosolic ribosomal protein L9	RPL9	CaO19.236	ribosome [GO:0005840]; rRNA binding [GO:0019843]; structural constituent of ribosome [GO:0003735]; translation [GO:0006412]
60S acidic ribosomal protein P0	RPP0	CaO19.7015	cytosolic large ribosomal subunit [GO:0022625]; large ribosomal subunit rRNA binding [GO:0070180]; structural constituent of ribosome [GO:0003735]; cytoplasmic translation [GO:0002181]; ribosomal large subunit assembly [GO:0000027]
Ribosomal protein of the small subunit, putative	RPS15	CaO19.5927	small ribosomal subunit [GO:0015935]; RNA binding [GO:0003723]; structural constituent of ribosome [GO:0003735]; translation [GO:0006412]
40S ribosomal protein S20 (Likely cytosolic ribosomal protein S20)	RPS20	CaO19.13732	hyphal cell wall [GO:0030446]; small ribosomal subunit [GO:0015935]; yeast-form cell wall [GO:0030445]; RNA binding [GO:0003723]; structural constituent of ribosome [GO:0003735]; translation [GO:0006412]
40S ribosomal protein S23, putative	RPS23	CaO19.13632	small ribosomal subunit [GO:0015935]; structural constituent of ribosome [GO:0003735]; translation [GO:0006412]
40S ribosomal protein S25-A (40S ribosomal protein S25-B) (Likely cytosolic ribosomal protein S25)	RPS25B	CaO19.6663	ribosome [GO:0005840]
40S ribosomal protein (Likely cytosolic ribosomal protein S5)	RPS5	CaO19.11812	membrane [GO:0016020]; small ribosomal subunit [GO:0015935]; RNA binding [GO:0003723]; structural constituent of ribosome [GO:0003735]; translation [GO:0006412]

40S ribosomal protein S6	RPS6	CaO19.4660	ribosome [GO:0005840]; structural constituent of ribosome [GO:0003735]; translation [GO:0006412]
40S ribosomal protein S8	RPS8	CaO19.14162	cell surface [GO:0009986]; ribosome [GO:0005840]; structural constituent of ribosome [GO:0003735]; translation [GO:0006412]
26S protease subunit RPT4	RPT4	CaO19.482	cytoplasm [GO:0005737]; proteasome complex [GO:0000502]; ATP binding [GO:0005524]; hydrolase activity [GO:0016787]; protein catabolic process [GO:0030163]
Likely 26S proteasome regulatory particle ATPase Rpt6p	RPT6	CaO19.3593	cytoplasm [GO:0005737]; proteasome complex [GO:0000502]; ATP binding [GO:0005524]; hydrolase activity [GO:0016787]; protein catabolic process [GO:0030163]
E3 ubiquitin-protein ligase (EC 6.3.2.-)	RSP5	CaO19.11111	ligase activity [GO:0016874]; ubiquitin-protein transferase activity [GO:0004842]
Fimbrin	SAC6	CaO19.5544	calcium ion binding [GO:0005509]
Adenosylhomocysteinase (EC 3.3.1.1)	SAH1	CaO19.3911	biofilm matrix [GO:0097311]; cytoplasm [GO:0005737]; adenosylhomocysteinase activity [GO:0004013]; NAD binding [GO:0051287]; one-carbon metabolic process [GO:0006730]; S-adenosylhomocysteine catabolic process [GO:0019510]
S-adenosylmethionine synthase (EC 2.5.1.6)	SAM2	CaO19.657	ATP binding [GO:0005524]; metal ion binding [GO:0046872]; methionine adenosyltransferase activity [GO:0004478]; one-carbon metabolic process [GO:0006730]; S-adenosylmethionine biosynthetic process [GO:0006556]
Small COPII coat GTPase, putative (EC 3.6.5.-)	SAR1	CaO19.3462	endoplasmic reticulum membrane [GO:0005789]; ER to Golgi transport vesicle membrane [GO:0012507]; Golgi membrane [GO:0000139]; GTP binding [GO:0005525]; GTPase activity [GO:0003924]; ER to Golgi vesicle-mediated transport [GO:0006888]; intracellular protein transport [GO:0006886]
Succinate dehydrogenase [ubiquinone] flavoprotein subunit, mitochondrial (EC 1.3.5.1)	SDH12	CaO19.10389	mitochondrial inner membrane [GO:0005743]; flavin adenine dinucleotide binding [GO:0050660]; succinate dehydrogenase (ubiquinone) activity [GO:0008177]; electron transport chain [GO:0022900]; tricarboxylic acid cycle [GO:0006099]
Seryl-tRNA synthetase	SES1	CaO19.269	cytoplasm [GO:0005737]; ATP binding [GO:0005524]; serine-tRNA ligase activity [GO:0004828]; seryl-tRNA aminoacylation [GO:0006434]
Serine hydroxymethyltransferase, cytosolic (SHMT) (EC 2.1.2.1) (Glycine hydroxymethyltransferase) (SHMII) (Serine methylase)	SHM2	CaO19.13173	cytoplasm [GO:0005737]; glycine hydroxymethyltransferase activity [GO:0004372]; pyridoxal phosphate binding [GO:0030170]; glycine metabolic process [GO:0006544]; L-serine metabolic process [GO:0006563]; tetrahydrofolate interconversion [GO:0035999]
Uncharacterized protein	SLB1	CaO19.778	
Integral membrane protein, eisosome component, putative	SLB2	CaO19.3149	eisosome [GO:0032126]
Uncharacterized protein	SLK19	CaO19.14055	integral component of plasma membrane [GO:0005887]; cellular response to pH [GO:0071467]; fungal-type cell wall organization [GO:0031505]; pathogenesis [GO:0009405]
Pyridoxine biosynthesis protein SNZ1 (Uncharacterized protein)	SNZ1	CaO19.10464	cytoplasm [GO:0005737]; catalytic activity [GO:0003824]; pyridoxal phosphate biosynthetic process [GO:0042823]; vitamin B6 biosynthetic process [GO:0042819]
6-phosphogluconolactonase (Uncharacterized protein)	SOL2	CaO19.1355	6-phosphogluconolactonase activity [GO:0017057]; carbohydrate metabolic process [GO:0005975]; pentose-phosphate shunt [GO:0006098]

Heat shock protein SSA1 (Heat shock protein YG100)	SSA2	CaO19.1065	biofilm matrix [GO:0097311]; cell surface [GO:0009986]; cytoplasm [GO:0005737]; fungal-type cell wall [GO:0009277]; hyphal cell wall [GO:0030446]; membrane [GO:0016020]; plasma membrane [GO:0005886]; ATP binding [GO:0005524]; peptide binding [GO:0042277]; interaction with host [GO:0051701]; peptide transport [GO:0015833]; response to toxic substance [GO:0009636]
Hsp75-like protein (Uncharacterized protein)	SSB1	CaO19.13724	cell surface [GO:0009986]; cytosol [GO:0005829]; fungal-type cell wall [GO:0009277]; plasma membrane [GO:0005886]; yeast-form cell wall [GO:0030445]; ATP binding [GO:0005524]; filamentous growth [GO:0030447]; filamentous growth of a population of unicellular organisms [GO:0044182]; induction by symbiont of host defense response [GO:0044416]; translation [GO:0006412]
Heat shock protein SSC1, mitochondrial (Cytoplasmic antigenic protein 6) (mtHSP70)	SSC1	CaO19.1896	biofilm matrix [GO:0097311]; cell surface [GO:0009986]; mitochondrial matrix [GO:0005759]; plasma membrane [GO:0005886]; yeast-form cell wall [GO:0030445]; ATP binding [GO:0005524]; unfolded protein binding [GO:0051082]; protein folding [GO:0006457]
Sti1	STI1	CaO19.3192	
Secreted beta-glucosidase SUN41 (EC 3.2.1.-)	SUN41	CaO19.11124	cell wall [GO:0005618]; extracellular region [GO:0005576]; hydrolase activity, acting on glycosyl bonds [GO:0016798]; cell wall organization [GO:0071555]; pathogenesis [GO:0009405]; polysaccharide catabolic process [GO:0000272]
Eukaryotic peptide chain release factor subunit, putative	SUP45	CaO19.11025	cytoplasm [GO:0005737]; translation release factor activity, codon specific [GO:0016149]
Transaldolase (EC 2.2.1.2)	TAL1	CaO19.11849	biofilm matrix [GO:0097311]; cell surface [GO:0009986]; cytoplasm [GO:0005737]; hyphal cell wall [GO:0030446]; yeast-form cell wall [GO:0030445]; sedoheptulose-7-phosphate:D-glyceraldehyde-3-phosphate glyceronetransferase activity [GO:0004801]; carbohydrate metabolic process [GO:0005975]; pentose-phosphate shunt [GO:0006098]
Glyceraldehyde-3-phosphate dehydrogenase (EC 1.2.1.12)	TDH3	CaO19.14106	biofilm matrix [GO:0097311]; cell surface [GO:0009986]; cytoplasm [GO:0005737]; fungal-type cell wall [GO:0009277]; hyphal cell wall [GO:0030446]; plasma membrane [GO:0005886]; yeast-form cell wall [GO:0030445]; extracellular matrix binding [GO:0050840]; fibronectin binding [GO:0001968]; glyceraldehyde-3-phosphate dehydrogenase (NAD+) (phosphorylating) activity [GO:0004365]; laminin binding [GO:0043236]; NAD binding [GO:0051287]; NADP binding [GO:0050661]; adhesion of symbiont to host [GO:0044406]; cell-matrix adhesion [GO:0007160]; glucose metabolic process [GO:0006006]; glycolytic process [GO:0006096]; induction by symbiont of host defense response [GO:0044416]; interaction with host [GO:0051701]
Elongation factor 1-alpha	TEF2	CaO19.382	cytoplasm [GO:0005737]; GTP binding [GO:0005525]; GTPase activity [GO:0003924]; translation elongation factor activity [GO:0003746]
V-type proton ATPase catalytic subunit A (V-ATPase subunit A) (EC 3.6.3.14)	TFP1	CaO19.9249	endomembrane system [GO:0012505]; proton-transporting V-type ATPase, V1 domain [GO:0033180]; vacuolar membrane [GO:0005774]; ATP binding [GO:0005524]; proton-transporting ATPase activity, rotational mechanism [GO:0046961]; ATP hydrolysis coupled proton transport [GO:0015991]; ATP metabolic process [GO:0046034]; pathogenesis [GO:0009405]

Uncharacterized protein	TFS1	CaO19.1974	
Threonyl-tRNA synthetase, cytoplasmic (Uncharacterized protein)	THS1	CaO19.5685	cytosol [GO:0005829]; ATP binding [GO:0005524]; threonine-tRNA ligase activity [GO:0004829]; threonyl-tRNA aminoacylation [GO:0006435]
Uncharacterized protein	TOS1	CaO19.1690	
Thioredoxin reductase (EC 1.8.1.9)	TRR1	CaO19.4290	biofilm matrix [GO:0097311]; cytosol [GO:0005829]; ferrous iron binding [GO:0008198]; thioredoxin-disulfide reductase activity [GO:0004791]; cell redox homeostasis [GO:0045454]; cellular response to oxidative stress [GO:0034599]; removal of superoxide radicals [GO:0019430]
Peroxiredoxin TSA1	TSA1	CaO19.7417	cell surface [GO:0009986]; cytoplasm [GO:0005737]; cytosol [GO:0005829]; fungal-type cell wall [GO:0009277]; hyphal cell wall [GO:0030446]; nucleus [GO:0005634]; high molecular weight kininogen binding [GO:0030985]; thioredoxin peroxidase activity [GO:0008379]; cell redox homeostasis [GO:0045454]; cellular response to hydrogen peroxide [GO:0070301]; cellular response to oxidative stress [GO:0034599]; filamentous growth [GO:0030447]; filamentous growth of a population of unicellular organisms in response to chemical stimulus [GO:0036171]; filamentous growth of a population of unicellular organisms in response to starvation [GO:0036170]; fungal-type cell wall organization [GO:0031505]; hydrogen peroxide catabolic process [GO:0042744]; interaction with host [GO:0051701]; negative regulation of sequence-specific DNA binding transcription factor activity [GO:0043433]; positive regulation of sequence-specific DNA binding transcription factor activity [GO:0051091]; positive regulation of transcription from RNA polymerase II promoter in response to hydrogen peroxide [GO:0061407]; response to hydrogen peroxide [GO:0042542]
Tubulin alpha chain, putative	TUB1	CaO19.7308	cytoplasm [GO:0005737]; microtubule [GO:0005874]; GTP binding [GO:0005525]; GTPase activity [GO:0003924]; structural constituent of cytoskeleton [GO:0005200]; microtubule-based process [GO:0007017]
Transcriptional repressor TUP1-homologue, putative	TUP1	CaO19.13528	cellular response to copper ion [GO:0071280]; cellular response to drug [GO:0035690]; cellular response to farnesol [GO:0097308]; cellular response to starvation [GO:0009267]; development of symbiont in host [GO:0044114]; entry into host [GO:0044409]; evasion or tolerance of defenses of other organism involved in symbiotic interaction [GO:0051834]; filamentous growth [GO:0030447]; filamentous growth of a population of unicellular organisms [GO:0044182]; filamentous growth of a population of unicellular organisms in response to biotic stimulus [GO:0036180]; filamentous growth of a population of unicellular organisms in response to chemical stimulus [GO:0036171]; filamentous growth of a population of unicellular organisms in response to starvation [GO:0036170]; negative regulation of filamentous growth of a population of unicellular organisms [GO:1900429]; negative regulation of isoprenoid metabolic process [GO:0045827]; negative regulation of transcription from RNA polymerase II promoter [GO:0000122]; negative regulation of transcription, DNA-templated [GO:0045892]; pathogenesis [GO:0009405]; phenotypic switching [GO:0036166]; quorum sensing [GO:0009372]; single

			organismal cell-cell adhesion [GO:0016337]; transcription, DNA-templated [GO:0006351]
Ubiquitin-conjugating enzyme, putative (EC 6.3.2.19)	UBC4	CaO19.7571	cytosol [GO:0005829]; nuclear SCF ubiquitin ligase complex [GO:0043224]; proteasome complex [GO:0000502]; ATP binding [GO:0005524]; ubiquitin conjugating enzyme activity [GO:0061631]; cellular response to heat [GO:0034605]; mitotic sister chromatid segregation [GO:0000070]; positive regulation of mitotic metaphase/anaphase transition [GO:0045842]; protein localization to Golgi apparatus [GO:0034067]; protein monoubiquitination [GO:0006513]; protein polyubiquitination [GO:0000209]; protein processing [GO:0016485]; protein ubiquitination involved in ubiquitin-dependent protein catabolic process [GO:0042787]; regulation of protein glycosylation [GO:0060049]; SCF-dependent proteasomal ubiquitin-dependent protein catabolic process [GO:0031146]; ubiquitin-dependent protein catabolic process via the multivesicular body sorting pathway [GO:0043162]
Ubiquitin fusion protein, putative	UBI3	CaO19.10599	extracellular region [GO:0005576]; ribosome [GO:0005840]; protein tag [GO:0031386]; structural constituent of ribosome [GO:0003735]; protein ubiquitination [GO:0016567]; ribosome biogenesis [GO:0042254]; translation [GO:0006412]
Aspartate transcarbamylase (Protein URA1)	URA2	CaO19.9896	amino acid binding [GO:0016597]; aspartate carbamoyltransferase activity [GO:0004070]; ATP binding [GO:0005524]; carbamoyl-phosphate synthase (glutamine-hydrolyzing) activity [GO:0004088]; metal ion binding [GO:0046872]; 'de novo' pyrimidine nucleobase biosynthetic process [GO:0006207]; glutamine metabolic process [GO:0006541]
Vacuolar inheritance protein, putative	VAC8	CaO19.745	fungal-type vacuole [GO:0000324]; vacuolar membrane [GO:0005774]; filamentous growth [GO:0030447]; filamentous growth of a population of unicellular organisms in response to biotic stimulus [GO:0036180]; hyphal growth [GO:0030448]; vacuole inheritance [GO:0000011]
Glucan 1,3-beta-glucosidase (EC 2.4.1.-) (EC 3.2.1.58) (Exo-1,3-beta-glucanase)	XOG1	CaO19.10507	cell surface [GO:0009986]; cell wall [GO:0005618]; extracellular region [GO:0005576]; cell adhesion molecule binding [GO:0050839]; glucan exo-1,3-beta-glucosidase activity [GO:0004338]; transferase activity [GO:0016740]; cell-substrate adhesion [GO:0031589]; cellular glucan metabolic process [GO:0006073]; fungal-type cell wall organization [GO:0031505]; pathogenesis [GO:0009405]; single-species biofilm formation in or on host organism [GO:0044407]; single-species biofilm formation on inanimate substrate [GO:0044011]
Potential mitochondrial carrier family protein Yhm2	YHM2	CaO19.11673	integral component of membrane [GO:0016021]; plasma membrane [GO:0005886]; transport [GO:0006810]
GTP-binding protein, putative	YPT31	CaO19.10153	intracellular [GO:0005622]; GTP binding [GO:0005525]; small GTPase mediated signal transduction [GO:0007264]
Actin	ACT1	Ca19.12474	
High-mobility group non-histone chromosomal protein, putative	NHP6A	CaO19.4623.3	
Putative uncharacterized protein	RPL14	CaO19.4931.1	
60S ribosomal protein L2, putative	RPL2	CaO19.2309.2	

60S ribosomal protein L6	RPL6	CaO19.3003.1	
Ribosomal protein, small subunit, putative	RPS10	CaO19.2179.2	
Ribosomal protein, small subunit, putative	RPS13	CaO19.4193.1	
Superoxide dismutase [Cu-Zn] (EC 1.15.1.1)	SOD1	CaO19.2770.1	

Table 2: Unique Proteins in *C. parapsilosis* extracellular matrix			
Protein Characteristics			
Protein Name	**Gene Name**	**ORF Number**	**Gene Ontology**
Cytochrome P450 52A5, putative (EC 1.14.14.-)	ALK1	CaO19.13150	integral component of membrane [GO:0016021]; heme binding [GO:0020037]; iron ion binding [GO:0005506]; oxidoreductase activity, acting on paired donors, with incorporation or reduction of molecular oxygen, reduced flavin or flavoprotein as one donor, and incorporation of one atom of oxygen [GO:0016712]
Uncharacterized protein	GUK1	CaO19.1115	guanylate kinase activity [GO:0004385]
Xanthine phosphoribosyltransferase, putative (EC 2.4.2.-)	HPT1	CaO19.13254	nucleoside metabolic process [GO:0009116]
Methylenetetrahydrofolate dehydrogenase	MTD1	CaO19.3810	methylenetetrahydrofolate dehydrogenase (NADP+) activity [GO:0004488]; folic acid-containing compound biosynthetic process [GO:0009396]
NADP(+)-coupled glycerol dehydrogenase, putative (EC 1.1.1.-)	orf19.14049	CaO19.14049	biofilm matrix [GO:0097311]; oxidoreductase activity [GO:0016491]; cellular response to drug [GO:0035690]
26S proteasome regulatory subunit RPN11 (Likely 26S proteasome regulatory particle subunit Rpn11p)	RPN11	CaO19.7264	mitochondrion [GO:0005739]; nuclear periphery [GO:0034399]; proteasome regulatory particle, lid subcomplex [GO:0008541]; proteasome storage granule [GO:0034515]; thiol-dependent ubiquitin-specific protease activity [GO:0004843]; mitochondrial fission [GO:0000266]; peroxisome fission [GO:0016559]; proteasome-mediated ubiquitin-dependent protein catabolic process [GO:0043161]; protein deubiquitination [GO:0016579]
4-aminobutyrate aminotransferase	UGA12	CaO19.854	4-aminobutyrate transaminase activity [GO:0003867]; pyridoxal phosphate binding [GO:0030170]; gamma-aminobutyric acid metabolic process [GO:0009448]

Table 2: Unique Proteins in *C. tropicalis* extracellular matrix			
Protein Characteristics			
Protein Name	**Gene Name**	**ORF Number**	**Gene Ontology**
Constitutive acid phosphatase, putative (EC 3.1.3.2)	PHO12	CaO19.11211	acid phosphatase activity [GO:0003993]

Appendix B: Abstracts for manuscripts published in collaboration

An abstract follows for the manuscript published in collaboration with A. Skop:

Gnazzo MM, Uhlemann EE, Vilarreal AR, Shirayama M, **Dominguez EG,** Skop AR. The RNA-binding protein ATX-2 regulates cytokinesis through PAR-5 and ZEN-4. Mol Biol Cell. 2016 Oct 15;27(20):3052-3064. Doi:10.1091/mbc.E16-04-0219. PMCID: PMC5063614.

The spindle midzone harbors both microtubules and proteins necessary for furrow formation and the completion of cytokinesis. However, the mechanisms that mediate the temporal and spatial recruitment of cell division factors to the spindle midzone and midbody remain unclear. Here we describe a mechanism governed by the conserved RNA-binding protein ATX-2/Ataxin-2, which targets and maintains ZEN-4 at the spindle midzone. ATX-2 does this by regulating the amount of PAR-5 at mitotic structures, particularly the spindle, centrosomes, and midbody. Preventing ATX-2 function leads to elevated levels of PAR-5, enhanced chromatin and centrosome localization of PAR-5-GFP, and ultimately a reduction of ZEN-4-GFP at the spindle midzone. Codepletion of ATX-2 and PAR-5 rescued the localization of ZEN-4 at the spindle midzone, indicating that ATX-2 mediates the localization of ZEN-4 upstream of PAR-5. We provide the first direct evidence that ATX-2 is necessary for cytokinesis and suggest a model in which ATX-2 facilitates the targeting of ZEN-4 to the spindle midzone by mediating the posttranscriptional regulation of PAR-5.

An abstract follows for the manuscript published in collaboration with L. Kaczmarek:

Sidoryk K, Switalska, M, Jaromin, A, Cmoch, P, Bujak, I, Kaczmarska, M, Wietrzyk, J, **Dominguez EG**, Zarnowski, R, Andes, DR, Bankowski, K, Cybulski, M, Kaczmarek L. The synthesis of indolo[2,3-b]quinoline derivatives with a guanidine group: highly selective cytotoxic agents. Eur J Med Chem. 2015 Nov 13;105:208-2019. Doi:10.1016/j.ejmech.2015.10.022. PMID: 26496013.

The synthesis of indolo[2,3-b]quinoline derivatives containing guanidine, amino acid or guanylamino acid substituents as well as their in vitro evaluation for the cytotoxic and antifungal activity are reported. The influence of the guanidine group on the selective cytotoxic and hemolytic properties of indolo[2,3-b]quinoline was investigated. Most of the compounds displayed a high cytotoxic activity in vitro and two of the most promising compounds (3 and 12) exhibited a high selectivity between normal and cancer cell-lines. The cytotoxic activity of compound 3 was about 600-fold lower against normal fibroblasts than against A549 and MCF-7 cancer cell lines. Novel entities acted as the DNA-intercalators when tested using a DNA-methyl green assay but demonstrated zero or low hemolytic activity in comparison to their unsubstituted analogs. The mechanism of action was studied for guanidine derivatives 3 and 12 and both compounds were found to be very effective inducers of apoptosis.